26 January 2007 | $10

Science

AAAS

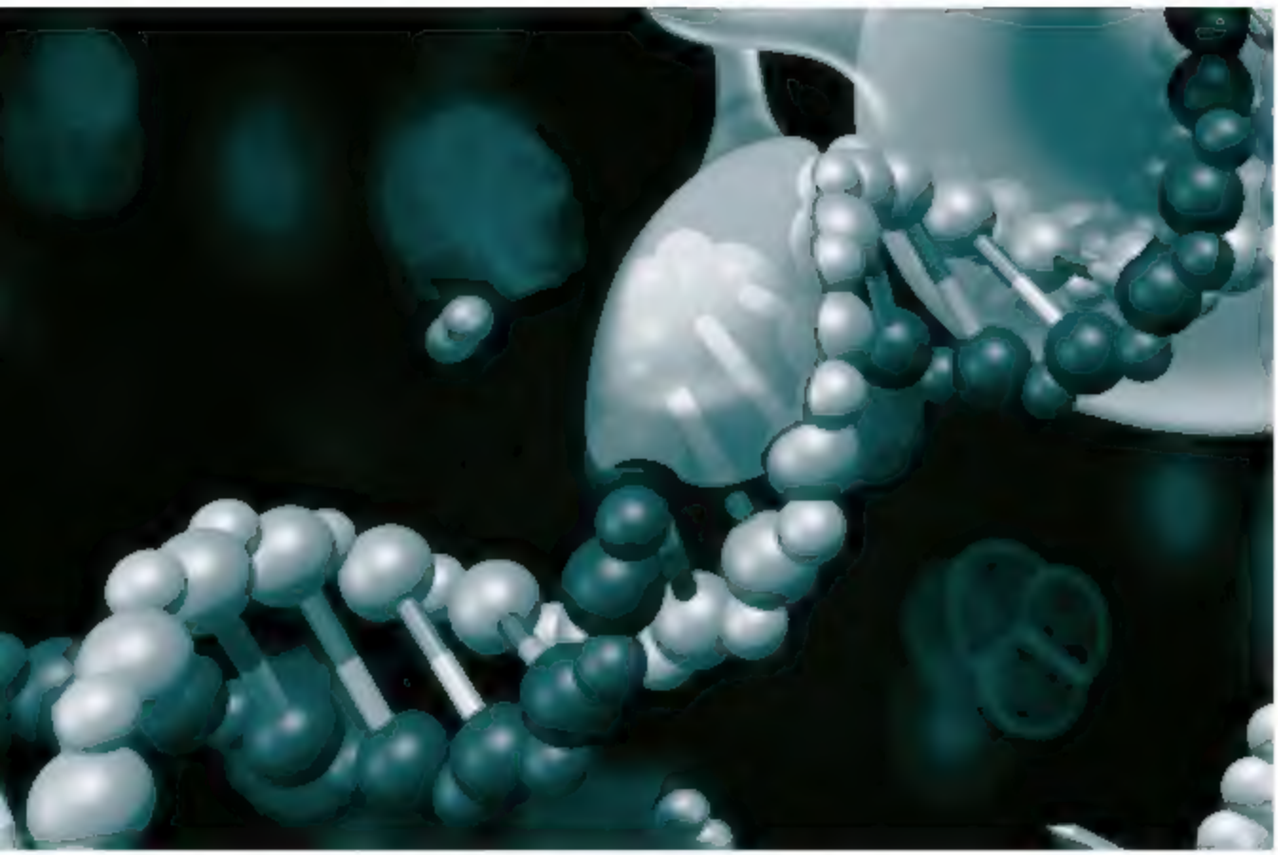

Redefining Fast PCR

Bio-Rad's unique iProof™ high-fidelity DNA polymerase delivers unsurpassed speed and fidelity, with higher yields and fewer reaction failures, for all your PCR needs.

Features and Benefits

- Extreme speed — Increased processivity dramatically reduces extension steps (to 15–30 sec/kb) and overall run times (to 25–35 min)
- Unmatched fidelity — Novel proofreading enzyme is the most accurate thermostable polymerase (52-fold more accurate than *Taq*)
- Minimal enzyme usage — Enhanced processivity enables the use of less enzyme (0.25–1 U/reaction)

For more information, visit us on the Web at **www.bio-rad.com/ad/iProof/**

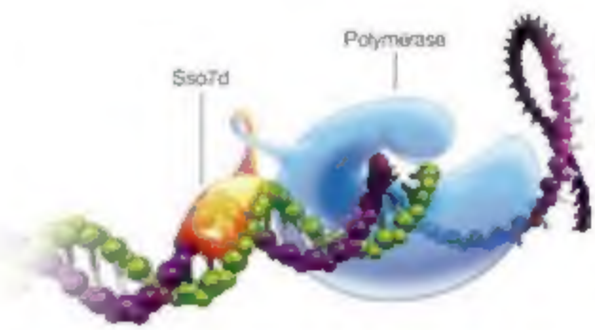

Fusing the double-stranded DNA binding protein Sso7d to iProof polymerase gives it a powerful sliding grip on the replicated DNA.

Practice of the polymerase chain reaction (PCR) may require a license.

Visit us on the Web at **discover.bio-rad.com**
Call toll free at 1-800-4BIORAD (1-800-424-6723); outside the US, contact your local sales office.

BIO-RAD

GE Healthcare

ÄKTA™

100,000 scientists working with proteins believe in ÄKTA, UNICORN and wizards.

To 100,000 scientists worldwide, ÄKTA™ sets the standard in protein purification. All systems in the ÄKTAdesign™ family work with intelligent UNICORN™ software, which makes it easy to control every stage of your purification process. But we're never content to stand still. The result is products like ÄKTAxpress™, which can solve low expression and double-tagged protein purification challenges, and ÄKTApurifier™, a time-saving automated protein purification system that can be configured to suit your personal application and workflow needs.

By continually developing technology that can turn your scientific ideas into reality, we're bringing science to life and helping transform healthcare.

We call it Protein Separations Re-imagined.

Discover the legendary purification power of UNICORN and ÄKTA, visit www.gehealthcare.com/akta

imagination at work

0659-06

Volume 315, Issue 5811

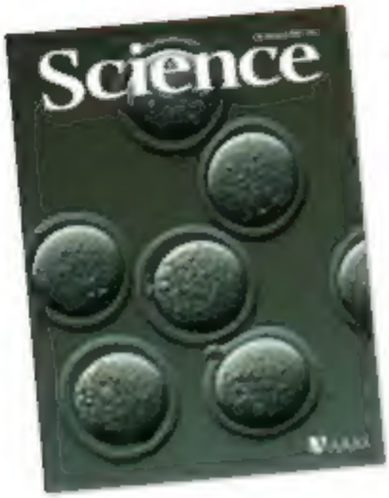

COVER

Mouse zygotes that are developing parthenogenetically (without fertilization) with a single polar body and two pronuclei. These zygotes develop into blastocysts, from which embryonic stem cells can be harvested. Such cell lines can provide a source of immunologically compatible tissues for transplantation. Zygote outer diameter, 70 to 80 micrometers. See page 482.

Image: K. Kim, K. Ng, A. Yabuuchi, and G. Q. Daley

DEPARTMENTS

EDITORIAL

NEWS OF THE WEEK

NEWS FOCUS

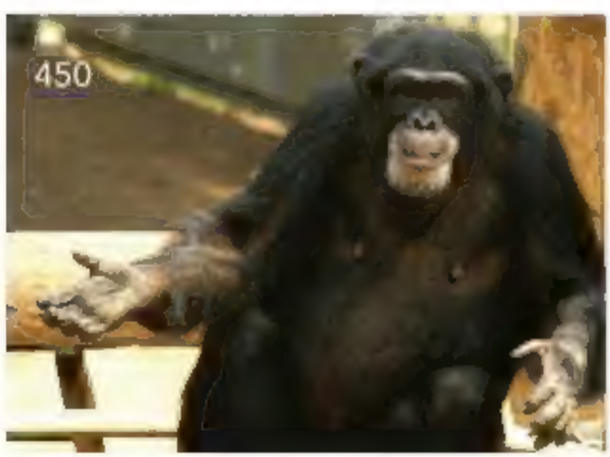

LETTERS

BOOKS *ET AL.*

EDUCATION FORUM

PERSPECTIVES

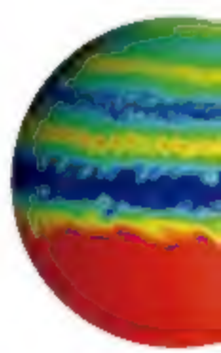

467

CONTENTS continued >>

Automated solutions by QIAGEN

Free up your time

- Largest portfolio of purification protocols
- Plug-and-play spin-column automation with QIAcube
- Low- to high-throughput automation
- Molecular diagnostics systems*
- Consultative Application Service and Instrument Care

Contact QIAGEN today or visit www.qiagen.com/goto/Automated .

* some PCR assays are not cleared for clinical use in USA and Canada.

QIAGEN®

Sample & Assay Technologies

Science

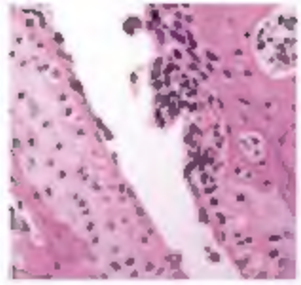

SCIENCE EXPRESS

www.sciencexpress.org

TECHNICAL COMMENT ABSTRACTS

REVIEW

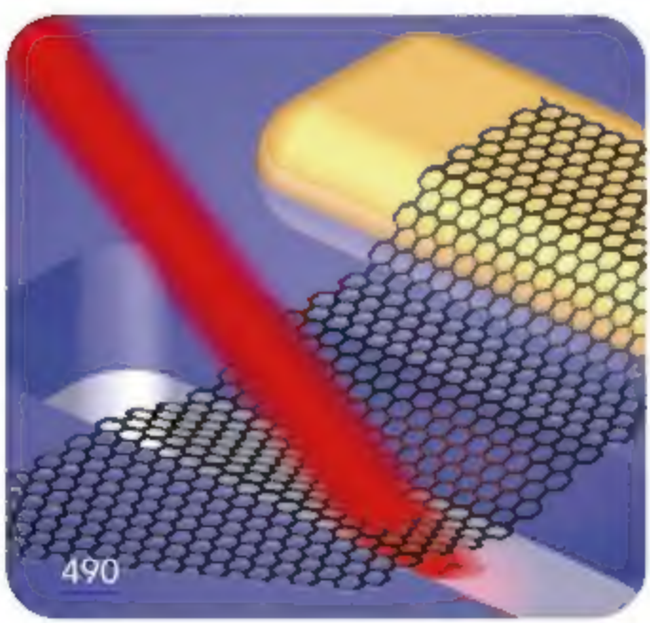

BREVIA

RESEARCH ARTICLE

REPORTS

CONTENTS continued >>

Astonishingly robust. Want to try some?

Comparison of amplifications using Taq DNA Polymerase and GoTaq® DNA Polymerase. A. Taq DNA Polymerase in Storage Buffer A. B. Taq DNA Polymerase in Storage Buffer A. C. GoTaq® DNA Polymerase in Colorless GoTaq® Reaction Buffer. D. GoTaq® DNA Polymerase in Green GoTaq® Reaction Buffer.

Promega GoTaq® Polymerase delivers better performance and it's more convenient. Plus, you get the same Promega PCR Guarantee as *Taq* in Buffer A or Buffer B. You'll save time, because GoTaq serves as both a loading buffer and tracking dye. This robust enzyme reliably amplifies large or small products.

Here's a sweet deal…**try it FREE!**
www.promega.com/gotaq/

PROMEGA CORPORATION • www.promega.com

Promega

REPORTS *CONTINUED...*

469 & 518

AAAS

ADVANCING SCIENCE, SERVING SOCIETY

SCIENCE (ISSN 0036-8075) is published weekly on Friday, except the last week in December, by the American Association for the Advancement of Science, 1200 New York Avenue, NW, Washington, DC 20005. Periodicals Mail postage (publication No. 484449) paid at Washington, DC, and additional mailing offices. Copyright © 2007 by the American Association for the Advancement of Science. The title SCIENCE is a registered trademark of the AAAS. Domestic individual membership and subscription (51 issues): $142 ($74 allocated to subscription). Domestic institutional subscription (51 issues): $710. Foreign postage extra: Mexico, Caribbean (surface mail) $55; other countries (air assist delivery) $85. First class, airmail, student, and canadian rates on request. Canadian rates with GST available upon request, GST #125488122. Publications Mail Agreement Number 1069624. **Printed in the U.S.A.**

Change of address: Allow 4 weeks, giving old and new addresses and 8-digit account number. **Postmaster:** Send change of address to AAAS, P.O. Box 96178, Washington, DC 20090-6178. **Single-copy sales:** $10.00 current issue, $15.00 back issue prepaid includes surface postage; bulk rates on request. **Authorization to photocopy** material for internal or personal use under circumstances not falling within the fair use provisions of the Copyright Act is granted by AAAS to libraries and other users registered with the Copyright Clearance Center (CCC) Transactional Reporting Service, provided that $30.00 per article is paid directly to CCC, 222 Rosewood Drive, Danvers, MA 01923. The identification code for *Science* is 0036-8075. *Science* is indexed in the Reader's *Guide to Periodical Literature* and in several specialized indexes.

CONTENTS continued >>

SCIENCENOW

www.sciencenow.org

Novel Synchrotron Shifts Into Neutral
Gently accelerated beams could probe the interactions between colliding molecules.

A Kiss to Help Forget a Fight
Some birds appear to manage fallout from conflicts much like primates do

Taking Blood Cells for a Spin
Tiny tornadoes might simplify blood tests

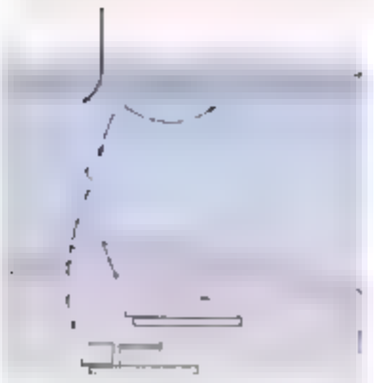

Cleaved to regulate transcription.

SCIENCE'S STKE

www.stke.org

PERSPECTIVE: EGFR Signaling Inhibits E2F1-Induced Apoptosis in Vivo—Implications for Cancer Therapy
D. Ginsberg
Insights from regulation of cell death during fly development offer clues to potential cancer therapy.

PERSPECTIVE: Split Personality of Transcription Factors Inside and Outside the Nuclear Border
J. R. Naranjo and B. Mellström
Three transcription factors act outside the nucleus to regulate calcium homeostasis.

Micella's back, as a postdoc.

SCIENCE CAREERS

www.sciencecareers.org

U.S. Educated Woman, Postdoc Edition—New Year, New Life
M. P. deWhyse
Now a postdoc, Micella discusses her recent transition and ponders what lies on the road ahead

U.S. Returning to Academia
S. Webb
Some scientists have made the move to industry a roundtrip

ITALY: Getting Up to I.T.
E. Pain
Valerie Materese left academia and her home country to set up an editing and information research company

SCIENCEPODCAST

Listen to the 26 January *Science* Podcast to hear about brain damage that disrupts smoking addiction, a three-way symbiosis that confers heat tolerance, clues to pneumonic plague progression, and more
www.sciencemag.org/about/podcast.dtl

Separate individual or institutional subscriptions to these products may be required for full-text access.

Phusion™ High-Fidelity DNA Polymerase from New England Biolabs

EXTREME PRECISION WITH UNPARALLELED SPEED AND ROBUSTNESS

We [illegible] PCR [illegible] A [illegible] 50 [illegible] DNA [illegible]

Advantages:

- Extreme fidelity – Highest of any thermostable polymerase
- High Speed – [illegible] are [illegible]
- Robustness – Reliable results [illegible] with minimal optimization
- High Yields – Increased product yields with minimal enzyme amounts
- Specificity – Hot start modification reduces non-specific [illegible]

Phusion High-Fidelity DNA Polymerase (R)	F-530S/L
Phusion Hot Start High-Fidelity DNA Polymerase (R)	F-540S/L
Phusion High-Fidelity PCR Master Mix (R) with HF Buffer	F-531S/L
with GC Buffer	F-532S/L
Phusion High-Fidelity PCR Kit (R)	F-553S/L

(R) = Recombinant

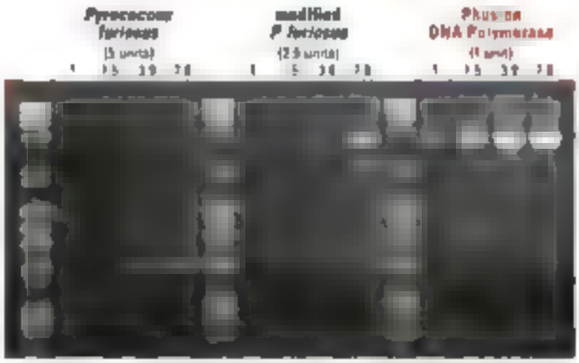

Experience extreme speed and yield with Phusion High-Fidelity DNA Polymerase. A [illegible] fragment from human beta-globin gene was amplified according to supplier recommendations using varying extension times. Phusion DNA Polymerase was able to amplify the fragment with a combined annealing and extension step of only 1 minute. Also, a single unit of Phusion DNA Polymerase produced higher yields than 2.5 or 5 units of *Pyrococcus furiosus* DNA Polymerases.

Phusion™ is a trademark of Finnzymes Oy.

For more information please visit www.neb.com

- **New England Biolabs Inc.** 1-800-NEB-LABS Tel: 978-927-5054 Fax: 978-921-1350 info@neb.com
- **Canada** Tel: (800) 387-1095 info@ca.neb.com
- **Germany** Tel: 0800 246 227 info@de.neb.com
- **UK** Tel: 0800 318486 info@uk.neb.com
- **China** Tel: 010-82378266 beijing@neb-china.com

Produced by

FINNZYMES

Distributed by

NEW ENGLAND BioLabs Inc.

the leader in enzyme technology

EDITED BY STELLA HURTLEY AND PHIL SZUROMI

Sunlight, Clouds, and Dimethylsulfide

Dimethylsulfide is produced in abundance by marine organisms and is a precursor for a major fraction of cloud-forming aerosols. Thus, it has been suggested that oceanic primary productivity could be part of an important feedback loop involving clouds. **Vallina and Simó** (p. 506) report that dimethylsulfide concentrations over the remote ocean are strongly correlated with the amount of solar radiation received by the upper mixed layer of the ocean. This response could produce a negative feedback in which dimethylsulfide emissions are inhibited as the increased cloudiness they cause reduces the amount of light received by the pelagic ecosystem.

Making a Stand

Many responsive materials, such as hydrogels, are made from polymers that can swell or shrink with changing exposure to a solvent. Although these materials can respond rapidly, there is a limit to the complexity in their shape change as well as to the amount of stress that can be exerted on such soft materials. **Sidorenko *et al.*** (p. 487) constructed two architectures in which silicon nanocolumns are either freely embedded in a polymer hydrogel or attached to the underlying substrate. When the hydrogel changes dimension upon exposure to water vapor, the nanocolumns are lifted up and stand up off the surface. This actuation is fast (on the order of seconds) and reversible. The hydrogel can also be templated so that the motion of the silicon nanocolumns occurs in a specific pattern.

Slow Rumble

Japan-installed seismic networks on the Nankai subduction zone after the Kobe earthquake, and the resulting measurements have revealed a wealth of new phenomena, including nonvolcanic tremor, long-period volcanic events, and slow earthquakes. **Ito *et al.*** (p. 503, published online 30 November; see the Perspective by **Dragert**) identify yet another type of seismic reverberation, that of very-low-frequency events with equivalent magnitudes of 3 to 3.5 and long periods of tens of seconds. The very-low-frequency earthquakes accompany and migrate with nonvolcanic tremor and slow slip events. The coincidence of these three phenomena improves the detection and characterization of slow earthquakes, which are thought to increase the stress on the updip megathrust earthquake rupture zone.

CREDITS (TOP TO BOTTOM): J. M. GRUNLAN; C. SC. VÖHRINGER-MARTINEZ ET AL.

Aqueous Acceleration

The role of water in many atmospheric reactions remains poorly understood at the molecular level because it is difficult to distinguish nonspecific effects, such as collisional activation, from direct participation of water as a catalyst. **Vöhringer-Martinez *et al.*** (p. 497; see the Perspective by **Smith**) combined precise kinetic measurements with quantum chemical calculations to implicate a catalytic role for individual water molecules in the gas-phase reaction of OH radicals with acetaldehyde. Their results suggest that water complexation to acetaldehyde lowers the subsequent barrier to attack by OH. The increasing instability of such complexes with rising temperature accounts for an unusual negative dependence on temperature of the magnitude of the catalytic effect.

Beating on a Graphene Drumskin

A resonator vibrates in response to an applied external force, and making a resonator thinner and less massive will generally cause it to operate at higher frequencies and have better sensitivity. **Bunch *et al.*** (p. 490) exfoliated ultrathin sheets of graphene from graphite and suspended the two-dimensional layers across a trench. They then actuated the thin sheets optically and electrically, thereby realizing the ultimate limit of resonators: only one atom in thickness.

Fewer Escapist Tendencies

Early in its history, Mars was once wet and humid and had a denser atmosphere than it has today. This atmosphere was supposedly battered by the solar wind and lost into space. **Barabash *et al.*** (p. 501) find that the escape rate today for gases in the martian atmosphere is very low, based on measurements from the orbiting Mars Express spacecraft. Propagating these rates backward over a period of 3.5 Gy would result in the removal of 0.2 to 4 mbar of CO_2 and a few centimeters of water. Rather than having left the planet, CO_2 and water could instead be locked away beneath its surface.

A Species by Another Name?

There is considerable uncertainty about what constitutes a species for bacteria because of the apparently rampant horizontal gene exchange that occurs between microorganisms, which seems to result in microbial populations being blended. **Fraser *et al.*** (p. 476) focus on the distribution and effect of mutation and recombination frequencies and, by combining a modeling approach with a review of the existing data, reveal the conditions under which bacterial speciation may occur.

Continued on page 435

Introducing Our Second Generation Genome Sequencing System

Genome Sequencer FLX

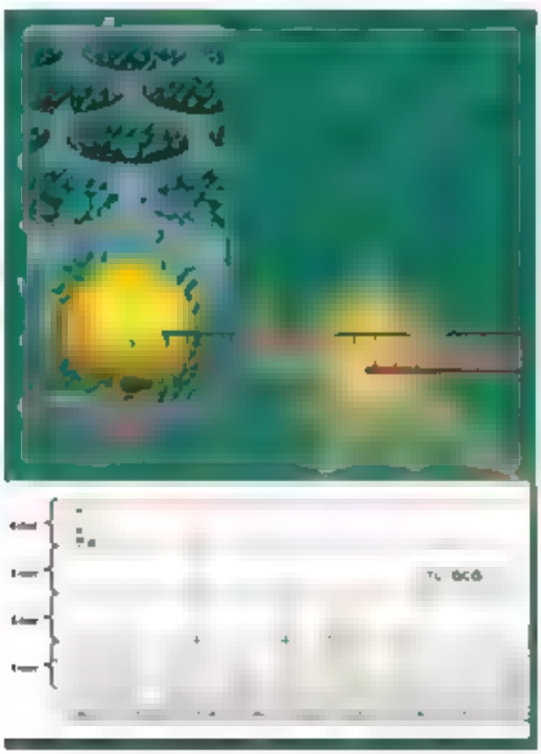

Be First to the Finish with...

- Increased read lengths averaging 200 to 300 bases per read
- Throughput of more than 400,000 reads per run
- High single-read accuracy greater than 99.5% over 200 bases
- Consensus-read accuracy greater than 99.99%

...more Flexibility and more Applications.

Visit ***www.genome-sequencing.com*** to learn about the expanding number of peer-reviewed publications appearing weekly

454 LIFE SCIENCES

Roche

Roche Diagnostics GmbH
Roche Applied Science
68298 Mannheim
Germany

Continued from page 433

Like Mother, Like Daughter

Tissues derived from embryonic stem cells may prove therapeutically useful, but a likely problem will be the rejection of stem cells that carry surface antigens dissimilar from those of the recipient. In order to create embryonic stem cell lines that carry matched surface antigens, **Kim *et al.*** (p. 482, published online 14 December; see the cover) have analyzed parthenogenetic derivation of embryonic stem cells in the mouse. Using oocytes from two separate phases of mitosis, they induced parthenogenetic development in which the cells carry two copies of the maternal genome. Stem cells derived from these embryos would be a specific match for the donor of the oocyte. Such parthenogenetically derived stem cells could produce many, but not all, tissues, possibly because of the absence of the paternally imprinted genome.

Plaguing the Lungs

Plague is not just transmitted by fleas; hypervirulent pneumonic plague can be transmitted directly among people by coughing. **Lathem *et al.*** (p. 509) show that a specific virulence factor from *Yersinia pestis*, plasminogen activator, is injected into host cells and promotes proliferation of the bacteria and massive lung inflammation. It is possible that this bacterial protease converts host plasminogen into plasmin, thereby releasing trapped bacteria from fibrin clots. Thus, inhibiting plasminogen activator during therapy might slow disease progression and allow antibiotics time to take effect.

Stop Smoking

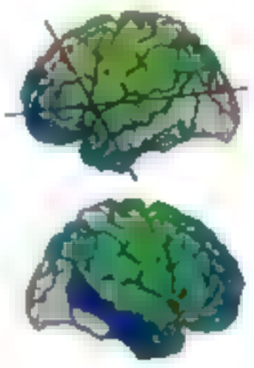

The region of the brain called the insula has received relatively little attention in drug addiction literature. **Naqvi *et al.*** (p. 531) now report the results of a retrospective anatomical analysis of a large cohort of brain-damaged patients. The analysis was prompted by their observation of a single patient with insula damage who quit a severe nicotine addiction immediately upon recovery from his acute neurological damage without any apparent difficulty or relapse. Damage to the insula appears to reduce the urge to smoke rather than, for example, reducing the reward or reinforcement associated with smoking.

Three-Way Partnership

A three-way endosymbiosis involving a grass, a fungus, and a virus has been discovered in the hot springs of Yellowstone National Park by **Márquez *et al.*** (p. 513). A virally infected fungus infects the developing grass's roots and confers heat tolerance to both grass and fungus. Furthermore, it is the virus in the fungus that allows the endophyte to confer this tolerance. Fungus lacking the virus did not provide heat resistance to its host grass until it was reinfected.

Heads, I Win

One of the enduring observations in support of human irrationality is that we are disproportionately sensitive to losses relative to gains. When offered a 50/50 gamble, the potential gain needs to be twice as large as the potential loss in order for subjects to exhibit a region-wise willingness to accept or to reject the gamble. **Tom *et al.*** (p. 515) have mapped a set of brain regions that respond parametrically to the sizes of potential gains and losses, and show that these regions are more sensitive to losses. Furthermore, the between-subject differences in neural responses reflect the between-subject differences in their behavioral aversion to losses.

Inside B Cell Central

B cells become effective factories for antibody production only after they have gone through a series of maturation steps that select clones of B cells carrying somatic mutations for high-affinity antibodies. This process takes place in the germinal center, where B cells are also thought to compete vigorously for available antigen. Using intravital microscopy, **Allen *et al.*** (p. 528, published online 21 December) observe that the behavior of germinal center B cells is more consistent with a competition for the attention of helper T cells than for scarce antigen. This finding could prove useful in considering how best to stimulate robust immune responses with vaccines.

CREDIT: NAQVI ET AL.

Monica Bradford is the executive editor of *Science*

Catalytic Connections

WE ALL KNOW THAT AT CONFERENCES THE REAL EXCHANGE OF IDEAS HAPPENS DURING the breaks and meals. Through informal communications, we discover common bonds and passions on which we build future collaboration. The International Conference of Women Leaders in Science, Technology and Engineering in Kuwait this month, which brought together Arab scientists and engineers from the Middle East and North Africa (ME NA) with U.S. women holding similar positions, was an effort to spark such connections. Against the backdrop of the present political climate, charged with concerns about terrorism, spread of proliferation, and economic vulnerability, I was thrilled to see business cards being swapped at an astonishing rate. The richness and sincerity of these interactions provided tangible evidence of the catalytic effect that women could have on the region.

The conference was organized by the Kuwait Foundation for the Advancement of Science, the Kuwait Institute for Scientific Research, the Arab Fund for Economics and Social Development, the American Association for the Advancement of Science (publisher of *Science*), and the U.S. Department of State, under the auspices of the prime minister of Kuwait. A central purpose of the meeting was to foster leadership skills by creating networks among female scientists in the region and between those scientists and U.S. women. As Yasmin A. Almubarak Alfawaz, an epidemiologist from Saudi Arabia, wrote, "Our mere presence together there, created a dialogue that will lay down the foundations for future collaborations."

Clearly, a vibrant community of women scientists is emerging in the region. At the conference, many Arab women met regional counterparts for the first time. As personal stories were shared, generalizations quickly vanished. Some of the attendees were international students, whereas others had moved outside their home country to pursue their studies; some were single, others married, and many had children before pursuing their degrees; some had returned home hoping to make a difference after years abroad, while others had found opportunities in their own countries. Yet all remained focused on making a contribution through their work, even when societal norms presented obstacles. Confident and articulate, these women understand that socioeconomic development of the region depends on global capacity building and strategic investments in science and technology.

Before the meeting, my own image of Arab women was of an oppressed and marginalized group. Yet statistics presented during the meeting by Samia Islam painted a more nuanced picture. Drawing from a 2005 United Nations Educational, Scientific and Cultural Organization report, she noted that 74% of science graduates in Bahrain are women, as compared to 43% in the United States. Unfortunately, this positive indicator is offset by the World Bank Group GenderStats data for 2004, which point out that women make up only 19% of the total labor force in Bahrain, while they account for 46% in the United States. The World Bank sector brief *Gender in ME NA* focuses on this paradox and notes that "unlike in other regions of the world, significant progress to reduce the gender gaps in education and in lower mortality rates has not carried through into ME NA's labor market." These observations were borne out by some of the attendees for whom a science education is a reality, but full participation in the work force is still elusive. As the 2006 InterAcademy Council report *Women for Science* stated, "global capacity building . . . is impossible without full engagement of women at the grassroots." Hopefully, this conference will signal to the region that the time for full engagement is now.

In stepping out of my own comfort zone to attend the conference, I carried some unease. I was not eager to fly over Baghdad and felt I must acknowledge that the Arab world is an editor provides intellectual stimulation and, I thought, a sufficient level of engagement. But the eyes of a Yemeni woman—all that I could see of her—showed me that there is more to encounter, and her gaze spoke volumes. I share hers for knowledge, professional achievement, and the chance to make a difference. On the meeting's last day, she spoke of her gratitude for the conference and of how it had liberated her. Her eyes, her presence, had equally liberated me and, no doubt, others.

Monica Bradford

10.1126/science.1140004

CREDIT: CATHERINE O'DON

EDITED BY GILBERT CHIN AND JAKE YESTON

CELL BIOLOGY

Caught in the NET

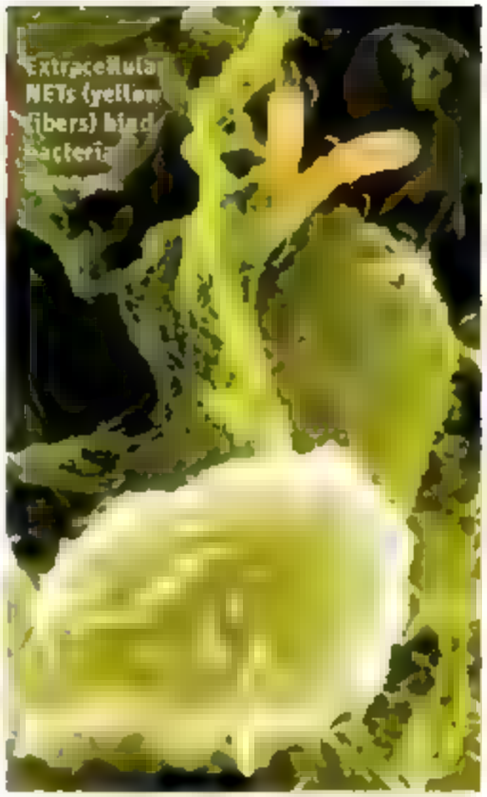

When circulating neutrophils are challenged by microbes, they can transform themselves into neutrophil extracellular traps or NETs, which are constructed out of chromatin (from the nucleus) and granule proteins (from the cytoplasm). These NETs grab hold of and sequester bacteria—and in doing so, they keep them within the range of antimicrobial enzymes and peptides.

Fuchs *et al.* show that this process involves a new type of cell death program. After neutrophils are stimulated, the normal segregation of chromatin into regions that are actively transcribing genes and those that are inactive disappears, and the nuclei become deformed. Subsequently, intracellular membranes, including the nuclear envelope and also granule membranes, disintegrate; this leads to the mixing and assembly of the NET components, which are then released from the dying cell as its plasma membrane ruptures. This sequence of cell death is distinct from other known forms of programmed cell death and appears to involve reactive oxygen species (superoxide and peroxide) that are produced by NADPH oxidase. Chronic granulomatous disease patients are deficient in this enzyme and cannot make NETs, which may explain in part why they suffer recurrent infections. Thus, even with their last breath, neutrophils contribute to the fight against invasive microbes. — SMH

J. Cell Biol. **176**, 231 (2007)

CHEMISTRY

Through the Looking Glass

Amino acids exist predominantly as L isomers, although the mirror-image D isomers figure in several biochemical pathways. Pyridoxal phosphate–dependent enzymes racemize amino acids for this purpose by binding them through a hydrogen bond–stabilized imine linkage. Park *et al.* have prepared a small molecule receptor that binds amino acids through a similar motif but also incorporates a chiral binaphthyl backbone. When L amino acids are bound in the presence of triethylamine base, they are selectively epimerized by proton exchange to the D isomers in order to relieve steric constraints imposed by the framework. The authors could efficiently invert the configurations of 13 chiral amino acids, including those with acidic or basic side chains. Selectivities ranged from 7:1 (for alanine) to 20:1 (for threonine). Acid hydrolysis liberated the epimerized product from the framework, after which the receptor could be recycled. — JSY

J. Am. Chem. Soc. **129**, 10.1021/ja067724g (2007)

BIOCHEMISTRY

Three of a Kind

Nitrogen is, of course, an essential element for life, and the primary mode by which microbes acquire nitrogen is by ammonia uptake through the trimeric ammonia channel AmtB. Two crystal structures of bacterial AmtB and one of archaeal Amt1 revealed that each monomer features a passageway for ammonia (NH_3) and a pseudosymmetric pair of five transmembrane helix domains (for more on how this dual topology arrangement might have evolved, see Rapp *et al.*, Reports, Science Express, 25 January 2007). When intracellular nitrogen is limiting, the primary AmtB regulator, the trimeric protein GlnK—dissociates to allow ammonia entry: an unregulated channel (and persistent ammonia influx) would be fatal given its effect on pH homeostasis.

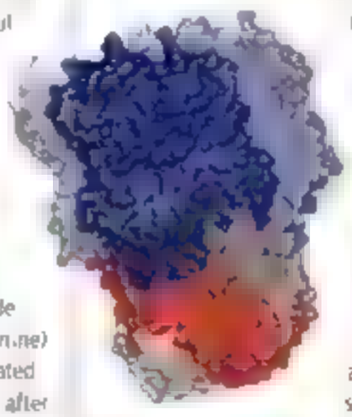

The AmtB (blue)–GlnK (red) complex, with detergent (yellow).

Gruswitz *et al.* and Conroy *et al.* have solved the structure (at 2.0 and 2.5 Å, respectively) of the bacterial AmtB–GlnK complex, and Yildiz *et al.* have contributed an electron microscopic study of the archaeal Amt1–GlnK1 complex. They find that an extended region of GlnK referred to as the T loop, which contains an arginine residue at its tip, inserts into the cytoplasmic vestibule of AmtB and physically impedes the passage of ammonia. All five hydrogens of the guanidinium cation find partners on the interior surface of the AmtB pore, which seems fitting because the channel has, after all, adapted to conduct ammonia. How is such an ornate association disrupted? As intracellular nitrogen drops, the small molecule 2-oxoglutarate accumulates and binds to GlnK (precisely where is not quite clear yet) along with Mg·ATP; these interactions and perhaps ATP hydrolysis may be involved in the extension and retraction of the T loop. — GJC

Proc. Natl. Acad. Sci. U.S.A. **104**, 42 1213 (2007).
EMBO J. 10.1038/sj.emboj.7601492 (2007)

IMMUNOLOGY

Keeping It Brief

The cytokine interleukin-2 (IL-2) is both produced by and exerts strong effects on T cells. Despite its fundamental importance for T cell development and immune regulation, IL-2 is only fleetingly expressed, consistent with a need to keep the potent effects of this growth factor under tight control.

Villarino *et al.* have investigated the management of IL-2 expression by helper T (T_H) cells and find that several feedback mechanisms exist to ensure the brevity of its expression. Selection cytokines—including some that use receptors bearing the common γ chain—exhibited the ability to suppress IL-2 expression. Most potent

CREDITS: TOP TO BOTTOM: V. BRINKMANN/MAX PLANCK INSTITUT FOR INFECTION BIOLOGY; GRUSWITZ *ET AL.* PROC. NATL. ACAD. SCI. U.S.A. **104**, 42 2007

among these was IL-2 itself, and it was at its best in combination with one or more of the other cytokines. Negative feedback was also mediated by the intracellular STAT family of transcription factors, which assist with the differentiation of T_H1 and T_H2 cells. These in vitro observations were supported by in vivo experiments, in which treatment of mice with recombinant IL-2 measurably reduced the levels of IL-2 produced after immunization. It will be of interest to investigate whether these pathways cooperate in distinct ways to control early T cell immunity, regulatory T cells, and the formation of T cell memory. — SJS

J. Exp. Med. 10.1084/jem.20061198 (2007)

MATERIALS SCIENCE

Wiggling into Something Thinner

Nanoscale features can be fabricated in polymer thin films by room temperature forging or embossing, in which the material undergoes inelastic flow from beneath a die to create an impression. The thinness of the layer remaining below the die is limited by friction, the shear strength of the material, and the pressure created by material building up outside the die, as well as by the amount of force the die itself can tolerate before it deforms. Cross *et al.* show that applying a small amplitude shearing motion (approximately 10 nm) in the plane of

Nanoscale die used to pattern films.

the film activates surface flow. The shear motion not only allows much thinner layers to be formed but also decreases the number of defects that often limit the yield of structures with the necessary critical dimensions for a given application. Finite element simulations were used to confirm the underlying mechanism. — PDS

Nano Lett. 7, 10.1021/nl0624566 (2007)

CLIMATE SCIENCE

A Splash of Cold Water

During the last deglaciation, a large and rapid injection of glacial meltwater from the Laurentide Ice Sheet to the North Atlantic (called meltwater pulse 1a, or mwp-1a) raised sea level by ~20 m in only about two centuries. This enormous freshwater addition has variously been posited as the trigger of the Bølling warming period 14,600 years ago or as the cause of the Older Dryas cold event that terminated the Bølling 14,000 years ago; uncertainty about the age of mwp-1a has prevented resolution of these conflicting claims. Stanford *et al.* present a record of North Atlantic Deep Water (NADW) flow intensity from Erik Drift that, combined with previously published improved dating for mwp-1a, establishes a relatively minor 200-year weakening of NADW flow 14,600 years ago, coincident with mwp-1a. The data also show that no discernible sea-level rise accompanied the clear NADW slowdown during the Younger Dryas. These results demonstrate that NADW formation and climate are not controlled exclusively by the magnitude or rate of meltwater addition, because the largest meltwater pulse resulted in the relatively minor Older Dryas whereas the climatologically much more dramatic Younger Dryas was not associated with discernable rises in sea level. Thus, the location of meltwater additions may be important. — HJS

Paleoceanography **21**, PA4103 (2006)

GENETICS

Not Cheaper by the Dozen

Fitness, defined as an individual's reproductive success, is measured by the number of offspring, and parents with more offspring are generally considered fitter. However, Penn and Smith show that in married couples in preindustrial societies, the survival of both the mother and the father depended on the number of offspring the wife had and families with fewer children had more surviving grandchildren. In an analysis of 21,000 records of survival in late 19th-century Utah, survival rates of the parents and children were significantly lower in the largest families, that is, those with 12 or more children. The negative effect of bearing children on fitness was stronger in females, lasted after menopause, and was evident even in women with only 1 to 3 offspring. However, after the birth of the fourth child, the risk of death became significantly greater in fathers, too. In addition, those children with the largest number of siblings were less likely to survive to the age of 18, with the youngest siblings at greatest risk. The ability of human females to survive long after the loss of reproductive function has previously been explained by the positive effect a mother's survival has on the success of her offspring; without a mother, survivorship of the children is lowered. Nevertheless, this study demonstrates that there may be a selective pressure for females to stop reproducing before they complete child rearing. EMZ

Proc. Natl. Acad. Sci. U.S.A. **104**, 553 (2007)

CREDITS: CROSS ET AL., NANO LETT. 7, 10.1021/NL0624566 (2007)

www.sciencemag.org

Science

1200 New York Avenue, NW
Washington, DC 20005
Editorial: 202-326-6550, FAX 202-289-7562
News: 202-326-6500, FAX 202-371-9227

Bateman House, 82-88 Hills Road
Cambridge, UK CB2 1LQ
+44 (0) 1223 326500, FAX +44 (0) 1223 326501

Subscription Services For change of address, missing issues, new orders and renewals, and payment questions: 866-434-AAAS (2227) or 202-326-6417, FAX 202-842-1065. Mailing addresses: AAAS, P.O. Box 96178, Washington, DC 20090-6178 or AAAS Member Services, 1200 New York Avenue, NW, Washington, DC 20005

Institutional Site Licenses please call 202-326-6755 for any questions or information

Reprints: Author Inquiries 800-635-7181
Commercial Inquiries 803-359-4578
Corrections 202-326-6501

Permissions 202-326-7074, FAX 202-682-0816

Member Benefits Bookstore: AAAS/BarnesandNoble.com bookstore www.aaas.org/bn; Car purchase discount: Subaru VIP Program 202-326-6417; Credit Card: MBNA 800-847-7378; Car Rentals: Hertz 800-654-2200 CDP#343457, Dollar 800-800-4000 #AA1115; AAAS Travels: Betchart Expeditions 800-252-4910; Life Insurance: Seabury & Smith 800-424-9883; Other Benefits: AAAS Member Services 202-326-6417 or www.aaasmember.org.

science_editors@aaas.org	(for general editorial queries)
science_letters@aaas.org	(for queries about letters)
science_reviews@aaas.org	(for returning manuscript reviews)
science_bookrevs@aaas.org	(for book review queries)

Published by the American Association for the Advancement of Science (AAAS), *Science* serves its readers as a forum for the presentation and discussion of important issues related to the advancement of science, including the presentation of minority or conflicting points of view, rather than by publishing only material on which a consensus has been reached. Accordingly, all articles published in *Science*—including editorials, news and comment, and book reviews—are signed and reflect the individual views of the authors and not official points of view adopted by the AAAS or the institutions with which the authors are affiliated.

AAAS was founded in 1848 and incorporated in 1874. Its mission is to advance science and innovation throughout the world for the benefit of all people. The goals of the association are to: foster communication among scientists, engineers and the public; enhance international cooperation in science and its applications; promote the responsible conduct and use of science and technology; foster education in science and technology for everyone; enhance the science and technology workforce and infrastructure; increase public understanding and appreciation of science and technology; and strengthen support for the science and technology enterprise.

Information for Authors

See pages 120 and 121 of the 5 January 2007 issue or access www.sciencemag.org/feature/contribinfo/home.shtml

EDITOR-IN-CHIEF **Donald Kennedy**
EXECUTIVE EDITOR **Monica M. Bradford**
DEPUTY EDITORS **R. Brooks Hanson, Barbara R. Jasny, Katrina L. Kelner**
NEWS EDITOR **Colin Norman**

Editorial SUPERVISORY SENIOR EDITOR Phillip D. Szuromi; SENIOR EDITOR/PERSPECTIVES Lisa D. Chong; SENIOR EDITORS Gilbert J. Chin, Pamela J. Hines, Paula A. Kiberstis (Boston), Marc S. Lavine (Toronto), Beverly A. Purnell, Bruce Ray, Guy Riddihough, H. Jesse Smith, Valda Vinson, David Voss; ASSOCIATE EDITORS Jake S. Yeston, Laura M. Zahn; ONLINE EDITOR Stewart Wills; ASSOCIATE ONLINE EDITOR Tara S. Marathe; BOOK REVIEW EDITOR Sherman J. Suter; ASSOCIATE LETTERS EDITOR Etta Kavanagh; INFORMATION SPECIALIST Janet Kegg; EDITORIAL MANAGER Cara Tate; SENIOR COPY EDITORS Jeffrey E. Cook, Cynthia Howe, Harry Jach, Barbara P. Ordway, Jennifer Sills, Trista Wagoner; COPY EDITORS Lauren Kmec, Peter Mooreside; EDITORIAL COORDINATORS Carolyn Kyle, Beverly Shields; PUBLICATION ASSISTANTS Ramatoulaye Diop, Chris Filiatreau, Joi S. Granger, Jeffrey Hearn, Lisa Johnson, Scott Miller, Jerry Richardson, Brian White, Anita Wynn; EDITORIAL ASSISTANTS Maris M. Bish, Emily Guise, Patricia M. Moore; EXECUTIVE ASSISTANT Sylvia S. Kihara; ADMINISTRATIVE SUPPORT Maryrose Police

News SENIOR CORRESPONDENT Jean Marx; DEPUTY NEWS EDITORS Robert Coontz, Eliot Marshall, Jeffrey Mervis, Leslie Roberts, John Travis; CONTRIBUTING EDITORS Elizabeth Culotta, Polly Shulman; NEWS WRITERS Yudhijit Bhattacharjee, Adrian Cho, Jennifer Couzin, David Grimm, Constance Holden, Jocelyn Kaiser, Richard A. Kerr, Eli Kintisch, Andrew Lawler (New England), Greg Miller, Elizabeth Pennisi, Robert F. Service (Pacific NW), Erik Stokstad; John Simpson (intern); CONTRIBUTING CORRESPONDENTS Barry A. Cipra, Jon Cohen (San Diego, CA), Daniel Ferber, Ann Gibbons, Robert Irion, Mitch Leslie, Charles C. Mann, Evelyn Strauss, Gary Taubes, Ingrid Wickelgren; COPY EDITORS Linda B. Felaco, Rachel Curran, Sean Richardson; ADMINISTRATIVE SUPPORT Scherraine Mack, Fannie Groom; BUREAUS: Berkeley, CA: 510-652-0302, FAX 510-652-1867, New England: 207-549-7755, San Diego, CA: 760-942-3252, FAX 760-942-4979, Pacific Northwest: 503-963-1940

Production DIRECTOR James Landry; SENIOR MANAGER Wendy K. Shank; ASSISTANT MANAGER Rebecca Doshi; SENIOR SPECIALISTS Jay Covert, Chris Redwood; SPECIALIST Steve Forrester; PREFLIGHT DIRECTOR David M. Tompkins; MANAGER Marcus Spiegler; SPECIALIST Jessie Mudjitaba

Art DIRECTOR Kelly Buckheit Krause; ASSOCIATE ART DIRECTOR Aaron Morales; ILLUSTRATORS Chris Bickel, Katharine Sutliff; SENIOR ART ASSOCIATES Holly Bishop, Laura Creveling, Preston Huey; ASSOCIATE Nayomi Kevitiyagala; PHOTO EDITOR Leslie Blizard

Science International

Europe (science@science-int.co.uk) EDITORIAL: INTERNATIONAL MANAGING EDITOR Andrew M. Sugden; SENIOR EDITOR/PERSPECTIVES Julia Fahrenkamp-Uppenbrink; SENIOR EDITORS Caroline Ash (Geneva: +41 (0) 222 346 3106), Stella M. Hurtley, Ian S. Osborne, Stephen J. Simpson, Peter Stern; ASSOCIATE EDITOR Joanne Baker; EDITORIAL SUPPORT Alice Whaley, Deborah Dennison; ADMINISTRATIVE SUPPORT Janet Clements, Phil Marlow, N. White; NEWS: INTERNATIONAL NEWS EDITOR Daniel Clery; CORRESPONDENT Gretchen Vogel (Berlin: +49 (0) 30 2809 3902, FAX +49 (0) 30 2809 8365); CONTRIBUTING CORRESPONDENTS Michael Balter (Paris), Martin Enserink (Amsterdam and Paris), John Bohannon (Vienna)

Asia Japan Office: Asca Corporation, Eiko Ishioka, Fusako Tamura, 1-8-13, Hirano-cho, Chuo-ku, Osaka-shi, Osaka, 541-0046 Japan; +81 (0) 6 6202 6272, FAX +81 (0) 6 6202 6271; asca@os.gulf.or.jp; ASIA NEWS EDITOR Richard Stone +66 2 662 5818 (rstone@aaas.org); JAPAN NEWS BUREAU Dennis Normile (contributing correspondent, +81 (0) 3 3391 0630, FAX 81 (0) 3 5936 3531; dnormile@gol.com); CHINA REPRESENTATIVE Hao Xin, + 86 (0) 10 6307 4439 or 6307 3676, FAX +86 (0) 10 6307 4358; haoxin@earthlink.net; SOUTH ASIA Pallava Bagla (contributing correspondent +91 (0) 11 2271 2896; pbagla@vsnl.com)

Africa Robert Koenig (contributing correspondent, rob.koenig@gmail.com)

EXECUTIVE PUBLISHER **Alan I. Leshner**
PUBLISHER **Beth Rosner**

Fulfillment & Membership Services (membership@aaas.org) DIRECTOR Marlene Zendell; MANAGER Waylon Butler; SYSTEMS SPECIALIST Andrew Vargo; CUSTOMER SERVICE SUPERVISOR Pat Butler; SPECIALISTS Laurie Baker, Tamara Alfson, Karena Smith, Vicki Linton, Latoya Casteel; CIRCULATION ASSOCIATE Christopher Refice; DATA ENTRY SUPERVISOR Cynthia Johnson; SPECIALISTS Tomeka Diggs, Tarrika Hill, Erin Layne

Business Operations and Administration DIRECTOR Deborah Rivera-Wienhold; BUSINESS MANAGER Randy Yi; SENIOR BUSINESS ANALYST Lisa Donovan; BUSINESS ANALYST Jessica Tierney; FINANCIAL ANALYST Michael LoBue, Farida Yeasmin; RIGHTS AND PERMISSIONS: ADMINISTRATOR Emilie David; ASSOCIATE Elizabeth Sandler; MARKETING: DIRECTOR John Meyers; MARKETING MANAGERS Darryl Walter, Allison Pritchard; MARKETING ASSOCIATES Julianne Wielga, Mary Ellen Crowley, Catherine Featherston, Alison Chandler, Lauren Lamoureux; INTERNATIONAL MARKETING MANAGER Wendy Sturley; MARKETING/MEMBER SERVICES EXECUTIVE: Linda Rusk; JAPAN SALES Jason Hannaford; SITE LICENSE SALES: DIRECTOR Tom Ryan; SALES AND CUSTOMER SERVICE Mehan Dossani, Kiki Forsythe, Catherine Holland, Wendy Wise; ELECTRONIC MEDIA: MANAGER Lizabeth Harman; ASSISTANT MANAGER Lisa Stanford; PRODUCTION ASSOCIATES Nichele Johnston, Kimberly Oster

Advertising DIRECTOR WORLDWIDE AD SALES Bill Moran

Product (science_advertising@aaas.org); MIDWEST Rick Bongiovanni: 330-405-7080, FAX 330-405-7081 • WEST COAST/W. CANADA Teola Young: 650-964-2266 EAST COAST/E. CANADA Christopher Breslin: 443-512-0330, FAX 443-512-0331 • UK/EUROPE/ASIA Julie Skeet: +44 (0) 1223-326-524, FAX +44 (0) 1223-325-532 JAPAN Mashy Yoshikawa: +81 (0) 33235 5961, FAX +81 (0) 33235 5852 TRAFFIC MANAGER Carol Maddox; SALES COORDINATOR Deiandra Simms

Commercial Editor Sean Sanders: 202-326-6430

Classified (advertise@sciencecareers.org); U.S.: RECRUITMENT SALES MANAGER Ian King: 202-326-6528, FAX 202-289-6742; U.S./INDUSTRY: Darrell Bryant: 202-326-6533; MIDWEST/CANADA: Daryl Anderson: 202-326-6543; NORTHEAST: Allison Millar: 202-326-6572; SOUTHEAST: Fernando Junco: 202-326-6740; WEST: Katie Putney: 202-326-6577; SALES COORDINATORS Erika Bryant, Rohan Edmonson, Shirley Young; INTERNATIONAL: SALES MANAGER Tracy Holmes: +44 (0) 1223 326525, FAX +44 (0) 1223 326532; SALES Christina Harrison, Svitlana Barnes; SALES ASSISTANT Kellie Jones; JAPAN: Jason Hannaford: +81 (0) 52 757 5360, FAX +81 (0) 52 757 5361; ADVERTISING PRODUCTION OPERATIONS MANAGER Deborah Tompkins; ASSOCIATES Christine Hall; Amy Hardcastle; PUBLICATIONS ASSISTANTS Robert Buck; Mary Lagnaoui

AAAS Board of Directors RETIRING PRESIDENT, CHAIR Gilbert S. Omenn; PRESIDENT John P. Holdren; PRESIDENT-ELECT David Baltimore; TREASURER David E. Shaw; CHIEF EXECUTIVE OFFICER Alan I. Leshner; BOARD Rosina M. Bierbaum; John E. Dowling; Lynn W. Enquist; Susan M. Fitzpatrick; Alice Gast; Thomas Pollard; Peter J. Stang; Kathryn D. Sullivan

ADVANCING SCIENCE, SERVING SOCIETY

WALLACE REVEALED

After spending years collecting specimens in exotic locales, a young British naturalist dreams up an explanation for how one species transforms into another. The description fits Charles Darwin, but it also matches Alfred Russel Wallace (1823–1913), the co-discoverer of natural selection and one of the 19th century's leading biologists. Wallace was also one of the founders of biogeography, the study of organisms' distribution.

NET WATCH

A new online exhibit from the Natural History Museum in London documents Wallace's work and life with annotated selections from his writings and other memorabilia, such as a plate (above) of a ring-tailed lemur from a 1900 collection of his articles. You can browse some of his travel dispatches, including the letter in which he describes the destruction of all his South American specimens in a shipboard fire. Other offerings indicate that Wallace didn't resent being overshadowed by the older scientist. For example, Wallace wrote a friend that he was "thankful that it has not been left to me to give the theory to the public." >>

www.nhm.ac.uk/naturedotcom/collections-at-the-museum/wallace-collection/themes.jsp

CREDITS: (TOP TO BOTTOM) NATURAL HISTORY MUSEUM; NATIONAL LAND IMAGE INFORMATION (COLOR AERIAL PHOTO); MINISTRY OF LAND, INFRASTRUCTURE, AND TRANSPORT OF JAPAN

Snow Over Ireland

Scientists have found cocaine on a sampling of Dublin bank notes, adding to concern that Ireland is becoming the cocaine capital of Europe.

A team led by Brett Paull, an environmental chemist at Dublin City University, analyzed 45 bills collected from around the city, using chromatography and mass spectrometry, and found coke residues on all of them. Three bills also had traces of heroin.

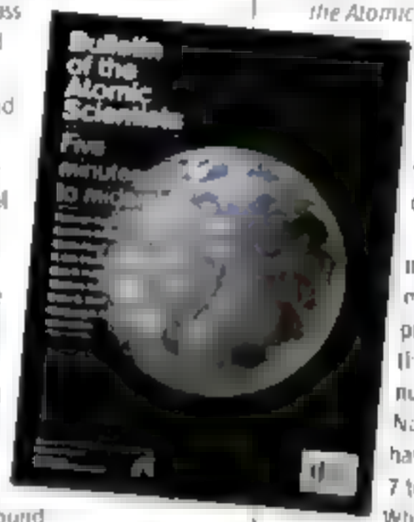

"The chemicals produce a nice, clear signal down to picogram concentrations," says Fritz Sörgel, a chemist at the Institute for Biomedical and Pharmaceutical Research in Nuremberg, Germany. This isn't the first study of its kind. A 2001 U.S. study of $1 bills, for example, found cocaine, heroin, methamphetamine, and phencyclidine. But it is the latest in a recent burst of reports by European researchers that suggests increasing drug abuse on the continent. "Spain is thought to be the number one country for cocaine abuse," says Sörgel, "but Ireland appears to be rising to the top."

Paull says that in 5% of the samples, particularly €20 and €50 notes, the concentration was about 100 times higher than the rest. "That suggests that those bills were rolled up and used for snorting," he says. "The rest may have been contaminated during processing in banks."

Apocalyptic Adjustment

The famous Doomsday Clock of the *Bulletin of the Atomic Scientists* (*BAS*) has begun to factor another global concern into its timing: Instead of reflecting only the threat of nuclear annihilation, its end of the world calculus now includes climate change.

Flooding, destructive storms, increased drought, and polar ice melt are causing loss of life and property," *BAS* says of the risks that sparked the move. That and nuclear proliferation, including North Korea's recent bomb test, have pushed the minute hand from 7 to 5 minutes before midnight. What do the stalwarts of weapons control think of this fuzzier doom? "I understand their concern about broadening the appeal," says Ivan Oelrich of the Federation of American Scientists in Washington, D.C., but "I hope it does not distract attention" from the nuclear-weapons threat.

It's the 14th time the clock has shifted since its 1947 debut. The safest we've been was in 1991, when weapons reductions moved the clock back to 17 minutes.

Tombs Open Up >>

Japan's archaeologists are about to get long-sought peeks into the tombs of the country's early emperors.

In July 2005, the Japanese Archaeological Association led 15 academic societies in asking Japan's Imperial Household Agency for permission to investigate 11 ancient imperial tombs that have gotten only cursory, if any, inspection by scientists. Included on the list is the tomb of Emperor Nintoku, who ruled in the 4th or 5th century and is said to rest in one of the world's largest burial complexes, near present-day Osaka. Last month, the agency decreed that one representative from each society will be allowed to enter some of the tombs.

In the past, critics have accused the Imperial Household Agency, which oversees some 900 burial sites, of blocking delayed investigations on the grounds that scientists might turn up evidence that the ancestors of today's royal family really came from Korea. Japanese legend traces the line age back through 125 emperors to the Shinto sun goddess Amaterasu Omikami. Myths aside, there is academic debate over which older tombs house which imperial bones.

Kop Takahashi, a Toyama University archaeologist on the association's board, says researchers won't be allowed to touch anything, so they are likely to concentrate on mapping tomb layouts and details of interiors. "Until now, we couldn't get in at all, so this is a step in the right direction," says Takahashi.

For news and research with impact, turn to *Science*

There's only one source for news and research with the greatest impact – *Science*. With over 700,000 weekly print readers, and millions more online, *Science* ranks as one of the most highly read multidisciplinary journals in the world. And for impact, *Science* can't be beat. According to the recently released Thomson ISI Journal Citation Report 2005, *Science* ranked as the No. 1 most cited multidisciplinary journal with a citation factor of 31. Founded in 1880 by inventor Thomas Edison, and published by the nonprofit AAAS, *Science*'s reputation as the leading source for news, research, and leading edge presentation of content continues to grow. Looking for news and research that will impact the world tomorrow? Then look in *Science*.

www.sciencemag.org

To join AAAS and receive your own personal copy of *Science* every week go to www.aaas.org/join

Science
AAAS

Movers

UPWARD GAZE. The new head of the European Southern Observatory (ESO) hopes to make the 45-year-old organization even more of a player on the international astronomical scene.

Dutch astronomer Tim de Zeeuw, now scientific director of Leiden Observatory in the Netherlands, says his biggest challenge will be to persuade ESO's 13 member states to build the 42-meter European Extremely Large Telescope. The observatory is also a partner with the United States in the Atacama Large Millimeter Array being built in Chile.

Matt Mountain, director of the Space Telescope Science Institute in Baltimore, Maryland, says de Zeeuw is a "fantastic choice" for ESO. De Zeeuw, 50, succeeds French astronomer Catherine Cesarsky, who is leaving to become president of the International Astronomical Union (*Science*, 8 September 2006, p. 1385).

AWARDS

WOLF PRIZES. George Feher has always had a knack for cracking tough problems. Growing up in Czechoslovakia in the 1930s, he taught himself radio electronics. In 1941, he and eight Jewish friends escaped Nazi persecution and fled to British-ruled Palestine. After a stint in British detention, Feher worked out a way to decode radio transmissions between the British High Commissioner and 10 Downing St. that later proved pivotal in the Israeli war for independence. Feher moved to the United States in 1946 and eventually wound up at the University of California, San Diego, where he turned his sleuthing to uncovering the workings of the reaction center, the molecular machine that drives photosynthesis.

CREDITS: (TOP TO BOTTOM) ESO; © ISAACSON/JACKSON; (LEFT TO RIGHT) KOSTEL, RUTGERS UNIVERSITY

Last week, Feher's detective work earned him a share of the 2007 Wolf Prize in Chemistry. Feher (above) shares the $100 000 prize with Ada Yonath, a chemist and structural biologist at the Weizmann Institute of Science in Rehovot, Israel, who pioneered ways to use x-rays to map the three-dimensional structure of the ribosome. Other Wolf Prizes this year go to Stephen Smale of the University of California, Berkeley, and Harry Furstenberg of the Hebrew University of Jerusalem (mathematics), and Albert Fert of CNRS in Orsay, France, and Peter Grunberg of the Julich Research Center in Germany (physics).

IN THE COURTS

DEVASTATED. A mathematics professor who was fired from a Korean university 11 years ago shot an arrow at a Seoul high court judge last week after losing his appeal of the dismissal. The judge suffered only minor injury, and the researcher has been charged with attempted murder.

Myung Ho Kim lost his job at Sungkyunkwan University in 1996 after telling institutional authorities about an error in a math problem on the university's entrance exam. He claimed retaliation, but administrators said he was sacked because he had been rude to students and contemptuous toward the university (*Science*, 5 September 1997, p. 1441).

On 15 January, Seoul high court justice Park Hong Woo upheld the university's decision. "Although we recognize Kim as a man of decent scholarship who has a clean conscience, we did not find him as a qualified member of the academic membership," the judge said.

Kim then whipped out a crossbow and fired a stone arrow at the judge, wounding his midriff. "When my appeal was dismissed, I felt that my life was over," Kim told reporters, denying that he had tried to kill the judge. The Korean Professors Union issued a statement after the incident decrying the ruling as biased. Kim, who's been unemployed for the past several years, could now even face a death sentence if the attempted murder charge is proved, officials say.

In Brief >>

CRAFOORD PRIZES. Earth scientist Wallace Broecker has won the 2006 Crafoord Prize from the Royal Swedish Academy of Sciences. Broecker (left), a researcher at Columbia University, receives the $500,000 award for his pioneering studies of the link between ocean chemistry and carbon dioxide levels in the atmosphere. The academy has also announced the winner of the 2007 prize: anthropologist Robert Trivers (above, right) of Rutgers University in New Brunswick, New Jersey, who receives the honor for his contributions to the understanding of cooperation and conflict in the animal world.

Got a tip for this page? E-mail people@aaas.org

UC punts on tobacco funds 447

Harvard's multidisciplinary move 449

Pact men. GE's Jeffrey Immelt (*left*) and WRI's Jonathan Lash helped organize an industry-environmentalist partnership on climate change

CLIMATE CHANGE

New Congress May Be Warming Up to Plans for Capping Emissions

The first winter storm of the season, long overdue, blew through Washington, D.C., last weekend. But proponents of federal legislation to limit carbon emissions continued to bask in the glow of increasing support for their cause.

The new Democratic majority in both houses of Congress has made it more likely that a bill capping carbon emissions will land on President George W. Bush's desk before he leaves office in January 2009. Of course, the final form of any legislation will be shaped by the demands of various powerful industries, and it could well encounter a presidential veto. But few question the new-found political momentum behind some type of federal action. "The tide is turning," says Jonathan Lash of the nonprofit World Resources Institute (WRI) in Washington, D.C., which has joined a new partnership between environmentalists and industry announced this week.

The president's State of the Union address, delivered after *Science* went to press, was expected to focus on ethanol as part of a nonmandatory climate strategy. But most observers expect Congress to be more aggressive in tackling greenhouse gas emissions. Two senators hoping to become president, Arizona Republican John McCain and Illinois Democrat Barack Obama, have cosponsored a bill that would slash emissions steeply by 2050. And on 22 January, the newly formed United States Climate Action Partnership, a group that includes 10 major U.S. companies such as General Electric and BP America, as well as WRI and the Natural Resources Defense Council (NRDC), advocated for a "mandatory [and] flexible ... emissions trading system that has impressed energy analysts.

"You couldn't have imagined 2 years ago a group of such companies getting behind such targets," says Jason Grumet of the National Commission on Energy Policy in Washington, D.C., a similar consensus-building group that in 2004 recommended less aggressive goals. NRDC's David Doniger says the conventional wisdom at the time was that the group's principles went as "far as the political center of gravity would go." In 2005, for example, then-energy committee chair Senator Pete Domenici (R-NM) urged Congress to "proactively address climate change." But the best that the Republican-led body could do was make a vague, nonbinding statement calling for "mandatory steps" to cap greenhouse gas emissions. House Republicans stuck to voluntary approaches while promoting federal research.

The statement by the new climate partnership is easily the most aggressive yet from industry. It aims to halt growth of U.S. emissions within a decade and to lower current levels by 60% to 80% by 2050. The group wants to control the cost of emission permits, perhaps with a price limit, but not in a way that would undermine the system, and to bar old-fashioned coal plants from getting free credits. Coalition members say they want to avoid piecemeal state emissions caps, such as a tough new California system, and more draconian measures down the road.

Another set of once-odd bedfellows also lobbied Congress last week. "We dare to imagine a world in which science and religion cooperate" to tackle climate change and other problems, said Reverend Richard Cizik of the National Association of Evangelicals (NAE), one of several evangelical Christian leaders who have joined with Harvard entomologist E. O. Wilson and Missouri Botanical Garden botanist Peter Raven and other researchers for "responsible care for creation." NAE has agreed to distribute a "pastor's tool kit" with information on the warming atmosphere and other environmental problems to counter what Cizik calls "junk science" from climate skeptics.

Such coalitions seem likely to strengthen the hand of lawmakers such as Senator Barbara Boxer (D-CA), head of the Environment and Public Works committee, who wants to pass a carbon cap "as soon as possible." House Speaker Nancy Pelosi (D-CA), meanwhile, has created a special committee to explore and publicize climate change legislation. House energy committee chair and auto industry supporter John Dingell (D-MI) opposes the new committee, which won't have legislative authority. But its creation, says Grumet, demonstrates that Pelosi "is not going to defer to the committee structure" in moving her agenda.

Yet aggressive action won't be easy. Some of the 49 Republicans in the 100-seat Senate will be needed to override a veto by the White House of any emissions legislation, notes Senate Energy committee staff director Robert Simon. McCain and Obama's bill is a positive step, says another aide, but is unlikely to win the support of a majority of senators.

-ELI KINTISCH

CREDIT: REGGIE LIPSCOMB/NPS PHOTOGRAPHY

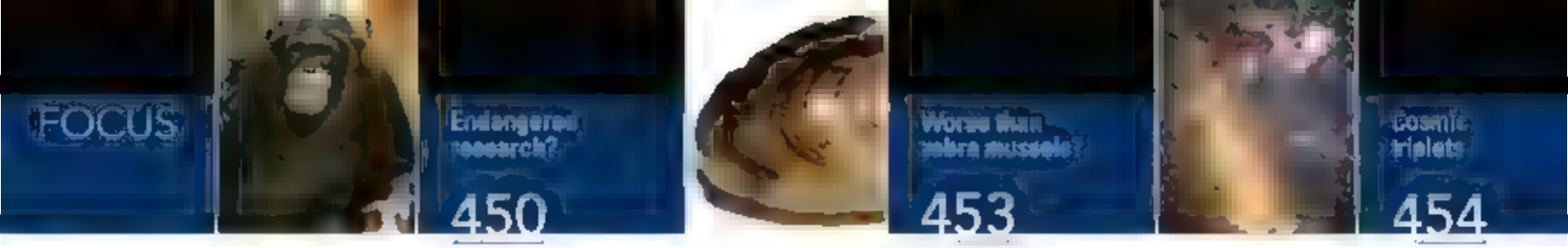

SPACE SCIENCE

LUNAR-A Moon Mission Gets an 'F'

TOKYO—A mission to explore the moon's origin and evolution has crashed before launch. Earlier this month, Japan's space agency terminated its LUNAR-A probe because its ambitious technology was still not ready to go even after the launch had been delayed for 12 years.

The cancellation of the ill-starred mission has sent tremors through the global space science community. "The feeling is one of uniform regret that this mission is not flying," says Clive Neal, a geologist at the University of Notre Dame in South Bend, Indiana. Despite the setback, Japan's space scientists say they remain committed to pursuing technically challenging missions.

Planned by the Institute of Space and Astronautical Science (ISAS) in Sagamihara, near Tokyo, LUNAR-A called for an orbiting spacecraft to drop two torpedo-shaped probes onto the moon's surface—one on the near side and one on the far side. These "penetrators" would lodge 2 meters below the surface, activating seismometers to detect faint moonquakes and other sensors to measure heat flow, then relay the data to Earth. Scientists had hoped to deduce details of the largely unknown lunar interior, such as whether the moon has an iron core. A better picture of lunar anatomy would constrain models of how the moon formed.

Mission planning began with high hopes in the early 1990s. While ISAS planetary scientists sketched out key unresolved questions about the moon's interior, colleagues on the engineering side huddled over how to get inside the moon. They opted to design a probe to drop from orbit and embed instruments firmly and intact in the lunar soil, something that has never been tried before. They thought this would be more practical than developing a rover to traverse the moon's expanses, says Manabu Kato, an ISAS planetary scientist. And burying the instruments would shield them from the extreme day-night temperature fluctuations that fried instruments left on the surface by previous missions.

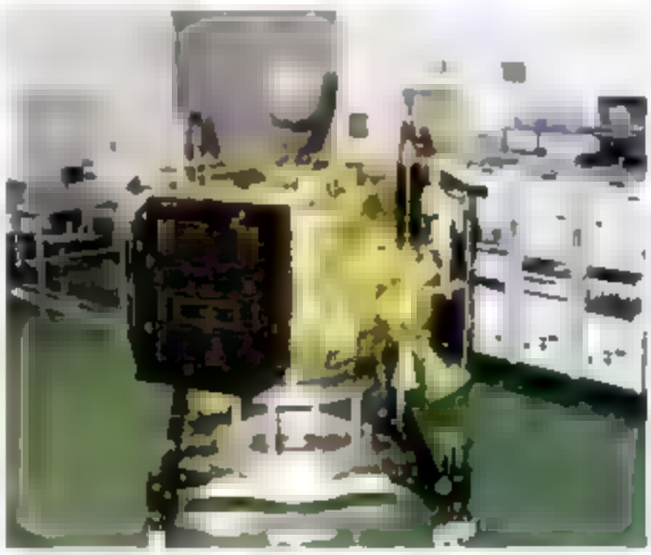

Sidelined. The LUNAR-A orbiter has been ready for years, but problems with the payload led to its cancellation.

By 1995, the planned launch date, the orbiter was ready to go. The penetrators were not. They're still not, even after 12 additional years of development and escalating costs. The original price tag for the satellite alone was $106 million, and $132 million has been spent so far.

What went wrong? Kato says the team vastly underestimated the challenges of girding instruments and electronics to survive an impact imparting a force of up to 10,000 times that of gravity. "Modeling had indicated that just some hardening of components would be sufficient," Kato says. But testing proved otherwise.

The first snag was finding a proper test site. Only after the first launch date passed did engineers realize that ISAS lacked suitable equipment and facilities. In 1997, with the project already 2 years behind schedule, they finally found an adequate testing ground: Sandia National Laboratories in Albuquerque, New Mexico. There a device akin to a giant upside-down ▶

India Inches Closer to Crewed Space Flight

THIRUVANANTHAPURAM, KERALA—India took another small step this week toward a place at the top table of space-faring nations. The Indian Space Research Organization (ISRO) launched a crewless spacecraft into orbit on 10 January, and on 22 January, controllers guided it back to Earth for a splashdown in the Bay of Bengal, 140 kilometers from its launch site. The feat of launching and retrieving a probe has to date only been achieved by Russia, the United States, and China, and is an essential step toward sending astronauts into orbit. "Both the launch and splashdown of the space capsule were completed with textbook precision," says ISRO spokesperson S. Krishnamurthy.

The Space Capsule Recovery Experiment is part of an effort to eventually launch Indian nationals into space. Toward that goal, the 5000 researchers here at the Vikram Sarabhai Space Center hope to launch another experimental capsule soon. In 2008, the plan calls for the launch of a remote-sensing mission to the moon called Chandrayaan-1. The first Indian in orbit is planned for 2014, with astronauts on the moon by 2020. ISRO is seeking $250 million in start-up funds to loft the first astronaut.

One of the key technologies on test during the recovery experiment was thermal protection to shield potential astronauts from the intense heat caused by friction during reentry. A team of 40 researchers here produced the lightweight heat-resistant materials made from pure silica that coated the outside of the 550-kilogram capsule. "The thermal protection system was one of the important experiments being carried out in the space recovery module. This is a precursor for all forthcoming reusable launch vehicles—and in the long run, to the manned mission too," says space center director B. N. Suresh.

The mission also carried two materials science experiments in which crystals were grown under near zero gravity conditions. Researchers are now studying the capsule to see whether all the experiments went according to plan.

—PALLAVA BAGLA

CREDIT: COURTESY OF JAXA

cannon uses explosives to fire test penetrators into the sandy earth. But due to schedule constraints, ISAS could use the Sandia facilities only once every 10 months, resulting in an excruciatingly slow process of trial and error. At last, after the instruments were hardened sufficiently, ISAS engineers determined that the electrical wiring was too frail. Once that was fixed, they found that they had to develop a circuit to reset the CPU after impact. The launch date slipped again and again.

During the most recent round of testing in June 2006, the scientific instruments, circuits, and software all passed muster, Kato says. But further work is necessary to make the communications systems more robust, he says. Another round of testing is scheduled for this summer.

That's too late to save LUNAR-A. After a series of internal reviews, ISAS's parent organization, the Japan Aerospace Exploration Agency (JAXA), on 15 January scrapped the mission. A JAXA spokesperson says the decision was based on the orbiter's deterioration in storage and the fact that the penetrators are not ready for prime time.

Not all hope is lost. Takashi Nakajima, current LUNAR-A manager, says that the penetrator project is not being abandoned. ISAS will complete development work and then try to get the penetrators added on another moon mission. "Researchers will still request this kind of investigation," says Hiroshi Mizutani, a space scientist who headed the mission until his retirement 2 years ago.

Planetary scientists outside Japan agree. "The community would very much like to see a geophysical network on the moon to study internal structure and heat flow, but two penetrators do not make a network," says Andrew Cheng, a planetary scientist at Johns Hopkins University in Baltimore, Maryland. Kato says ISAS had hoped LUNAR-A would gather enough data to determine whether the moon has an iron core, proving that the penetrators work. Subsequent missions could have then expanded their use on the moon and, perhaps, Mars.

But he vows that ISAS will remain at the forefront of space engineering and space science. "If you don't develop new technologies, you won't make new scientific discoveries," Kato says.

ISAS's next marriage of engineering and science is its $300 million Selenological and Engineering Explorer (SELENE). Set for launch in late March, SELENE comprises an orbiter and a pair of smaller satellites that will aim instruments at the moon to collect the most detailed data yet on its topography, the elemental makeup of its surface, its magnetism, and its gravitational field. "We're confident," says Kato. "We've tested it, and we're ready to go." If so, that would take some of the sting out of the humbling demise of LUNAR-A.

–DENNIS NORMILE

RESEARCH MANAGEMENT

Report Backs NSF Prize to Spur Innovation

The National Science Foundation (NSF) should test the waters before plunging into a costly program to award prizes to encourage innovation. That's the verdict of an expert panel of the National Academies' National Research Council, which has cautiously endorsed an idea Congress had ordered NSF to consider. Ironically, legislators may have lost interest.

In 2005, Representative Frank Wolf (R-VA), then chair of the spending panel that sets NSF's budget, asked the agency to think about offering megaprizes for solutions to important scientific challenges with societal implications. At one hearing, for example, Wolf speculated about how a $1 billion prize could yield an elegant technological solution to the nation's dependence on foreign oil. Last summer, NSF officials turned for guidance to the National Academies, which this week issued a 44-page report urging NSF to adopt "an experimental approach" by piloting a handful of small prizes before considering spending big bucks.

Prizewinner? The self-assembly of nano-scale materials might be the sort of technology ripe for an NSF contest.

CREDIT: CHAD MIRKIN/NORTHWESTERN UNIVERSITY

Such prizes are useful, says panelist and former NSF Director Erich Bloch, because they bring in new people who don't normally participate in government programs and because it allows you to tackle controversial ideas. But I wouldn't spend $1 billion on it.

Panel chair Mark Myers, a retired research executive at Xerox, believes that NSF needs to develop a methodology" on how to run such a program and then evaluate each step of the way. The panel did not recommend any topics for NSF to tackle, although for illustrative purposes it mentioned areas such as nano self-assembly, green chemistry, low-carbon energy technologies, and teaching software. The report suggests that NSF should start with a handful of prizes ranging from $200,000 to $2 million and raise the payout to as much as $30 million if the concept proves successful. Myers says Congress should increase NSF's budget to make room for the program so that its cost doesn't undermine ongoing activities.

The report recommends starting the prizes this year, but with NSF facing a budget freeze (*Science*, 5 January, p. 24) that's not likely to happen. "It's a solid report, and piloting is always the right way to go," says senior NSF administrator Norman Pitts, who has tracked the issue. "But it's an expensive proposition, and I don't see how we could afford it this year."

An even bigger obstacle, however, may be the recent changes on Capitol Hill. Wolf is no longer on the spending subpanel, and House Republicans are in the minority. A Democratic aide on the House Committee on Science and Technology, which oversees NSF, says that prizes probably make more sense at a mission-oriented agency, such as NASA or the Defense Department. And the aide questions the idea that a prize will attract new players into the research game. "I have a hard time believing that there are many people doing basic research who aren't already familiar with NSF and its programs."

–JEFFREY MERVIS

RESEARCH FUNDING

UC Balks at Campus-Wide Ban on Tobacco Money for Research

Concerned about academic freedom, the University of California (UC) has delayed voting on a plan to impose a blanket ban on research funding from tobacco companies. If approved, the ban would make UC the only U.S. university to forbid tobacco dollars campus-wide. Faculty members anguished over the issue for 4 years before calling on UC's governing body—the regents—to take a stand. Instead, the regents punted it back to the faculty last week.

Faculty fission. Stanton Glantz (*left*) would like to see a blanket ban on tobacco funding at UC, but James Enstrom (*right*) says such a ban would violate academic freedom.

"It's a very good decision," says James Enstrom, an epidemiologist at UC Los Angeles who uses Philip Morris's money. "Academic freedom makes this a great university, and the faculty need time to consider this issue more thoroughly." But Stanton Glantz, a bioengineer and antitobacco crusader at UC San Francisco, turns the argument around: "The tobacco industry funds research to confuse the public," he says. "This manipulation of the scientific process subverts academic freedom and is another example of the fundamental erosion of the university."

Momentum for a UC-wide ban on tobacco funding has been building. Since 2003, seven units within the university system, including UC Berkeley's School of Public Health and the UC San Diego Cancer Center, have shut their doors to tobacco money. But UC's faculty-composed Academic Senate voided these bans in May 2005, declaring that only the regents had the authority to decline funding—and that they had to do it for the entire system or not at all.

Currently, UC researchers can take money from any source, as long as terms of the grant do not violate university policy (for example, by excluding foreigners). As of last year, there were 19 active grants at UC supported by the tobacco industry, totaling $15.8 million. (UC's total grants and contracts added up to $4 billion that year.)

Before the regents would consider a tobacco-funding ban, however, they asked the senate for input. That's when things got complicated. "The tobacco issue put our principles in conflict," says senate member and UC Santa Cruz social psychologist Faye Crosby. "Most of us agreed that academic freedom trumps all other principles. But then the senators reviewed documented evidence that the tobacco industry had manipulated researchers into publishing biased results—by tweaking manuscripts or threatening to cut off funding, Glantz charges. "We realized academic freedom can be illusory," says Crosby. For many, allowing the university to accept tobacco money was allowing a threat to academic freedom.

Enstrom disagrees. "I do not feel that any tobacco funding arrangements I've had have manipulated my academic freedom," he says. In 2003, Enstrom published a study in the *British Medical Journal* that found no relation between secondhand smoke and lung cancer deaths. The project was partially funded by the Center for Indoor Air Research, which itself is funded by tobacco companies. Enstrom says the study was methodologically sound and that it added an important minority opinion to the smoking debate. "Thankfully, UC doesn't allow only certain points of view to be funded," he says. "My entire career has been based on the academic freedom I've had."

The senate's recommendation to the regents reflected the divisiveness of the issue. On one hand, the faculty asserted that "grave issues of academic freedom would be raised" if the regents banned funding based solely on its source. On the other, they declared that academic freedom could be suppressed, and that the tobacco industry had a history of such suppression.

The seemingly contradictory wording proved too much for the regents. At an ▶

CREDITS (LEFT TO RIGHT): BY S. GLANTZ/UCSF; PROVIDED BY J. E. ENSTROM

Kansas Standards Evolve Again

Eighteen months after its state education board adopted science standards promoting the teaching of intelligent design (ID), Kansas is set to toss them out. Next month, a newly aligned board expects to adopt standards that emphasize evolution.

The change follows elections that flipped the board's 6–4 conservative majority to a 6–4 margin for moderates (*Science* 11 August 2006, p. 743). As a result, the board replaced the former chair, ID proponent Steve Abrams, with Bill Wagnon, who has fought against the ID-tainted standards since their adoption in August 2005.

The pending standards have been written by a committee appointed by the board that delivered a product deemed unacceptable by conservatives. "We'll be glad to bring back standards that do not contain supernatural explanations and are in line with national and international norms," says Sue Gamble, a moderate board member. "These standards will help teachers to strengthen the teaching of evolutionary content."

–YUDHIJIT BHATTACHARJEE

No Roving for Moon Rovers

Budget troubles at NASA will likely nix plans to send a series of sophisticated robotic rovers to the moon after the agency sends an orbiter there next year. NASA officials blame a tight exploration budget and the rising cost of the rovers, which were meant to find possible human landing sites and gather scientific data. Industry and agency sources say that up to half of the roughly $800 million set aside over the next 3 years for rover development at Marshall Space Flight Center in Huntsville, Alabama, could go to Goddard Space Flight Center in Greenbelt, Maryland, and Ames Research Center in Mountain View, California, to design smaller and cheaper spacecraft that could do similar jobs.

The decision to cancel the original set of rovers comes just a few months after NASA chief Michael Griffin moved the program from Ames to Marshall. That decision, sources say, was made to please Congress's Republican dominated Alabama delegation, but the recent election, which put Democrats in the driver's seat, took pressure off the agency. The remainder of the would-be rover funding would cover budget shortfalls in NASA's effort to develop a launcher to replace the space shuttle, slated for retirement in 2010. The proposed cuts are part of the agency's 2009 budget request to be announced on 5 February.

–ANDREW LAWLER

18 January meeting at U.C. San Francisco the governing body appeared as divided as the senate. "I believe a yes vote [on this ban] would establish a very dangerous precedent which threatens our culture of academic freedom," said Regent Jefferson Coombs at the meeting. "It would convey a signal that we do not trust our world-class faculty." Regent Richard Blum countered that "none of us take academic freedom lightly. ... but [accepting tobacco money] hurts academic freedom, not helps it."

In the end, the regents voted overwhelmingly to send the issue back to the faculty. An amendment charges the senate to clarify whether a blanket tobacco funding ban truly threatens academic freedom before the regents meet again in May.

Michael Cummings, an authority on smoking issues who runs the Tobacco Control Program at the Roswell Park Cancer Institute in Buffalo, New York, says he's disappointed with the delay. "It's good to debate academic freedom," he says, but "if you can't choose on this, you can't choose on anything."

–DAVID GRIMM

AVIAN INFLUENZA

With Change in the Seasons, Bird Flu Returns

An upsurge in H5N1 bird flu outbreaks in poultry across Asia is driving home the message that even countries that have eliminated the virus once shouldn't become complacent. The continuing high death toll in humans, including two recently detected cases of infection with a Tamiflu-resistant strain in Egypt, is also a grim reminder of how devastating the virus might be if it acquires the ability to spread easily among humans.

High alert. Since H5N1 virus was detected in Japan this month, officials have been checking blood samples from poultry at neighboring farms.

Over the past 3 weeks, Thailand and Vietnam reported their first H5N1 outbreaks among poultry in 6 months. Japan, which seemed to have dodged the bullet since its cluster of outbreaks in 2004 confirmed that the virus hit one farm on 11 January and probably a second farm on the 23rd. South Korea, which last November suffered its first outbreak since containing the virus in 2004, reported that the virus had turned up on a fifth poultry farm. Several wild birds found dead in Hong Kong tested positive for H5N1. And Indonesia on 20 January reported its fifth human death from the virus in just 10 days, bringing its death toll to 62, by far the most of any country.

The increase in outbreaks in the Northern Hemisphere follows what has become an established pattern. The reason for the seasonality is still not well understood, says Les Sims, a veterinarian based in Miranda, Australia, who advises the U.N.'s Food and Agriculture Organization (FAO). It is likely to be some complex interaction among several factors, including cooler temperatures enabling the virus to survive longer in the environment, greater poultry trade in preparation for winter festivals, and movements of wild birds.

The recurrence of the virus in South Korea and Japan is particularly notable. In both the winter of 2003–'04 and this year, outbreaks in South Korea were followed 4 to 6 weeks later by outbreaks in Japan. "The outbreaks in Japan and South Korea suggest to me free-flying birds as the most likely origin," says Sims. Both countries are trying to determine how the virus was reintroduced.

"The reasons for these failures need to be examined and the lessons applied elsewhere," says Sims. But overall, he says the speed of the response, particularly in Thailand and Vietnam, "is a positive sign and shows that the surveillance systems are working."

In Indonesia, four of the five recent human deaths occurred in the Jakarta area. In response, the city government on 17 January ordered residents who keep backyard poultry to eat, sell, or cull their birds by the end of the month or have them confiscated and destroyed. The government is talking about gradually replacing the live markets that currently account for 80% of poultry sales in the city with slaughterhouses. "It would be a sea change culturally," says John Weaver, senior adviser to FAO in Jakarta. If done properly, he says, eliminating backyard poultry could reduce the opportunity for the virus to survive in the environment. But he cautions against a sudden prohibition, which could lead smallholders to hide their fowl and refuse to cooperate with animal disease control efforts.

Early this week, meanwhile, experts were poring over the puzzling and potentially worrisome details of a recent cluster of human H5N1 cases in Egypt. Late December, a 16-year-old girl and her 27-year-old uncle, living in the same house in Gharbiya province, both died of H5N1 infection. Sequence information made public on GenBank on 23 January by the U.S. Naval Medical Research Unit 3 (NAMRU-3) in Cairo shows that both were infected with a virus strain that is moderately resistant to the antiviral drug Tamiflu.

Tamiflu resistance has been reported in a few other human H5N1 cases after patients were given the drug. However, the Egyptian samples showing resistance were taken just 2 days after Tamiflu treatment began, an unusually short period in which to develop resistance, says NAMRU-3 commanding officer Bruce Boynton. What's more, the virus in both patients had a rare resistance-conferring mutation, called N294S, seen only in one previous H5N1 patient in Vietnam.

That's why Boynton says the evidence suggests "a more disturbing" theory: that both were infected by a sick bird that already harbored the mutated virus. If more such birds exist, doctors may see more H5N1 patients who don't respond well to Tamiflu. And if such a resistant strain were to spawn a pandemic, the world's vast Tamiflu stockpiles might be less helpful.

Tests are currently under way to determine whether the patients had the resistant strain before they took the drug and whether virus from a third suspected H5N1 patient in the household, who also died, has the same mutation, Boynton says. Veterinary virologists are also checking to see whether the mutated virus can be found in birds in Egypt.

–DENNIS NORMILE AND MARTIN ENSERINK

CREDIT: MIYAZAKI PREFECTURAL GOVERNMENT/AP PHOTO

ACADEMIC RESEARCH

Harvard Proposes One for the Team

Talk about greater collaboration across academic departments is cheap. But making it happen can be very expensive. Last week Harvard University made a $50 million down payment on the concept, including seed money for a first-ever university-wide department in developmental and regenerative biology. The move is part of a major expansion of the university's science and engineering programs, including a planned $500 million campus across the Charles River that was unveiled earlier this month.

"There's a lot of life left in the disciplinary sciences, but at the same time, there is a trend toward concentration of resources and larger scale collaborative science," says Harvard Provost Steven Hyman, who last week announced the creation of a Harvard University Science and Engineering Committee (HUSEC). The committee, which will report to Harvard's president and its governing board, will use the $50 million to [illegible] the new department—which will include stem cell research—and seed other initiatives, some of which could lead to similar new departments.

Harvard professors have traditionally conducted their research and trained within the confines of a particular school, be it the Faculty of Arts and Sciences (FAS), the medical school and affiliated hospitals, or the schools of public health and of engineering and applied sciences. Although some universities erased those lines decades ago, working across departmental boundaries at Harvard is "not unlike [working] with two entirely separate institutions," says Douglas Melton, co-director of the Harvard Stem Cell Institute.

Hyman will chair the university-wide committee, which he hopes will keep the 366-year-old institution among the leaders in all fields of science and engineering through the 21st century. And Hyman is considered to be on the short list of Harvard presidential candidates, assumes that many of the committee's recommendations will cost money. "We expect [the committee] to propose a budget, and we know that a lot more will be needed," he says. "But this shows the faculty that we are serious."

The new department will eventually have 25 to 30 faculty members, says Hyman, about half migrating from existing programs and the rest new appointments—and report to both FAS and medical school deans. It will serve as a focal point for the work of nearly 700 people, a cluster that Melton calls "one of the highest concentrations in the world of stem cell scientists." Stem cell institute co-director David Scadden says the new department will be a "critical complement" to the activities of the institute, which will occupy space in the department's new building on the Allston campus, scheduled for completion in 2010. All the members of the new department will be part of the institute, which now has 45 principal faculty members.

Nancy Andrews, dean of basic sciences at the medical school and a co-author of a report last summer that recommended the formation of HUSEC, calls the department "the obvious first choice" for interdisciplinary research because of the field's rapid growth.

Hyman expects the new committee to have a detailed plan in place for the new department by 1 April. "They are keen to begin recruiting," he notes. And he compares what Harvard is doing to the road map created a few years ago by National Institutes of Health Director Elias Zerhouni for more interdisciplinary programs across the agency's 27 institutes and centers. "That was his response to the changing world of science," says Hyman. "And this is our response."

–JEFFREY MERVIS

With reporting by Constance Holden.

CREDIT: HARVARD UNIVERSITY

All together. Steven Hyman will lead a Harvard panel fostering interdisciplinary science.

SCIENCESCOPE

New Cell Rules

The Wisconsin Alumni Research Foundation (WARF) has scaled back tough licensing rules restricting academic research on its broadly patented human stem cell lines. Previously, a company needed a license even for university-based research using the WARF lines. That restriction has been lifted, although a company must still have a license to do its own work or develop products. The foundation also clarified its fees and how academics can transfer cell lines.

Jon Soderstrom, managing director of Yale's Office of Cooperative Research, says the old rules were confusing, restrictive, and inconsistent. The change is "coming at a very crucial time for us," he says, as the school is now setting up a new stem cell program. The Santa Monica, California–based Foundation for Taxpayer and Consumer Rights (FTCR) says the move alleviates its concerns about restrictive policies that would hinder work at the new California Institute for Regenerative Medicine. However, FTCR still believes WARF's patents are invalid, and the U.S. Patent and Trademark Office is currently reviewing an administrative request filed by the group to review the patents.

–ELI KINTISCH

Big Bucks for ALS

The latest sign of the increasing focus of disease advocacy groups on research is a $36 million pledge by two nonprofit groups to identify new molecular targets against amyotrophic lateral sclerosis (ALS). The venture comes as one of the groups abandons efforts to tackle ALS via published drug targets. After testing 150 existing drugs in 22,000 mice, "we've pretty much exhausted all the logical targets for ALS," says Sean Scott, president of the ALS Therapy Development Institute (ALS TDI) in Cambridge, Massachusetts.

ALS TDI is partnering with the wealthier Muscular Dystrophy Association (MDA) in Tucson, Arizona. Scott's research staff of 24 will add 10 scientists probing gene and protein expression across healthy and diseased mice and human tissue collected through MDA's network of medical clinics. The goal is to identify genes that behave differently in ALS in hopes of finding out how those differences affect the disease.

Jeffrey Rothstein, who is supporting work on new ALS mouse models at the Robert Packard Center for ALS Research through Johns Hopkins University in Baltimore, Maryland, has high hopes for the new partnership. But he worries that existing mouse models may not be reliable enough to serve as a guide.

–JENNIFER COUZIN

The Endangered Lab Chimp

Almost human. Yerkes has more than 1000 chimpanzees like this one. At Yerkes that, owing to their similarities to us, are set aside for biomedical research.

CREDIT: YERKES NATIONAL PRIMATE RESEARCH CENTER

A decline in the number of chimpanzees available for biomedical research in the U.S. has sparked a growing debate on the opportunities and costs of studies with our closest relatives

FIFTEEN YEARS AGO, THE UNITED STATES was one of a half-dozen countries that had captive chimpanzees available to biomedical researchers. Today, it stands alone. Every country except perhaps Gabon has abandoned this type of experimentation for a bramble of ethical, financial, scientific and political reasons. Now the U.S. National Institutes of Health (NIH)—the main supporter of chimpanzees maintained for biomedical research—finds itself facing an incendiary debate over whether it should phase out such studies or breed more animals for future generations of investigators.

The issue has become especially acute over the past few months, in the face of a new projection about the fate of the captive chimps set aside for biomedical research. For the past decade, NIH has imposed a moratorium on breeding any federally supported chimps, which are housed at six primate centers across the country. It enforces the ban by refusing to support any newborns. In 2000, the U.S. Congress also mandated that older "surplus" chimps no longer needed for research be moved from primate centers to retirement sanctuaries. As a result, the population has dropped from 1500 in 1996 to 1139 in October 2006. Now, many researchers who conduct biomedical research on chimpanzees are worried that the number of breeding animals is declining so rapidly that there will soon not be enough left to sustain the population. "The population is heading for a cliff," says Todd Preuss, a neuroscientist at Yerkes National Primate Research Center in Atlanta, Georgia, which has the country's oldest colony of research chimpanzees. "If we don't start breeding these chimpanzees soon, they're going to go away, and they're going to be gone for good."

The push to breed more chimpanzees is forcing a reexamination of questions that have long surrounded research with our closest relatives, an endangered species that is rapidly disappearing in the wild. Where is the line that separates ethical from unethical research? What type of housing do chimps require? Where will the money come from to support the care of animals that routinely live 30 years in captivity and can live twice as long? Has NIH properly managed what it calls the "chimpanzee resource"? And why do scientists need chimpanzees for biomedical research anyway?

On one end, the Humane Society of the United States and the New England Anti-Vivisection Society have launched campaigns to stop all "invasive" experiments with chimpanzees that might harm them and to have all the animals moved to sanctuaries. Some primate researchers, too, have misgivings about conducting the types of vaccine, drug, and pathogenesis studies that are done in the United States on chimpanzees. "If you talk to a lot of primate researchers, they're not comfortable with it," says virologist Jonathan Allan, who conducts AIDS research with monkeys at the Southwest National Primate Research Center in San Antonio, Texas, one of the facilities that does biomedical chimp experiments. "You *shouldn't* be comfortable with it. You should have to search your soul as to the balance

between the research and the good that comes from it and the bad part, which is what happens to the animals. It's a difficult place to be. If you're comfortable with it and you don't have any problem with it, *that's* a problem."

Then again, a growing number of researchers, such as Preuss at Yerkes, conduct so-called noninvasive biomedical studies in these chimpanzees that they say cause them no physical harm. Behavioral researchers—who are allowed to work at some zoos and sanctuaries—also study this population. "There's so much we can do without a destructive approach to captive chimps," says Pascal Gagneux, a primatologist at the University of California, San Diego (UCSD) who conducts reproductive biology research with chimpanzee sperm samples. Gagneux, Preuss, and others contend that with new body-imaging technologies and the recent sequencing of the chimpanzee genome, the opportunities are greater than ever to use noninvasive techniques to learn about everything from human disease and aging to behavior and evolution.

Still other researchers caution against making a blanket proclamation that invasive experiments with chimpanzees are unethical. "To draw a hypothetical line in the air I don't think does justice to the subtlety of these questions," says Norman Letvin, an immunologist at the Beth Israel Deaconess Medical Center in Boston, who has done AIDS vaccine experiments in chimpanzees and monkeys. "These kinds of discussions need to be focused on very specific questions about a particular study." Letvin no longer experiments on chimps and says he can't see any compelling reason today to use large numbers of them for biomedical research. But he stresses, as do many other investigators, that this animal model has led to "enormously valuable" medical advances in the past and may well in the future.

Unfashionable model

Scientists have conducted biomedical research on chimpanzees for more than a century. As many proponents of this animal model note, such research played a crucial role in the development of the vaccine for hepatitis B, a sometimes lethal virus that has infected 2 billion people. But scientists around the world have also performed studies that are now considered bizarre or brutal. The U.S. Air Force's chimponaut program shot them into space. Other researchers harvested their organs for human transplants, implanted electrodes into their brains to study sleep, and used them to gauge the effects of alcohol and marijuana. And a Soviet scientist attempted to inseminate them with human sperm to make a "humanzee."

NIH formally entered the chimpanzee research business in 1960, when Congress established a network of regional primate centers for basic and clinical research. Some of these great apes were bred in captivity, but many more were taken from Africa until 1973, when the United States signed the Convention on International Trade in Endangered Species of Wild Fauna and Flora, which barred the importation of wild chimpanzees. In 1986, faced with increasing demands for chimpanzees from researchers studying the emerging AIDS epidemic, NIH started a breeding program. Numbers quickly grew, with the initial 315 male and female breeders producing nearly 400 offspring by 1997.

But the chimpanzee AIDS model had problems from the get-go. Researchers had to pay a steep user's fee, at least $50,000 per animal, and experiments often used so few animals that only the most dramatic results would reach statistical significance. It also soon became clear that HIV typically doesn't cause disease in chimps, undermining the model's reliability. Once scientists discovered in 1987 that SIV, a simian cousin of HIV, caused an AIDS-like disease in rhesus macaques, that became the model of choice.

In 1995, with few chimps being used to test AIDS vaccines, NIH's National Center for Research Resources (NCRR) established a moratorium on breeding the chimpanzees it supported "until further notice." Although researchers continued to use chimpanzees to study vaccines for hepatitis C and respiratory syncytial virus, as well as treatments for other diseases, NCRR reasoned that the demand could be met with existing animals. In 1997, the National Research Council (NRC) essentially concurred, issuing a report, *Chimpanzees in Research*, that recommended extending the breeding moratorium until 2001. NRC's panel of experts cited "compelling" reasons for maintaining a population of about 1000 chimpanzees for research. But it concluded that the existing population was "more than adequate to meet research needs for at least five years." It also expressly recommended that no facilities euthanize chimpanzees for population control.

NCRR imposed the breeding and euthanasia bans and, as the NRC panel recommended, set up a Chimpanzee Management Program (ChiMP) to monitor the status of the population and promote the appropriate use of these animals in research. NCRR simultaneously established a working group of outside experts to advise ChiMP. The working group has recommended extending the breeding moratorium three times, most recently in May 2005. There was "a huge number of chimps that weren't being used" for research, says veterinarian William Morton, a member of the ChiMP working group who runs a primate consulting company, Pans NHP in Edmonds, Washington. "They were just sitting there."

With the publication of the first draft of the chimpanzee genome in September 2005, calls mounted for NCRR to lift the moratorium. In a commentary in that same issue of *Nature*, the heads of the U.S. primate centers again extolled the benefits of maintaining this "unique resource" and warned that if the moratorium were not lifted, the population would sharply decline within 5 years.

Since then, one of the co-authors, John VandeBerg, director of Southwest National Primate Research Center, has performed a more detailed analysis of the age and health status of the chimps housed at all six facilities. At a chimp meeting at Yerkes in October 2006, VandeBerg said that of the 1133 animals then available, just 200 females were potential breeders. If the breeding moratorium were not lifted, he added, there will be no research chimps left by 2037, when

Number of Chimpanzees Available for Breeding or Research in the U.S.*

* Projection assumes no further breeding.

CREDIT: PRIMATE FOUNDATION OF ARIZONA; SOURCE: JOHN VANDEBERG, SOUTHWEST FOUNDATION FOR BIOMEDICAL RESEARCH

all of these chimpanzees will have died (see graph, p. 451).

VandeBerg concedes that his model is "simplistic"—for instance, it doesn't take into account the fact that some facilities, at their own expense, have bred a few chimpanzees despite the moratorium. Even so, his bleak projections startled many at the meeting, including Ajit Varki, a glycobiologist at UCSD who helped lead the drive to sequence the chimpanzee genome. "What's happening now is really a disaster," says Varki. Others noted that the aging of the population is already limiting brain and behavioral research that depends on younger animals.

Yerkes head Stuart Zola, who is a member of the ChiMP working group and the broader NCRR advisory council, emphasizes that many of these "potential breeders" may not become pregnant or may not take care of offspring if they do. "It's almost too late unless there's substantial breeding initiated quickly," says Zola.

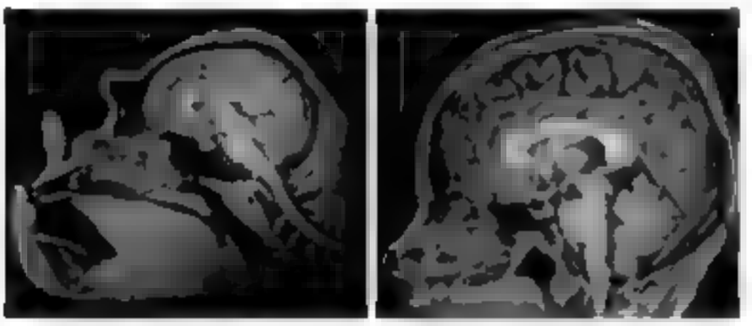

Like-minded? Using MRI, Emory University's James Rilling does comparative analyses of chimp (*left*) and human brains to study aging and evolution.

Although Zola is not one of them, several researchers fault NCRR for the way it has managed the chimpanzee resource. "Most of what they do is fund mass spectrometers and clinical research centers," says Varki, who would like the breeding moratorium lifted. "I think the chimpanzees are a thorn in their side." Even Morton, who supports the moratorium, criticizes NCRR for its failure to hold regular meetings of the working group he sits on "in order to follow its advice and develop a financial and management plan for the population. "Somebody needs to grasp this thing and show some leadership at NCRR," says Morton, who previously ran the NCRR-funded primate center at the University of Washington, Seattle. "What are the issues, and what are the facts?"

John Harding, who heads primate resources for NCRR, would not explicitly address why no long-term plan exists. But Harding stresses that the institution works closely with the primate centers and has "active policies and processes to manage and oversee its chimpanzee resource program." NCRR plans to convene its working group in March to reassess the moratorium, which is in effect until December 2007.

Ethical lines

Should NCRR lift the moratorium, debate will likely intensify over what type of chimp research is ethically acceptable and worth the expense—especially now that almost everyone else has gotten out of the business.

The Netherlands, the last European country to conduct invasive research on chimpanzees, outlawed the practice as of 2004 and has been moving its colony of more than 100 animals to zoos and safari parks. In October 2006, the one Japanese pharmaceutical company still conducting invasive research in that country decided to stop, with support from Kyoto University, the company plans to open a retirement sanctuary for its 80 animals in April. The Hepatitis Research Foundation in Poughkeepsie, New York, which has also conducted biomedical research at a chimpanzee colony in Liberia, decided last fall to release the rest of its 74 animals onto island sanctuaries. Gabon's Centre International de Recherches Medicales in Franceville has done biomedical research on its small population of captive chimps in the past, but future plans are unclear.

Morton says he'd like to see the United States phase out biomedical research with chimpanzees, too. "It settles on the side of people who have ethical arguments, but for financial reasons," says Morton. "If you lift the moratorium, there's going to be breeding like crazy, and once again we'll have all these chimps and who'll be supporting them?"

In fiscal year 2005, NCRR spent $8.7 million on chimpanzee care. More than 20% of that went to Chimp Haven in Keithville, Louisiana, the country's only publicly funded sanctuary for the retirement of surplus chimpanzees, and that amount is certain to rise as more animals are retired. Primatologist Linda Brent, who heads Chimp Haven, which depends on both public and private funding, questions how the federal government could possibly afford to breed more chimpanzees. The estimated lifetime cost of caring for a chimpanzee—captive males live for 30 years on average, females for 45—ranges from $300,000 to $500,000, she notes.

If the U.S. government does decide to invest more money in maintaining the research chimp population, many investigators contend that it should rethink what types of experiments can be done and how the animals are housed. "Chimpanzees should not be used as furry test tubes," says Beatrice Hahn, a virologist at the University of Alabama, Birmingham, who hunts for AIDS viruses in feces collected from wild chimpanzees. Hahn, who conducts no invasive research, contends that "95% of the experiments done with them are not necessary."

In their 2005 *Nature* commentary, VandeBerg and co-authors argued that chimpanzees should remain available for disease research and for testing drugs and vaccines. VandeBerg notes that some proprietary experiments with monoclonal antibodies done for commercial companies have led to illness or even death of chimps—preventing harmful drugs from entering human trials. "It's unethical from a human standpoint to not do this research," he says.

In an opposing commentary in the same issue, UCSD's Varki, Gagneux, and primatologist James J. Moore argue that chimpanzees should be used only in experiments that could also be done ethically in humans. That would rule out vaccine studies that intentionally infect animals with potentially harmful viruses, for instance. Even with such constraints, they predict demand for animals to rise. "I suspect in 5 to 10 years from now, there's going to be much greater interest in studying chimps in nondangerous ways," says Varki. If these chimps die off, he says, "history will look back and say how could you let that happen." In their commentary, they also called for increasing funding to provide chimpanzees with "optimal living conditions," such as Chimp Haven's facility, where chimps can socialize outdoors for much of the day.

Just how many chimpanzees the country needs to maintain a viable breeding population remains a hot-button issue. Nate Flesness, executive director of the International Species Information System and a member of the 1997 NRC committee, notes that North American zoos have fewer than 350 chimpanzees that they share for breeding. Flesness and others say the U.S. government should simply support a core breeding group of chimpanzees for biomedical research as an insurance policy for future emergencies. Beth Israel's Letvin agrees with this minimalist strategy. "If we've learned anything over the years, it's that we don't know what the next epidemic will be and what the next major health crisis is going to be," says Letvin. "It would be foolhardy to take any potential animal model off the table."

—JON COHEN

CREDIT: JAMES RILLING/EMORY UNIVERSITY

INVASIVE SPECIES

Feared Quagga Mussel Turns Up in Western United States

Scientists are trying to assess the potential for ecological and economic damage after finding a relative of the infamous zebra mussel in the Colorado River

For 2 decades, the zebra mussel has tormented the Great Lakes. Along with its close cousin, the quagga mussel, the fantastically prolific mussels have clogged the intake pipes of power plants, coated the hulls of boats, and thrown ecosystems out of whack. Western states have been so concerned that in 1998, they started a major campaign, called the 100th Meridian Initiative, designed to prevent boaters from accidentally transporting the mussels or other exotic species to their waters.

Now the initiative has suffered a major defeat. Earlier this month, quagga mussels were found in Lake Mead, a 50 000-hectare reservoir in Nevada. And last week, they were confirmed downstream in the Colorado River. There's no sign of zebra mussels yet, but observers fear their arrival is only a matter of time. State officials in Nevada and California are convening scientific advisory panels to figure out what to expect and how to cope with the quagga. "This is an organism that would be devastating for California's aquatic ecosystems and for freshwater infrastructure," says Richard Soehren, water policy adviser for the California Department of Water Resources.

Both zebra (*Dreissena polymorpha*) and quagga (*D. bugensis*) mussels are native to Eastern Europe. They are thought to have arrived in the Great Lakes by the late 1980s via the ballast water of container ships. In some places, up to 700,000 zebra mussels crowd together in a single square meter. By clogging intake pipes, the mussels cost the power industry many millions of dollars in added maintenance. Inexorably, the mussels have spread down the Mississippi River and throughout much of the eastern United States.

As a popular destination for boaters from across the country, Lake Mead was clearly in the mussels' path, and officials there have been on the alert after several close calls. In 2004, for example, they found dead zebra mussels on a half-dozen houseboats arriving at Lake Mead, 1800 kilometers from the most westerly sighting of zebra mussels.

Now it's clear that the quagga mussel already beat the zebra across the Great Divide. On 6 January, a diver doing a routine inspection of a breakwater found a quagga mussel at a Lake Mead marina, a few kilometers upstream from Hoover Dam. "I was heartbroken," says Wen Baldwin, president of the Lake Mead Boat Owners Association, after the diver showed it to him. Since then, divers with the National Park Service (NPS), which runs the Lake Mead National Recreation Area, have found mussels in four more locations. Based on the size of the mussels sent to him for identification, Robert McMahon of the University of Texas, Arlington, estimates that they have been in the lake for at least 2 years. The deep, cool water and rocky bottom offer an ideal habitat for the quagga mussels, notes Charles Ramcharan, a limnologist at Laurentian University in Sudbury, Canada. "Lake Mead is going to have a huge infestation," he predicts.

CREDITS (TOP TO BOTTOM): DAVE BREMNER/MICHIGAN SEA GRANT; SOURCE: CALIFORNIA DEPARTMENT OF WATER RESOURCES

Officials are worried about the impact on Hoover Dam, which last year generated 3.3 billion kilowatt-hours of electricity, and on the two drinking-water plants that also draw water from Lake Mead. Another big concern is the potential effect on sport fisheries in the lake. The mussels filter huge volumes of water, removing phytoplankton and boosting nutrients. This seems to have harmed commercial fish stocks in some but not all of the Great Lakes.

An emergency task force of NPS and state agencies in California and Nevada is scrambling to prevent further spread. As a temporary measure, Park Service boats have been grounded and concessionaires have been told not to transport rental boats. They have ramped up inspections of private boats at the lake as well. California is trying to increase boat inspections at its three border stations that receive traffic from Lake Mead. Ann Malcolm, general counsel for the state's Department of Fish and Game, says the agency will ask the legislature for the authority to inspect any possible sources of water on boats and force owners to drain them.

But the mussel seems to have already spread downstream. On 17 January, divers with the Metropolitan Water District (MWD) of Southern California found quagga mussels in Lake Havasu, near the intake to the Colorado River Aqueduct, which supplies water to 18 million people. "We are going to be taking aggressive action," says Debra Man, MWD's chief operating officer. They plan to use chlorine or copper sulfate to kill any mussels or larvae in the 386-km-long canal. Luckily, quagga mussels prefer deeper, cooler water with relatively few nutrients, so they probably won't thrive in the canals, says Ed Mills, an ecologist at the Cornell Biological Field Station in Bridgeport, New York.

However, if zebra mussels arrive as well, the situation could be worse. Not only might zebra mussels flourish in the aqueduct, but they could also cause serious problems with the many ditches and pipes in the Imperial Irrigation District, which takes its water from the Colorado River. "It's conceivable those canals could require extensive maintenance," says Michael Mizumoto, the district's biological control unit supervisor.

For the moment, however, scientists and managers will have enough headaches with the unfolding western drama of the quagga mussel. Says Ramcharan, "Y'all just bought front-seat tickets to the invasion show."

–ERIK STOKSTAD

Three-Headed Quasar Promises to Shed Light on Universe's Past

Triple plays are rare in baseball, but not as rare as triplet formations of quasars in space. In fact, images depicting multiple quasars in close proximity have always been routinely interpreted as mirages, different views of a single real quasar.

But not always. Of roughly 100 000 known quasars—cosmic beacons that beam luminous radiation across the universe—about 400 have been identified as being pairs. Quasars are powered by massive black holes in the cores of galaxies, and when two such galaxies collide, their central black-hole quasars regain their separate identities, so pairs can survive at least for a while.

Collision of a third quasar with such a doublet would be an extremely rare event, but astronomers say they have now witnessed the birth of quasar triplets.

"We have found the first case of a physical triple-quasar system," said astronomer George Djorgovski of the California Institute of Technology (Caltech) in Pasadena, leader of an international team reporting the discovery at the meeting. Two of the quasars in the group, designated QQQ 1432-0106, were discovered before 1989. Astronomers originally believed that the pair was an illusion created by gravitational lensing of a single quasar. Such lensing, an effect of Einstein's general theory of relativity, occurs when an intervening mass's gravity bends the light arriving from distant objects. In many known cases, such lensing bends the light from a distant quasar so much that it appears to arrive at Earth from multiple pathways, creating the impression of more than one object.

Later observations of that quasar system questioned the mirage interpretation, however. Many astronomers concluded that it consisted of two distinct nearby quasars at a redshift of 2.1, corresponding to a time when the universe was about 3 billion years old.

More recently, astronomers from Caltech and the École Polytechnique Federale de Lausanne in Switzerland, using data from the Keck Telescope in Hawaii, spotted evidence for a third nearby quasar, fainter than the others but also at about the same redshift distance. Further observations with the European Southern Observatory's Very Large Telescope in Chile confirmed the Keck finding.

Efforts to explain the triplet as a gravitational-lensing effect have failed, Djorgovski said, as have efforts to find any intervening massive body that could have acted as a lens. And scrutiny of the colors of light emitted by the quasars revealed subtle differences, further suggesting that the three quasars are distinct. "This is almost certainly not a gravitational lens," Djorgovski said, "so we are left with the alternative explanation that it is a physical triple-quasar system."

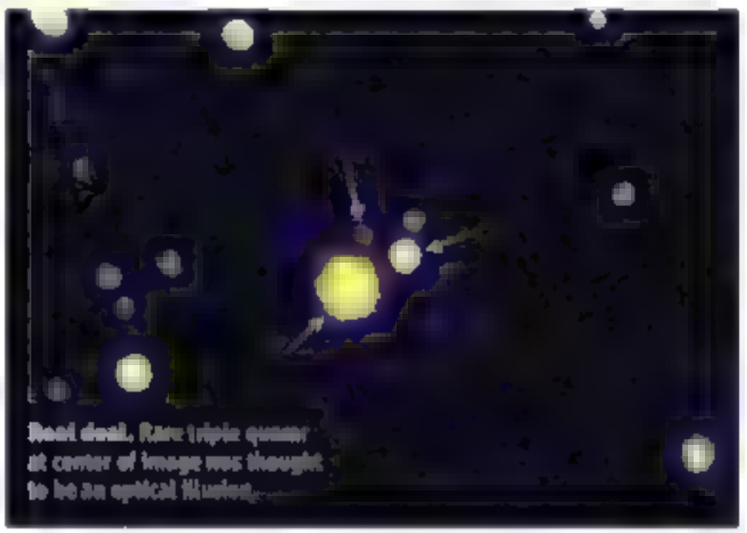

Real deal. Rare triple quasar at center of image was thought to be an optical illusion.

CREDIT: S. G. DJORGOVSKI ET AL./CALTECH AND ESFRI

Although such systems should be rare, they are not entirely surprising, and their existence could aid efforts to understand the dynamics of galaxy mergers in the early universe. Light from the triplets departed on its journey to Earth more than 10 billion years ago, at a time when galaxies occupied a smaller universe and crowding led to frequent collisions.

"These interactions are in fact quite common," said Frederic Rasio of Northwestern University in Evanston, Illinois. In fact, his computer simulations show that galaxies would often collide and merge to form larger galaxies, and when two galaxies containing central black hole–powered quasars merged, the two black holes would begin orbiting each other similarly to a binary star system.

Eventually, such orbiting black holes will swirl closer together and collapse into each other. Before that happens, however, another colliding galaxy could bring a third black hole to the dance, at which point the interactions get more complicated, Rasio's simulations show. "The three black holes interact rather violently and unpredictably," Rasio said. "What happens at the end is these black holes basically kick themselves out of the center of that galaxy."

Their rapid exit occurs after the latecomer black hole pairs up with one of the original two, giving the remaining loser a gravitational kick that hurls it out of the galaxy. The new pair recoils in the opposite direction. In both cases, the black holes depart their parent galaxies at speeds reaching thousands or even tens of thousands of kilometers per second.

These speeds are high enough that the black holes recoil certainly out into the halos of the galaxies and sometimes can even be kicked all the way out, meaning they become wandering black holes that go through empty intergalactic space, Rasio said.

In the observed triplet quasar system, the black holes have just begun to come together to perform their partner-swapping dance; they are still about 100 000 light-years apart. The entire process of merging and eventual splitting up will take about 100 million years, Rasio's simulations indicate.

"The process that Dr. Rasio has modeled is very, very far in the future," said astronomer Virginia Trimble of the University of California, Irvine. "So in some sense, the prediction has been verified by the observation, and the observation has been explained by the theory." But 100 million years is a long time to wait to see whether the future behavior of the triplet really matches the theoretical forecast.

Evidence that such triplet interactions occur could come sooner, however. A recoiled pair of black holes would soon merge and generate gravitational waves that might be detectable, Rasio said. And there also exists the possibility of detecting a wandering black hole speeding through space, ideally not heading too close to Earth.

Middle-Earth Denizens Mob the Milky Way

The mystery of the missing dwarf galaxies may have been solved. Instead of looking for dwarfs, astronomers should have been searching for hobbits.

Researchers from the Sloan Digital Sky Survey reported the discovery of seven previously unknown dwarf galaxies surrounding the Milky Way, plus an eighth at the edge of the Milky Way's gravitational influence. Because those small galaxies were found in a survey of only one-fifth of the sky, dozens more are likely to exist, team member Daniel Zucker of the University of Cambridge, U.K., said at the meeting.

Computer simulations based on current theories of galaxy formation suggest that large galaxies such as the Milky Way should be surrounded by dozens or even hundreds of dwarf satellites. Until recently, however, only a few such satellites were known.

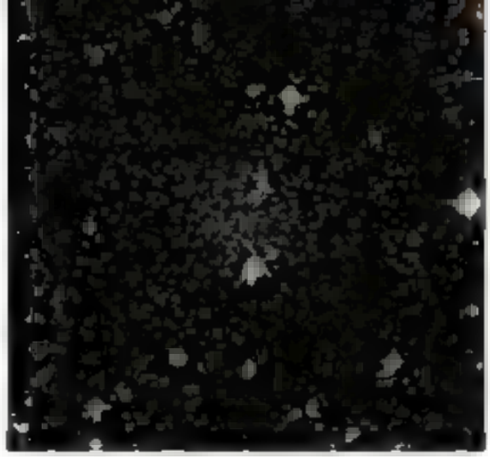

Fecund "hobbit." Leo T (central white cluster) is the smallest known star-forming galaxy.

A possible explanation for the discrepancy, supported by the Sloan results, is that many of the dwarfs are too dim to be easily detected.

These new dwarfs are extremely faint, Zucker said. "We're finding lots of them, and they seem to be much fainter than anyone suspected galaxies could be before. So perhaps rather than dwarf galaxies, we should give them the name 'hobbit galaxies.'"

The eighth of the new galaxies, designated Leo T, is stranger still. At a distance of 1.4 million light-years, it is probably not a Milky Way satellite but rather a free-floating dwarf within the Local Group of galaxies, Zucker said.

Leo T contains both old and new stars, generating a total brightness only about 50 000 times that of the sun. The presence of new stars is surprising because most other dwarfs ceased star formation long ago.

"This is basically the smallest, faintest star-forming galaxy known," Zucker said. The Local Group could be filled with faint objects like this.

More such dim, free-floating galaxies could help explain the lack of dwarfs in past observations, said Nitya Kallivayalil of the Harvard-Smithsonian Center for Astrophysics in Cambridge, Massachusetts.

This missing-satellites problem is really one of the great mysteries," she said. "The point that there could be free-floating satellites bound to the Local Group but not necessarily to any major member of the Local Group is very interesting, and it's something that is not outlandish when you look at the simulations."

–TOM SIEGFRIED

Tom Siegfried is a writer in Los Angeles, California.

Snapshots From the Meeting >>

Caught speeding. Long believed to be the Milky Way's most prominent satellite galaxies, the Magellanic Clouds may turn out to be mere passers-by. Rather than pursuing a tightly bound path, both the Large and Small Magellanic clouds appear to be speeding by at more than 300 kilometers per second, possibly fast enough for them to escape our galaxy's gravity. "We do have to now consider the possibility that the clouds are perhaps unbound to the Milky Way," said Nitya Kallivayalil of the Harvard-Smithsonian Center for Astrophysics in Cambridge, Massachusetts. Kallivayalil and two other astronomers calculated the clouds' velocities by using data from the Hubble Space Telescope to compare the cloud motion across the sky to that of very distant (and hence effectively stationary) quasars. The Milky Way could still keep the clouds in orbit, Kallivayalil said, if it is twice as massive as current estimates suggest or if its invisible halo of dark matter has an odd shape.

Supernova solution. The space-based Chandra X-ray Observatory has helped clear up a long-standing mystery about a famous supernova. Spotted by Johannes Kepler in 1604, the supernova has seemed likely to be Type Ia, a thermonuclear explosion detonated when a white dwarf star accumulates too much mass to remain stable. Yet surrounding the explosion site [illegible] are commonly seen with Type II supernovae, which occur after a massive star burns out, collapses, and explodes. X-rays from the 1604 supernova remnant, recorded by Chandra, confirm the case for Type Ia, astronomer Stephen Reynolds of North Carolina State University in Raleigh reported at the meeting. The x-rays reveal large amounts of iron, a telltale sign of a thermonuclear blast. Type II supernovae produce more oxygen than iron. "There's iron everywhere; oxygen is hard to find" around the blast, Reynolds said. "But at the same time, we've confirmed the presence of circumstellar material." That material, Reynolds said, suggests that Kepler's supernova might belong to a new class of Type Ia supernovae from a slightly more massive than average progenitor.

Mapping the darkness. Using almost 1000 hours of observation time with the Hubble Space Telescope, astronomers have produced the highest resolution map yet of dark matter's distribution in the cosmos. "It's the largest project that has ever been done with the space telescope," said Nick Scoville of the California Institute of Technology (Caltech) in Pasadena, principal investigator of the NASA project. Known as COSMOS (for Cosmic Evolution Survey), the project traced the location of dark matter across a wide patch of the sky (nine times the area covered by the moon) at various distances out to a depth corresponding to a time when the universe was about half its present age. The dark matter, unknown material that gives off no visible light, was detected by the way its gravity blurred the shapes of faraway galaxies. The new maps, published last week in *Nature*, show that dark matter provides a massive scaffolding around which the universe's ordinary (or "baryonic") matter conglomerates in clusters of galaxies. "Without this dark matter, the universe wouldn't exist as it is today," said COSMOS collaborator Richard Massey, also of Caltech. There are hints, however, that ordinary matter does not always coincide with the dark-matter skeleton. "There are some interesting discrepancies within the map," said Massey. Previous dark-matter mapping by Anthony Tyson of the University of California, Davis, and colleagues showed similar discrepancies. "There is something funny going on," said Tyson, who is not involved in the COSMOS project.

–T.S.

CREDITS: (TOP TO BOTTOM) MIKE IRWIN/THE SDSS; COLLABORATION; NASA/CHANDRA/CNRS

Near-perfect eyes. Vampire squid lenses are designed for seeing details, even in virtual darkness.

Loopy Lens Proteins Provide Squid With Excellent Eyesight

When Alison Sweeney wanted to learn about eye evolution, she went to sea. While the ship rolled beneath her, she dissected the eyes of squid freshly retrieved from 1000 meters below and tested how well each lens resolved the details of a panel of ever-narrower black and white stripes. Back at Duke University in Durham, North Carolina, as a graduate student in the lab of Sönke Johnsen, she combined those results with biochemical and modeling data on the optical and chemical properties of lens proteins to reconstruct the history of vision in cephalopods—squid, octopi, and their relatives. From just one ancestral lens protein—vertebrates started with several—these marine invertebrates have evolved lens-based eyesight more than once, Sweeney reported at the meeting.

The work "is one of the first times that people have dissected the origins of the complexity in the lens" used by many underwater creatures, says evolutionary biologist Todd Oakley of the University of California, Santa Barbara. Seeing clearly underwater requires a special spherical lens with a high refractive index in the center but a lower index toward the edge. This gradation is achieved with progressively lower concentrations, from the lens's center outward, of proteins called crystallins.

The genes for crystallins evolved from the duplicated genes of small enzymes often involved in stress responses. Vertebrates have several unique families of crystallins, but cephalopods have just one family, the S-crystallins, which descend from a liver enzyme.

To study this simpler protein family, Sweeney divided the squid lens into four concentric layers and analyzed its protein makeup using mass spectrometry and other techniques. With the help of Duke's David Des Marais and Yih-Jin Andrew Bun, she figured out evolutionary relationships among that squid's crystallins and determined how the proteins fold and interact. She and Nikhat Manz of the University of Florida, Gainesville, also sequenced 600 genes for S-crystallins from a dozen other cephalopod species. "It's the breadth of approach that I am most impressed with," says Thomas Wolcott, a physiological ecologist at North Carolina State University in Raleigh.

Researchers already knew that S-crystallins have an extra loop compared to the ancestral liver enzyme. Early on in evolution, this loop was short. But in newer S-crystallin variants, it is longer, and the proteins are more positively charged, Sweeney reported. The older, shorter proteins were evenly distributed throughout the cephalopod lens. But there was a gradient for the more recent crystallins, with almost none in the center and relatively more near the edge. (Amounts dropped at the edge itself.) Sweeney's analysis suggested that there had been positive selection for the longer loops in the younger proteins.

For a lens to be transparent, crystallins must stay folded and evenly dispersed to create a glassy state. That's not a problem in the close-packed proteins in a lens's center. But in the outer half of the lens, proteins can have the freedom to form clumps and cause cataracts. It could be that the longer loop helps prevent this by further stabilizing the protein, Sweeney noted. In addition, the high positive charge helps keep the proteins apart.

"It's amazing how finely tuned the squid lens is to do its job," says Jonathan Henry, a developmental biologist at the University of Illinois, Urbana-Champaign.

When Sweeney sequenced the S-crystallin genes from various cephalopods, she expected to find that all these lens proteins had descended from a common cephalopod ancestor that had co-opted the liver enzyme. Instead, the sequences indicated that this adaptation of the enzyme into lens proteins occurred later, after the ancestral cephalopod had begun to diverge into squid, octopi, and other species. How many cephalopod lineages independently came up with this solution remains unclear, but "it looks like there's been novel evolution [of the enzyme] at least twice," she reported.

After her study, Sweeney is deeply impressed by cephalopod vision. Indeed, she noted, the shipboard tests showed that the vampire squid's lens, which is considered a "living fossil" in the evolutionary history of cephalopods, "has a visual acuity better than in a state-of-the-art Zeiss dissecting microscope."

Muscle Fibers Shift Into High Gear

One look at a ballerina as she pirouettes and poses drives home the remarkable ability of our muscles to adapt to diverse biomechanical demands. Manny Azizi and Thomas Roberts, biomechanists at Brown University, have now found that as certain muscles contract, they vary their shape to balance the need for speed and force. "It's as if these muscles have a built-in automatic transmission," says Azizi.

"Their study ... takes us one step closer to understanding how skeletal muscle works in active animals," says David Carrier, a comparative physiologist at the University of Utah, Salt Lake City. The data could even inspire better robots. "Their results may provide a simple means for automatically varying the gearing of a robotic [muscle] with changes in load," says William Kier of the University of North Carolina, Chapel Hill.

The body has several kinds of muscles, each characterized by a particular alignment

CREDIT: STEVEN HADDOCK/MBARI

Whale Worm Sperm Factories

Five years ago, researchers were thrilled by a decomposing whale carcass they found on the floor of California's Monterey Canyon, 2900 meters underwater. The carcass was home to a thriving community of bacteria-filled tubeworms, called *Osedax*, embedded in its decaying bones. The visible worms were all females, each attended by up to 100 microscopic males that live in the female's gelatinous tube (*Science*, 30 July 2004, p. 668). Now, biologists have taken a closer look at these dwarf males and found that they have a distinctly odd but highly targeted development: They fail to mature, except with respect to their ability to produce sperm.

Since 2002, Robert Vrijenhoek and his colleagues at the Monterey Bay Aquarium Research Institute in Moss Landing, California, have visited several more whale falls, some of which are less than 1000 meters deep. At the meeting, marine biologist Greg Rouse of Scripps Institution of Oceanography in San Diego, California, reported finding at least nine *Osedax* worm species on these carcasses. "They are finding new species every time they go down," says Mark Martindale, an experimental embryologist at the University of Hawaii, Honolulu.

Rouse has also brought worm-covered whale bones back to the lab, where he used electron and confocal laser scanning microscopy to detail the males' anatomy. In his earlier studies, Rouse noticed that the male *Osedax* worms look like larvae of tubeworms typically seen at deep ocean vents. But the new work shows them to be even less well developed than these larvae.

The dwarf males have no mouth, no anus, and no gut at all. There's no circulatory system, nor any of the internal stores of bacteria that females depend on for nourishment, he reported. Smaller males have lots of yolk from the egg from which they were born, and larger males have almost none, suggesting that males deplete this resource as they grow.

Instead of internal organs, sperm at different stages of development stuff the male worm's body cavity. Rouse discovered a unique sperm duct that opens out at the top of the male's head. His studies indicate that sperm precursor cells start out at the worm's head, migrate toward the "tail," and finally move forward again before being released.

Rouse had previously suggested that as females age, they accumulate a harem of males. New data based on worms collected during recent underwater expeditions buttress this view. The work suggests that immature worms that land on bone become female, whereas those that settle on existing female tubes become males—a pattern known in at least one other annelid, Rouse pointed out.

The analysis of the male whale worm is exciting, says marine biologist Kenneth Halanych of Auburn University in Alabama. "It reminds us that there are still many interesting discoveries that await [us] in the oceans' depths."

–E.P.

of individual fibers. Biceps have parallel fibers and excel as fast contractors, for example. In contrast, calf muscles are pinnate with short fibers arranged at an angle to the direction of contraction. This configuration packs in more fibers per square centimeter, making the muscle stronger, but sacrifices contractile speed.

To build a computer model of how pinnate muscles behave under different demands, Azizi initially turned to programs for designing video games, which also require three-dimensional animation. His virtual muscle could contract, shortening along the vertical dimension—that is, its height—and expand along other dimensions to maintain a constant volume. For each new muscle shape, Azizi observed whether and to what degree the fibers changed their angle.

The simulations showed that certain muscle shapes caused contracting pinnate fibers to shift to a less steep angle. When that happens, the muscle's overall height decreases more than it would have had the fibers maintained their angle. In other words, the virtual muscle shifted into the equivalent of a high gear ratio, increasing the speed of contraction. Other simulations indicated that pinnate muscles with unchanging angles were the strongest.

Azizi then looked at whether real muscles acted this way. He had expected that each pinnate muscle would have just one gear ratio—that is, undergo a characteristic shape change and therefore be strong or contract fast but not have both features.

When he and Roberts evaluated how the drumstick muscle of turkeys shortened under different conditions, the results surprised Azizi. "A single muscle undergoes not one shape change but a range of different shape changes under different circumstances," he said.

Paralleling the virtual muscle, the turkey fibers themselves shortened about the same amount under the various test conditions. But the overall muscle contracted more under lighter forces, kicking into a high gear. With a heavy load, the angle of the fibers remained constant and the muscle contracted only a little and instead became more oval, just as in the simulations. In this way, the muscle operated at a lower gear and took full advantage of the dense packing of pinnate fibers, Azizi noted.

Fast and strong. Most of the hamstring muscles have parallel fibers (diagram, *left*), whereas those in the calf are pinnate (*right*).

Just as one changes gears on a bicycle to crawl up an ever-steeper hill, "the direction of change in the muscle gears matches the mechanical demands of contraction," Azizi said. Moreover, the muscle's shifting of gears required no nervous system input, occurring automatically depending on the load applied.

Azizi proposes that although pinnate muscle fibers often rotate as they contract, heavy loads pull against the fibers too much for them to do that. Thus, although pinnate muscles are supposedly specialized for force, under light demand, they can also work fast. The study is "outstanding and very important for assessing muscle architecture with relation to function," says Andrew Biewener, a biomechanist at Harvard University. "It's something that many of us have thought about but never worked or thought through."

–ELIZABETH PENNISI

CREDITS: (TOP) MIKE USICH, JUPITER; S. MANNY AZIZI/BROWN UNIVERSITY

Science Magazine's

State of the Planet 2006-2007

Donald Kennedy, Editor-in-Chief
and the Editors of *Science*

The American Association for the Advancement of Science

The most authoritative voice in science, *Science* magazine, brings you current knowledge on the most pressing environmental challenges, from population growth to biodiversity loss.

COMPREHENSIVE • CLEAR • ACCESSIBLE

ISLAND PRESS

Science AAAS

islandpress.org

LETTERS

edited by Etta Kavanagh

Pretty Structures, But What About the Data?

THE "GREAT PENTARETRACTION" (A SCIENTIST'S NIGHTMARE: SOFTware problem leads to five retractions," G. Miller, News of the Week, 22 Dec. 2006, p. 1856; "Retraction," G. Chang *et al.*, 22 Dec. 2006, p. 1875) in the wake of one of protein crystallography's greatest blunders, while an embarrassment to the authors, nevertheless provides the rest of the field with some small measure of comfort beyond mere schadenfreude. The mistake so clearly illustrates two lessons that we (senior, baby boomer professors ram down the throats of our protein-crystallographically aroused graduate students: (i) that those lovely colored ribbons festooning the covers and pages of journals are just models, not data, and (ii) that you invite disaster if you don't know what your software is actually doing down there in the computational trenches. Students have a hard time subsuming these dicta into their souls for two reasons: the tyranny of authority (the vanity journals occupying the vanguard) and the inherent beauty of the macromolecular models that emerge, as if by magic, from the user-friendly crystallographic software accumulated over decades through the generous labor of the field's talented reciprocal space-cadets. This case highlights the dangers of ignoring biochemical results, conventional but logically solid, as was done in the original papers and as is now outlined in the politely flaccid news report published along with the retractions. Seth Fraser's group, for instance, had shown in careful studies published in unglamorous workaday journals that the upside-down topology inferred from the erroneous structures of the multidrug-resistance pump could not possibly apply to the protein in its membrane home [e.g., (*1*)]. It's too bad these results were dismissed as just old-fashioned biochemistry.

> "[T]hose lovely colored ribbons festooning the covers and pages of journals are **just models, not data** ..."
> —Miller

CHRIS MILLER

Howard Hughes Medical Institute, Department of Biochemistry, Brandeis University, Waltham, MA 02454, USA

Reference

1. S. Reyes, Y. Ubaz, S. Schuldiner, *FEBS Lett.* **562**, 193 (2004).

Crop Models, CO_2, and Climate Change

IN THEIR RESEARCH ARTICLE "FOOD FOR thought: lower-than-expected crop yield stimulation with rising CO_2 concentrations" (30 June 2006, p. 1918), S. P. Long *et al.* argue that crop models have to be improved to enable estimation of future food production under rising CO_2 and climate change. Their conclusion is based on a very selective sample of crop models used in climate change studies. A larger group of process-based crop models have already been improved and/or tested satisfactorily with data from field experiments, but they are ignored by Long *et al.* (*1*–*3*).

Furthermore, the effects of rising CO_2 on crop yields in the past have been relatively small. Other factors such as technology development have been more important and are likely to be so in the future (*4*). For instance, yields of wheat in Europe have nearly tripled between 1961 and today, mainly because of the development of new varieties and improved management (*4*, *5*). Changes in CO_2 concentration over the same period explain less than 4% of this yield increase, assuming 0.08% increase per ppm CO_2 (*4*), which is similar to the data by Long *et al.* This relative insignificance of the CO_2 signal negates much of Long *et al.*'s contention that the experimental technology used to estimate yield changes has a considerable effect on predictions of global food supply (*6*).

Long *et al.* are also extrapolating from the crop productivity per unit area of plots, ignoring important regional and higher level relationships. For instance, crop management, which is largely determined by socio-economic conditions, is often suboptimal, reducing potential yields and some of the benefits of rising CO_2. Estimations of regional crop yields will also depend on relationships between climate and land use change (*4*). Clearly, future food production depends on several factors such as technology development, including crop management, land use change, and climate effects, which require a much more integrated approach than that offered by Long *et al.*

FRANK EWERT,[1]* JOHN R. PORTER,[2] MARK D. A. ROUNSEVELL[3]

[1]Department of Plant Sciences, Group Plant Production Systems, Wageningen University, P.O. Box 430, 6700 AK Wageningen, The Netherlands. [2]Faculty of Life Sciences, University of Copenhagen, 10 2630 Taastrup, Denmark. [3]Department of Geography, Université Catholique de Louvain, Place Pasteur, 3, Louvain-la-Neuve, Belgium.

*To whom correspondence should be addressed. E-mail: frank.ewert@wur.nl

References

1. S. Asseng *et al.*, *Field Crops Res.* **85**, 85 (2004).
2. F. Ewert *et al.*, *Agric. Ecosyst. Environ.* **93**, 249 (2002).
3. P. D. Jamieson *et al.*, *Agric. Ecosyst. Environ.* **82**, 27 (2000).
4. F. Ewert, M. D. A. Rounsevell, I. Reginster, M. J. Metzger, R. Leemans, *Agric. Ecosyst. Environ.* **107**, 101 (2005).
5. Food and Agriculture Organization of the United Nations (FAO), *FAO Statistical Databases*, www.fao.org (2005).
6. F. M. Tubiello *et al.*, *Eur. J. Agron.*, in press.

Response

OUR RESEARCH ARTICLE DID NOT CRITICIZE the design of models used to predict global change impacts on future food supply. We argued that reliable model projections require accurate model parameterization. Data from the fully open-air field treatments with elevated CO_2 (FACE) indicate that the commonly used parameterization for the CO_2–fertilization effect is overoptimistic. We recognized that rising CO_2 is only one of many factors affecting future food supply, but CO_2 has been shown to be pivotal in projecting an increase versus a decrease in future food supply under global change (*1*–*4*).

Ewert *et al.* suggest that rising CO_2 has had, and will have, little impact, attributing only 4% of wheat yield improvement over the past 30 years to rising CO_2. This 4% is consistent with FACE but not non-FACE results (extrapolating from Fig. 2A). We agree that the 50 ppm increase in CO_2 may have played a relatively minor role in the past 30 years. But it is projected to increase to 180 ppm over the next 50 years and thus has the potential to be far more important.

Ewert *et al.* note the tripling of wheat yield since 1960, due to technology development, and imply that this will continue. Large increases in cereal crop yields have been achieved by improved harvest index and nitrogen fertilization, but returns on these strategies are diminishing (*5*, *6*). Although we hope that the improvements of past decades can be maintained, it will not happen without innovative new approaches and a perceived need for crop adaptation. In our judgment, urgent action is needed given the long times required to develop new cultivars adapted to change and able to realize in farmers' fields the higher CO_2 fertilization effect observed in protected environments. Equally, field-scale manipulations of CO_2, including, for example, tropical locations, interactions with rising ozone, and genetic variation, are needed. Without this more secure parameterization, projections of future global food security may have feet of clay. If we fail in taking these practical measures, then might history say, were they modeling while the world's grain supply burned?

STEPHEN P. LONG,[1] ELIZABETH A. AINSWORTH,[2] ANDREW D. B. LEAKEY,[3] DONALD R. ORT,[2] JOSEF NÖSBERGER,[4] DAVID SCHIMEL[5]

[1]Departments of Plant Biology and Crop Sciences, University of Illinois at Urbana-Champaign, Urbana, IL, 61801, USA. [2]Photosynthesis Research Unit, U.S. Department of Agriculture–Agricultural Research Service, Urbana, IL 61801, USA. [3]Institute for Genomic Biology, University of Illinois at Urbana-Champaign, Urbana, IL 61801, USA. [4]Institute for Plant Sciences, ETH Zurich, 8902 Zurich, Switzerland. [5]Climate and Global Dynamics Division, National Center for Atmospheric Research, Boulder, CO 80307, USA.

References

1. M. Parry, C. Rosenzweig, M. Livermore, *Philos. Trans. R. Soc. Lond. B Biol. Sci.* **360**, 2125 (2005).
2. C. Rosenzweig, M. L. Parry, *Nature* **367**, 133 (1994).
3. H. Gitay, S. Brown, W. Easterling, B. Jallow, in *Climate Change 2001: Impacts, Adaptation, and Vulnerability*, J. J. McCarthy *et al.*, Eds. (IPCC/Cambridge Univ. Press, Cambridge, 2001), pp. 237–342.
4. M. L. Parry, C. Rosenzweig, A. Iglesias, M. Livermore, G. Fischer, *Global Environ. Change Human Policy Dimensions* **14**, 53 (2004).
5. M. P. Reynolds, A. Pellegrineschi, B. Skovmand, *Ann. Appl. Biol.* **146**, 39 (2005).
6. V. J. Shearman, R. Sylvester-Bradley, R. K. Scott, M. J. Foulkes, *Crop Sci.* **45**, 175 (2005).

Problems with University Hiring in Spain

SPAIN HAS COME A LONG WAY IN THE PAST 30 years, but in regards to science and technology the country is suffering from growing pains on its way to claiming its proper place as one of the top 10 economies of the world [Spain ranked eight in total GDP in 2005 according to the World Bank (*1*)]. The abuse suffered by Antonio Ferriz ("Spain reconsiders its university reform law," X. Bosch, News of the Week, 10 Nov. 2006, p. 911) would be inconceivable in a system where merit is the principal factor for hiring faculty.

Although in recent times, the top universities in Spain have followed well-established procedures in the selection of faculty, the process is riddled with irregularities at smaller universities, which are managed by local governments that place a low priority on research. Increased autonomy for universities must come with increased responsibility. Not hiring the best candidate available constitutes dereliction of duty by university officials. They are responsible to the community that maintains the university.

The new university reform law represents a step forward in the process of qualification of candidates, but there are no incentives for universities to hire the best possible candidates. Inbreeding and ethical violations are likely to continue at all but the best universities in Spain until autonomy and responsibility run concurrently.

JUAN J. MANFREDI

Professor and Chair, Department of Mathematics, University of Pittsburgh, Pittsburgh, PA 15260, USA.

Reference

1. See http://web.worldbank.org/WBSITE/EXTERNAL/DATASTATISTICS/0,,contentMDK:20399644~menuPK:3504474~pagePK:64133150~piPK:64133175~theSitePK:239419,00.html.

ALTHOUGH DISCUSSION OF THE PROBLEM OF inbreeding in Spanish university hiring practices is welcome ("Spain reconsiders its university reform law," X. Bosch, News of the Week, 10 Nov. 2006, p. 911), it is frustrating to see the debate so narrowly centered around the regulations related to details of hiring procedures. The present system is focused on controlling the procedures (not unlike other European systems) instead of the outcomes. It is sadly true that if universities were left to their own devices, too many decisions would be plainly wrong. But legislating to force academies to make the right choice is a poor remedy for a deeper illness. The real questions are why universities are making poor hiring decisions, and how to reverse this tendency. The answers must be based on the current reality that the general interests of a university and its drive toward excellence are at odds with the interests of its members. A Spanish academic nowadays benefits much less from hiring a world-class, independent new colleague than from promoting a less-qualified subordinate already at the university. This is the heart of the matter and where the debate should be focused: not how to force academies to act against their interests, but how to align these interests with those of their universities. A culture of excellence sinks in very slowly, and growing numbers of excellent academies are thriving in Spain by swimming against the tide. It is time to turn it. If temporary measures are necessary, they should be clearly identified as such, distinguishing them from the final model, in which universities and their members face the consequences of their decisions, as in any other sector of society.

EMILIO ARTACHO

Department of Earth Sciences, University of Cambridge, Cambridge CB2 3EQ, UK.

CORRECTIONS AND CLARIFICATIONS

News of the Week: "Astrobiology fights for 'its life'" by A. Lawler (19 Jan., p. 318). The picture credits on page 320 were reversed. The picture of Lynn Rothschild is courtesy of Roberto Antoni/Lynn Rothschild/NASA, and the Centro de Astrobiología building in Madrid is courtesy of the center.

News Focus: "Don't pretty up that picture just yet" by J. Cousin (22 Dec 2006, p. 1866). The caption accompanying this image in the story was misleading. The original version of the image is on the left, and the modified one is on the right.

Breakthrough of the Year: "The Poincaré conjecture—proved" by D. Mackenzie (22 Dec. 2006, p. 1848). The news story stated that of the three groups that have worked through the missing details of Perelman's papers, only Cao and Zhu claim to have finished the complete proof of the Geometrization Conjecture. In fact, Kleiner and Lott also make that claim.

TECHNICAL COMMENT ABSTRACTS

COMMENT ON "Evolutionary Paths Underlying Flower Color Variation in *Antirrhinum*"

Mark D. Rausher

Although Whibley *et al.* (Reports, 18 August 2006, p. 963) argue for the presence of high-fitness ridges in the *Antirrhinum* floral-color adaptive landscape, their data are equally compatible with adaptive landscapes having a single peak and no ridges. Their demonstration of divergent selection across a hybrid zone argues against the presence of adaptive ridges.

Full text at www.sciencemag.org/cgi/content/full/315/5811/461a

RESPONSE TO COMMENT ON "Evolutionary Paths Underlying Flower Color Variation in *Antirrhinum*"

Annabel C. Whibley, Nicolas B. Langlade, Christophe Andalo, Andrew I. Hanna, Andrew Bangham, Christophe Thebaud, Enrico Coen

Rausher's assertion that divergent selection across a hybrid zone is incompatible with adaptive ridges, although intuitively reasonable, is incorrect on several fronts. His alternative hypothesis of a single moveable peak predicts a sharp environmental transition across the hybrid zone that is not supported by observations. Thus, a high fitness path still provides the most straightforward explanation of our data.

Full text at www.sciencemag.org/cgi/content/full/315/5811/461b

MUSIC

Riffs on Numerical Themes

On a recent frigid evening in New York City, I went downtown to hear some jazz. In most respects it was a perfectly normal concert: a quartet led by the saxophonist Rudresh Mahanthappa promoting a new CD in the sort of high-end jazz bar that seats about 100 people, all of them squinting in disbelief at the price of drinks. But there was also a tantalizing secret for those in the know. Mahanthappa composed the music for his latest album, *Codebook*, using number theory—the branch of mathematics that has born such fruits as the Fibonacci sequence (the inspiration for centuries of art and mysticism, including the best-selling if often reviled *Da Vinci Code*), and the tools of cryptography.

One could say that mixing math and music is nothing new. As the German philosopher Gottfried Leibniz put it, "Music is the pleasure the human mind experiences from counting without being aware that it is counting." But whereas all music is built to some extent on mathematical structures, Mahanthappa takes the relationship to the next level. Math isn't just the medium of his art, it is also his subject.

Take for example his tune "Farther and In Between." The melodies batted between sax, bass, and piano are permutations of a scale built on the semitone intervals (1,4,2,8,5,7). It happens that 142,857 is one of the so-called cyclical numbers, which have long fascinated number theorists and numerologists alike (not to conflate the two). Cyclical numbers with *n* digits have the interesting property that multiplying one of them by a whole number between 1 and *n* generates a new number having the same digits rearranged (e.g., $142857 \times 3 = 428571$). Mahanthappa uses this arithmetical curiosity as a constraint for improvisation: play anything as long as it generates a cyclical number.

But what does the audience get out of such mathematical mischief? The pessimist in me says that they get nothing at all, that it's just a gimmick. Let's call that the null hypothesis. If you've been to modern art museums, you'll know immediately what I mean. (I cannot forward to read the artist's explanation of the pile of tin cans covered in panty hose and melted bubble gum, you learn that it represents space-time evolution, artificial intelligence, or ...)

To test the null hypothesis, I gave Mahanthappa the best chance possible to prove it wrong by assembling an ideal audience. Sitting around the table with me were two musicians with no formal mathematical training, a mathematician with no musical training, a couple of mathematicians who are also accomplished musicians, and, as a control group, a lawyer and a social worker. I passed around a cheat sheet so that everyone knew what to listen for. (The day before the concert, I met with Mahanthappa and wrote down the order of the pieces to be played and the mathematical basis of each.) The lights dimmed, the band mounted the stage, and the experiment began.

Mahanthappa launched us into the deep end right away, both musically and mathematically. Before the rest of the instruments joined, he broke the silence with a sequence of notes so fast and jittery it was like a spider dancing on his sax. The manic melodies of the tune "The Decider," are a mapping of the Fibonacci sequence (2) onto the 12-tone musical scale. From that initial shock, the band carried the piece aloft in what felt like a series of booster rockets before reaching the seemingly free-floating (but actually quite structured) space of improvisational jazz.

Using the Fibonacci sequence seems like an arbitrary choice, perhaps verging on a gimmick. Wouldn't a random sequence do just as well? According to Mahanthappa, the choice rises above gimmickry for two reasons. For one, he says, taking the sequence as his inspiration and constraint generates music he could not have produced otherwise. For another, he claims, the mapped sequence has unique musical behaviors. "It sounds right no matter what key the others are comping (3) in," he told me. "I tried alternative sequences and they didn't have that property."

Fair enough. However, such subtleties didn't immediately come across to my test audience. "The mathematical themes are difficult to hear," remarked Michael Thaddeus (an algebraic geometer at Columbia University) with furrowed brow. "Well, it is called *Codebook* after all," he quipped. And for some of the pieces—such as "Frontburner," in which a Coltrane melody has been run through several layers of encryption—no human ear, no matter how prepared, would be able to detect Mahanthappa's invention.

Far more apparent than any of the individual mathematical tropes was an overall sense of lush complexity. "The drummer in particular was using rhythmic elements from Indian classical music in a way that was clearly far beyond that of an amateur," observed Manjul Bhargava, a number theorist (and tabla performer) at Princeton University. (Indeed, the drummer, Dan Weiss, is a student of the renowned Calcutta tabla player Samir Chatterjee.)

But as the show went on, mathematical neurons did begin to fire. Thaddeus deduced that the melodies in "Farther and In Between" get their jumpy quality from the lack of consecutive digits in the cyclical numbers. He and Bhargava were also wise to the math within another tune, "Enhanced Performance," which is built on a nested set of accelerating polyrhythms. (Mahanthappa dedicated the piece to steroid use among Olympic athletes, and knowing this contributed an extra squirt of adrenaline.) Nor did you have to be a mathematician (or a musician) to observe many of the tricks. Caroline Trowbridge, a recent graduate of Yale Law School, easily detected that layered within several of the tunes—but especially "Play It Again Sam," dedicated to Samuel Morse—were the performers' names in Morse code, like signatures on sound paintings.

So on this basis, I can already rule out the null hypothesis. The math is definitely more than just a gimmick, even to the untrained ear. But what then does the audience get out of the experience? This is where the experiment got interesting. The band played two sets, and the breather between them, like a coffee break between lectures at a good scientific conference, brimmed with heated, cross-disciplinary conversation. Topics ranged from how constraints act as dynamos for creativity (for example, the sonnet form in poetry) and the

CREDIT: JOE SCRUFF

biological constraints that produce Fibonacci numbers in nature to the independent discovery (far earlier than in Europe) and use of Fibonacci numbers in ancient Indian poetry. With our brains fizzing from such cross-talk, the second set was all the more enjoyable.

And that supports my alternative hypothesis for what an audience can get out of a Masada harpa performance—a unique jazz-based occasion to explore ideas. Trowbridge called it "the secret knowledge effect"—that heightening of the senses from an awareness of hidden layers of meaning—and I agree. In addition, the quartet's virtuosity makes their playing a pleasure to behold, no matter how one feels about jazz. But before taking my word for it, I recommend replicating the experiment for yourself—with the CD if you can't catch a performance.

–John Bohannon

Notes

1. The quartet comprises Rudresh Mahanthappa, Vijay Iyer, François Moutin, and Dan Weiss.
2. The sum of each pair of consecutive numbers in the Fibonacci sequence {0, 1, 1, 2, 3, 5, 8, 13, 21, ...} generates the next. The ratios of consecutive Fibonacci numbers {1/2, 2/3, 5/8, 8/13, ...} converge on the irrational number Φ (0.618033989...), known as the golden mean.
3. That's jazz-speak for "accompanying."

10.1126/science.1139629

SCIENCE AND RELIGION

Arguing for Atheism

Michael Shermer

> There is no position on which people are so immovable as their religious beliefs. There is no more powerful ally one can claim in a debate than Jesus Christ, or God, or Allah, or whatever one calls this supreme being. The religious factions that are growing throughout our land are not using their religious clout with wisdom. They are trying to force government leaders into following their position 100 percent. If you disagree with these religious groups on a particular moral issue, they complain, they threaten you with a loss of money or votes or both. I'm frankly sick and tired of the political preachers across this country telling me ... that if I want to be a moral person, I must believe in A, B, C, and D. Just who do they think they are?

The reviewer is at *Skeptic* magazine, 2761 North Marengo Avenue, Altadena, CA 91001, USA. E-mail: mshermer@skeptic.com

Such stirring words, spoken with such moral conviction, must surely come from an outraged liberal exasperated with the conservative climate of America today, and one can be forgiven for thinking that in a review of *The God Delusion* these are the words of Richard Dawkins himself, who is well known for not suffering religious fools gladly. But no. They were entered into the *Congressional Record* on 16 September 1981 by none other than Senator Barry Goldwater, the fountainhead of the modern conservative movement, the man whose failed 1964 run for the presidency was said to have been fulfilled in 1980 by Ronald Reagan, and the candidate whose campaign slogan was "In Your Heart You Know He's Right."

If Goldwater had been president for the past six years, I doubt that Dawkins would have penned such a powerful polemic against the infusion of religion into nearly every nook and cranny of public life. But here we are, and like Goldwater, Dawkins is sick and tired of being told that atheists are immoral, second-class, back-of-the-bus citizens. *The God Delusion* is his way of, like the Howard Beale character in the 1976 film *Network*, sticking his head out the window and shouting, "I'm as mad as hell, and I'm not going to take this anymore."

But *The God Delusion* is so much more than a polemic. It is an exercise to "raise consciousness to the fact that to be an atheist is a realistic aspiration, and a brave and splendid one. You can be an atheist who is happy, balanced, moral, and intellectually fulfilled." Dawkins wants atheists to quit apologizing for their religious skepticism. "On the contrary, it is something to be proud of, standing tall to face the far horizon, for atheism nearly always indicates a healthy independence of mind and, indeed, a healthy mind."

Dawkins also wants to raise consciousness about the power of Darwin's dangerous idea of natural selection. He believes that most people—even many scientists—do not fully understand just how powerful an idea it is. He attributes that failure to the need to be steeped and immersed in natural selection before you can truly recognize its power. In this context, natural selection "shatters the illusion of design within the domain of biology, and teaches us to be suspicious of any kind of design hypothesis in physics and cosmology as well."

Out of obligation, of course, Dawkins reviews and offers rebuttals to all the standard arguments for God's existence. He concentrates on dissecting the anthropic principle and dismantling intelligent design creationism. (As part of the latter efforts, he redirects the creationists' argument from complexity to show that God must have been designed by a superintelligent designer.) He then builds a case for "why there almost certainly is no God." The remainder of the book outlines possible evolutionary origins of morality and religious belief, a justification for being hard on religion, childhood religious indoctrination as child abuse, and an elegant commentary on the progressively changing moral zeitgeist. Dawkins closes with a tribute to the power and beauty of science, which no living writer does better.

When I received the bound galleys for *The God Delusion*, I cringed at the title, wishing it were more neutral (why not, say, *The God Question*?). As I read the book, I found myself wincing at Dawkins's references to religious people as "faith-heads," as being less intelligent, poor at reasoning, or even deluded, and to religious moderates as enablers of terrorism. I shudder because I have religious friends and colleagues who do not fit these descriptors, and I empathize at the pain such pejorative appellations cause them. In addition, I am not convinced by Dawkins's argument that without religion there would be "no suicide bombers, no 9/11, no 7/7, no Crusades, no witch-hunts, no Gunpowder Plot, no Indian partition, no Israeli Palestinian wars, no Serb Croat Muslim massacres, no persecution of Jews as 'Christ-killers,' no Northern Ireland 'troubles'...." In my opinion, many of these events—and others often attributed solely to religion by atheists—were less religiously motivated than politically driven, or at the very least involved religion in the service of political hegemony.

I also never imagined a book with this title would ever land on bestseller lists in the United States. But I was wrong. The data have spoken. *The God Delusion* is a runaway bestseller: a market testimony to the hunger many people—far more, I now think, than polls reveal—have for someone in a position of prestige and power to speak for them in such an eloquent voice. Dawkins's latest book deserves multiple readings, not just as an important work of science, but as a great work of literature.

10.1126/science.1138989

THE EARLY YEARS

Algorithm-Guided Individualized Reading Instruction

First grade students achieved stronger learning outcomes in reading when teachers fine-tuned instruction to individual students under the guidance of A2i software

Carol McDonald Connor,[1]* Frederick J. Morrison,[2] Barry J. Fishman,[3] Christopher Schatschneider,[1] Phyllis Underwood[1]

Reading and writing are among the most important skills in today's information-driven world. Yet, according to the National Assessment of Educational Progress (*1*), more than one-third of children in the United States lack fundamental reading skills. This rate is even higher for children living in poverty. Illiteracy is a society-wide and costly problem and is associated with increased rates of grade retention, referral to special education, high school dropout, and juvenile delinquency (*2*). Many children fail to reach proficient levels in reading only because they do not receive the amount and type of instruction they need (*3*–*5*).

Much of the controversy regarding the best way to teach children how to read has focused on whether instruction should be code-based, such as phonics, or based on whole language and meaning (*6*–*8*), but this debate may miss the point. Although most children develop stronger reading skills when they receive a balance of explicit decoding instruction in combination with meaningful reading activities (*7*, *9*–*12*), even a balanced approach theory assumes that one approach, if it is the right one, will be equally effective for all children (*13*, *14*). Instead, the efficacy of any particular instructional practice may depend on the skill level of the student. Instructional strategies that help one student may be ineffective when applied to another student with different skills (*15*–*21*).

About the Intervention

In a previous study, children who began first grade with below-average letter-word reading skills demonstrated greater improvement with greater amounts of time in explicit teacher-managed code-focused instruction (table S1) (*16*). For students who began with above-average reading skills, greater growth in letter-word reading skills was actually related to less time in teacher-managed code-focused activities. We also found an interaction between vocabulary and instruction. Children with above-average vocabulary scores at the start of the school year made greater gains in word reading when they spent more time throughout the year in child-managed meaning-focused instruction (such as independent reading). In contrast, children who began with below-average vocabulary scores achieved the strongest growth in word reading skills with a combination of instruction patterns. Their reading skills grew more when they initially spent more time on code-based activities, with increased child-managed meaning-focused instruction as the school year progressed.

Reading instruction. Lessons are tailored to individual students.

Algorithms used by Assessment to Instruction (A2i) Web-based software (*22*) incorporate these child-by-instruction interactions and, for each child, provide recommendations updated monthly regarding amounts and types of instruction (figs. S1 and S2).

Individualizing instruction with the use of A2i does not represent a new reading curriculum but rather a new way of implementing current reading programs. All literacy activities are indexed to dimensions of instruction (code- versus meaning-focused, teacher- versus child-managed, and change over time (*16*) (table S1). The dimension that describes code- versus meaning-focused instruction captures the content of the activity. Code-focused instruction includes those activities designed to help students achieve proficient phonological decoding and word reading skills (*14*). Meaning-focused instruction is designed to teach children how to extract and construct meaning from text (*23*). The dimension teacher- versus child-managed instruction identifies who is responsible for focusing the students' attention on the learning activities at hand—the teacher or the student (*14*–*16*). Teacher-managed instruction may be highly interactive, such as when the teacher is leading a discussion. Child-managed instruction includes activities in which students are expected to work independently (see photograph, left) or with peers. Change over time captures the impact of changing the focus of instruction time through the school year (*16*).

These dimensions operate simultaneously so that any language arts activity falls in one of four sectors (table S1). For example, children reading together in the library are participating in a child-managed, meaning-focused activity. The teacher instructing the children in how to segment or blend phonemes in words is leading a teacher-managed, code-focused activity.

In addition to recommending amounts and types of instruction, A2i algorithms use children's reading scores to help teachers effectively group the children for instruction. Lesson planning software helps teachers implement this individualized instruction on a daily basis (appendix SA and fig. S2).

The individualizing instruction intervention asked teachers to teach reading for at least 90 minutes a day during a dedicated block of time, to provide instruction to children with similar reading skills in small groups, and to follow the A2i recommended amounts and specific types of instruction. Control teachers were also expected to have a dedicated daily reading block (of 90 minutes) and to use small groups according to school policies. Assessment results were shared with all teachers (appendices SA and SB). All teachers in the treatment group received the same amount of training on how to plan and implement individualized reading instruction using A2i. Control teachers received no professional development from our program during this

[1]Florida Center for Reading Research, Florida State University, Tallahassee, FL 32301, USA. [2]Department of Psychology, [3]School of Education, University of Michigan, Ann Arbor, MI 48109, USA.

*Author for correspondence. E-mail: cconnor@fsu.edu

CREDIT: TARO MASUYAMA

experimental phase. Thus, expectations for amount and structure of reading instruction were similar across groups, whereas the access to A2i recommendations and professional development was different.

Methods

This cluster-randomized field trial asked whether providing individualized reading instruction (as guided by A2i algorithms) would cause stronger student reading outcomes. The study was conducted in an ethnically and economically diverse school district in Florida in 10 schools, with 47 teachers and 616 first-grade students. Schools were matched and paired on key indicators, with one randomly assigned to the treatment group (n = 22 teachers) and the other to the control group (n = 25 teachers). All participating schools had students living in poverty (table S2 and appendix SB).

Students' language and literacy skills were assessed in August 2005 and in January and May 2006 with the use of the *Woodcock Johnson Tests of Achievement III* (24), which are predictive of performance on state and federal achievement tests (*1*) (table S3).

Results and Implications

Our results revealed that individualized instruction, guided by A2i and supported by professional development, promoted stronger student reading growth compared with that of the control group, controlling for fall reading and vocabulary scores as well as child and school characteristics (residualized mean difference = 2.63, 95% confidence interval = 0.37 to 4.90; appendices SB and SC and table S5).

However, individualizing student instruction using A2i software even with professional development, proved challenging for some of the teachers in the study. We captured fidelity of treatment in two ways, through classroom observations and by recording time spent using A2i (appendix SC). Based on classroom observations, by February, nine teachers (41%) implemented the intervention with moderate to high fidelity (table S4). Two teachers (9%) did not implement the intervention until toward the end of the year. Teachers' use of A2i software also varied. On average, they used A2i for 180 minutes from 1 September to 31 May (range 15 to 374 minutes, median = 191 minutes). Six teachers used the software for less than 100 minutes, whereas 11 teachers used the software for more than 200 minutes. Teachers who used A2i more frequently also tended to better implement individualized instruction in the classroom (correlation, r = 0.34, P = 0.014).

Although it is not possible to fully disentangle the impact of individualizing instruction using A2i and the professional development teachers received, it is unlikely that the reading outcomes were due to teacher training alone. The treatment teachers all received the same amount of training, yet varied in the number of minutes they used A2i and the extent to which they individualized instruction. Thus, we could examine these two markers of fidelity as they related to children's reading outcomes, holding the amount of training constant. We found that the more time teachers spent using A2i, the stronger were their students' reading skills by the end of the year (a 1-point increase in *W* score for every additional 50 minutes teachers used A2i, $t(20)$ = 2.97, P = 0.008, table S6). There was also an interaction with students' initial vocabulary scores. When teachers used A2i more frequently, on average, their students demonstrated stronger outcomes compared with children who had similar initial vocabulary scores in the control classrooms. Additionally, in higher fidelity classrooms, students with below-average initial vocabulary skills (including many children from high-poverty families) achieved reading scores that were generally comparable to students with higher initial vocabulary scores (tables S7 and S8, fig. S3, and the figure shown below). Taken together, using A2i and implementing A2i recommendations in the classroom appear to contribute to stronger student outcomes over and above the training teachers received, although no doubt both aspects contribute to better reading results.

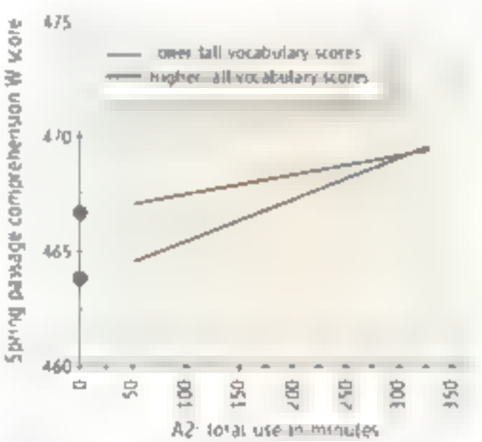

Interaction between A2i use and vocabulary. Spring scores for first graders who started the year with below-average vocabulary (blue) (25th percentile; *W* score = 474, age equivalent, 6 years) and above-average vocabulary (red) (75th percentile; *W* score = 486, age equivalent, 8 years). Mean terminal scores are shown for children in the control group (circles) and the treatment group (lines); treatment group results vary depending on teachers' A2i use (table S6).

Thus, individualized reading instruction guided by the A2i algorithm and coupled with professional development supports teachers in their efforts to provide optimally effective reading instruction for all children.

References and Notes

1. National Assessment of Educational Progress, *The Nation's Report Card* (National Center for Education Statistics, Washington, DC, 2005).
2. A. J. Reynolds, S.-R. Ou, *Child. Youth Serv. Rev.* **26**, 1 (2004).
3. F. R. Vellutino *et al.*, *J. Educ. Psych.* **88**, 601 (1996).
4. E. J. Morrison, H. J. Bachman, C. M. Connor, *Improving Literacy in America: Guidelines from Research* (Yale Univ. Press, New Haven, CT, 2005).
5. B. R. Foorman *et al.*, *J. Educ. Psych.* **90**, 37 (1998).
6. D. Ravitch, in *The Great Curriculum Debate: How Should We Teach Reading and Math?*, T. Loveless, Ed. (Brookings Institution Press, Washington, DC, 2001), pp. 210–228.
7. K. Rayner *et al.*, *Psych. Sci. Public Interest* **2**, 31 (2001).
8. K. L. Dahl, P. A. Freppon, *Reading Res. Q.* **30**, 50 (1995).
9. J. T. Guthrie *et al.*, *J. Educ. Res.* **94**, 145 (2001).
10. B. M. Taylor *et al.*, *Elem. Sch. J.* **101**, 121 (2000).
11. P. Cunningham, D. Hall, in *Teaching Every Child Every Day: Learning in Diverse Schools and Classrooms*, K. R. Harris, S. Graham, D. Deshler, Eds. (Brookline Books, Cambridge, MA, 1998), pp. 32–78.
12. M. Pressley, *Reading Instruction That Works: The Case for Balanced Teaching* (Guilford, New York, 1998).
13. S. M. Ross *et al.*, *Psych. Sch.* **34**, 171 (1997).
14. National Reading Panel, "Teaching children to read: an evidence-based assessment of the scientific research literature on reading and its implications for reading instruction" (NIH Pub. No. 00-4769, National Institute of Child Health and Human Development, Washington, DC, 2000).
15. C. M. Connor *et al.*, *J. Educ. Psych.* **96**, 682 (2004).
16. C. M. Connor *et al.*, *Sci. Stud. Reading* **8**, 305 (2004).
17. C. Juel, C. Minden-Cupp, *Reading Res. Q.* **35**, 458 (2000).
18. C. M. Connor *et al.*, *Sci. Stud. Reading* **11**, 243 (2007).
19. C. M. Connor *et al.*, *J. Educ. Psych.* **98**, 665 (2006).
20. J. K. Torgesen, *Learn. Disabil. Res. Pract.* **15**, 55 (2000).
21. R. J. Sternberg, in *Human Abilities: Their Nature and Measurement*, J. Dennis, Ed. (Lawrence Erlbaum, Hillsdale, NJ, 1996), pp. 167–181.
22. A teacher version of A2i will be available after 1 August 2007. Information about A2i is available online (http://kinetics.coe.umich.edu/A2i/login.asp), with login A2idemo and password ISI06. Click the Classroom View button located under the ISI logo to view A2. The software and protocol are currently available to other researchers upon request.
23. C. E. Snow, *Reading for Understanding* (RAND Education and the Science and Technology Policy Institute, Santa Monica, CA, 2001).
24. N. Mather, R. W. Woodcock, *Woodcock Johnson III Tests of Achievement: Examiner's Manual* (Riverside, Itasca, IL, 2001).

25. We thank A. Goldberg (the software programmer), the school district, teachers, parents, students, and the ISI Researchers. Funding was provided by the U.S. Department of Education, Institute for Education Sciences, Cognition and Student Learning (R305H04013) and the National Institute of Child Health and Human Development (RO1 HD48539). World Class Schools, and James Campbell and Associates. C.M.C., F.J.M., and B.J.F. may, in the future, have a financial interest in the A2i intervention.

Supporting Online Material
www.sciencemag.org/cgi/content/full/315/5811/464/DC1

10.1126/science.1134513

GENETICS

SNPs, Silent But Not Invisible

Single nucleotide polymorphisms that are considered "silent" can affect protein folding.

Anton A. Komar

Single nucleotide polymorphisms (SNPs) are small genetic changes found in both coding and noncoding regions of the genome. The genetic code is degenerate in that most amino acids are represented by more than one triplet of nucleotide bases (a codon). Such codons are considered synonymous. Many SNPs are "silent" as they result in synonymous codon substitutions. Because these silent SNPs do not change the amino acid composition of the protein product, they have largely been assumed to exert no discernible effect on gene function or phenotype. But are silent SNPs indeed always silent? On page 525 in this issue Kimchi-Sarfaty *et al.* (*1*) provide evidence that naturally occurring silent SNPs can affect in vivo protein folding and, consequently, function. The study shows that substrate specificity of P-glycoprotein, the product of the multidrug resistance 1 (*MDR1*) gene, is altered by SNPs presumed to be synonymous and silent. How is this possible?

The original Beadle and Tatum hypothesis of "one gene, one enzyme"—the essence of the classic view of gene structure and function—started to break down almost as soon as it had been completely formulated (*2*). Cellular processes, including alternative RNA splicing and posttranslational protein modifications, create more than one protein product from a given sequence in the genome. Yet, it is widely assumed that a single messenger RNA (mRNA) encoding a polypeptide chain with a defined amino acid sequence will give rise to, during the process of translation, identical protein products in terms of their structure and activity, assuming that these products undergo the same co- and posttranslational modifications in the cell. This assumption is based on the widely accepted Anfinsen's principle, which states that the information necessary to specify the native three-dimensional structure of a protein—which largely defines its function—is contained solely in its amino acid sequence (*3*).

Although these two principles can still be applied to a wealth of genes and proteins, a polypeptide chain can exist in the cell in a number of alternative conformations, revealing different functions and/or activities. For example, a neuronal isoform of cytoplasmic polyadenylation element binding protein in the sea slug (*Aplysia californica*) exists in two different forms, a soluble inactive form and an insoluble active form that regulates synaptic protein synthesis (*4*). The molecular mechanisms that can drive the folding of a polypeptide chain in vivo into alternative conformations are still mostly obscure.

The crowded cellular environment, folding catalysts, and accessory proteins all contribute to protein folding in the cell (*5*). Could there be other factors affecting the final conformation of a protein? In 1987, Purvis and colleagues proposed that "the way in which some proteins fold is affected by the rates at which regions of their polypeptide chains are translated in vivo" (*6*). They hypothesized that certain "gene sequences have evolved to control the rate of translational elongation such that the synthesis of defined portions of their polypeptide chains is separated temporally."

The rate of ribosome traffic on mRNA is known to be nonuniform and mainly modulated by both the general degeneracy of the genetic code (namely, the use of specific synonymous codons that is characteristic for a given organism) and the availability of cognate aminoacyl–transfer RNAs (tRNAs) that surround the ribosome during translation, poised to deliver amino acids. Within many organisms, a strong codon bias exists (*7*) and the amount of cognate tRNAs is directly proportional to the frequency of codon usage. Thus, infrequent codons in mRNA appear to be slowly translated, whereas frequent codons are rapidly translated.

Optimization of in vivo protein folding, which is thought to be cotranslational (*5*), might include the adaptation of codon selection along DNA (and hence, along corresponding mRNA) to a particular translation kinetics. Temporal separation of folding events during protein synthesis on the ribosome might thus avoid "unwanted" interactions within the growing polypeptide, ensuring high yield of the correctly folded protein. Therefore, altered translation kinetics of a defined mRNA due to, in particular, synonymous codon substitutions (which would not alter the amino acid sequence of the encoded polypeptide) might drive the in vivo folding of the same polypeptide chain into different conformations (see the figure).

This hypothesis is very difficult to prove using in vivo systems, because numerous quality-control mechanisms exist to get rid of incorrectly or abnormally folded and misfolded proteins (*8*). So far, supporting experimental data have been scarce, making the findings of Kimchi-Sarfaty *et al.* particularly important. The authors show that combinations of the three previously known SNPs for the *MDR1* gene (C1236T, G2677T, and C3435T) alter P-glycoprotein activity. P-glycoprotein is a multiple-transmembrane protein pump that transports various drugs out of cells. Its function can thus reduce the efficacy

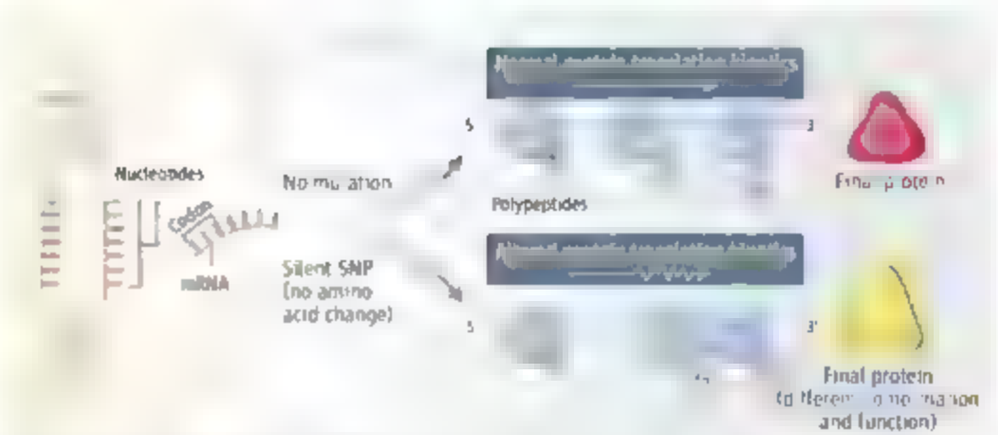

Translation kinetics and protein folding. Unaffected translation kinetics results in a correctly folded protein. Abnormal translation kinetics, caused by the ribosome moving faster or slower through certain mRNA regions, can produce a different final protein conformation. Abnormal kinetics may arise from a silent single nucleotide polymorphism (SNP) in a gene that creates a codon synonymous to the wild type codon. However, this synonymous codon substitution may lead to different kinetics of mRNA (protein) translation, thus yielding a protein with a different final structure and function.

The author is in the Department of Biological, Geological and Environmental Sciences, Cleveland State University, Cleveland, OH 44115, USA. E-mail: a.komar@csuohio.edu

of chemotherapy treatments. Kimchi-Sarfaty *et al.* found that P-glycoprotein inhibitors CsA and verapamil were less effective against proteins that were produced from haplotypes that consist of the polymorphic double (C1236T-G2677T, C1236T-C3435T, G2677T-C3435T) or triple (C1236T-G2677T-C3435T) variant combinations, suggesting that these protein products have altered conformations. Yet C1236T and C3435T polymorphisms do not change the amino acid sequence of P-glycoprotein. The C1236T polymorphism changes a CGC codon to CGT at amino acid position 412 of the polypeptide (both encode glycine) and the C3435T polymorphism changes ATC to ATT at position 1145 (both encode isoleucine). However, both polymorphisms result in changes from frequent to infrequent codons and therefore may slow down the ribosome traffic at the corresponding mRNA regions. These alterations may thus affect the co-translational folding pathway of P-glycoprotein, resulting in a different final conformation. Limited proteolysis and the use of a conformation-sensitive monoclonal antibody indeed revealed structural differences between the wild-type protein and the polymorphic haplotypes.

Artificial site-directed silent mutagenesis of synonymous codons (changing from infrequent to frequent) in certain genes also support the hypothesis that altered translation kinetics of mRNA might affect final protein conformation (*9*). However, until the study by Kimchi-Sarfaty *et al.*, there had been no example demonstrating that naturally occurring variations in synonymous codons in a defined gene can give rise to a protein product with the same amino acid sequence but different structural or functional features. By demonstrating that this is indeed the case, the study opens up a new avenue of research and suggests that silent SNPs might contribute to development and progression of certain diseases. If this is the case, then silent SNPs should not be neglected in determining the likelihood of the development and progression of many diseases such as Alzheimer's disease, myopia (a disease leading to a refractive defect of the eye), and others that are strongly linked to SNPs. This knowledge should also be taken into account in personalized drug treatment and development programs.

References and Notes

1. C. Kimchi-Sarfaty *et al.*, *Science* **315**, 525 (2007); published online 21 December 2006 (10.1126/science.1135308).
2. G. W. Beadle, E. L. Tatum, *Proc. Natl. Acad. Sci. U.S.A.* **27**, 499 (1941).
3. C. B. Anfinsen, *Science* **181**, 223 (1973).
4. K. Sakamoto *et al.*, *Cell* **115**, 893 (2003).
5. J. Frydman, *Annu. Rev. Biochem.* **70**, 603 (2001).
6. L. J. Purvis *et al.*, *J. Mol. Biol.* **193**, 413 (1987).
7. P. M. Sharp, T. M. Tuohy, K. R. Mosurski, *Nucleic Acids Res.* **14**, 5125 (1986).
8. B. Bulmer, *Nature* **325**, 728 (1987); A. Hamilton, A. Horwich, *Cell* **125**, 443 (2006).
9. A. A. Komar, T. Lesnik, C. Reiss, *FEBS Lett.* **462**, 387 (1999).

Published online 21 December 2006.
10.1126/science.1138239
Include this information when citing this paper.

ATMOSPHERES

The Jet-Stream Conundrum

Mark P. Baldwin, Peter B. Rhines, Huai-Ping Huang, Michael E. McIntyre

Fluid jets occur in Earth's atmosphere and oceans, and on other planets. A new theoretical view of jets has helped reveal why they form and how they interact with the surrounding fluid.

Jet streams, or "jets" for brevity, are concentrated, intense, elongated flows that often contain most of the kinetic energy in a flowing fluid. They are pervasive features of Earth's atmosphere and oceans, where they transport heat, chemicals, and even biota such as krill, and they are also abundant on other planets (see the figure).

Jets are observed to occur spontaneously on rotating planets whenever stratified atmospheres or oceans are forced into turbulent motion. Yet there is a mystery as to why jets exist at all—why is there this propensity to concentrate energy and momentum? A second mysterious property of jets is that they can act as flexible material barriers, inhibiting mixing across their axes. The strongest eastward jets provide expressways for the transport of chemicals and biota along their axes but severely inhibit mixing across their axes. A new theoretical paradigm (*1*) explains the abundance of jets, in any planetary atmosphere or ocean, in a simple manner. The paradigm combines field theory with chaotic (turbulent) fluid motion; in doing so, it captures delicate interactions that are crucial for forming and stabilizing jets. It shows that mixing a fluid on a rotating planet will invariably produce jets and that the two mysteries, jet formation and the inhibition of mixing, formerly regarded as two separate phenomena, are intimately related to each other.

Both jet formation and the inhibition of mixing are completely enigmatic in terms of

M. P. Baldwin is at Northwest Research Associates, Bellevue, WA 98009, USA. E-mail: mark@nwra.com. P. B. Rhines is in the Department of Oceanography, University of Washington, Seattle, WA 98195, USA. E-mail: rhines@ocean.washington.edu. H.-P. Huang is at the Lamont-Doherty Earth Observatory, Palisades, NY 10964, USA. E-mail: huai@ldeo.columbia.edu. M. E. McIntyre is in the Department of Applied Mathematics and Theoretical Physics, University of Cambridge, Cambridge CB3 0WA, UK. E-mail: m.e.mcintyre@damtp.cam.ac.uk

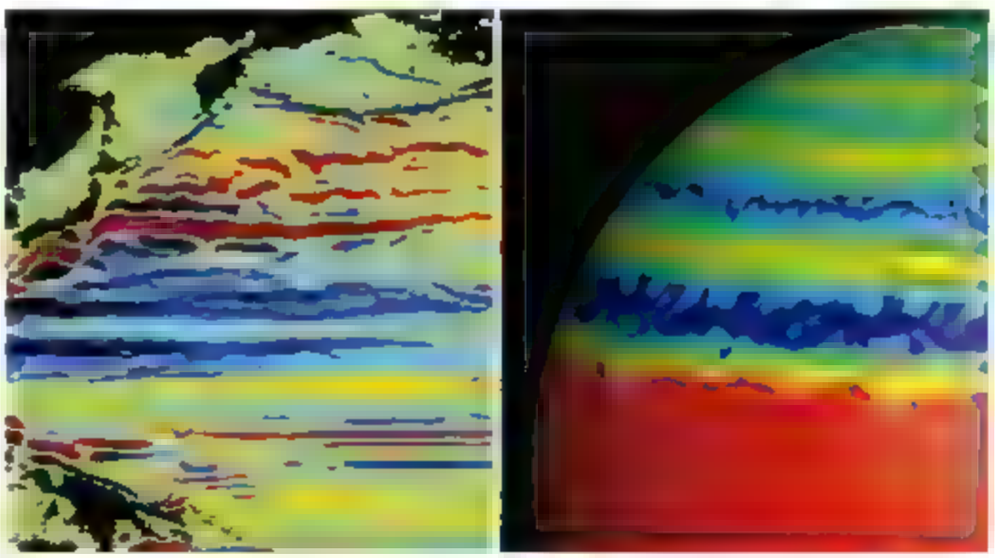

Jets near and far. (Left) Map of east-west current speeds at 400-m depth, simulated by an eddy-resolving ocean model. Red and blue indicate eastward and westward flows. [Adapted from Richards *et al.* (*11*)] **(Right)** Snapshot of a simulation for Jupiter, with red and blue indicating eastward and westward flows. [Adapted from Hempel *et al.* (*16*)]

standard turbulence theory. In the standard paradigm, a turbulent flow puts fluid particles into random walks that cause local mixing everywhere. Mixing implies that any quantity carried with the flow, such as a chemical tracer, will eventually become uniformly distributed. However, this contradicts the observed inhibition of mixing across jet axes. For example, the stratospheric polar night jet has different chemical properties on either side of the jet axis, thereby containing the ozone hole (2). Furthermore, in the standard paradigm, momentum is locally mixed like a chemical tracer. If this were the case, jets would immediately begin to dissipate, again contradicting observation. One reason for the persistence of jets is that there are wave motions and long-range, nonlocal interactions, the latter are not considered in the standard paradigm. It is these long-range interactions that are best understood using field theory.

The new paradigm keeps the idea of mixing but combines it with the long-range interactions. All waves involve restoring forces like those in an elastic medium, and they give rise to subtle long-range effects—outside the scope of the standard paradigm—including long-range momentum transport by waves (radiation stresses).

Also among the nonlocal effects are simple fields somewhat like the electrostatic field of a positively charged atomic nucleus. An atom in its ground state consists of the nucleus and its electrostatic field, together with a quantum field described by Schroedinger's equation. The quantum field represents the electron orbitals, which are carried along with the atomic nucleus no matter how the nucleus moves, as long as it moves slowly enough.

The fluid analog to the nuclear charge that holds the atom together is a scalar field called the potential vorticity (PV). PV is a unified measure of actual or potential swirl or shear (including planetary rotation) and is carried with the flow like a chemical tracer (*3*). Strong, compact PV anomalies carry with them recognizable velocity, buoyancy, and pressure fields in the surrounding fluid, just as atomic nuclei carry electron orbitals (again provided that the motion is slow enough). These structures are the familiar pancake-like vortices of cyclones and anticyclones, from ordinary cyclonic depressions to Hurricane Katrina and Jupiter's Great Red Spot. Knowing the PV anomaly is enough to deduce the entire vortex structure, just as knowing the nuclear charge is enough to deduce the entire atomic orbital structure. The deduction of the vortex structure from the PV field is called PV inversion (*4*). The new paradigm comes from combining the turbulence-theoretic idea of mixing with the field-theoretic idea of PV inversion and from giving the two ideas an equal status.

Planetary rotation provides a vast reservoir of PV, with a south-north gradient that enables wave propagation. PV inversion allows us to deduce the velocity field corresponding to displacements of the fluid (and PV contours). For example, the velocity field corresponding to a large-scale east-west wave pattern causes the wave (called a Rossby wave) to propagate westward. The PV contours therefore behave somewhat like elastic bands, and it is this so-called Rossby elasticity of the PV gradient that supports the propagation of Rossby waves.

The key to understanding jets is that PV, not momentum, tends to behave like a tracer. It is therefore PV that is mixed when the fluid becomes turbulent. Mixing weakens the south-north PV gradients, reducing the Rossby-wave elasticity and encouraging further mixing. This positive feedback tends to make the mixing spatially inhomogeneous. Thus, strong mixing creates a profile in latitude of alternating steep and weak PV gradients, called a PV staircase. This staircase corresponds (through PV inversion) to thin, fast eastward jets located at the latitudes of the steepest PV gradients and strengthened elasticity. Furthermore, the strengthened elasticity there, together with the jet shear, strongly inhibit mixing across the eastward jets (*2*, *5*). Thus, the new paradigm explains both jet formation and the inhibition of mixing.

The new paradigm demonstrates how a rotating planet can concentrate energy and momentum into jets, with faster rotation yielding not just one jet but several or many (*5*–*7*). Thus scaling theory links the planet's radius, its rotation rate, and the turbulent kinetic energy level of the fluid to the scale and spacing of its jets. In accord with this theory, Earth's atmosphere has just one or two jets per hemisphere, whereas Jupiter and Earth's oceans have many (see the figure).

Several new planetary flight missions—including NASA's Mars Reconnaissance Orbiter, the European Space Agency's Venus Express, and NASA's planned Juno mission to Jupiter—are poised to provide detailed observations of extraterrestrial atmospheres. These observations are needed to understand, for example, Jupiter's Great Red Spot, which owes its persistence to the surrounding jets and Rossby waves (*8*).

Although the new paradigm helps us understand the mystery of jet formation and persistence, the emerging details of many jet-related phenomena in nature remain to be fully explored. Earth's atmospheric jets have shifted poleward by about 1° since 1979 (*9*), with corresponding shifts in climate zones. New data sets and high-resolution computer simulations have revealed a previously unknown set of mid-ocean jets (*10*–*11*) (see the figure) as well as velocity extremes within the Antarctic Circumpolar Current (*12*). The first hints of how Antarctic krill use the circumpolar jets are emerging, promising new insights into the life cycle and food-chain role of the krill (*13*, *14*).

There remain open questions with important implications for climate prediction. For example, the precise circumstances under which PV staircases form remains elusive. Quantitative predictions of devastating storms, of thermohaline shutdown, and of dislocations in ecosystems and in Earth's heat balance also require a more detailed understanding of jets.

References and Notes

1. The paradigm emerged at an American Geophysical Union Chapman Conference, "Jets and Annular Structures," held in Savannah, GA, 9 to 15 January 2006. The proceedings will be published in a special issue of the *J. Atmos. Sci.*; also available at www-mete.kugi.kyoto-u.ac.jp/yoden/research/Chapman_Web/ChapmanConference2006/jets.htm
2. M. N. Juckes, M. E. McIntyre, *Nature* **328**, 590 (1987).
3. The Rossby-Ertel PV is the component of absolute vorticity normal to the stratification surfaces, divided by the mass per unit area enclosed between neighboring surfaces. When the surfaces move apart adiabatically, conservation of angular momentum can convert potential swirl into actual swirl, or actual shear, relative to the planet.
4. PV inversion is similar to finding the electric field due to a charge or the electron wave function of an atom. For a minimal tutorial, see www.atm.damtp.cam.ac.uk/people/mem/papers/ENCYC/epv-times.pdf
5. P. B. Rhines originated the idea of turbulently generated jets (*15*).
6. D. G. Dritschel, M. E. McIntyre, *J. Atmos. Sci.*, in press; also at Web site in (*2*).
7. T. J. Dunkerton, R. K. Scott, *J. Atmos. Sci.*, in press; also at Web site in (*2*).
8. S. Shetty, X. S. Asay-Davis, P. S. Marcus, paper presented at the American Physical Society annual meeting of the Division of Fluid Dynamics, 19 to 21 November 2006, Tampa Bay, Florida, U.S.A. (*2*).
9. Q. Fu *et al.*, *Science* **312**, 1179 (2006).
10. H. Nakano, H. Hasumi, *J. Phys. Oceanogr.* **35**, 474 (2005).
11. K. J. Richards *et al.*, *Geophys. Res. Lett.* **33**, L03605, 10.1029/2005GL024645 (2006).
12. C. W. Hughes, N. A. Maximenko, personal communication.
13. H. A. Fach, J. M. Klinck, *Deep-Sea Res. Part I Oceanogr. Res. Pap.* **53**, 987 (2006).
14. H. A. Fach, E. E. Hofmann, E. J. Murphy, *Deep-Sea Res. Part I Oceanogr. Res. Pap.* **53**, 1011 (2006).
15. P. B. Rhines, *J. Fluid Mech.* **69**, 345 (1975).
16. M. Heimpel, J. Aurnou, J. Wicht, *Nature* **438**, 193 (2005).

17. We thank M. Allison, Y. Hayashi, B. Harris, P. H. Haynes, B. J. Hoskins, W. A. Robinson, D.W.J. Thompson, G. Vallis, and S. Yoden for discussions, and NSF and NASA for funding the Chapman Conference. M.P.B. was supported by NSF's Climate Dynamics Program (under the U.S. CLIVAR Program), NOAA's Office of Global Programs, NASA's Supporting Research and Technology Program for Geospace Sciences, NASA's Living with a Star Program, and NASA's Oceans, Ice, and Climate Program.

10.1126/science.1131375

DEVELOPMENTAL BIOLOGY

The Mother of All Stem Cells?

Allan C. Spradling and Yixian Zheng

Partitioning of centrosomes during division of *Drosophila* germline stem cells may help keep one daughter as a stem cell and move the other toward differentiation.

The stem cells that sustain metazoan tissues face a difficult challenge. Each time a stem cell divides—it can divide indefinitely—it risks damage from errors in the duplication and segregation of genetic and cellular material that could stunt its vitality or propel it toward a cancerous state. Normally, each division must be asymmetric to ensure that only one daughter cell differentiates, while the other becomes a stem cell, thus renewing the stem cell population. Yet stem cells safely grow and divide many more times than other cell types, including their own daughters. On page 518 of this issue, Yamashita *et al.* (*1*) examine the role of one of the most fundamental cellular components in supporting stem cell function—the centrosome. Centrosomes organize the microtubule-rich mitotic spindle that directs how chromosomes and other materials are distributed between daughter cells at cell division (mitosis). The authors show that male germline stem cells in the fruit fly *Drosophila melanogaster* differentially position their mother and daughter centrosomes during mitosis. As part of this strategy, which ensures asymmetric division, the stem cell permanently retains the mother centrosome across many cell divisions, raising the possibility that differential centrosomal inheritance is essential to stem cell biology.

Unlike other known animal cell organelles, the two centrosomes inherited by daughter cells at division are not identical. All normal cells initially have one centrosome comprising a mother and daughter centriole as well as pericentriolar material. The mother centriole contains structures and proteins that are absent from the daughter centriole, and it nucleates more microtubules than the daughter. During each cell division cycle, the centrosome replicates. The mother centrosome retains the original mother centriole. In contrast, the daughter centrosome undergoes maturation during mitosis and during the G_1 phase of the next cell division cycle, converting its inherited daughter centriole into a new mother centriole (*2*). Whether this intrinsic asymmetry facilitates asymmetric stem cell division has remained a mystery.

The authors are in the Department of Embryology and Howard Hughes Medical Institute, Carnegie Institution, 3520 San Martin Drive, Baltimore, MD 21218, USA. E-mail: spradling@ciwemb.edu

Yamashita *et al.* took advantage of centrosomal asymmetry to follow the fates of mother and daughter centrosomes during germline stem cell division in the testes of *Drosophila*. These germline stem cells, which give rise to sperm, have already divided 12 or more times when they become established in their niche adjacent to stromal cells known as the hub (see the figure). Germline stem cells complete as many as 30 additional cell cycles over the life of the animal, each time sustaining themselves while producing one non–stem cell daughter, the gonialblast. Each gonialblast divides just six times before differentiating.

The authors genetically engineered flies to produce a centrosomal protein, known as PACT, tagged with green fluorescent protein. By inducing the expression of this fluorescent protein at different times, they could selectively label either mother or daughter centrosomes. Mother centrosomes were almost always located near the hub, which ensured that after mitosis they would be inherited by the daughter that remains in the niche and remains a stem cell. Daughter centrosomes, on the other hand, always migrated to the opposite end of the stem cell and were inherited by the daughter cell destined to become a gonialblast. Thus, germline stem cells retain their mother centrosome from the time they first enter their niche.

What advantage might such a strategy confer on the stem cell? The most likely answer is to help control the orientation of cell divisions. Germline stem cells in the *Drosophila* testis position their mitotic spindles at right angles to the hub, a mechanism that facilitates the proper specification of their daughters (*3*). Because one centrosome retains its hub proximity while the other moves to the opposite side of the cell, assembly of a mitotic spindle is always perpendicular to the hub. As a result, after cell division, one of the daughter cells remains associated with the hub and receives signals from the hub to remain a stem cell. Meanwhile, the hub-distal daughter cell moves away from the niche and initiates gonialblast differentiation. Yamashita *et al.* show that the hub-proximal mother centrosome is associated with robust microtubules during interphase (the nondividing stage) and that some of these microtubules extend to the adherens junctions that connect the stem cell to hub cells. These microtubules may firmly tether the mother centrosome to the hub, ensuring the proper orientation of stem cell division as well as the stem cell–specific inheritance of the mother centrosome.

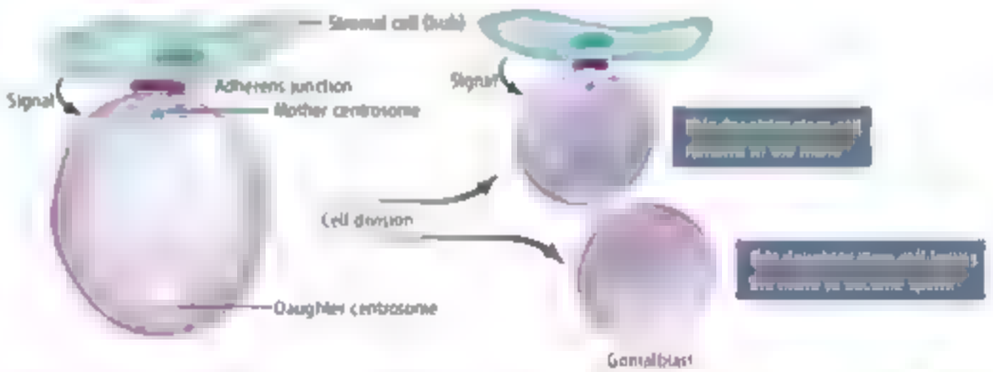

Centrosome inheritance and daughter cell fate. During the division of a germline stem cell in the *Drosophila* testis, the mother centrosome remains adjacent to the hub. The greater microtubule nucleating capacity of the mother centrosome probably stabilizes its association with the adherens junction, maintaining stem cell function.

Studies of other asymmetrically dividing cells suggest possible additional roles for programmed centrosome inheritance in stem cells. Aside from their participation in spindle assembly, centrosomes associate with membrane-bound organelles such as the Golgi and recycling endosomes. Centrosomes also regulate cytokinesis by delivering membranes asymmetrically to the cleavage furrow (*4*, *5*). Thus, differential centrosome inheritance might contribute to stem cell maintenance and daughter cell programming by partitioning membrane-bound organelles and signaling molecules asymmetrically between the germline stem cell and gonialblast. Indeed,

asymmetric segregation of cell fate determinants through recycling endosomes has been implicated in specifying cell fate in the developing *Drosophila* nervous system (*5*). The mother centrosome may also serve as a basal body that nucleates a primary cilium, at least in mammalian stem cells (*6*). Primary cilia can serve as signaling organelles (*7*) and might provide a means for stem cells to communicate with their niche and to receive a maintenance signal.

Could retention of the mother centrosome contribute to stem cell longevity as well as to developmental programming? The most relevant information comes from studies of asymmetric cell division in the budding yeast *Saccharomyces cerevisiae*. Mother cells have a lower replicative potential than buds they produce, and selectively retain damaged molecules (*8*, *9*). Interestingly, the fungal counterpart of the mother centrosome, the mother spindle pole body, is selectively inherited by the bud (*10*). By inheriting mother centrosomes, stem cells may likewise use the robust microtubule array to repel molecules that promote replicative senescence. However, in yeast, other types of damage, such as chromosome breaks that cause loss of heterozygosity, accumulate preferentially in the bud (*11*), so the importance of maternal centrosome inheritance in promoting longevity remains unclear.

Is differential centrosome inheritance the long-sought secret of stem cell function? It should now be possible to determine whether maternal centrosomes are retained by several other well-characterized *Drosophila* stem cells. In male germline stem cells, such behavior seems likely to contribute to the stable asymmetric programming of stem cell and daughter. And it is satisfying to contemplate the possibility that this strategy might also promote stem cells' remarkable stability and longevity.

References

1. Y. M. Yamashita, A. P. Mahowald, J. R. Perlin, M. T. Fuller, *Science* **315**, 518 (2007).
2. M. Deshaies, P. Gonczy, *J. Cell Sci.* **117**, 1619 (2004).
3. Y. M. Yamashita, D. L. Jones, M. T. Fuller, *Science* **301**, 1547 (2003).
4. A. Gromley *et al.*, *Cell* **123**, 75 (2004).
5. G. Emery *et al.*, *Cell* **122**, 763 (2005).
6. A. M. Preble, T. M. Giddings, S. K. Dutcher, *Curr. Top. Dev. Biol.* **49**, 207 (2000).
7. V. Singla, J. F. Reiter, *Science* **313**, 629 (2006).
8. H. Aguilaniu, L. Gustafsson, M. Rigoulet, T. Nyström, *Science* **299**, 1751 (2003); published online 27 February 2003 (10.1126/science.1080418).
9. K. J. Bitterman, M. Oliver, D. A. Sinclair, *Microbiol. Mol. Biol. Rev.* **67**, 376 (2003).
10. G. Pereira, T. U. Tanaka, K. Nasmyth, E. Schiebel, *EMBO J.* **20**, 6359 (2001).
11. M. A. McMurray, D. E. Gottschling, *Science* **301**, 1908 (2003).

10.1126/science.1138737

CHEMISTRY

Single-Molecule Catalysis

A single water molecule can act as a catalyst in a gas-phase reaction by forming a complex with a reactant that reacts faster than the "bare" reactant.

Ian Smith

To some, the word catalysis conjures up images of large-scale industrial processes. For example, the Haber process, discovered about 100 years ago, makes use of supported iron catalysts to speed up the conversion of nitrogen and hydrogen to ammonia at moderate temperatures. Worldwide, this process is responsible for the annual manufacture of more than 100 million metric tons of ammonia (*1*). In contrast, the paper by Vohringer-Martinez *et al.* on page 497 of this issue (*2*) addresses a fundamental question: Can single molecules serve as catalysts? That is, can individual molecules accelerate chemical reactions?

This question is best answered by experiments in the gas phase, where the overall reaction comprises a series of elementary reactions, each involving a small number of molecules. One well-known example is the catalytic destruction of ozone in the upper atmosphere by species such as halogen atoms, nitric oxide, and hydroxyl radicals (*3*). These species (X) participate in chain reactions ($X + O_3 \rightarrow XO + O_2$ and $XO + O \rightarrow X + O_2$), whose net effect is to speed up the conversion of "odd oxygen" (O atoms and O_3 molecules) to dioxygen O_2, thereby lowering the amount of ozone present in the stratosphere.

This destruction of ozone can be thought of as an example of homogeneous catalysis (the catalyst is in the same phase as the reactants), familiar in reactions in solution. By contrast, Vohringer-Martinez *et al.* provide an example of gas-phase catalysis more akin to heterogeneous catalysis. They report that the reaction between hydroxyl radicals and acetaldehyde, $OH + CH_3CHO \rightarrow H_2O + CH_3O$, is accelerated by the participation of single molecules of water. They argue convincingly that this is because hydrogen-bonded complexes of CH_3CHO and H_2O form and that these complexes react faster with OH radicals than do individual molecules of CH_3CHO. The binding to water is thus analogous to binding to a surface in

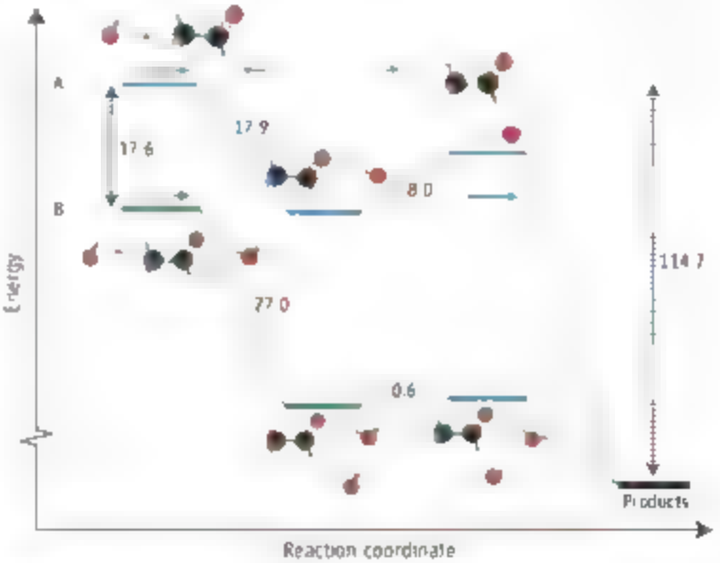

Catalysis by single water molecules. Energy profiles for (**A**) reactions between hydroxyl radicals and "bare" acetaldehyde molecules (the "higher road" traced in blue) and (**B**) reactions between hydroxyl radicals and acetaldehyde molecules that are associated with single molecules of water (the "lower road" traced in green). The horizontal lines show maxima and minima along the reaction path of minimum energy, with energy differences given in kJ mol^{-1}. The arrows are used to indicate that on pathway B all the reactive flux that reaches the minimum associated with the prereaction complex passes through the inner transition state and becomes products, whereas on pathway A some of the flux is reflected at the inner transition state, reducing the reaction rate. The cartoons show the structures at the maxima and minima in most cases of hydrogen-bonded complexes. More details are given in (*2*).

CREDIT: K. HAYNES

The author is in the University Chemical Laboratory, Lensfield Road, Cambridge CB2 1EW, UK. E-mail: i.w.m.smith@bham.ac.uk

heterogeneous catalysis. Their experiments make use of gas mixtures cooled to several different temperatures, as low as 58 K, by expansion through a convergent-divergent "Laval" nozzle (*4*). Information about the rate of reaction is then obtained by a standard method. OH radicals are generated by pulsed laser photolysis of hydrogen peroxide, and the rate of their reactive loss is measured with the use of a second laser that induces the OH radicals to fluoresce. The decrease in the fluorescence signal as the time delay between the two laser pulses is increased provides information about the reaction rate. Adding water to the expanded gas increases the rate of loss of OH, especially at the lowest temperatures of the experiments.

The interpretation of the experiments is that the reaction between OH radicals and hydrogen-bonded complexes of acetaldehyde with water is faster than that between OH radicals and "bare" acetaldehyde molecules—as supported by first-principles quantum chemical calculations. Even for reactions with uncomplexed CH_3CHO, there is no energy barrier on the pathway from reactants to products, that is, there is no configuration that the reaction must pass through that has a higher energy than that of the initially separated reactants. But there is a "submerged barrier" or "reef." As for an increasing number of fast elementary reactions, the ideas of transition state theory must be applied rather subtly (*5*). There are, in effect, two transition states, an "outer" one that leads into a shallow well on the energy pathway (corresponding to a prereaction complex), followed by an "inner" transition state with an energy lower than that of the separated reactants but higher than that of the well (see figure). It is the inner transition state that is the true "bottleneck" to reaction because the internal quantum states at this configuration are more widely spaced than those for the outer transition state—or, equivalently, it represents a free energy maximum along the reaction pathway.

Quantum chemical calculations show that H_2O forms a complex with CH_3CHO bonded by 17.6 kJ mol^{-1}, through two hydrogen bonds. Interaction of this complex with an OH radical forms a further hydrogen bond, so that the energy of this tertiary prereaction complex is 44.6 kJ mol^{-1} below fully separated $CH_3CHO + H_2O + OH$ and 27 kJ mol^{-1} lower than the energy of $CH_3CHO \cdot H_2O + OH$. The prereaction complex can then convert to products, $2H_2O + CH_3O$, through an almost energetically equivalent transition state (see the figure).

The combined experimental and theoretical arguments about the relative reactivity of CH_3CHO and $CH_3CHO \cdot H_2O$ toward OH radicals are convincing. However, it is not yet possible to put a figure on the extent of the acceleration of the reaction caused by the single water molecule acting as a catalyst. To convert the measured phenomenological rate constants for reaction into rate constants for reaction of OH with $CH_3CHO \cdot H_2O$, one needs to know the concentration of the complexes present in the experiments. Two difficulties arise. First, it is not easy to measure these concentrations, for example by infrared spectroscopy, in the environment of the jet. Second, it is not easy to estimate the concentrations, especially as these may depend on the kinetics of the $CH_3CHO + H_2O$ association, not just the thermodynamics of this process.

Interesting as these results are, an important question is whether they have any relevance to atmospheric chemistry. Aldehydes arise in the troposphere during the atmospheric oxidation of hydrocarbons; ethane oxidizes to acetaldehyde. The lifetimes of both ethane and acetaldehyde (*6*), determined by their reaction with OH radicals, are short, so atmospheric acetaldehyde is found chiefly at low altitudes where the average temperature is around 288 K. Even at 100% relative humidity, the equilibrium fraction of acetaldehyde complexed with water is likely to be very small, and therefore the acceleration of the $OH + CH_3CHO$ reaction will probably be minimal.

References

1. J. A. Pool, E. Lohilavsky, P. J. Chirik, *Nature* **427**, 527 (2004).
2. E. Vöhringer-Martinez *et al.*, *Science* **315**, 497 (2007).
3. R. P. Wayne, *Chemistry of Atmospheres* (Oxford Univ. Press, Oxford, ed. 3, 2000), p. 164.
4. I. W. M. Smith, B. R. Rowe, *Acc. Chem. Res.* **33**, 261 (2000).
5. E. E. Greenwald, S. W. North, Y. Georgievskii, S. J. Klippenstein, *J. Phys. Chem. A* **109**, 6031 (2005).
6. A. R. Ravishankara, E. R. Lovejoy, *J. Chem. Soc. Faraday Trans.* **90**, 2159 (1994).

10.1126/science.1138496

GEOPHYSICS

Mediating Plate Convergence

Herb Dragert

Movement of Earth's tectonic plates generates low-frequency seismic events. These events are not background noise, but represent slower and deeper earthquakes.

With improvements in the technology and density of networks used to monitor seismicity and crustal deformation, Earth scientists are discovering a rich spectrum of rupture phenomena deep within subduction zones. These zones are where Earth's crustal plates collide, resulting in one plate moving underneath the other and eventually re-entering the upper mantle.

A recently discovered phenomenon called "episodic tremor and slip" (ETS) involves small crustal motions over periods of days to weeks. The direction of motion is in the same sense as plate convergence and often these motions propagate along the coastal margin. The slip episodes repeat at intervals of months to years, accompanied by distinct seismic tremors whose records look more like background noise than earthquakes. Although the processes involved are not fully understood, researchers have identified this plate-boundary behavior along the Cascadia Subduction Zone in the Pacific Northwest (*1*) and the Nankai Subduction Zone off the eastern coast of southwest Japan (*2*). On page 503 of this issue (*3*), Ito *et al.* show that ETS is also marked by the occurrence of very-low-frequency (VLF) earthquakes. This adds yet another piece to the puzzle of contemporary deeper plate dynamics.

As seen in the great Sumatra-Andaman earthquake of 2004 (*4*), the most awesome tectonic characteristic of the world's subduction zones is the repeated occurrence of great thrust earthquakes. Although the average recurrence intervals for these devastating temblors are directly related to plate convergence rates, the nature of the stress buildup that culminates in these large fault ruptures is not well known. Scientists agree that it is the inexorable aseismic plate motions (i.e., motions without earthquakes) at depth that increase stress on the overlying locked portion of the fault that will ultimately be relieved by a great earthquake. Until recently, it was assumed that this deep aseismic slip or ductile shearing between plates occurred at a uniform speed. The observation of small (<5 mm) systematic surface displacements at continuous Global Positioning System (GPS) stations over a period of several weeks led to the discovery of a "silent slip event" on the Cascadia Subduction

The author is at the Geological Survey of Canada, Pacific Geoscience Centre, Sidney, British Columbia V8L 4B2, Canada. E-mail: hdragert@nrcan.gc.ca

Zone (5). This study established that distinct episodes of aseismic slip of a few centimeters can occur on the deeper plate interface immediately downdip from a completely locked plate boundary, unrelated to any local earthquake activity.

A reexamination of all available regional continuous GPS data over the past decade showed that such slip events have occurred repeatedly along the northern Cascadia margin and with surprising regularity (6). Although these slip events can be modeled by simple dislocations in an elastic medium, the physical processes involved in this dynamic behavior on the deeper plate interface are not well understood.

Another key insight into real-time dynamics of convergent plate boundaries was established by the discovery of a "nonvolcanic deep tremor" along the Nankai Subduction Zone (7). Data from the National Research Institute for Earth Science and Disaster Prevention (NIED) high-sensitivity seismograph network (Hi-net) enabled the identification of small-amplitude seismic tremors that lasted from a few minutes to a few days, with predominant frequencies ranging from 1 to 10 Hz and source depths averaging about 30 km. From the location, duration, and mobility of the tremor activity, it was surmised that the generation of tremors may be related to the movement of fluids originating from the dehydration of metabasalts in the subducting oceanic crust, or triggered by the addition of fluids to a critically stressed medium, or perhaps triggered by nearby earthquake activity. It was not until the study of Cascadia tremors (1) that the intimate relationship between tremors and episodic plate slip was established. These tremors were found to be identical to those observed in Japan, and they occurred predominantly at times of episodes of slip.

In subsequent examination of tilt changes recorded by Hi-net accelerometers, it was discovered that the previously identified tremor episodes in southwestern Japan were indeed accompanied by crustal displacements attributable to deep plate slip (2). Although no clear mechanisms for tremor generation were established, the similarity of the ETS phenomena occurring in both the Nankai and Cascadia regions points to an ongoing plate dynamic process common to young subduction zones.

The findings of Ito *et al.* reveal that VLF earthquakes may be another key aspect of episodic plate slip at depth, at least for southwestern Japan so far. The authors characterize these VLF earthquakes by a distinct lack of high-frequency components (2 to 8 Hz) relative to similar-magnitude ordinary earthquakes, and by signals that are predominantly body waves. Because the seismicity due to VLF earthquakes accompanies and migrates with the deep low-frequency tremors and slip events, and because the spectral content for VLF events suggests a rupture duration on the order of 10 s, the authors propose a "continuum" model of slip processes in the transition zone of the plate interface (see the figure).

In this model, the transition zone consists primarily of weakly coupled fault areas that are subject to episodic aseismic slip that occurs over days to weeks during one episode. However, there are numerous small, slightly stronger patches that rupture in VLF events in response to increased shear stress caused by slow slip in the surrounding material. The limited size of these patches, along with the presence of high pore-fluid pressure, characterize the VLF earthquake and its rupture duration. Tremors are attributed to "microcracking" within the transition zone over source sizes and rupture times much smaller than those for VLF earthquakes.

This model is aesthetically pleasing in its simplicity. The nature of the slip and the stress release is ultimately dependent on the distribution of fluids and their pore pressures. The regions of the subduction zone where great thrust (i.e., megathrust) earthquakes occur are characterized by a paucity of fluids and/or low pore-fluid pressures, resulting in very large brittle asperities that rupture in great earthquakes every hundred years or so. The deeper regions of the convergent plate interface, where high temperatures (>550°C) and abundant free fluids render materials plastic, are characterized by continuous aseismic plate motions. The transition region between these two is characterized by spatial and temporal asperities in fluid content and pore-fluid pressures, leading to the phenomena of episodic slow slip events accompanied by VLF earthquakes and deep tremors.

Can the extensive depth distribution of tremors observed in Cascadia (8) be accommodated within this framework? What determines the recurrence intervals for slow slip events, and how are they dependent on plate convergence rates, plate age, and external stress triggers? Basically, what are the necessary and sufficient conditions for episodic tremor, slow slip, and these deep VLF earthquakes? Perhaps the most important question concerns the relationship of these phenomena to present-day regional seismicity. It is clear that episodes of deep slip will modulate the rate of stress accumulation on the locked portion of the plate interface, thereby modulating the cumulative probability (and conceivably acting as a trigger) for great subduction thrust earthquakes (9). But what about earthquakes occurring within the subducting slab and the overlying crust? Does the stress release from these more subtle and benign plate-slip phenomena influence the location and timing of regional seismicity? Understanding these relationships could provide solid underpinnings for earthquake forecasting in subduction zones.

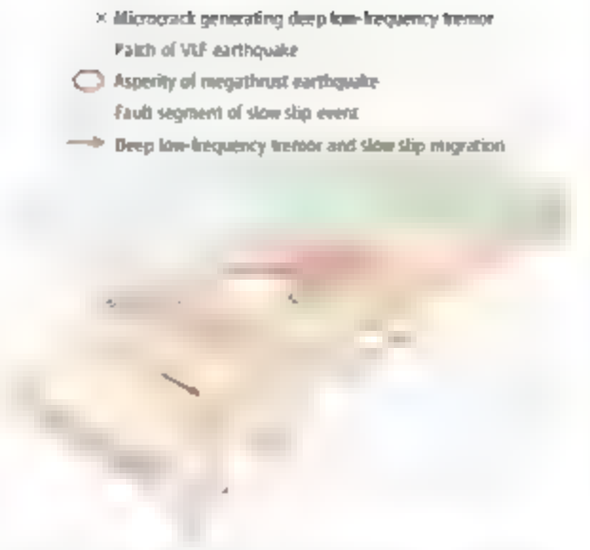

Weak faults, slow slip, and low-frequency earthquakes. The way stress is released at convergent plate boundaries is governed by the distribution of fluids or high pore pressures, and by the mean size of stronger, fluid-poor asperities. The shallow portion of the subducting plate interface is fluid-poor and has large, strong asperities that rupture in great earthquakes. The deeper plate interface, hot and fluid rich, allows continuous aseismic plate motion. The transition zone between these two regions marks a heterogeneous, time-dependent mixture of fluid-rich material and small-scale brittle asperities that gives rise to episodes of ETS and VLF earthquakes. [Adapted from Ito *et al.* (3)]

References

1. G. Rogers, H. Dragert, *Science* **300**, 1942 (2003); published online 8 May 2003 (10.1126/science.1084783).
2. K. Obara, H. Hirose, F. Yamamizu, K. Kasahara, *Geophys. Res. Lett.* **31**, L23602, doi:10.1029/2004GL020848 (2004).
3. Y. Ito, K. Obara, K. Shiomi, S. Sekine, H. Hirose, *Science* **315**, 503 (2007); published online 30 November 2006 (10.1126/science.1134454).
4. T. Lay *et al.*, *Science* **308**, 1127 (2005).
5. H. Dragert, K. Wang, T. S. James, *Science* **292**, 1525 (2001); published online 19 April 2001 (10.1126/science.1060152).
6. M. M. Miller, T. Melbourne, D. J. Johnson, W. Q. Sumner, *Science* **295**, 2423 (2002).
7. K. Obara, *Science* **296**, 1679 (2002).
8. H. Kao *et al.*, *Nature* **436**, 841 (2005).
9. S. Mazzotti, J. Adams, *Bull. Seismol. Soc. Am.* **94**, 1954 (2004).

10.1126/science.1137171

ASSOCIATION AFFAIRS

Baltimore: Time for Scientists to Take Role in Public Life

If the Nobel Prize is supposed to be the crowning achievement of a scientific career, someone forgot to tell David Baltimore. After sharing the 1975 Prize in Medicine for the discovery of reverse transcriptase at age 37, Baltimore has published more than 600 papers, including seminal research on the genetics of cancer, the workings of the HIV virus and AIDS vaccine candidates, and fundamental observations in molecular immunology. He was a founder of the Whitehead Institute for Biomedical Research, president of Rockefeller University and the California Institute of Technology, and a leading figure in national policy commissions on stem cell–based DNA and AIDS research.

David Baltimore

"Much of my life since the Prize has been taken up with doing science," Baltimore said. As he assumes the presidency of AAAS in February, he wants to remind the public that "science is the driving force" of all modern life, not just his own.

It's an idea Baltimore thinks has been lost in the classroom and Congress in recent years. "With science feeling itself under attack from various sides, it's never been a more important time for scientists to take a role in public life … and there is hardly any other organization that can speak as broadly for science as AAAS," he noted in a recent interview.

Schools are one place where "increasing skepticism about rational thinking" has placed science under siege, according to Baltimore. In his candidacy statement, he said, "Raising children who do not know that life and our planet evolved over 4.5 billion years of change and development hamstrings them from participating in modern life."

Baltimore wants AAAS to continue its strong support of science education from kindergarten to college, noting that it has already had much success with curriculum and science literacy programs such as Project 2061 and outreach at the AAAS Annual Meeting.

AAAS should remind its members that "there is an opportunity for every scientist to be involved with a local school board," providing curriculum advice and helping teachers understand "the experimental nature of science," Baltimore said.

Throughout his career, Baltimore has played a key role in creating national science policy, as an organizer of the 1975 Asilomar Conference that set standards for recombinant DNA technology, as co-chair of the 1986 National Academy of Sciences Committee on a National Strategy for AIDS, and head of the National Institutes of Health AIDS Vaccine Research Committee in 1996. He received the 1999 National Medal of Science in part for his work on AIDS research policy.

Baltimore has been outspoken about what he sees as government efforts to distort and suppress scientific research, and he thinks that AAAS has a role to play in fighting this trend as well. AAAS congressional testimony and science-based briefings for new members of Congress will be AAAS Center for Science, Technology and Congress's chief contributions to national policy, he said.

In particular, the controversy over federal funding for embryonic stem cell research has cast a shadow over America's labs, Baltimore said, noting that his own graduate students have been wary about funding woes in their future.

"It's unique in my experience in science that the government has put shackles on a certain kind of research. We've never had a richer set of opportunities put in front of any scientists than the opportunities put in front of biologists today, yet there is a pervasive sense of being abandoned by the National Institutes of Health," he said.

Baltimore stepped down as Caltech president last September, but continues as Robert Andrews Millikan Professor of Biology and head of the Baltimore Lab at the university. His current research, supported by a $17.9-million grant from the Gates Foundation, is looking for ways to genetically boost the immune system against infectious pathogens, particularly HIV.

Baltimore laughed when asked if he had ever envisioned himself as an international advocate and spokesperson for science in the early days of his career. "No, I was just a lab rat and loving it. I've sort of grown into this as a consequence of my interest in institutions."

Baltimore will succeed the current president, John P. Holdren, at the close of the 2007 Annual Meeting on 19 February. Holdren will become chair of the AAAS board, as Gilbert S. Omenn steps down as chair. James J. McCarthy has been elected to succeed Baltimore as president-elect. McCarthy is the Alexander Agassiz Professor of Biological Oceanography at Harvard University.

Becky Ham

AAAS

Call for Nomination of AAAS Fellows

AAAS Fellows who are current members of the Association are invited to nominate members for election as Fellows. A Fellow is defined as "a Member whose efforts on behalf of the advancement of science or its applications are scientifically or socially distinguished." A nomination must be sponsored by three AAAS Fellows, two of whom must have no affiliation with the nominee's institution.

Nominations undergo review by the Steering Groups of the Association's sections (the Chair, Chair-Elect, Retiring Chair, Secretary, and four Members at Large of each section). Each Steering Group reviews only those nominations designated for its section. Names of Fellow nominees who are approved by the Steering Groups are presented to the AAAS Council for election.

Nominations with complete documentation must be received by 11 May 2007. Nominations received after that date will be held for the following year. The nomination form and a list of current AAAS Fellows can be found on the AAAS Web site at www.aaas.org/about/aaas/fellows. To request a hard copy of the nomination form, please contact Ellen Carpenter at the AAAS Executive Office, 1200 New York Ave., N.W., Washington, DC 20005, at 202-326-6635, or at ecarpent@aaas.org.

HUMAN RIGHTS

AAAS Expands Human Rights "Eye in the Sky"

After a successful yearlong pilot program, AAAS will [illegible] powerful satellite imagery and related technologies to help investigate international reports of human rights violations with a new 3-year $700,000 grant from the John D. and Catherine T. MacArthur Foundation.

During the pilot project, AAAS, in partnership with other organizations, used geospatial technologies to document human rights violations around the world, including in the Darfur region of Sudan, Burma, and Zimbabwe.

With the new grant, the Science and Human Rights program will expand upon its 2005–2006 pilot project with a new emphasis on tailoring its activities to the priorities of intergovernmental organizations and courts like the International Criminal Court and the African Court on Human and Peoples' Rights.

"This grant is extremely exciting because it will allow us to develop the first steps of a worldwide information system using advanced technologies that should help prevent human rights violations before they accelerate," said Lars Bromley, senior program associate in the AAAS Office of International Initiatives.

In late May 2006, AAAS released its first human rights report, in partnership with Amnesty International and the Zimbabwe Lawyers for Human Rights, based on satellite imagery.

The report presented evidence that the government of Zimbabwe had destroyed entire settlements, including the town of Porta Farm, forcing thousands of residents to flee their homes. Reports on the Zimbabwean satellite imagery were published in several outlets, including the *Washington Times*, National Public Radio, the *Guardian*, and Reuters.

"With a global reach and reputation for independence, human rights organizations are able to sound the alarm and mobilize millions quickly, often before governments or the international community have even admitted there is a problem," said Ariela Blätter, director of the Crisis Prevention & Response Center at Amnesty International USA, a partner of AAAS's Science and Human Rights program.

Since 1978, the MacArthur Foundation has provided support to advance human rights around the world, with a special interest in innovative uses of technology that advance its grant-making goals. The foundation's November 2005 pilot grant of $1,250,000 to AAAS was used to help international organizations, government agencies, and nongovernmental organizations (NGOs) rapidly collect, evaluate, and distribute information about human rights violations using geospatial technologies.

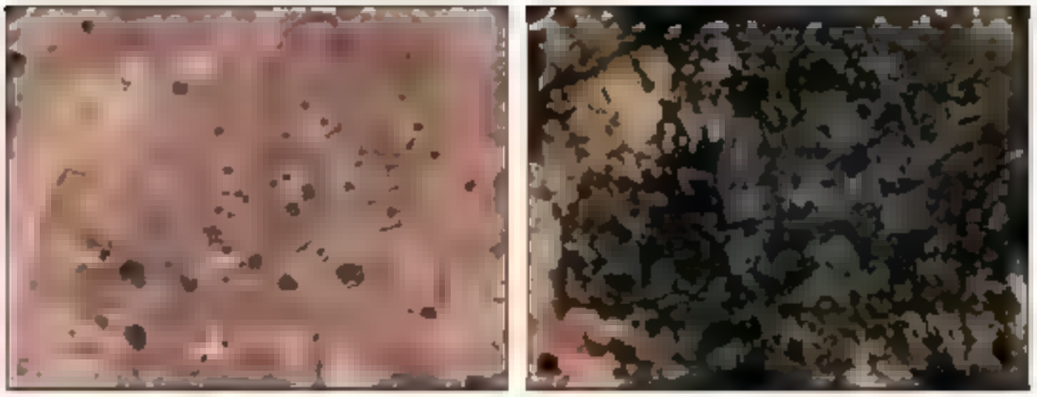

Before and after satellite images of Birkedoias, Chad, burned during an attack in December 2005 by janjaweed militants in the Darfur conflict.

Within the past year, NGOs such as Amnesty International, the U.S. Committee for Human Rights in North Korea, and the U.S. Campaign for Burma have worked with AAAS to analyze high-resolution satellite imagery with geographic information systems and human intelligence to raise public awareness and alert governments, media outlets, and others about human rights violations.

While the overall price of new satellite imagery and powerful computers to analyze the images has recently fallen, AAAS has received other grants from a variety of organizations, including an award of $50,000 from the Open Society Institute for monitoring in the Karen State of Burma. A report on Burma will be released later this year, as will reports on Darfur and elsewhere.

In addition to gathering and analyzing the images from companies like DigitalGlobe and GeoEye, SHR plans to use the grant money to develop an outreach program through Web sites, workshops, meetings, and correspondence with organizations that have expertise applicable to human rights projects.

AAAS has been a pioneer in bringing science and technology to bear on international human rights issues with regular reports and workshops sponsored by its Science and Human Rights program. The program also supports scientists whose human rights are threatened, through the AAAS Human Rights Action Network.

In January 2006, the network coordinated an appeal to the government of Guatemala to protect Fredy Peccerelli, executive director of Guatemalan Forensic Anthropology Foundation, who had received death threats against him and his family for his efforts to locate and exhume mass graves from the country's bloody civil war.

Benjamin Somers

ANNUAL MEETING

Sustainability from All Sides

The AAAS Annual Meeting stands apart from other scientific gatherings in its emphasis on the connection between science and society, a critical crossroads that is explored in depth with this year's theme of "Science and Technology for Sustainable Well-Being."

At the 173rd Annual Meeting in San Francisco next month, scientists, journalists, and the public can explore the idea of sustainability across a wide number of disciplines, from climate change science and the future of the oceans to the politics of energy reserves, endangered languages, and environmental justice.

In his invitation to the conference, AAAS President John Holdren said, "The character of the challenges to the human condition—energy, water, health, climate, security, development, and more" are best tackled by AAAS's interdisciplinary approach.

For the first time this year, a AAAS Annual Meeting blog [http://news.aaas.org] will provide extensive coverage from San Francisco, featuring reports and podcasts from the staff of *Science* and *ScienceNOW*, AAAS's award-winning Science Update radio program, and AAAS's writers, along with links to U.S. and international news coverage of the meeting.

— Becky Ham

Results of the 2006 Election of AAAS Officers

Following are the results of the 2006 election. Terms begin on 20 February 2007

General Offices
President-Elect: James , McCarthy
Board of Directors: Cherry Murray, Linda P B. Katehi
Committee on Nominations: Rita R. Colwell, Jane Lubchenco, Floyd E. Bloom, Mary L. Good

Section on Agriculture, Food, and Renewable Resources
Chair-Elect: Roger N. Beachy
Member-at-Large: Charles J. Arntzen
Electorate Nominating Committee: Sally A. Mackenzie, Richard A. Dixon

Section on Anthropology
Chair-Elect: Eugenie C. Scott
Member-at Large: Jeslie C. Aiello
Electorate Nominating Committee: G. Philip Rightmire, Payson Sheets
Council Delegate: Michael A. Little

Section on Astronomy
Chair-Elect: Jr. Cornell Tarter
Member-at-Large: Carey Michael Lisse
Electorate Nominating Committee: Alan Marscher Heidi Newberg
Council Delegate: Heidi B. Hamme

Section on Atmospheric and Hydrospheric Sciences
Chair-Elect: Anne M. Thompson
Member-at-Large: Peter H. Gleick
Electorate Nominating Committee: Jennifer A Francis, Patricia Quinn

Section on Biological Sciences
Chair-Elect: Mariana Wolfner
Member-at-Large: Yolanda P Cruz
Electorate Nominating Committee: Kate Barald, Joel Huberman
Council Delegates: Brenda Bass, Nancy Beckage, Johanna Schmitt, Catherine Krull, Michael Cox, Rob Steele, Toby Kellogg, David Queller, Diane Shakes

Section on Chemistry
Chair-Elect: Wayne L. Gladfelter
Member-at-Large: Dennis A. Dougherty
Electorate Nominating Committee: Linda C. Hsieh-Wilson, Gregory C. Fu
Council Delegates: C. Bradley Moore, Jon Clardy, Nicholas Winograd

Section on Dentistry and Oral Health Sciences
Chair-Elect: Mary MacDougall
Member-at-Large: Paul H. Krebsbach
Electorate Nominating Committee: Luisa Ann DiPietro, Ichiro Nishimura

Section on Education
Chair-Elect: George D. Nelson
Member-at-Large: Gerald Wheeler
Electorate Nominating Committee: Cathryn A. Manduca, Carlo Parravano

Section on Engineering
Chair-Elect: Priscilla P. Nelson
Member-at-Large: Debbie A. Niemeier
Electorate Nominating Committee: Melba M. Crawford, Rafael L. Bras

Section on General Interest in Science and Engineering
Chair-Elect: Barbara Gastel
Member-at-Large: Lynne Tompani Friedmann
Electorate Nominating Committee: Don M. Jordan, Susan Pschorr

Section on Geology and Geography
Chair-Elect: Victor R. Baker
Member-at-Large: Lonnie G. Thompson
Electorate Nominating Committee: Neil D. Opdyke, Sherilyn C. Fritz
Council Delegate: Douglas J. Sherman

Section on History and Philosophy of Science
Chair-Elect: Thomas Nickles
Member-at-Large: Karen A. Rader
Electorate Nominating Committee: Kathryn M. Olesko, Richard M. Burian

Section on Industrial Science and Technology
Chair-Elect: Stan Bull
Member-at-Large: Thom Mason
Electorate Nominating Committee: Ana Ivelisse Aviles, Joyce A. Nettleton

Section on Information, Computing, and Communication
Chair-Elect: Michael R. Nelson
Member-at-Large: Christine L. Borgman
Electorate Nominating Committee: Deborah Estrin, Gladys A. Cotter

Section on Linguistics and Language Science
Chair-Elect: Frederick J. Newmeyer
Member-at-Large: Wendy K. Wilkins
Electorate Nominating Committee: Sarah Grey Thomason, Barbara Lust

Section on Mathematics
Chair-Elect: William Jaco
Member-at-Large: Claudia Neuhauser
Electorate Nominating Committee: Francis Sullivan, Juan Meza
Council Delegate: Joel L. Lebowitz

Section on Medical Sciences
Chair-Elect: Gail H. Cassel
Member-at-Large: R. Alan B. Ezekowitz
Electorate Nominating Committee: Peter F. Weller Michael Lederman

Section on Neuroscience
Chair-Elect: John H. Byrne
Member-at-Large: Charles D. Gilbert
Electorate Nominating Committee: Alison Goate, Theodore W. Berger
Council Delegate: Patricia K. Kuhl

Section on Pharmaceutical Sciences
Chair-Elect: Danny D. Shen
Member-at-Large: Ian A. Blair
Electorate Nominating Committee: John D. Schuetz, Kenneth W. Miller

Section on Physics
Chair-Elect: Cherry Murray
Member-at-Large: Sally Dawson
Electorate Nominating Committee: Barbara Goss Levi, Elizabeth Beise
Council Delegates: Miriam P. Sarachik, W. Carl Lineberger

Section on Psychology
Chair-Elect: Lila Gleitman
Member-at-Large: Morton Ann Gernsbacher
Electorate Nominating Committee: John F. Kihlstrom, Richard L. Doty

Section on Social, Economic, and Political Sciences
Chair-Elect: Russell Hardin
Member-at-Large: Arnold Zellner
Electorate Nominating Committee: Gary L. Albrecht, Gary King

Section on Societal Impacts of Science and Engineering
Chair-Elect: Lewis M. Branscomb
Member-at-Large: Ruth L. Fischbach
Electorate Nominating Committee: Ann Bostrom, Robert Cook-Deegan

Section on Statistics
Chair-Elect: William F. Eddy
Member-at-Large: Francoise Seillier-Moseiwitsch
Electorate Nominating Committee: Judith M. Tanur, Norman Breslow

Recombination and the Nature of Bacterial Speciation

Christophe Fraser,* William P. Hanage, Brian G. Spratt

Genetic surveys reveal the diversity of bacteria and lead to the questioning of species concepts used to categorize bacteria. One difficulty in defining bacterial species arises from the high rates of recombination that results in the transfer of DNA between relatively distantly related bacteria. Barriers to this process, which could be used to define species naturally, are not apparent. Here, we review conceptual models of bacterial speciation and describe our computer simulations of speciation. Our findings suggest that the rate of recombination and its relation to genetic divergence have a strong influence on outcomes. We propose that a distinction be made between clonal divergence and sexual speciation. Hence, to make sense of bacterial diversity we need data not only from genetic surveys but also from experimental determination of selection pressures and recombination rates and from theoretical models.

Bacteria are promiscuous. They often live in environments with an abundant diversity of donor DNA, and studies of the genomes of members of the same, or similar, species indicate the dynamic nature of gene acquisition, loss, and transfer (*1*). It is probably possible, through a series of intermediates and vectors, to transfer genes between any two bacteria. Besides the illegitimate recombinational process that leads to gene acquisition from distantly related sources, there is convincing evidence that homologous recombination may frequently replace small regions of the genome of a bacterium with those from other members of the same species or from closely related species (*2*). The rate of homologous recombination varies greatly. In some species it appears to be rare and leads to the evolution of distinct clonal lineages, whereas in others these localized recombinational imports arise much more frequently than mutations (*3*). In recent years, extensive homologous recombination has been shown to be so widespread that it may be regarded as the norm rather than the exception.

Nonetheless, surveys of genetic diversity in the bacterial kingdom are revealing that, far from a continuum mediated by promiscuous gene exchange, bacteria seem to form clusters of genetically related strains (species), at least for those genera studied so far (*4*–*6*). There is thus uncertainty regarding the nature of bacterial speciation and the influence that homologous recombination exerts upon it (*7*).

One proposition is that speciation (by which we mean the generation of permanently distinct clusters of closely related bacteria) could arise not because of fundamental ecological constraints or geographic separation but rather as a consequence of recombination failing more frequently between DNA sequences that are different than between those that are similar (*8*–*10*). In experimental studies of recombination in bacteria from widely differing genera, a consistent pattern of decline in the recombination rate as a function of genetic distance has been observed (Fig. 1A) (*11*). This effect has been shown to be associated with the various mechanisms that detect the sequence similarities between donor and recipient DNA, principally MutS-mediated mismatch repair and RecA-mediated recombination (*12*–*14*). RecA is involved in initiating recombination between donor and recipient DNA and is thus essential for recombination, whereas MutS inhibits recombination between mismatched sequences. One mechanism that has received particular attention is the requirement of RecA for minimally efficient processing segments (MEPS), which are short regions of sequence identity located at either end of the donor DNA strand and hypothesized to be required for recombination to occur (*15*). This mechanism can generate the general relationship seen in Fig. 1A and provides a corroborative estimate for the length of MEPS of between 20 and 30 base pairs (bp) (*16*). Whatever mechanism underlies the decline in recombination with increasing sequence divergence, this relationship results in constraints on recombination that operates at the genomic level, potentially allowing species distinctness to emerge as a dynamic corollary to diversification and adaptation (*8*, *9*).

Although this picture of speciation driven by recombinational (i.e., sexual) incompatibility is appealing, especially for the parallels it offers with the biological species concept of Mayr (*17*), the elucidation of the quantitative detail of recombinational incompatibility is only one aspect of the story (or stories) of bacterial speciation. What drives new strains to cross these "soft" genetic barriers and form new species? How distinct must clusters be for this soft barrier to be effective enough to maintain separation and for the evolutionary fate of each cluster to be distinct? Is there a consistent mechanism of speciation that applies to all bacteria, irrespective of the rates and mechanisms of recombination, which are known empirically to be extremely variable?

Department of Infectious Disease Epidemiology, Imperial College London, London W2 1PG, UK.

*To whom correspondence should be addressed. E-mail:

Modeling Bacterial Diversity

Genetic surveys of bacterial populations usually provide a static picture of the patterns of genotype clustering; consequently, exploring the dynamics of populations requires theoretical models studied using computer simulations and analytical approximations. Clustering in natural populations can then be compared with those from simulated populations if the genotypes of strains are defined in the same way. Isolates within bacterial populations are commonly characterized by the alleles at seven housekeeping loci [multilocus sequence typing (MLST)], where each allele corresponds to a different sequence (*18*). We have developed a model in which strains are defined in the same way and in which alleles change at defined rates by mutation or recombination. We also showed that genetic diversity in several bacterial pathogens could be explained by this simple model of neutral drift (*19*).

The use of neutral models of mutation and drift is not a denial of selection but a recognition that much observed population genetic structure can be explained in simple terms. It makes sense, as a null model, to explore the dynamics of neutral diversification and the conditions under which populations do, or do not, separate into distinct genotypic clusters that mimic the emergence of species. Estimates for the rates of mutation and recombination are available from empirical studies of a variety of bacteria [e.g., (*2*, *20*)], as is the relationship between sequence divergence and recombination rate shown in Fig. 1A.

We estimated population mutation rates (denoted θ) in the range 1 to 26, whereas recombination rates (denoted ρ) are more variable, ranging from 0 to 100 (*19*, *20*). These values are expressed per gene sequence per generation and are related to the underlying biological mutation and recombination rates (denoted m and r, respectively) by a constant known as the effective population size N_e, such that $\theta = 2mLN_e$ and $\rho = 2rN_e$. Our estimates of θ are based on genes approximately $L = 500$ bp long, and if we take a plausible estimate of the DNA mutation rate (m) at 5×10^{-10} per base pair per replication (*21*), we get a ballpark estimate for the effective population size N_e of 10^7.

The effective population size is not directly related to the census population size but is rather a measure of how much neutral diversity the environment can carry. It may be considerably smaller than the census population size as a result of factors such as regular bottlenecks,

genome-wide selective sweeps, or hierarchical structure (22). Consider, for example, an infectious agent such as *Streptococcus pneumoniae*. At least three factors result in an effective population size many orders of magnitude smaller than the actual number of bacteria. First, the bacterial population is divided into distinct populations within individual humans and is transmitted by small inocula, so that the number of infected people may be a better measure of population size than the number of bacteria. Second, transmission is seasonal, with peaks occurring during the winter months, creating bottlenecks during the low season, so that the effective population size may reflect the number of people infected during these bottlenecks. Third, the human contact network is hierarchically structured into communities, communities of communities, and so on, so that the effective number of people infected is lower than the actual number of people infected (23). Thus, a population of trillions of bacteria can have a low effective population size. Similar considerations may influence effective population sizes in many environments, such as the partitioning of marine bacteria around nutrient-rich coastal regions, seasonal regulation caused by the "bloom-bust" cycle of algal nutrient availability, and local clustering of populations around small particles of nutrients (24). In general, most natural populations of bacteria live in structured environments with well-defined patches of growth, where serious limits exist on the dispersion of novel types between patches. Establishing plausible estimates for N_e for a diverse range of bacteria, as well as identifying the factors that affect it, should be a research priority.

To explore speciation, we extended our previous model (19) to simulate simplified genomes (Fig. 1C), with an effective population size $N_e = 10^5$ and a population mutation rate θ 2, and defined each strain by the alleles at a larger number of loci (70) to counter the effect that occasional recombination at a single locus has in distorting relationships between otherwise divergent or similar strains (25). This model ignores several heterogeneities that may arise in populations (e.g., fitness, ecology, and recombination rate) but may nonetheless provide a preliminary description of the generation of diversity by drift. Our choice of parameters and model structure is an inevitable compromise between plausibility and computational limitations, achieved principally by reducing the effective population size and by using an approximation algorithm for modeling mutation of DNA sequences (25).

The Clonal-Sexual Threshold

The most salient feature of this simple model is a sharp transition in population structure with increasing rates of homologous recombination. When recombination rates are low, the population is effectively clonal in structure. In some sense, each clone has a separate evolutionary fate, because novel alleles that arise are unlikely to spread horizontally through the population. A feature of neutral population structure in the clonal region is strong genotypic clustering (Fig. 2, A and B). These clusters are unstable, and the long-term dynamics are characterized by a constant process in which major clusters regularly emerge by chance, split, drift apart, and eventually become extinct (Fig. 2C).

When recombination rates are increased to values between one-fourth and twice the mutation rate (per locus), a threshold is passed where clusters no longer diverge but are constantly reabsorbed into the parent population by the cohesive force of recombination. Alleles can succeed through horizontal spread even when the parental lineage does not. The degree of clustering is much reduced compared with the clonal situation (Fig. 2, D and E), and dynamic analysis (Fig. 2F) reveals that the clustering that does occur is transient.

It is worth noting that in both situations, the degree of diversity at each locus is the same and is governed by the balance between extinction and mutation. The sexual population contains more distinct genotypes, based on different combinations of a similar number of alleles. Recombination is frequent enough that the fate of alleles at one locus is not tied to their association with alleles at other loci. In the clonal situation, in contrast, clusters regularly become extinct (Fig. 2C), and extinction of clones is the principal regulator of diversity as a whole. Clustering can be defined as overdispersion of the genetic distances between isolates (Fig. 2, B, E, and H), and a measure of this is the index of association (26). In earlier work, we showed how to calculate this index for neutral models (without the dependence on sequence divergence of Fig. 1) (19), and we have shown that the threshold between clonal and sexual regimes holds for a wide range of parameters (20). The transition between clonal and sexual population structure is studied in more detail in the accompanying Supporting Online Material (27).

Diversity-Driven Speciation in Sexual Bacteria?

In populations with high rates of recombination, the reduced rate of recombination between two closely related species, compared to that within each species, provides a mechanism of sexual isolation that can maintain the separation of species, but it is unclear whether the relationship between divergence and recombination rate is sufficient to cause species to arise by drift. In other words, is it plausible that chance variation would occasionally result in strains different enough from the founder population that they no longer recombine with the founders often enough to maintain genetic proximity, and thus become sufficiently genetically isolated to form a new species? Our simulations suggest that although this type of distance-scaled recombination can lead to the emergence of separate populations, this only occurs under conditions in which the recombination rate declines with divergence more rapidly than is suggested by experimentation (Fig. 2, G and I). For values of this decline consistent with Fig. 1A, we did not observe distinct populations emerging in our simulations because the amount of variability within simulated populations is too low for the recombination rate to vary appreciably (Fig. 2, D to F). Thus, although this conceptual model is appealing, it is not supported by the quantitative detail of the interplay between genetic diversification and sexual isolation.

Experimental studies of the relationship between sequence divergence and recombination have focused on interspecific transfer of DNA, that is, between organisms that are up to 20% divergent and are already presumed to be at least somewhat sexually isolated. For the process of speciation modeled here, we are initially interested in the process of intraspecific transfer, so the most important question is how very small amounts of sequence divergence, up to 5%, affect recombination. We know that bacteria may vary

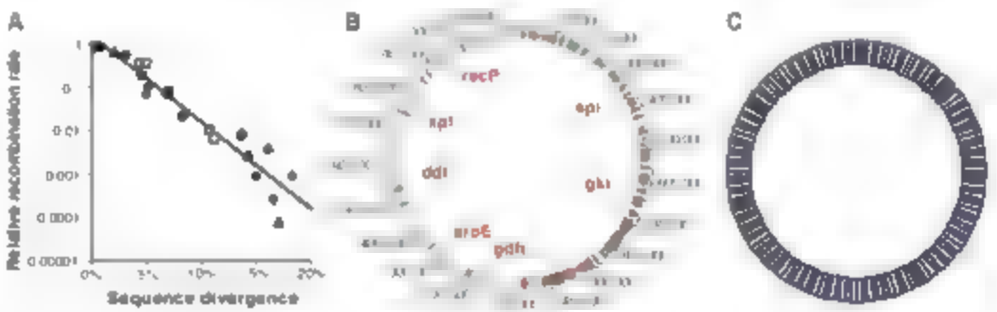

Fig. 1. (**A**) Recombination rate for a range of related donors, as a function of the proportion of sequence that is different (sequence divergence), for a variety of bacteria, recipients. Circle, *Bacillus subtilis*; square, *Bacillus mojavensis*; diamond, *S. pneumoniae*; triangle, *Escherichia coli*. The best fit log-linear curve is shown with intercept 0.8% and slope 19.8. [Data are from (*12*, *14*).] Slopes for individual named species range from 17.9 for *S. pneumoniae* to 25.7 for *E. coli*. (**B**) Genome of *S. pneumoniae* (from (*35*)] and location of the MLST genes. (**C**) Schematic representation of the simulated genomes in a stochastic neutral model. MLST genes are highlighted.

in their mechanisms of recombination, and hence the pattern shown in Fig. 1A may not be universal. In a yeast, for example, a different relation between genetic distance and recombination rates has been observed (*78*), in which the recombination rate declines very rapidly for the first few mismatches (85% reduction for 5 bp) because of a mechanism linked to the MutS mismatch-repair system, and this mechanism then saturates so that the decline thereafter follows a log-linear relationship very similar to that seen in bacteria studied to date (Fig. 1A). Similarly, anomalies such as the reported 10^4-fold reduction in recombination rate (by phage-mediated transduction) between *Salmonella enterica* serovar Typhimurium and *S. enterica* serovar Typhi that are only about 1% divergent (*8*, *79*). Thus before conclusions can be reached about the feasibility of speciation occurring by distance-related recombination, details of the dependence of the recombination rate on sequence divergence must be known (*11*).

Using methods based on MLST (*36*), we can identify strains from natural populations of bacteria separated by single recombination events and calculate the divergence between the ancestral and inserted allele (*36*). In species supporting sufficient levels of sequence diversity, such as *Neisseria meningitidis* and *S. pneumoniae*, these may frequently be highly divergent (up to 5%). Thus demonstrates that, at least within some species, extensive sequence divergence is no bar to recombination. Mechanisms of reproductive isolation other than sequence divergence certainly exist, such as niche differentiation, differences in DNA exchange by

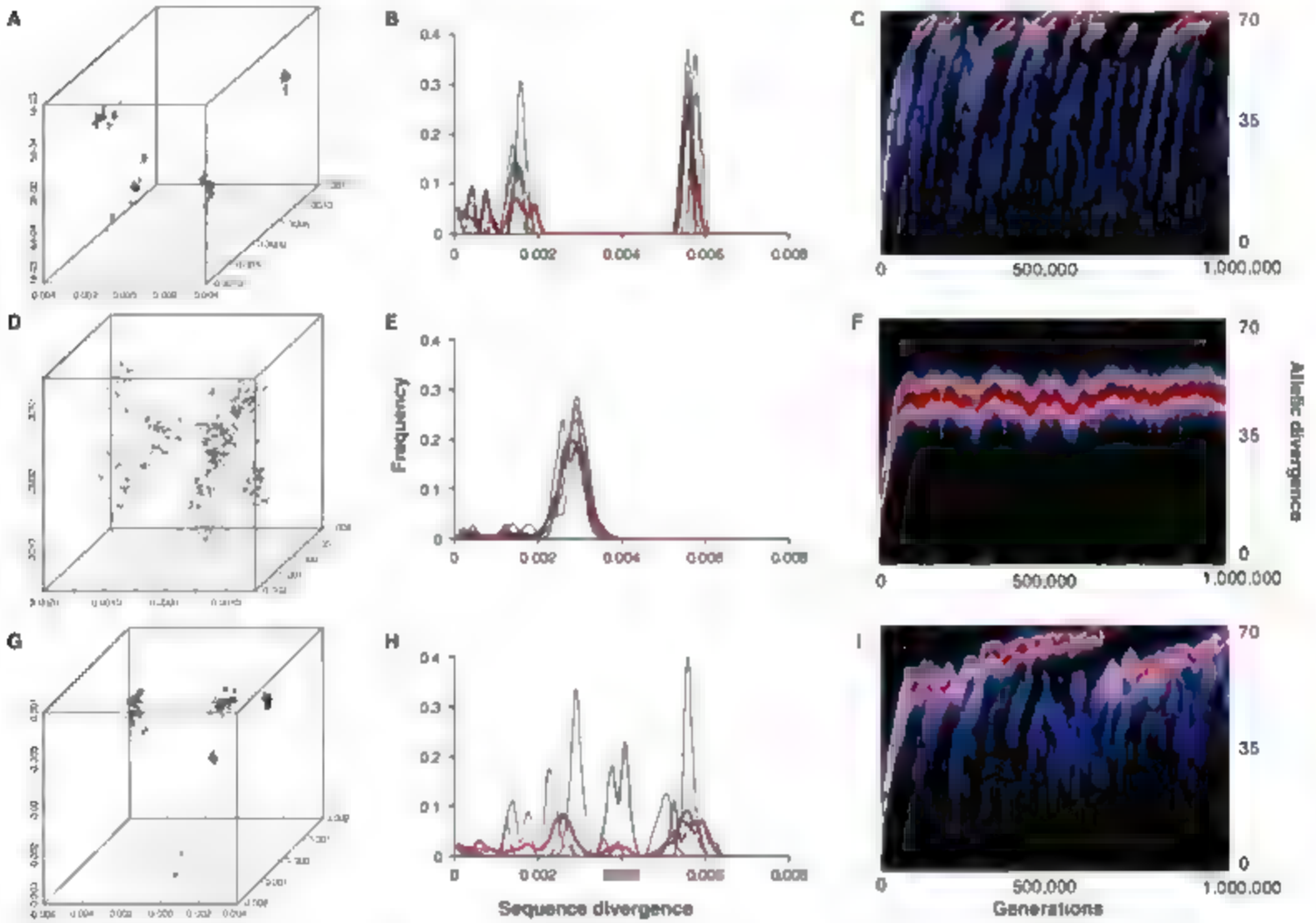

Fig. 2. Simulated genetic structure of a clonal population (A to C) and sexual population (D to F). All populations are evolving under neutral drift and are homogeneously mixing. (**A**, **D**, and **G**) Genetic maps, which are determined by principal coordinate analysis (*36*), represent the genetic distances between 1000 randomly chosen isolates from the simulated population after 10^6 generations have elapsed. Coordinates are expressed in units of sequence divergence. (**B**, **E**, and **H**) An alternative way to represent clustering is the distribution of sequence divergence between pairs of isolates in the population. The thin lines show the distance between five random strains and all the other strains in the sample, whereas the thick red line shows the distribution of all the pairwise distances. Where there is little clustering (E), all pairwise distances are similar and the distribution has a single peak; where there is strong clustering [(B) and (H)], the distribution has multiple peaks corresponding to pairwise comparisons within and between clusters. (**C**, **F**, and **I**) Distribution of the pairwise comparisons evolving over 10^6 generations. To normalize the distribution, pairs of isolates are compared for the number of alleles that are different, between 0 and 70, rather than for the proportion of base pairs as in (B), (E), and (H). The height of the distribution is represented by color shade ranging from black (0.0) to red (>0.1), so that peaks in (B), (E), and (H) correspond to red shaded areas in (C), (F), and (I). (C) and (I) show clusters moving apart, visible as red peaks moving up through time. When clusters split, a new peak appears at the bottom; extinctions are apparent from peaks disappearing. (F) shows instead more stable population structure, with a stable diffuse cluster being maintained throughout the simulation. Parameter values for θ and ρ, the population mutation and recombination rates, are θ = 2, ρ = 0.01 [(A) to (C)], $\rho = 20 \times 10^{-300x}$, where x is the sequence divergence [(D) to (F)]. We also explored under which conditions clustering could occur in the presence of high recombination rates [(G) to (I)]. Clusters with high within-cluster recombination can be generated, mimicking spontaneous speciation [(G) to (I)], but require that recombination rate declines as a function of sequence divergence at a very rapid rate uncharacteristic of most bacteria studied to date, such that $\rho = 20 \times 10^{-300x}$.

phage-mediated transduction owing to incompatibility in susceptibility to phage infection or restriction-modification systems, or differences in transformability in response to hormones (*11*, *31*). These mechanisms have not yet been implicated in the process of bacterial speciation, but their impact could be profound.

Slow Allopatric Speciation in Sexual Bacteria

So far, we have considered only the case of a single population. Prolonged physical separation (allopatry) will reduce mixing and recombination between bacteria, and by random accumulation of mutations, two separated populations will genetically diverge at twice the mutation rate ($2m$). As this happens, the intrinsic capacity for recombination between the populations is reduced. The question then arises, at what point should they be termed species?

For sexual populations (above the critical recombination threshold), speciation can be said to have occurred when the populations fail to blend even if the barrier isolating them has been removed. If the rate at which two populations can exchange genes depends on the genetic distance between the populations, then if this distance is below a threshold, recombination can cause distinct populations to converge and blend. If, on the other hand, this genetic distance is above a threshold, then recombinational incompatibility between the populations is such that the populations can never blend and could legitimately be considered distinct species (*27*). Thus, the degree of divergence induced by allopatry or other mechanisms of separation required for speciation to occur is not a constant but depends on the rate of recombination between similar genotypes. When separation is not sufficient to cause speciation, and sympatry is restored, blending will occur more rapidly than allopatric divergence (Fig. 3); however, genetic diversity is transiently enhanced owing to the long-term persistence of alleles from both populations. Separation thresholds and the dynamics of blending are explored further in (*27*). In summary, simple allopatry will only generate distinct clusters of strains over very long periods.

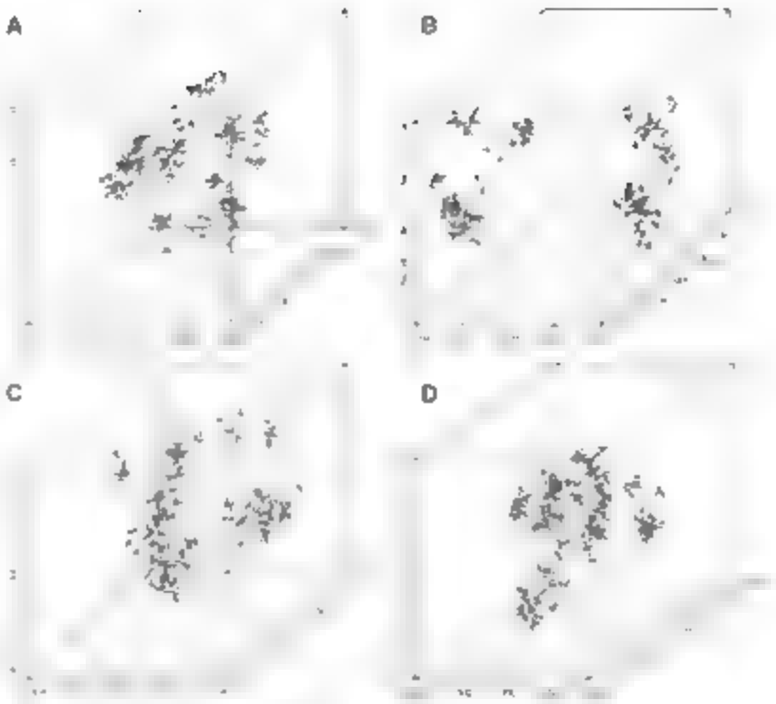

Fig. 3. Genetic maps of a population temporarily divided by a strong barrier. With parameters as in Fig. 2 for the sexual population, a split is introduced after 300,000 generations (A). After 300,000 generations apart, the populations have drifted and are clearly distinct (B). At this point, the populations are reunited; after 10,000 generations, little distinction remains (C), and after a further 10,000 generations, no remnants of the separation are evident (D).

Comparison with Multilocus Sequence Analysis

The inferred genetic map for a sample of bacteria from the mitis group *Streptococci* (Fig. 4) (*30*) was obtained from the sequences of six of the seven genes that define the streptococcal MLST scheme and from calculating the matrix of sequence divergence between isolates. *ddl* is excluded because it is linked to genes determining penicillin resistance, which undergo interspecific transfer more frequently than others (this is an interesting example of selection directly affecting the genetic interrelatedness of populations, albeit at one locus). Named species are currently defined by a strict series of phenotypic tests, and these indeed correspond to clear clusters of related bacteria. However, these clusters are not uniform, for example, *S. pneumoniae* is less divergent than the other named species.

For *S. pneumoniae*, the recombination rate has been estimated as roughly three times the mutation rate (per locus) (*19*), that is, above the clonal/sexual threshold, so it should behave as a sexual population. The distance between species is quite variable. The divergence between *S. pneumoniae* and *S. oralis* is >10%, on the basis of Fig. 1A, we presume that the recombination rate between them is suppressed by a factor of about 100. Thus, even if opportunities for recombination between these were as frequent as intraspecific recombination, they would not blend owing to genetic divergence. By contrast, the divergence between *S. pneumoniae* and *S. pseudopneumoniae* is about 3%, so that interspecific recombination should only be reduced by a factor of 4 relative to intraspecific recombination. In sympatry, this is not sufficiently divergent to prevent blending. Interestingly, the two types of streptococci appear to share a similar niche within the human nasopharynx, and we hypothesize that a mechanism must act to separate the two populations and that they could thus be considered nascent species. Speciation could be considered complete once these populations have diverged enough for blending by sympatric recombination to be genetically impossible.

Conclusions

Our model is an oversimplified caricature of genetic diversification and speciation but nonetheless gives some insight into the interplay between mutation, recombination, and genetic divergence. For the case of diversity generated by neutral drift, we have derived a simple phenomenology of species. If recombination is less common than mutation, the situation is essentially clonal and the population is characterized by a high degree of clustering. In this case, we expect that, although natural selection and geographic structure will act to influence a process of clustering that may be inherent to clonal populations, they do not actually cause the clustering. If recombination is more frequent than this, a threshold is crossed and recombination starts to act as a cohesive force on the population by breaking linkage between alleles and reducing genetic clustering. Such a situation could in principle lead to dynamic speciation by chance drift, but only if the amount of variation within the population is sufficient for recombination rates to vary appreciably between members of the population. On the basis of current estimates for the species we have studied, this does not occur, but it should not be ruled out. Thus, in general, bacteria can and do form sexual species, and mechanisms involving allopatry or niche specialization must be invoked in speciation. In this case, the situation is largely analogous to speciation in higher organisms, without the complications associated with sexual mating choice (*32*).

In our analysis, we have not discussed the role that natural selection may play in driving speciation. This is not because we do not believe selection to be important; quite the contrary. Rather, it is instructive to understand the dynamics of neutral diversification and speciation to then understand how different types of selection might influence this process. Also, we might plausibly hypothesize that even in a structured adaptive landscape, adaptation to different niches may involve selection at a small proportion of loci, and thus that the generation of genomic barriers to recombination arises by the accumulation of selectively neutral mutations, a process governed by simple rules similar to

those described here. In this sense, we may expect our results to be applicable to much larger values of the effective population size where selective forces are amplified relative to drift. Some additional simulations and discussion of the effect of increasing N_e are in (*27*). The derivation of analytical approximations to the processes of cluster dynamics (i.e., splitting, extinction, blending, and relative drift) described here will help in exploring this subject further.

An alternative perspective on bacterial speciation has been provided by Cohan, who identified the clonal-sexual threshold for neutral drift

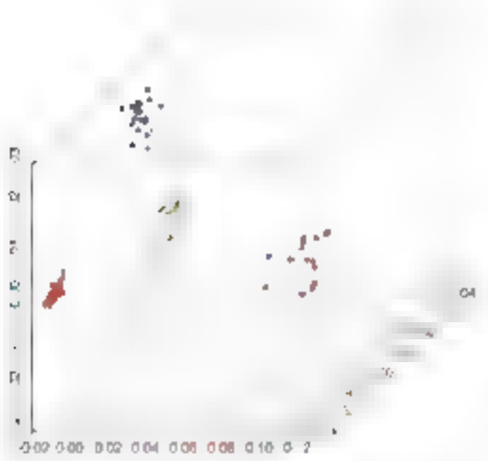

Fig. 4. Genetic map of the *Streptococcus* genus, based on concatenated sequences of MLST genes (excluding *ddl*). Samples from four named species are highlighted: Red, *S. pneumoniae*; yellow, *S. pseudopneumoniae*; purple, *S. mitis*; and brown, *S. oralis*. The three light blue dots represent strains for which the named species status could not be assessed.

but who has emphasized that the threshold for sharing adaptive polymorphisms is much higher (*33*), leading to the notion that populations may be adaptively distinct but indistinguishable by neutral markers. These studies have emphasized the role of adaptive mutations in designating "ecotypes" as putative species (*34*). Our analyses suggest that for populations with recombination rates above the sexual threshold, ecotypes could rapidly blend should the adaptive landscape change and the barriers between niches be removed, and that below the sexual threshold differentiation into distinct genetic clusters arises even in the absence of selection.

Our model highlights the importance of a detailed quantitative description of the processes that drive speciation. The simulations used here are based on generic plausible parameters, but further work is required to produce simulations properly calibrated to individual sets of experimental observations. For example, although the log-linear relation observed in Fig. 1A seems to be general—and strikingly similar among bacteria as different as *Streptococcus*, *Haemophilus* and *Bacillus* species—more effort is needed to measure recombination rates between closely related bacteria because exceptions and anomalies have been documented in some systems (*11*, *28*, *29*), and also to estimate gene flow within and between natural populations. Examination of streptococci (Fig. 4) reveals a diversity of patterns between relatively closely related species, as well as apparent asymmetries in gene flow that are not easily explained by simple models. More work is also required to explore the interplay between recombination and adaptation in more realistic selective landscapes, including in particular the role of epistatic interactions that can promote diversity and limit the scope for genome-wide selective sweeps.

In our opinion, understanding the nature and organization of genetic diversity can only be achieved by taking a multifaceted approach to the problem. Genetic surveys can reveal the extent and nature of the diversity that surrounds us. Careful experimentation can highlight potential mechanisms for creating the observed patterns. Theoretical models can then be used to explore whether the link between mechanisms and observation is plausible. Because the technological capacities for sequencing and simulating sequences are both growing exponentially, the ability to link them into a consistent picture may soon be limited only by our imagination.

References and Notes

1. H. Ochman, J. G. Lawrence, E. A. Groisman, *Nature* **405**, 299 (2000).
2. E. J. Feil *et al.*, *Proc. Natl. Acad. Sci. U.S.A.* **98**, 182 (2001).
3. B. G. Spratt, W. P. Hanage, E. J. Feil, *Curr. Opin. Microbiol.* **4**, 602 (2001).
4. S. G. Acinas *et al.*, *Nature* **430**, 551 (2004).
5. W. P. Hanage, C. Fraser, B. G. Spratt, *BMC Biol.* **3**, 6 (2005).
6. J. C. Venter *et al.*, *Science* **304**, 66 (2004).
7. D. Gevers *et al.*, *Nat. Rev. Microbiol.* **3**, 733 (2005).
8. D. Falush *et al.*, *Philos. Trans. R. Soc. London Ser. B* **361**, 2045 (2006).
9. W. Hanage, B. G. Spratt, K. M. E. Turner, C. Fraser, *Philos. Trans. R. Soc. London Ser. B* **361**, 2039 (2006).
10. J. G. Lawrence, *Theor. Popul. Biol.* **61**, 449 (2002).
11. J. Majewski, *FEMS Microbiol. Lett.* **199**, 161 (2001).
12. M. Vulic, F. Dionisio, F. Taddei, M. Radman, *Proc. Natl. Acad. Sci. U.S.A.* **94**, 9763 (1997).
13. J. Majewski, P. Zawadzki, P. Pickerill, F. M. Cohan, C. G. Dowson, *J. Bacteriol.* **182**, 1016 (2000).
14. P. Zawadzki, M. S. Roberts, F. M. Cohan, *Genetics* **140**, 917 (1995).
15. P. Shen, H. V. Huang, *Genetics* **112**, 441 (1986).
16. J. Majewski, F. M. Cohan, *Genetics* **153**, 1525 (1999).
17. E. Mayr, *Systematics and the Origin of Species* (Columbia Univ. Press, New York, 1942).
18. M. C. J. Maiden *et al.*, *Proc. Natl. Acad. Sci. U.S.A.* **95**, 3140 (1998).
19. C. Fraser, W. P. Hanage, B. G. Spratt, *Proc. Natl. Acad. Sci. U.S.A.* **102**, 1968 (2005).
20. W. P. Hanage, C. Fraser, B. G. Spratt, *J. Theor. Biol.* **239**, 210 (2006).
21. J. W. Drake, B. Charlesworth, D. Charlesworth, J. F. Crow, *Genetics* **148**, 1667 (1998).
22. J. Maynard Smith, *Proc. R. Soc. London Ser. B. Biol. Sci.* **245**, 37 (1991).
23. D. J. Watts, P. S. Dodds, M. E. J. Newman, *Science* **296**, 1302 (2002).
24. J. R. Thompson *et al.*, *Science* **307**, 1311 (2005).
25. Briefly, the model is defined as follows. It is a neutral Fisher-Wright model, that is, in each discrete generation, N_e isolates are sampled with replacement from the previous generation with equal probability. Each isolate has a genotype defined by 70 alleles, and each allele is assigned coordinates within an abstract six-dimensional sequence space. Mutation and recombination occur with probability μ and r per gene, respectively, where L is the length of the gene (600 bp). If mutation occurs, one of the six coordinates is incremented by 1. At the start of the simulation, all coordinates are set to 1. Distances in the abstract sequence space are related to real genetic distances by using a probabilistic model. Based on considering the probability of mutations recurring at the same location in real sequences, sequence (Hamming) distance is estimated as $h = L(1-(1-1/L)^D)$, where D is the block distance in the abstract sequence space, a measure of the number of mutations that separates two alleles. Recombination succeeds with probability matched to the relation observed in Fig. 1A, namely $10^{-3.8x}$, where x is the local sequence divergence, equal to the Hamming distance estimated at the altered gene and its two neighbors divided by the total length being compared (*31*).
26. J. Maynard Smith, N. H. Smith, M. O'rourke, B. G. Spratt, *Proc. Natl. Acad. Sci. U.S.A.* **90**, 4384 (1993).
27. Materials and methods are available as supporting material on *Science* Online.
28. A. Delfa, M. Hendrix, M. Upsjch, S. Jinks Robertson, *Proc. Natl. Acad. Sci. U.S.A.* **94**, 9757 (1997).
29. T. C. Zahrt, S. Maloy, *Proc. Natl. Acad. Sci. U.S.A.* **94**, 9786 (1997).
30. W. P. Hanage, C. Fraser, B. G. Spratt, *Philos. Trans. R. Soc. London Ser. B* **361** (2006).
31. L. S. Hausmann, R. Hakenbeck, P. Gaustad, *J. Bacteriol.* **179**, 6589 (1997).
32. D. Schluter, *Trends Ecol. Evol.* **16**, 372 (2001).
33. F. M. Cohan, *Am. Nat.* **143**, 965 (1994).
34. F. M. Cohan, *Annu. Rev. Microbiol.* **56**, 457 (2002).
35. H. Tettelin *et al.*, *Science* **293**, 498 (2001).
36. R Development Core Team, *A Language and Environment for Statistical Computing* (R Foundation for Statistical Computing, Vienna, Austria, 2006); www.R-project.org.

37. C.F. is funded by a Royal Society University Research Fellowship. W.P.H. and B.G.S. thank the Wellcome Trust for funding. The authors acknowledge useful comments from D. Falush and D. J. Smith. The authors have no conflict of interest.

Supporting Online Material

www.sciencemag.org/cgi/content/full/315/5811/476/DC1
Materials and Methods
Figs. S1 to S7
References

10.1126/science.1127573

Sex-Specific UV and Fluorescence Signals in Jumping Spiders

Matthew L. M. Lim,[1] Michael F. Land,[2] Daiqin Li[1,3]*

There is widespread evidence for animal photoreceptions that are sensitive to ultraviolet (UV) wavelengths, and numerous functions for UV reflectance have also been shown (1). In addition, visible light fluorescence induced by UV wavelengths has been implicated in animal signaling in certain marine invertebrates and in the plumage of parrots (2, 3). We report a case of courtship signaling in which both UV reflectance and UV-induced fluorescence are used on a sex-specific basis. In the ornate jumping spider *Cosmophasis umbratica*, the males have UV-reflective patches of scales on the face and body that are displayed during courtship posturing (4). These are lacking in females (Fig. 1) but females have palps with a UV-excited bright green fluorescence that is absent in males (Fig. 1, A to C).

[1]Department of Biological Sciences, National University of Singapore, 14 Science Drive 4, 117543 Singapore. [2]Department of Biology and Environmental Science, University of Sussex, Brighton BN1 9QG, UK. [3]College of Life Sciences, Hubei University, Wuhan 430062, Hubei, China.

*To whom correspondence should be addressed. E-mail: dbsldq@nus.edu.sg

We examined the consistency of courtship behavior in environments that were either lacking in UV wavelengths (by using a transparent filter that specifically blocked UV wavelengths (fig. S1)) or removed UV reflectance cues in males (UV−) and prevented the fluorescence of females (F−). We also restricted nonvisual communication by using individual glass arenas. By manipulating UV-blocking filters over both either, or none of the glass arenas, we obtained four scenarios: UV+, F+; UV+, F−; UV−, F+; and UV−, F−.

Under full-spectrum light, males readily courted females by adopting a courtship posture comprising a flexed-up abdomen, arched legs, and extended vibrating palps; females responded either with displays comprising hunched legs and bent abdomen or by briefly running away (4). Without UV, females either made no response or simply turned away (without courting). Similarly, males courted more nonfluorescing females by orienting toward them, but responded with a reduced display lacking some behavioral elements. We found that a larger proportion of the same pairs that successfully interacted in the presence of UV (UV+, F+) failed to show intersexual behavior in its absence (UV−, F+) (Fig. 1D).

To ensure that the courtship responses of the spiders were an effect of sexual colors and not behavioral changes in the opposite sex, we compared the behavioral responses of individuals of one sex under full-spectral light when the partner of the opposite sex was illuminated by UV-deficient light. Among the 20 UV+ males that actively courted F+ females, most (16) failed to court the female when she lacked fluorescence (UV+, F−) (Fig. 1E), even though her behavioral reactions remained statistically the same as under normal light. And among 12 F+ females that responded to courting UV+ males (UV+, F+), most (9) ignored the same male that now lacked UV cues (UV−, F+) (Fig. 1F), even though these males also continued to show consistency in courtship. We conclude that sexual coloration is a crucial prerequisite to courtship.

Jumping spiders have excellent eyesight (5), and the retinas of the principal eyes are known to have photoreceptors with maximal sensitivities to UV and to green light (6, 7). The UV receptors have already been shown to have a role in male-male interactions (8). Our study strongly suggests a role for green wavelengths as well. The reflectance spectra of *C. umbratica* males have prominent peaks in both UV and green wavelengths, and the UV-induced green fluorescence is restricted entirely to the palps of females (fig. S2).

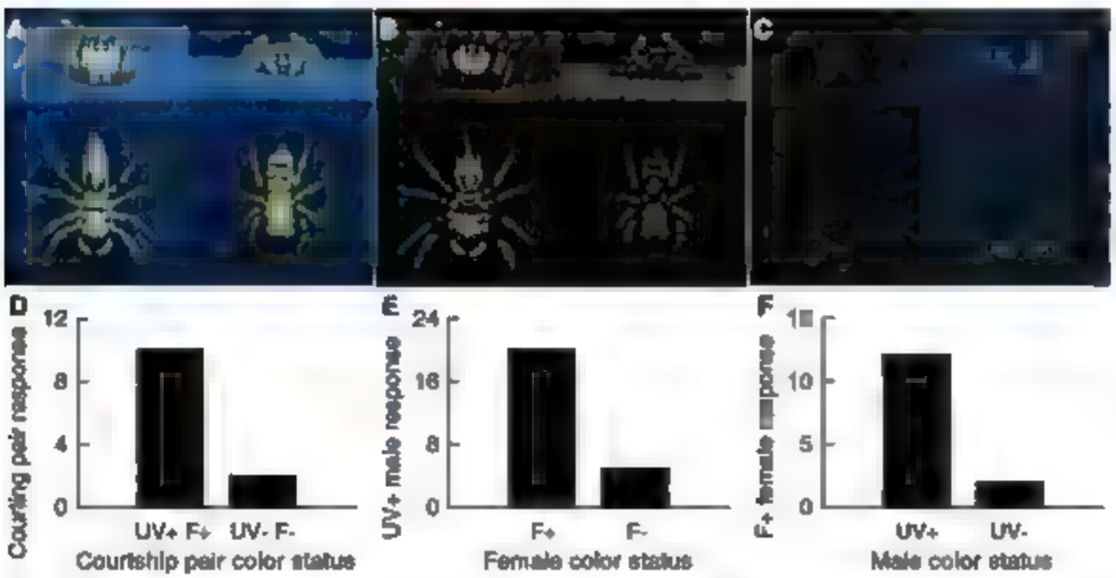

Fig. 1. (**A** to **C**) *C. umbratica* showing UV and fluorescent markings. Males (left) and females (right) from frontal (top) and dorsal (bottom) in (A) human visible color images, (B) UV images with whiter regions showing strong UV-reflective parts, and (C) color images of UV-induced fluorescence in females (Materials and Methods). (**D** to **F**) Decrease in the number of courtship responses when UV wavebands were removed. (D) Reduction in courtship interactions ($P = 0.004$, one-tailed sign test) when UV was absent from both sexes. (E) Males were uninterested when females lacked fluorescence ($P = 0.0003$, one-tailed sign test), and (F) females were uninterested in males that lacked UV colors ($P = 0.001$; one-tailed sign test).

References and Notes

1. M. J. Tovée, *Trends Ecol. Evol.* **10**, 455 (1995).
2. C. H. Marshall, T. W. Cronin, R. L. Caldwell, N. J. Marshall, *Science* **303**, 51 (2004); published online 13 November 2003 (10.1126/science.1089803).
3. K. E. Arnold, I. P. F. Owens, N. J. Marshall, *Science* **295**, 92 (2002).
4. M. L. M. Lim, D. Li, *Biol. J. Linn. Soc.* **89**, 397 (2006).
5. M. F. Land, in *Neurobiology of Arachnids*, F. G. Barth, Ed. (Springer-Verlag, Berlin, 1985), pp. 53–78.
6. A. D. Blest, R. C. Hardie, P. McIntyre, D. S. Williams, *J. Comp. Physiol. A* **145**, 227 (1981).
7. A. G. Peaslee, G. Wilson, *J. Comp. Physiol. A* **164**, 359 (1989).
8. M. L. M. Lim, D. Li, *J. Comp. Physiol. A* **192**, 871 (2006).

9. We thank R. K. Colwell, L. P. Koh, and T. M. Lee for comments on the manuscript. Financial assistance came from the National University of Singapore Academic Research Fund to D.L. (R-154-000-140-112).

Supporting Online Material

www.sciencemag.org/cgi/content/full/315/5811/481/DC1

Materials and Methods
Figs. S1 and S2
References

23 August 2006; accepted 31 October 2006
10.1126/science.1134254

Histocompatible Embryonic Stem Cells by Parthenogenesis

Kitai Kim,[1,2,4] Paul Lerou,[1,4,5] Akiko Yabuuchi,[1,2,4] Claudia Lengerke,[1,2,4] Kitwa Ng,[1,2,4] Jason West,[1,2,4] Andrew Kirby,[6] Mark J. Daly,[6] George Q. Daley[1,2,3,4]*

Genetically matched pluripotent embryonic stem (ES) cells generated via nuclear transfer or parthenogenesis (pES cells) are a potential source of histocompatible cells and tissues for transplantation. After parthenogenetic activation of murine oocytes and interruption of meiosis I or II, we isolated and genotyped pES cells and characterized those that carried the full complement of major histocompatibility complex (MHC) antigens of the oocyte donor. Differentiated tissues from these pES cells engrafted in immunocompetent MHC-matched mouse recipients, demonstrating that selected pES cells can serve as a source of histocompatible tissues for transplantation.

Parthenogenesis entails the development of an embryo directly from a mature oocyte without fertilization. Many animal and plant species reproduce via parthenogenesis, but in mice, parthenogenetic embryos develop only to the early limb bud stage because mammalian embryonic development requires gene expression from the paternal genome. Parthenogenetic embryonic stem (pES) cells have been isolated from parthenogenetic blastocysts of mice and primates (*1*, *2*). Both mouse and primate pES cells undergo extensive differentiation in vitro (*2*, *3*), and pES cells contribute widely to adult tissues in chimeric mice (*1*). A human case of parthenogenetic chimerism has been described in which the hematopoietic system and skin were derived from parthenogenetic cells (*4*). In addition to pluripotent stem cells from fertilized embryos and embryos created by somatic-cell nuclear transfer (*5*), parthenogenesis is another method for creating pluripotent stem cells that might serve as a source of tissue for transplantation.

Highly efficient methods of experimental murine parthenogenesis exist in which oocytes arrested at the second meiotic metaphase (MII) are chemically activated in the presence of cytochalasin, a drug that prevents extrusion of the second polar body (*6*). Diploidy is maintained, and the resulting pseudozygote can develop into a blastocyst from which ES cells can be isolated, which we term p(MII)ES cells (*7*). In some cases, pES cells harbor a duplication of a haploid genome and are thus believed to be predominantly homozygous (*7*, *8*). Because tissues derived from homozygous pES cells would express only one of two sets of parental histocompatibility antigens, they can be more readily matched to patients and might pose less risk of tissue rejection (*9*). However, in heterozygous recipients, major histocompatibility complex (MHC) homozygous tissues may be rejected by natural killer (NK) cells that recognize the lack of one set of histocompatibility antigens, a phenomenon called "hybrid resistance" that is particularly relevant to bone marrow transplantation (*10*). As compared with mismatched organs, partial MHC antigen matching enhances allograft survival, but full MHC-matched tissues are the most favorable for transplant (*11*). The only certain strategy for avoiding immunologic complications is to transplant genetically identical tissues, but this limits transplantation to autologous tissues, transplants between monozygotic twins, or cells created by somatic cell nuclear transfer.

Here we characterize pluripotent ES cell lines generated by parthenogenesis in which both of the maternal MHC loci have been maintained. Differentiated tissues from such MHC-matched ES cells can be transplanted into the oocyte donor strain without rejection, suggesting that these cells could be a favorable source of histocompatible tissues for transplantation.

Recombinant MHC-matched p(MII)ES cells. We reasoned that during the isolation of p(MII)ES cells from hybrid F_1 mice, recombination events occurring between paired homologous chromosomes in meiosis I would produce cells that had restored heterozygosity at the MHC loci (Fig. 1B). Recombination frequencies place the murine H-2 MHC locus at ~18.5 centimorgans (cM) from the centromere of mouse chromosome 17 (*12*), thus predicting that approximately one

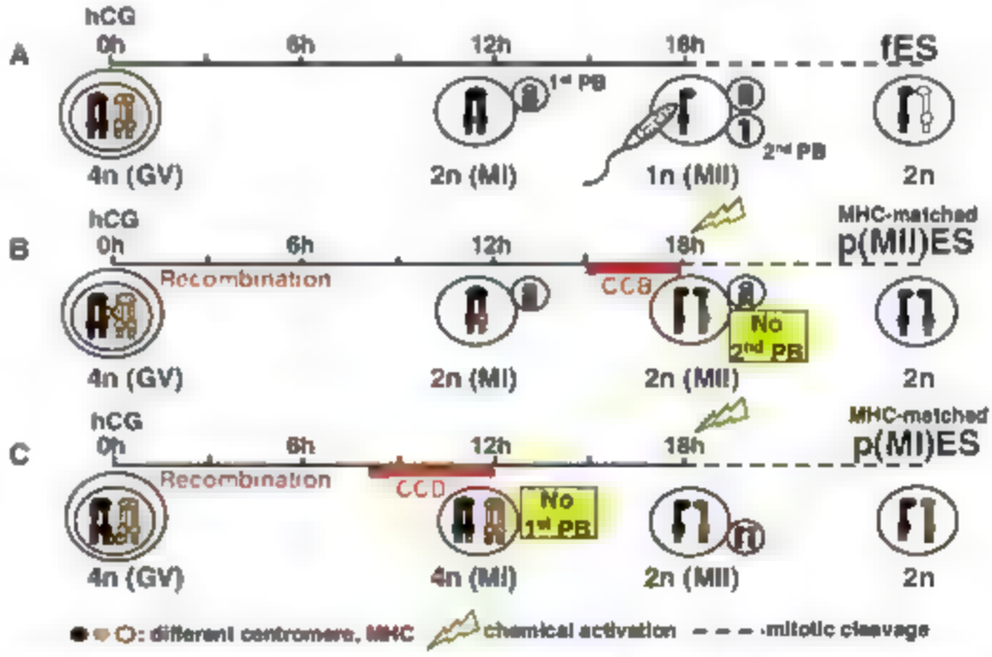

Fig. 1. Chromosome dynamics during normal and artificial murine oocyte maturation. (**A**) Normal fertilization. Immature oocytes arrested at diplotene of the first meiotic prophase harbor 20 sets of paired homologous chromosomes (bivalents). A single bivalent pair is illustrated at left, without recombination. The maternal or paternal chromosomes segregate into the first polar body (1st PB) during MI. At fertilization, half of the chromosomes are extruded via the second polar body (2nd PB), and the incoming sperm restores the diploid chromosome complement. Blastocysts derived by fertilization yield fES cells. hCG, human chorionic gonadotropin; GV, germinal vesicle. Timeline is shown at top, h, hours. (**B**) Parthenogenetic oocyte maturation. MII-arrested oocytes are activated in cytochalasin B, blocking extrusion of the second polar body. Diploidy is maintained, and the resulting blastocysts yield p(MII)ES cells. Recombination events produce MHC-matched p(MII)ES cells. (**C**) Parthenogenetic activation of immature oocytes (*26*). Inhibiting extrusion of the first polar body prevents segregation of the homologous chromosome pairs. Extrusion of a polar body restores diploidy.

[1]Division of Pediatric Hematology/Oncology, Children's Hospital Boston and Dana Farber Cancer Institute, Boston, MA 02115, USA. [2]Department of Biological Chemistry and Molecular Pharmacology, Harvard Medical School, Boston, MA 02115, USA. [3]Division of Hematology, Brigham and Women's Hospital, Boston, MA 02115, USA. [4]Harvard Stem Cell Institute, Cambridge, MA 02138, USA. [5]Division of Newborn Medicine, Brigham and Women's Hospital and Children's Hospital, Harvard Medical School, Boston, MA 02115, USA. [6]Center for Human Genetic Research, Massachusetts General Hospital, Boston, MA 02115, USA.

*To whom correspondence should be addressed. E-mail: george.daley@childrens.harvard.edu

in five meioses will yield a crossover event. We collected mature oocytes from C57BL/6 × CBA F_1 mice and initiated parthenogenetic embryo development via a protocol that prevents extrusion of the second polar body. From the 74% of activated oocytes that developed to blastocysts, we isolated 72 p(MII)ES cell lines (Table 1).

We used polymerase chain reaction (PCR) amplification followed by allele-specific restriction enzyme digestion or direct sequencing of single-nucleotide polymorphisms (SNPs) within the H-2 region of chromosome 17 to determine whether recombination had restored heterozygosity at the MHC loci (*13*). 24 out of 72 p(MII)ES cells (33%) harbored the heterozygous MHC genotype of the oocyte donor (fig. S1A, black circles, and fig. S1, B and C). Genotyping of flanking markers on chromosome 17 confirmed the MHC heterozygosity in a subset of eight selected cell lines (fig. S1C). We call ES cells selected in this manner recombinant MHC-matched p(MII)ES cells.

Recombinant MHC-matched p(MII)ES cells were differentiated into embryoid bodies (EBs) for 14 days, followed by culture on gelatin-coated tissue culture plates for an additional 14 days in order to examine MHC antigen expression on a differentiated population of epithelial-like cells (*14*). Differentiated p(MII)ES cells that had not recombined at the MHC loci by polymorphism analysis expressed only one of the parental MHC proteins ($H2K^b$ for C57BL/6 mice; Fig. 2B), whereas MHC-matched p(MII)ES cells that had recombined expressed both $H2K^b$ and $H2K^k$ on all cells (Fig. 2C). These data confirm the heterozygous genotype by MHC antigen expression. A majority of p(MII)ES cells had a normal karyotype (fig. S2A, $n = 16$ normal karyotypes out of 19 lines tested). A majority of p(MII)ES cells showed the loss of one X chromosome, a phenomenon known to occur in female ES cells (*15*).

MHC-matched p(MI)ES cells. In a second method aimed at generating genetically matched pES cells from C57BL/6 × CBA F_1 mice, we induced parthenogenetic development of immature oocytes while interfering with the segregation of the paired homologous chromosomes during the first meiotic metaphase (MI; Fig. 1C). This protocol has been reported to yield parthenogenetic embryos that are genetic clones of the oocyte donor by preventing segregation of the homologous maternal and paternal chromosomes (*16*). From the 56% of activated oocytes that developed into blastocysts, we isolated 23 ES cell lines, which we term p(MI)ES cells (Table 1). We determined the genotypes of the MHC region of the p(MI)ES cell lines by PCR amplification followed by allele-specific restriction enzyme digestion or direct sequencing of SNP loci on chromosome 17, and we observed MHC heterozygosity in 21 of 23 cell lines (fig. S1A, white circles, and fig. S3). Genotyping of flanking markers on chromosome 17 confirmed the heterozygous MHC genotype and MHC identity with the oocyte donor in 10 members of a selected set of 12 p(MI)ES cell lines (fig. S1C).

MHC-matched p(MI)ES cells were differentiated for 28 days in culture as described above and examined by flow cytometry. The differentiated derivatives expressed both $H2K^b$ and $H2K^k$ on all cells, confirming heterozygosity of the MHC locus by surface protein expression (Fig. 2D). In seven p(MI)ES cell lines, we documented a normal diploid chromosome content by direct chromosome counting (fig. S2C). Seven p(MI)ES cell lines had 39 chromosomes, reflecting the tendency of female ES cells to lose an X chromosome (*7*, *15*). Nine lines showed variable chromosome content. A more detailed genomic analysis that distinguishes these diploid and aneuploid classes of p(MI)ES cells is presented below.

Pericentromeric genotype and patterns of recombination in p(MII) and p(MI)ES cells. To assess the pattern of chromosomal segregation observed under the different oocyte activation protocols and to determine the degree of genetic identity of the pES cells with the oocyte donor, we determined the pericentromeric genotype and distal recombination of the p(MII)ES and p(MI)ES cell lines using SNPs that distinguish the parental mouse strains (C57BL/6 and CBA) (*17*). We hypothesized that p(MII)ES cells would be predominantly homozygous, with recombination reflected by a telomeric predominance of heterozygous SNPs. Conversely, we reasoned that the p(MI)ES cells would be predominantly heterozygous, with recombination reflected by a telomeric predominance of homozygous SNPs. Moreover, ES cells isolated from embryos that resulted from natural fertilization events between strains of inbred mice (fES cells from F_1 matings) should show heterozygosity at

Table 1. Parthenogenetic oocyte activation and ES cell derivation from a C57BL/6 × CBA F_1 mouse. Numbers indicate embryos reaching a given stage/total oocytes.

	Efficiency of p(MII)ES cell derivation					
Stage	**1 cell**	**2 cells**	**4 cells**	**Morula**	**Blastocyst**	**p(MII)ES cells**
Rate of development	150/150 (100%)	125/150 (83%)	117/150 (78%)	115/150 (77%)	111/150 (74%)	72/111 (65%)
	Efficiency of p(MI)ES cell derivation					
Rate of development	112/112 (100%)	87/112 (78%)	81/112 (72%)	75/112 (67%)	63/150 (56%)	23/63 (37%)

Table 2. Teratoma formation after injection of differentiated fES, p(MII)ES, and p(MI)ES cells into MHC-matched and -mismatched recipients, observed for 3 months. $Rag2^{-/-}\gamma c^{-/-}$ mice are on the C57BL/6 background. Numbers represent teratomas formed/total mice injected. ($P < 0.001$ for the hypothesis that haploidentity or full MHC match predicts teratoma formation; see methods in supporting online material for assumptions in statistical analysis.)

	ES cell type (MHC)					
Recipient mouse	**fES cells (C57BL/6)**	**fES cells (CBA)**	**fES cells (C57BL/6 × CBA)**	**p(MII)ES cells (C57BL/6)**	**p(MII)ES cells (C57BL/6 × CBA)**	**p(MI)ES cells (C57BL/6 × CBA)**
$Rag2^{-/-}\gamma c^{-/-}$	+ (4/4)	+ (5/5)	+ (2/3)	+ (4/4)	+ (3/3)	+ (3/3)
CBA	− (0/4)	+ (5/5)	− (0/3)	− (0/3)	− (0/4)	− (0/4)
C57BL/6	+ (5/7)	− (0/5)	− (0/5)	+ (8/12)	− (0/5)	− (0/5)
C57BL/6 × CBA F_1	+ (3/5)	+ (3/5)	+ (6/8)	+ (12/12)	+ (4/5)	+ (5/5)

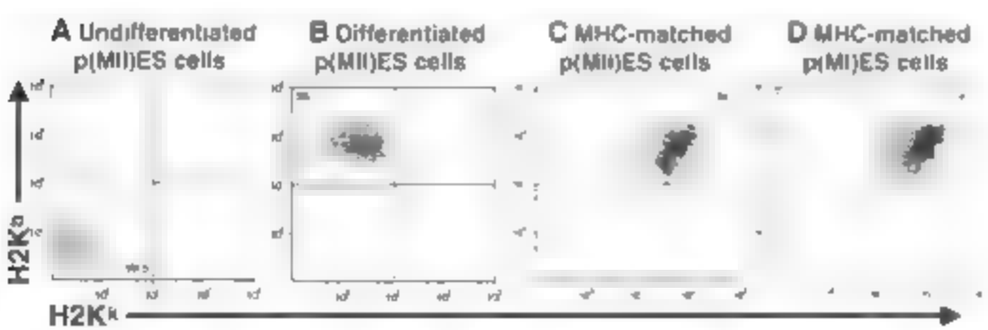

Fig. 2. MHC protein expression on pES cells. Flow cytometric detection of H2K protein expression is shown on (**A**) undifferentiated p(MII)ES cells, (**B**) differentiated MHC homozygous p(MII)ES, (**C**) MHC-heterozygous p(MII)ES, and (**D**) MHC-heterozygous p(MI)ES cells.

all loci, because the gametes derive from homozygous parents in which meiotic recombination is genetically invisible. We genotyped three SNPs on chromosome 17 in 72 p(MII)ES, 23 p(MI)ES, and 20 tES cell lines, and a single pericentromeric SNP on each chromosome in one p(MII)ES and five p(MI)ES cell lines (fig. S4). Based on the results of this low-resolution genotyping, we selected a set of 17 p(MII)ES and 20 p(MI)ES cells and performed higher-resolution genotyping using a standard panel of 768 mouse markers evenly spaced across the genome [an expansion of a previously described SNP set (*19*)]. A total of 514 markers spanning the 2.25 gigabases (Gb) across the 19 autosomes were informative. They were polymorphic between C57BL/6 and CBA and had a control F_1 correctly identified as heterozygous (resulting in an average intermarker distance of 4.6 Mb).

SNP genotyping confirmed the hypothesized patterns of recombination but revealed a surprisingly high degree of heterozygosity for the p(MII)ES cells. Because sister chromatid segregation is prevented in MII, all chromosomes were substantially homozygous near their centromeres for one of the two parental strains (Fig. 3A and figs. S5 and S6). Because of recombination, the heterozygosity of SNP markers increased in frequency in proportion to the genetic distance from the centromere (Fig. 3A, right panel, and fig. S6A). Despite the presumption of predominant homozygosity in p(MII)ES cells, we found homozygosity at only [illegible] loci in a survey of 17 p(MII)ES cell lines, with a range of homozygosity between 23.9 and 47.5% (fig. S7). These data demonstrate that, contrary to expectation, recombination renders the majority of loci in p(MII)ES cells heterozygous.

Some p(MII)ES cells harbored genotypes that showed homozygosity of SNPs from one parental strain near the centromere, followed by a region of heterozygosity and then a telomeric region of homozygosity of SNPs from the other parental strain (chromosomes 8 and 10 in Fig. 3A). This pattern is consistent with meiotic recombination between both sister chromatid pairs of homologous chromosomes, which occurs during MI, followed by segregation of the bivalents into separate cells upon extrusion of the first polar body, and then co-segregation of the recombinant sister chromatids into the same cell due to inhibition of extrusion of the second polar body (Fig. 1B). With both sister chromatids undergoing recombination separately, we postulated that p(MII)ES cells, although constrained to be homozygous at the centromeres, would manifest recombination at a rate that would be equivalent to an F_2 intercross between two F_1 mice. We calculated the genetic linkage map from the p(MII)ES genotypes using the program MAPMAKER EXP version 3 under the model of an F_2 intercross, and across all autosomes we estimated a total map length of 1339 cM. This is broadly consistent with the Massachusetts Institute of Technology Whitehead map, which reported a total autosomal map length estimate of 1338 cM (*19*).

Analysis of the recombination patterns of 70 p(MII)ES cells showed two distinct subgroups. Twelve of the p(MII)ES cells showed a predominant pattern of heterozygosity beginning at the centromere, followed on some chromosomes by telomeric regions of homozygosity (Fig. 3F and fig. S6B). When the genotype data of these 12 lines were similarly evaluated under the assumption of an F_2 intercross, the observed map length was significantly suppressed (910 cM). Despite the high density of polymorphic markers examined, 94 of the 228 autosomes in these 12 lines were observed to be completely heterozygous (fig. S7). These observations drive the estimated map length down as compared to that of the p(MII)ES cells and a standard F_2 recombination pattern. Indeed, the map length is suppressed because the recombinant chromosomes will in some cases co-segregate by chance (or by nondisjunction) into the same cell, thereby preserving heterozygosity in the genotyping assay (fig. S8).

A subset of eight p(MII)ES cells demonstrated complete heterozygosity across all loci, suggesting genetic identity of the parthenogenetic embryo with the oocyte donor—in effect, a parthenogenetic clone, as originally reported (*16*). However, all of the eight p(MII)ES cell lines that show complete heterozygosity are in fact aneuploid, with a range of chromosome counts between 38 and 77. Thus we speculate that these panheterozygous p(MII)ES cells derive from tetraploid blastocysts that manifest infidelity of chromosomal segregation during derivation and culture. Indeed, when oocytes are activated soon

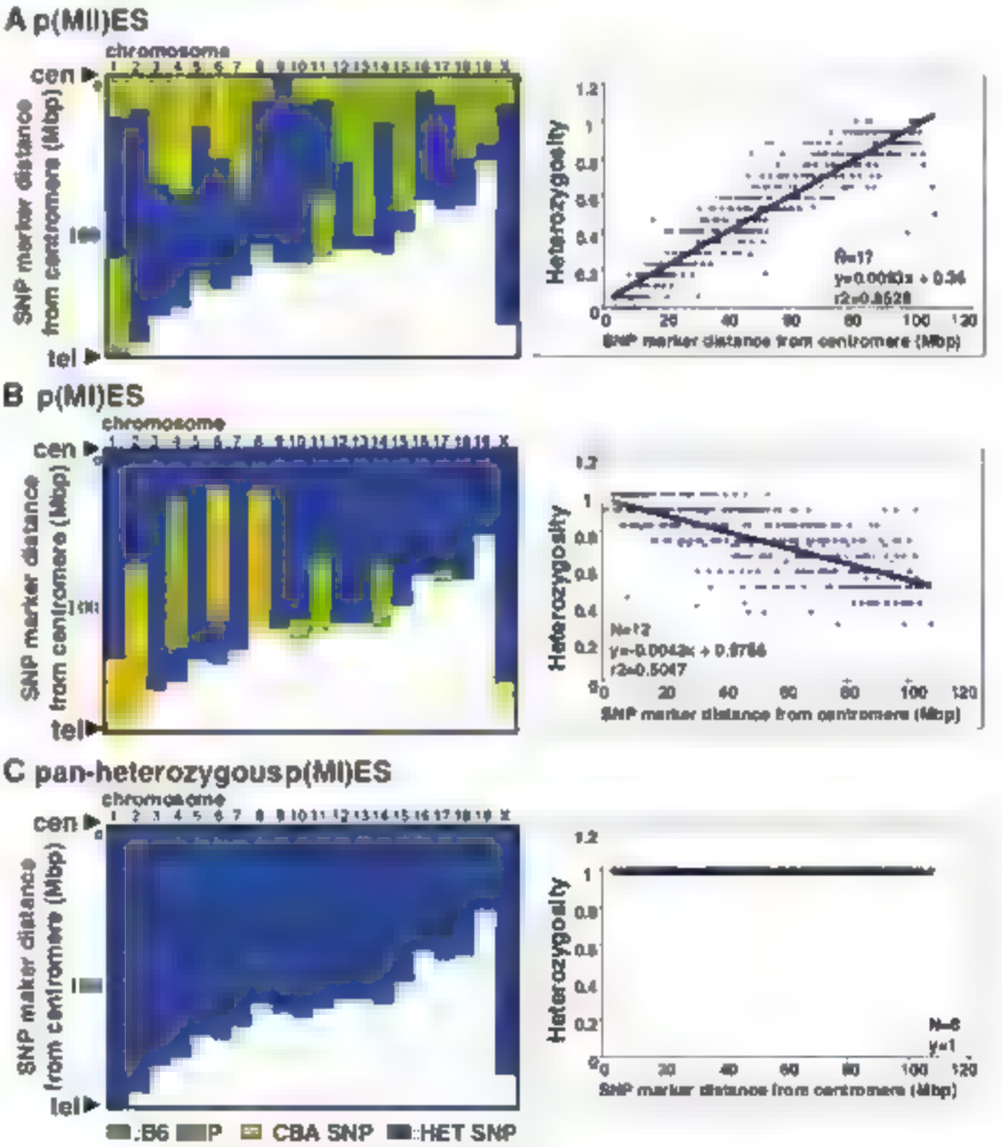

Fig. 3. Genome-wide SNP genotyping of a representative clone of p(MII)ES, p(MI)ES, and panheterozygous p(MII)ES cells. (**A**) p(MII)ES cells, (**B**) p(MI)ES cells, (**C**) panheterozygous p(MI)ES cells. (Left panels) show genotypes for each chromosome, from centromere (cen, top, to telomere (tel, bottom), revealing blocks, or haplotypes, of markers. Green, homozygous C57BL/6 (B6) SNP; orange, homozygous CBA SNP; blue, heterozygous (HET) SNP. Right panels show the heterozygosity of SNP markers plotted against SNP marker distance from the centromere.

after cytochalasin treatment to block MII, tetraploid blastocysts frequently result (figs. S2C and S9). Such embryos will yield tetraploid p(MII)ES cells, and it is possible that incubation with dimethylaminopurine may thereafter predispose them to abnormal chromosomal segregation or chromosomal loss. Such isolates maintain complete heterozygosity when genotyped as a population but do not represent a true clone of cells with genetic identity to the oocyte donor. Theoretically, parthenogenetic clones would arise only if the recombination events of MI are suppressed or if there is obligate co-segregation of the recombinant chromosomes into the same daughter cell. Based on our experience, we are skeptical that true parthenogenetic clones can be isolated.

Differentiation potential of p(MII)ES and p(MI)ES cell lines. To assess the pluripotency of the MHC-matched pES cells, we evaluated their differentiation potential by in vitro and in vivo assays. We injected cells subcutaneously into immunodeficient mice and observed robust teratoma formation from multiple p(MII)ES (n = 11), p(MI)ES (n = 4), and fES (n = 3) cell lines. The differentiation potential of p(MII)ES cells has been well documented (*1*), but not that of p(MI)ES cells. Histology of teratomas made from p(MI)ES cells revealed tissue elements of all three embryonic germ layers, mesoderm (bone, bone marrow, muscle, and cartilage), endoderm (respiratory epithelium and exocrine pancreas), and ectoderm (brain, melanocyte (iris), and skin) (Fig. 4). Using previously published methods for in vitro differentiation of ES cells, we observed rhythmic contractility in EBs that was consistent with cardiomyocyte development in p(MII), p(MI), and fES cells, and comparable numbers of hematopoietic elements as measured by methylcellulose-based colony-forming cell assays and flow cytometric analysis for the hematopoietic markers c-Kit, CD41, and CD45 (*20*) (fig. S10, A and B). We generated chimeric mice by injecting p(MII)ES (n = 4) and p(MI)ES (n = 3) cells into recipient blastocysts. Examples of p(MII)ES and p(MI)ES cells each demonstrated fetal liver chimerism and high-level skin chimerism of adult mice (Fig. 4I). No germline transmission of gametes from the p(MII)ES or p(MI)ES cells was noted in eight male and female chimeras that generated more than 700 progeny. Moreover, injection of over 50 tetraploid embryos with p(MII)ES cells failed to result in live births, consistent with the known developmental limitation of parthenogenetic mouse embryos (*1*). All were not fully competent to sustain organismal development because of a lack of paternal imprints, p(MII)ES and p(MI)ES cells appear to share a comparable degree of multilineage tissue differentiation as fES cells.

Histocompatibility of differentiated progeny of MHC-matched p(MII) and p(MI)ES cells. To test the immune compatibility of selected ES cell lines, we performed transplantation experiments in immunodeficient mice and in immunocompetent recipients that were either MHC-matched or -mismatched. When we injected 10^6 undifferentiated fES or pES cells subcutaneously into immunocompetent mice, we failed to observe efficient teratoma formation regardless of the genotypes of the ES cells or recipient mice. Like early embryonic tissues, undifferentiated mouse ES cells do not express MHC antigens, which we speculate renders them susceptible to rejection by NK cells (*5*). MHC antigens are expressed after differentiation of mouse ES cells in vitro (Fig. 2). To determine whether differentiated tissues derived from ES cells would be accepted as tissue grafts in recipient mice, we pre-differentiated ES cells into EBs for 2 weeks, then injected EB cells subcutaneously into immunodeficient mice or into immunocompetent MHC-matched and -mismatched recipients. We observed teratomas in all mice when we injected pre-differentiated ES cells into immunodeficient Rag2$^{-/-}\gamma c^{-/-}$ mice (Table 2). In immunocompetent recipient mice, we observed teratoma formation from pre-differentiated fES and pES cells only if there was no MHC mismatch with the recipient (Table 2). ABTS cells that carried both C57BL/6 and CBA MHC genotypes successfully engrafted in heterozygous MHC-matched C57BL/6 × CBA F_1 recipients, but failed to form teratomas in mismatched homozygous C57BL/6 or CBA recipi-

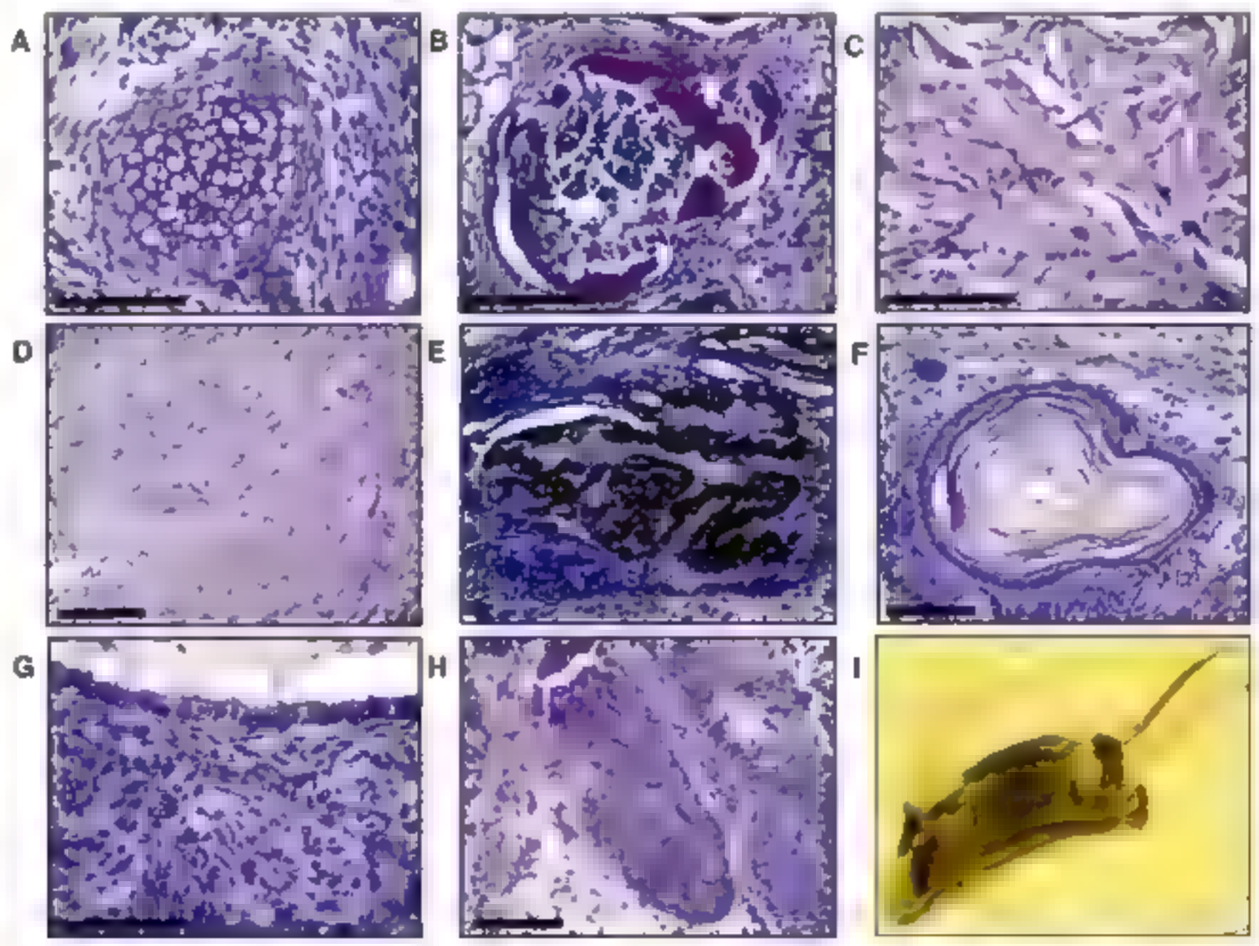

Fig. 4. Histopathology of teratomas from MHC-matched p(MI)ES cells and skin chimerism. (**A**) Cartilage. (**B**) Bone and bone marrow. (**C**) Muscle. (**D**) Brain. (**E**) Melanocyte (iris). (**F**) Skin. (**G**) Respiratory epithelium. (**H**) Pancreas. (**I**) Black coat color chimerism resulting from p(MI)ES cells injected into blastocysts from a BalbC5JL F_1 mouse (white coat color). Scale bar, 100 μm.

ents (Table 2). Homozygous fES or pMII ES cells engrafted in MHC-matched homozygous and heterozygous recipients (Table 2). Because ES cells of the CBA strain form teratomas in the $Rag2^{-/-}\gamma c^{-/-}$ mice, which are on the C57BL/6 background, we conclude that the immune response, and not host strain factors, is responsible for the failure of teratoma formation in immunocompetent MHC-mismatched recipients. These data demonstrate the histocompatibility of differentiated tissues from fES and pES cells that share genetic identity at the MHC loci with transplant recipients.

Discussion. We describe two strategies for isolating pluripotent murine ES cells that are genetically matched to the oocyte donor at the MHC loci. By applying genotyping analysis to pES cells isolated from hybrid C57BL/6 × CBA F_1 mice, we have selected lines that retain the maternal MHC genotype by virtue of sporadic meiotic recombination events and inheritance of the relevant sister chromatids. When these genetically defined pES cells are pre-differentiated into EBs before being injected into immunocompetent recipient mice, the tissues engraft as long as the MHC genotype of the donor cells is matched to the recipient mouse.

Although unable to sustain full organismal development because of the lack of paternal imprints, ES cells derived from parthenogenetic embryos appear to be pluripotent. Whether tissue differentiation and engraftment into all lineages are robust and whether the loss of heterozygosity of critical genomic regions might disrupt cell function in engrafted tissues remain central questions (*27*). These caveats notwithstanding, our data from the murine system establish a proof of principle for using parthenogenesis to generate MHC-matched tissues for transplantation.

Differentiated tissues from pES cells that express only one of the two sets of parental MHC haplotypes appear to engraft in heterozygous recipients (for example C57BL/6 into C57BL/6 × CBA F_1 recipients; Table 2). This suggests the theoretical possibility that a modest-sized bank consisting of pES cells homozygous for the major MHC haplotypes could serve as a source of transplantable tissues for cell replacement therapy. However, bone marrow and perhaps other tissues are subject to rejection by NK cells, which can distinguish tissues that express the full complement of MHC molecules from those expressing only a few (*10*). Moreover, minor histocompatibility antigens scattered across the genome might complicate transplantation from an allogeneic cell bank. Full MHC matching (or indeed, full genetic identity) is most favorable for predicting the survival and function of solid-organ allografts (*11*). More discriminating transplantation experiments are needed to distinguish the relative merits of tissues derived from homozygous MHC-matched pES cells, fully MHC-matched pES cells, or isogenic tissues derived by nuclear transfer.

A routine, highly efficient method for experimental parthenogenesis in mice interrupts MII and results in an embryo that carries a duplicated haploid genome that has been described as predominantly homozygous, except for regions that have reverted to heterozygosity because of recombination events during MI (*3*). Our data demonstrate quite unexpectedly that the majority of loci in pMIIES cells undergo recombination, thereby generating a predominantly heterozygous genome. Similarly, several rounds of mitotic divisions and inhibition of the first meiotic division ensure that substantial heterozygosity is preserved across the genome except for those regions that convert to homozygosity because of recombination. Both pMII and pMI cells can be selected to maintain the MHC genotype of the oocyte donor. All forms of pES cells retain the mitochondrial genome of the oocyte donor, unlike genetically matched ES cells that are created by nuclear transfer into oocytes from an unrelated donor, and therefore may avoid immunologic rejection due to antigens encoded by the mitochondrial genome (*22*).

Using a protocol that had been reported to create parthenogenetically cloned embryos (*16*), we generated a set of eight pMIIES cells that retained complete heterozygosity at all loci, implying genetic identity with the oocyte donor. However, these cells were all either tetraploid or aneuploid, suggesting that they arose from embryos that had failed to convert to diploidy during the parthenogenetic activation of immature oocytes. Although these cells retain essentially all of the maternal chromosomes, they are not true clones and are not likely to be a trustworthy source of tissues for transplantation.

The status of maternal- or paternal-specific imprint genes can be monitored to identify pES cells. Analyses of the imprinted status of the Rasgrf1 locus in 16 pMIIES cells confirmed the maternal pattern of methylation (fig. S11). However, the assessment of imprint loci in ES cells may be unreliable given their tendency toward epigenetic instability (*27*). The data presented here demonstrate that discerning the distinct patterns of homozygosity and heterozygosity in ES cell lines through SNP genotyping across the genome provides a definitive means to determine whether lines are the result of parthenogenesis, nuclear transfer, or natural fertilization. The diagnostic pattern of a pMIIES cell line is pericentromeric homozygosity and increasing heterozygosity as physical and genetic distance from the centromere increases. The diagnostic pattern of a pMIIES cell line is pericentromeric heterozygosity and an increasing frequency of homozygosity at markers distal to the centromere. A cell line derived from an embryo produced by nuclear transfer from a somatic cell will, for the most part, be a complete genetic match of the nuclear donor, because only rare occurrences of mitotic recombination would alter the expected pattern of SNP identity. Furthermore, there should be no discernable tendency for the recombination of genetic markers at greater distances from the centromere. Similarly, an ES cell line derived from a fertilized blastocyst should be a combination of sperm and egg donor haplotypes, again with no relationship between frequency of heterozygosity of markers and distance from the centromere.

Beyond demonstrating the potential for histocompatibility of parthenogenetically derived tissues, our experiments provide an analysis of genetic recombination during parthenogenetic activation and distinguish the patterns of recombination observed when karyokinesis is interrupted during meiosis I or II. Moreover, we note that isolation of pMIIES cells followed by SNP genotyping provides a means of genetic mapping of loci for phenotypes that can be defined through the study of ES cells.

References and Notes

1. M. D. Allen, S. C. Barton, K. Hilton, M. L. Norris, M. A. Surani, *Development* **120**, 1473 (1994)
2. J. B. Cibelli *et al.*, *Science* **295**, 819 (2002)
3. H. Lin *et al.*, *Stem Cells* **21**, 152 (2003)
4. L. Strain, J. P. Warner, T. Johnston, D. T. Bonthron, *Nat. Genet.* **11**, 164 (1995)
5. W. M. Rideout 3rd, K. Hochedlinger, M. Kyba, G. Q. Daley, R. Jaenisch, *Cell* **109**, 17 (2002)
6. H. Balakier, A. K. Tarkowski, *J. Embryol. Exp. Morphol.* **35**, 25 (1976)
7. E. J. Robertson, M. J. Evans, M. H. Kaufman, *J. Embryol. Exp. Morphol.* **74**, 297 (1983)
8. M. A. Surani, S. C. Barton, M. L. Norris, *Nature* **308**, 548 (1984)
9. C. J. Taylor *et al.*, *Lancet* **366**, 2019 (2005)
10. P. Hoglund *et al.*, *Immunol. Rev.* **155**, 11 (1997)
11. G. Opelz, T. Wujciak, B. Dohler, S. Scherer, J. Mytilineos, *Rev. Immunogenet.* **1**, 334 (1999)
12. National Center for Biotechnology Information.
13. S. H. Klebe, M. W. Hoffmann, P. B. Mushoff, B. Bayer, F. J. Marshall, *J. Immunol. Methods* **276**, 197 (2003)
14. E. Y. Fok, P. W. Zandstra, *Stem Cells* **23**, 1333 (2005)
15. I. Zvetkova *et al.*, *Nat. Genet.* **37**, 1274 (2005)
16. J. Kubiak, A. Paldi, M. Weber, B. Maro, *Development* **111**, 763 (1991)
17. The Jackson Laboratory. www.informatics.jax.org/ (2006)
18. J. L. Moran *et al.*, *Genome Res.* **16**, 436 (2006)
19. W. F. Dietrich *et al.*, *Nature* **380**, 149 (1996)
20. H. K. Mikkola, Y. Fujiwara, T. M. Schlaeger, D. Traver, S. H. Orkin, *Blood* **101**, 508 (2003)
21. L. Hernandez, S. Kozlov, G. Piras, C. L. Stewart, *Proc. Natl. Acad. Sci. U.S.A.* **100**, 13344 (2003)
22. J. Van de Water *et al.*, *N. Engl. J. Med.* **320**, 1377 (1989)
23. D. Humphreys *et al.*, *Science* **293**, 95 (2001)

24. This study was supported by grants from NIH and the NIH Director's Pioneer Award of the NIH Roadmap for Medical Research. G.Q.D. is a recipient of the Burroughs Wellcome Fund Clinical Scientist Award in Translational Research. K.K. was supported by the Cooley's Anemia Foundation and is a Special Scholar of the Leukemia and Lymphoma Society. P.L. was partly supported by NIH training grant Pathobiology of Newborn and Developmental Diseases (T32 HD007466). C.L. was supported by a Mildred Scheel Stiftung fuer Krebsforschung fellowship.

Supporting Online Material

www.sciencemag.org/cgi/content/full/1133542/DC1
Materials and Methods
Figs. S1 to S11
Table S1
References

7 August 2006; accepted 6 December 2006
Published online 14 December 2006;
10.1126/science.1133542
Include this information when citing this paper.

Reversible Switching of Hydrogel-Actuated Nanostructures into Complex Micropatterns

Alexander Sidorenko,[1] Tom Krupenkin,[1] Ashley Taylor,[1] Peter Fratzl,[2] Joanna Aizenberg[1]*

Responsive behavior, which is intrinsic to natural systems, is becoming a key requirement for advanced artificial materials and devices, presenting a substantial scientific and engineering challenge. We designed dynamic actuation systems by integrating high–aspect-ratio silicon nanocolumns, either free-standing or substrate-attached, with a hydrogel layer. The nanocolumns were put in motion by the "muscle" of the hydrogel, which swells or contracts depending on the humidity level. This actuation resulted in a fast reversible reorientation of the nanocolumns from tilted to perpendicular to the surface. By further controlling the stress field in the hydrogel, the formation of a variety of elaborate reversibly actuated micropatterns was demonstrated. The mechanics of the actuation process have been assessed. Dynamic control over the movement and orientation of surface nanofeatures at the micron and submicron scales may have exciting applications in actuators, microfluidics, or responsive materials.

Adaptive materials and devices that change properties and function in response to external stimuli are the focus of research in fields ranging from medicine and biology to chemistry, physics, materials science, and engineering. A wide range of artificial responsive materials, mostly involving polymers, has been reported (*1*–*9*). Hydrogels are prominent examples of such materials. Their elastic networks swell in water, allowing one to achieve the desired degrees of polymer hydration and volume changes. A variety of gels that are responsive to humidity, pH, temperature, electric fields, light, and ion strength have been designed (*1*–*7*) and patterned by means of lithography (*8*, *9*). These responsive gels have been shown to have potential applications in microfluidics, tissue engineering, and as shape-memory materials, artificial muscles, valves, and actuators (*1*–*9*).

Synthetic routes and fabrication strategies leading to new-generation, dynamically tunable materials are often inspired by biological systems that show a wide range of adaptive responses. Recently, a number of studies have demonstrated that various physicochemical properties of biological materials that are generally vital for survival arise from the presence of highly developed surface nano-roughness and exquisite nano- and microfeatures (*10*–*12*). Nano- and microstructures that develop on the surfaces of gecko feet, lotus leaves, and cicada and butterfly wings, for example, provide these organisms with exceptional adhesive, self-cleaning, water-repelling, and photonic properties.

Several efforts have been made to artificially produce nanostructured surfaces in polymeric materials that mimic biological structures and functions (*13*, *14*). The intrinsic flexibility of polymers frequently leads to undesired design outcomes because the features in soft materials are poorly controlled in general and are often susceptible to irreversible collapse (*15*). We reported an alternative approach to the fabrication of nanostructured surfaces, in which regular arrays of well-defined nanostructures with feature sizes of ~100 to 300 nm and aspect ratios reaching 100 were formed in silicon by means of the Bosch process (*16*). These structures are stable and their geometry is highly controlled. This rigidity, however, makes them unsuitable for use in adaptive materials and devices. A more promising approach is to create materials based on a hard-soft combination that capitalizes on the properties of both elements. Stable superhydrophobic surfaces have been fabricated by using polyelectrolyte multilayers overcoated with silica nanoparticles (*17*). Interesting examples of chemically, magnetically, and light-responsive photonic crystals, which were made by dispersing rigid colloidal particles into hydrogels, have been reported (*18*, *19*). Rodlike building blocks consisting of gold and polymer domains have been shown to self-assemble into a variety of superstructures (*20*).

We propose here to use the combination of soft and hard elements to enable reversible actuation of rigid surface nano- and microstructures that are set in motion by the polymer layer. We integrated a hydrogel (Fig. 1A) with an array of isolated, high aspect-ratio rigid structures (AIRS) (Fig. 1B) into hydrogel-AIRS assemblies (HAIRS) (Fig. 1, C to E). The AIRS provide rigidity, structure, and precision, whereas the hydrogel provides responsive behavior. We anticipated that the combination of the two would offer substantial dynamic responses based on geometrical rearrangements of the hydrogel-actuated nanostructures.

To achieve these designs, the hydrogel was formed in the confinement between AIRS and a secondary substrate (Fig. 1C) (*21*). Polyglycidyl methacrylate (PGMA) partially modified with acrylic acid, which forms an anchoring interface that is rich in reactive epoxy groups (*22*), was chemisorbed on one of the substrates. A layer of polyacrylamide gel (PAAG) grafted to the substrate via PGMA was formed by photo- or thermo-initiated in situ radical copolymerization of acrylamide and *N*,*N*′-methylene-bisacrylamide as a cross-linking agent (fig. S1). The AIRS used in our experiments consisted of square arrays of vertically oriented, uniform nanocolumns with diameters d = 100 to 300 nm, heights h = 5 to 8 μm, aspect ratios h/d = 15 to 80, and periodicities p = 2 to 4 μm (Fig. 1B).

We developed two hybrid architectures using either free-standing (HAIRS-1) or attached (HAIRS-2) nanocolumns. The key element of the HAIRS-1 design is the use of hydrogel-embedded silicon nanocolumns that detach from the original AIRS silicon wafer (Fig. 1D). To achieve the HAIRS-1 structure (fig. S2), the anchoring layer of chemisorbed PGMA and acrylic acid was applied to the second surface, whereas the AIRS remained unmodified. The prepolymerization solution was introduced between AIRS and the modified confining surface. After polymerization, the two surfaces were separated by applying shear stress to the "sandwich" that resulted in the complete breaking of the columns at the base. The detached columns remained embedded in the hydrogel film grafted via PGMA to the confining surface. This procedure was followed by rinsing and drying of the hydrogel to remove unreacted monomers and the solvent, causing the contraction of the film and the associated slanting of the unattached nanocolumns (Fig. 2, A and B). The surface revealed domains with non-uniform tilt directions, which were probably ordered by inhomogeneity of the hydrogel internal mechanical stresses. The tilt angle α of the columns observed in several experiments was 60° to 75°, and the exposed length l was 1.5 to 2.5 μm. Exposure to humidity led to swelling of the hydrogel and relaxation of the drying stresses. As a result, the tilted columns moved to their original orientation perpendicular to the surface (Fig. 2C). Upon drying, the columns returned to their tilted state. By adjusting the humidity level using the humidity chamber (and thus regulating the degree of hydration and the related volume change of the hydrogel), we can control the tilt angle of the nanocolumns.

To measure the actuation time, the process was recorded with a high-speed video camera (*21*). When a water droplet is placed on a dry sample, the switching to the perpendicular

[1]Bell Laboratories/Alcatel-Lucent, Murray Hill, NJ 07974, USA. [2]Max Planck Institute of Colloids and Interfaces, D 14424 Potsdam, Germany.

*To whom correspondence should be addressed. E-mail: jaizenberg@alcatel-lucent.com

orientation is extremely fast (~60 ms). Movie S1 depicts the process slowed down by about a factor of 7. The reverse transformation to the tilted state caused by unassisted drying of the sample takes ~4 s. Movie S2 depicts the reverse process slowed down by a factor of 2. The latter reorientation can be accelerated, if needed, by using airflow in the system and or by increasing the temperature. The actuation cycle was repeated on the same sample more than 20 times immediately after the preparation and more than 25 times 6 months later. No deterioration or change in the response rate was observed, demonstrating a remarkable stability and robustness of the designed actuation system.

When the anchoring layer of chemisorbed PGMA and acrylic acid is applied to the AIRS substrate and the confining surface is unmodified, the hydrogel film is grafted to the nanostructured surface (fig. S2). In this HAIRS-2 design (Fig. 1E), the hydrogel-embedded nanocolumns remain attached to the original substrate and bend upon the drying of the polymer film (Fig. 3A). The actuation cycle is similar to that described for HAIRS-1. Exposure to humidity causes the hydrogel to swell and relax, thus returning the nanocolumns to their perpendicular orientation. To visualize the reorientation process and the dependence of the tilt angle on the degree of hydration and or humidity, we placed a droplet of water on the HAIRS-2 surface and took an optical micrograph of the drying edge (Fig. 3B). The water content and the swelling of the hydrogel gradually decrease across this region, inducing a progressive increase in the tilt angles of the nanocolumns.

We further capitalized on these new actuation systems by expanding their capabilities to form reversibly actuated micropatterns with complex geometries. Because the tilt direction of the nanocolumns in the HAIRS-1 design depends on the local defects on the confining surface, we anticipated that this orientation could be controlled by deliberately introducing a topographic pattern onto this surface. Indeed, a highly uniform tilt direction of the nanocolumns was achieved by using a confining surface that was patterned with lines (Fig. 4A). A variety of more complex patterns can be achieved by using an underlying substrate of corresponding topography. One such example is given in Fig. 4B, where a honeycomblike pattern on the confining surface controls the formation of a complex structure in which arrays of radially oriented columns form "micrometer-wide flowers" that follow the geometry of the templating surface. An array of "micrometer-wide wraps," in which every group of four attached nanocolumns of the HAIRS-2 design is held together by a hydrogel, is shown in Fig. 4C. Such complex material movements would be impossible to accomplish in conventional microfluidic systems, in which the polymers are actuated by an electric or magnetic field. Even more important, these patterns are reversible, in contrast to the cases of structural rearrangement and assembly reported in (*20*, *21*). Structures shown in Fig. 4, B and C, open and close depending on

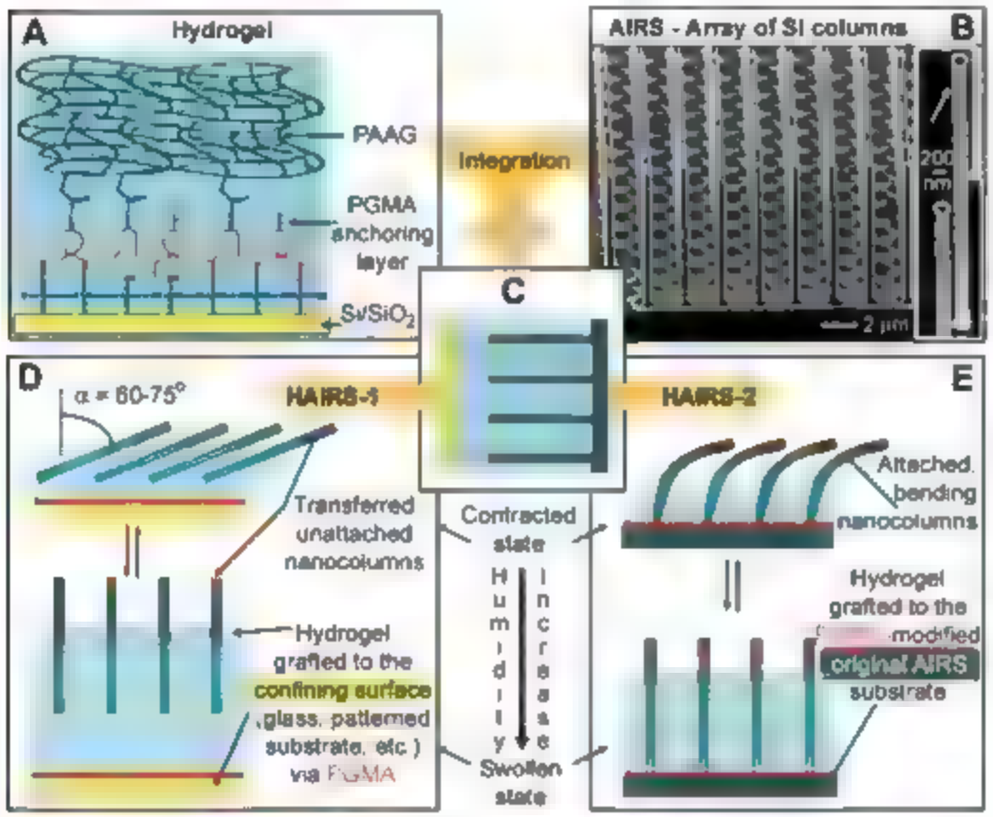

Fig. 1. (**A**) Schematic presentation of the structure and composition of the PAAG film grafted to the Si/SiO_2 substrate via the PGMA anchoring layer. (**B**) Scanning electron micrograph (SEM) of a sample AIRS structure composed of an array of silicon nanocolumns. An inset on the right reveals a banding pattern (scalloping) that is characteristic of the Bosch fabrication process. The band width is ~200 nm. (**C**) Hydrogel synthesis in the confinement of the AIRS and a secondary substrate (a glass slide or a silicon wafer, either flat or topographically patterned) separated by a spacer of the desired thickness that regulates the size of the polymer film. (**D**) Hybrid HAIRS-1 design. The nanocolumns, embedded into the hydrogel layer grafted to the PGMA-modified confining surface, break from the original wafer upon the separation of the confining substrates and become fully transferred onto the secondary surface. The surface topography changes from an array of highly tilted to vertically oriented nanocolumns. (**E**) Hybrid HAIRS-2 design. The hydrogel film is attached directly to the AIRS silicon wafer. Nanocolumns remain attached to the surface and bend upon drying.

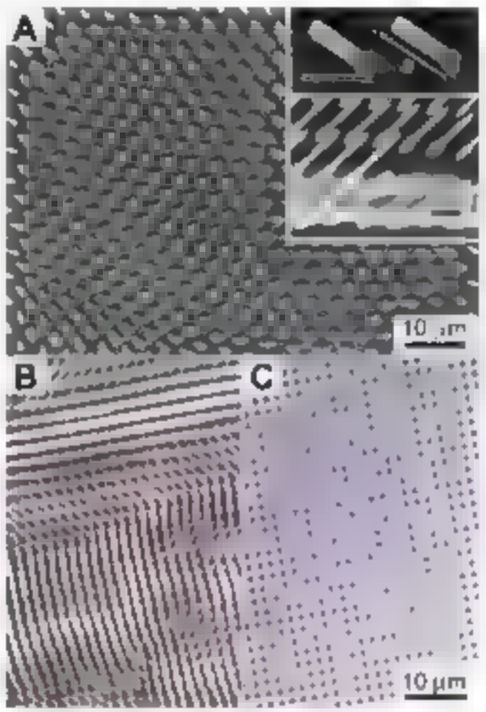

Fig. 2. Microscopy study of the HAIRS-1 design. (**A**) SEM image of a dry sample viewed perpendicular to the surface reveals tilted columns organized in domains with different tilt directions. The top inset shows a zoom-in view perpendicular to the surface. The number of 200-nm bands *n* on the emerging portion of the nanocolumns and the length of the column projections *a* were monitored to determine the length *l* of the exposed nanocolumns ($l = 200n$, measured in nm) and their tilt angle ($\sin \alpha = a/l$). The SEM of the cross section (bottom inset) clearly shows the tilted nanocolumns partially embedded into the hydrogel layer. Scale bars in insets, 2 μm. (**B** and **C**) Optical micrographs, imaging the same region of the HAIRS-1 system in a dry (B) and a wet (C) state, show the reorientation of the nanocolumns from a tilted to a vertical position upon the expansion of the hydrogel. Also see movies S1 and S2 and fig. S3.

the humidity level, as illustrated in Fig. 4, D and E. Their movements resemble the responsive behavior of carnivorous plants or pedicellaria multijawed microforceps-like structures found on echinoderms), whose movement between the open and closed states functions in feeding and defense and as an antifouling mechanism, preventing the settlement and growth of microorganisms (*34*). These biological structures essentially exist as arrays of environmentally responsive actuators, as do our artificial dynamic patterns. The potential of these unique structures for various applications is now being explored (*35*).

From a mechanical viewpoint, there is a major difference between the HAIRS-1 and HAIRS-2 systems in the way that the nanocolumns are deformed. In the case of the HAIRS-1 system, the columns correspond essentially to stiff elements loaded under compression, whereas the shrinking hydrogel exerts tensile forces. This type of design was recognized for a long time for its enormous potential in architectural construction by Buckminster-Fuller, who coined the term "tensegrity" (*26*), and the concept was later proposed as a mechanical model for the cell cytoskeleton (*27*). Such tensegrity structures consisting of stiff rods connected by soft springs under tension are currently being investigated in the context of mechanisms for their inherent shape memory and related potential as actuators (*28*). The HAIRS-1 system is a realization of tensegrity at the microscale, where the nanocolumns redirect the tensile forces from the gel (which a priori would just lead to a reduction of the gel-layer thickness) into a lateral actuation (Fig. 1D). The movement x is controlled by the volume change of the gel and the length of the nanocolumns. If v_w and v_d represent the volume of the gel in the wet and dry state, respectively, then $\cos\alpha = v_d / v_w$ and $\sin\alpha = \sqrt{1 - (v_d / v_w)^2}$. With the dimensions typically used in this study, the lateral actuation is on the order of $x = 4$ to 8 μm. A more complex topography of the confining surface (alternative, for example, to the uniform arrangements of the array of nanocolumns, the use of nanostructures of a different shape (such as blades), or a combination thereof) allows for a variety of reversible patterned movements at the micrometer scale (Fig. 4, A and B), which might be technically exploited, such as in the context of microfluidics or photonics (*25*).

HAIRS-2 systems go beyond the concept of tensegrity in the sense that the beams do not stay straight and carry compressive loads, but instead they bend (Fig. 1E). Typically, the stiffness of slim beams is much less in bending than in compression (assuming that no buckling occurs). As a consequence, a large fraction of the deformation energy is stored in the bent columns, which tend to go back to their straight shape when the tensile stresses from the gel are released upon rewetting. The amount by which each column bends is a measure of the force exerted by the gel. This is in contrast to the HAIRS-1 system, where the force developed by the gel has no direct influence on the structure after drying. Using simple beam theory, we estimated the force f at which the bending of the stacon nanocolumns in the HAIRS-2 design occurs (Eqs. S4 and S5). This force depends very sensitively on the aspect ratio. For an 8-μm-high column with an aspect ratio of either 80, 40, 20, or 10, the bending occurs at ~50 nN, ~500 nN, ~8 μN, or 100 μN, respectively. Moreover, the strain at the base cannot exceed the fracture strain of silicon. The consequence is that columns with a small aspect ratio can only undergo relatively

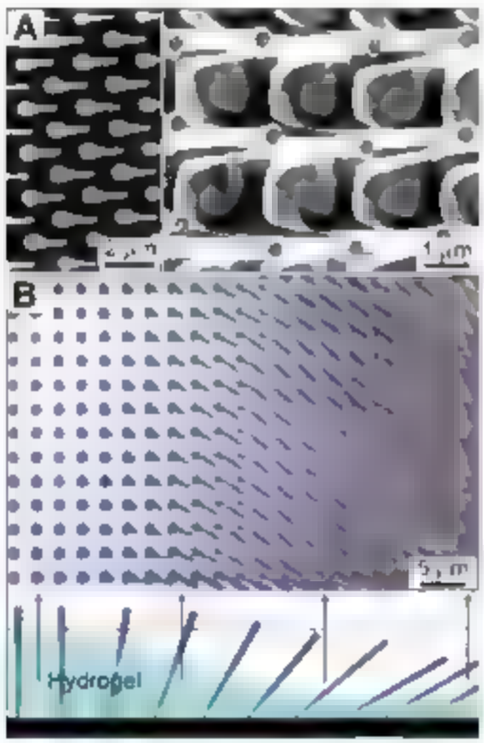

Fig. 3. Microscopy study of the HAIRS-2 structure. (**A**) Low-magnification SEM (left) and high-magnification SEM (right) show the hydrogel layer that forms characteristic onionlike or conical features at the bottom of the nanocolumns. (**B**) Optical micrograph of the drying edge of the HAIRS-2 structure taken perpendicular to the surface. The clarification of the actuation mechanism is shown schematically below the micrograph. A dashed line in the schematic corresponds to the focal plane in the image. The degree of hydration or swelling of the polymer layer decreases gradually across the sample from left to right. Correspondingly, the nanocolumns gradually change their orientation from perpendicular to tilted. The whole range of the orientations is depicted, thus providing a still image of the entire reorientation process.

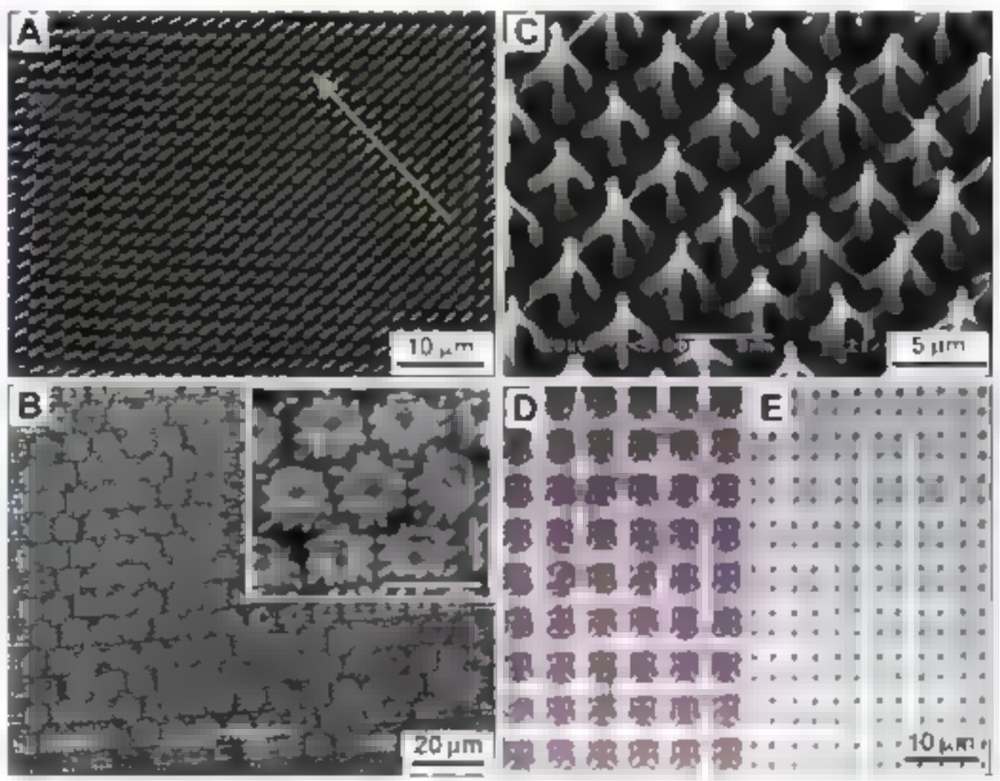

Fig. 4. SEM and optical images showing highly controlled pattern formation in the HAIRS designs. All the structures reversibly switch to the original vertical orientation of the nanocolumns upon rewetting. (**A**) Uniform orientation of the tilted nanocolumns in the HAIRS-1 structure templated by the patterned confining surface that is bearing lines. The direction of the lines is indicated by an arrow. (**B**) Regular array of microflorets in the HAIRS-1 structure templated by the substrate bearing a honeycomb pattern. (**C**) An example of a complex HAIRS-2 pattern, showing an array of microtraps, in which every group of four attached nanocolumns is held together by the hydrogel. (**D** and **E**) Optical micrographs imaging microtraps shown in (C) in a dry (D) and a wet (E) state. The switching of the nanocolumns from bent fourfold clusters to a vertical orientation is clear.

small bending and then must break, whereas columns with an aspect ratio of 80 can fully bend to touch the surface without breaking. An aspect ratio of at least 20 is needed for sufficient bending of each beam to touch its neighbors to obtain the structure shown in Fig. 4, C and D. This mechanical assessment makes it possible to design a hydrogel nanocolumns combination that enables a desired degree of directed actuation.

We have developed hybrid architectures in which arrays of high aspect-ratio silicon nanocolumns, either attached or free-standing, are embedded into a hydrogel film and are actuated into highly controlled, complex microstructures upon contraction and or swelling of the polymer. The actuation is fast, reversible, reproducible, and robust. We believe that these architectures may lead to a variety of applications, including actuators, controlled reversible-pattern formation, microfluidics, reversible switching of the wetting behavior, tunable photonic structures, artificial muscles, and release systems (*24*).

References and Notes

1. S. Minko, *Responsive Polymer Materials: Design and Applications* (Blackwell, Ames, IA, 2006) and references therein.
2. Y. Osada, H. Okuzaki, H. Hori, *Nature* **355**, 242 (1992).
3. Y. Osada, A. Matsuda, *Nature* **376**, 219 (1995).
4. D. J. Beebe *et al.*, *Nature* **404**, 588 (2000).
5. T. P. Russell, *Science* **297**, 964 (2002).
6. J. Lahann *et al.*, *Science* **299**, 371 (2003).
7. A. Lendlein, H. Y. Jiang, O. Junger, R. Langer, *Nature* **434**, 879 (2005).
8. F. Chellini *et al.*, *Macromol. Rapid Commun.* **22**, 1284 (2001).
9. M. Mayer, J. Yang, I. Gitlin, D. H. Gracias, G. M. Whitesides, *Proteomics* **4**, 2366 (2004).
10. T. Sun, L. Feng, X. Gao, L. Jiang, *Acc. Chem. Res.* **38**, 644 (2005) and references therein.
11. K. Autumn *et al.*, *Proc. Natl. Acad. Sci. U.S.A.* **99**, 12252 (2002) and references therein.
12. P. Vukusic, J. R. Sambles, *Nature* **424**, 852 (2003) and references therein.
13. A. K. Geim *et al.*, *Nat. Mater.* **2**, 461 (2003).
14. S. B. Lee, R. Koepsel, D. B. Stolz, H. E. Warriner, A. J. Russell, *J. Am. Chem. Soc.* **126**, 13400 (2004).
15. E. Delamarche, H. Schmid, B. Michel, H. Biebuyck, *Adv. Mater.* **9**, 741 (1997).
16. I. N. Krupenkin, J. A. Taylor, T. M. Schneider, S. Yang, *Langmuir* **20**, 3824 (2004).
17. L. Zhai, F. C. Cebeci, R. E. Cohen, M. F. Rubner, *Nano Lett.* **4**, 1349 (2004).
18. S. A. Asher, in *Nanoparticles: Building Blocks for Nanotechnology*, V. M. Rotello, Ed. (Kluwer, New York, 2004), pp. 145–172.
19. M. K. Mauzer, I. F. Sednev, S. A. Asher, *Adv. Funct. Mater.* **15**, 1401 (2005).
20. S. Park, J.-H. Lim, S.-W. Chung, C. A. Mirkin, *Science* **303**, 348 (2004).
21. Materials and methods are available as supporting material on *Science* Online.
22. K. S. Iyer, B. Zdyrko, H. Malz, J. Pionteck, I. Lunov, *Macromolecules* **36**, 6519 (2003).
23. B. D. Gates *et al.*, *Angew. Chem. Int. Ed.* **43**, 2780 (2004).
24. E. E. Ruppert, R. S. Fox, R. B. Barnes, *Invertebrate Zoology* (Brooks Cole Thomson, Belmont, CA, ed. 7, 2004).
25. In particular, our preliminary data show that these structures (i) direct the flow and particle transport (analogous to the function of cilia in organisms) and thus have potential in microfluidics, (ii) reversibly change their photonic properties and thus can be considered for tunable photonics, (iii) reversibly switch their wetting behavior from superhydrophobic in the humid environment to hydrophilic in the dry environment, and (iv) trap and release particles in microflowers.
26. R. Buckminster-Fuller, *Portfolio Art News Annu.* **4**, 112 (1961). Also available at www.rwgiaprojects.com/rbinotes/lpapers/tensegrity/tenseg01.html.
27. D. E. Ingber, *Annu. Rev. Physiol.* **59**, 575 (1997).
28. M. Debiossac, *Mech. Res. Comm.* **30**, 311 (2003).

29. We thank P. Kolodner, J. Weaver, I. Luzinov, and I. Sokolov for fruitful discussions. We thank R. Smith and N. Lippa for technical assistance. This work was supported in part by the Office of Naval Research, award N00014-05-1-0909.

Supporting Online Material

www.sciencemag.org/cgi/content/full/315/5811/487/DC1
Materials and Methods
Figs. S1 to S5
Table S1
References
Movies S1 and S2

25 September 2006; accepted 7 December 2006
10.1126/science.1135516

Electromechanical Resonators from Graphene Sheets

J. Scott Bunch,[1] Arend M. van der Zande,[1] Scott S. Verbridge,[1] Ian W. Frank,[2] David M. Tanenbaum,[2] Jeevak M. Parpia,[1] Harold G. Craighead,[1] Paul L. McEuen[1]*

Nanoelectromechanical systems were fabricated from single- and multilayer graphene sheets by mechanically exfoliating thin sheets from graphite over trenches in silicon oxide. Vibrations with fundamental resonant frequencies in the megahertz range are actuated either optically or electrically and detected optically by interferometry. We demonstrate room-temperature charge sensitivities down to 8×10^{-4} electrons per root hertz. The thinnest resonator consists of a single suspended layer of atoms and represents the ultimate limit of two-dimensional nanoelectromechanical systems.

The miniaturization of electromechanical devices promises to be as revolutionary in the coming decades as the miniaturization of electronic devices was in the previous ones. Devices ranging from nanoscale resonators, switches, and valves have applications in tasks as diverse as information processing, molecular manipulation, and sensing. The prototypical nanoelectromechanical system (NEMS) is a nanoscale resonator, a beam of material that vibrates in response to an applied external force (*1*, *2*). The ultimate limit would be a resonator one atom thick, but this puts severe constraints on the material. As a single layer of atoms, it should be robust, stiff, and stable.

Graphite consists of stacked layers of graphene sheets separated by 0.3 nm and held together by weak van der Waals forces (*3*). It has extremely high strength, stiffness, and thermal conductivity along the basal plane. In addition, graphite can be exfoliated onto an insulating substrate, producing micron-sized graphene sheets with thicknesses down to a single atomic layer (*4*–*8*). Thus far, research on these thin graphene sheets has focused primarily on their electronic properties. We demonstrate a method of suspending single- and multilayer graphene sheets over trenches and show that such sheets can be mechanically actuated. This work also makes a detailed study of the mechanical properties of these graphene resonators, including resonance frequency, spring constant, built-in tension, and quality factor.

Suspended graphene sheets are fabricated with a peeling process similar to that reported previously (*5*–*7*). In our case, the graphene sheets are mechanically exfoliated over predefined trenches etched into a SiO_2 surface (Fig. 1) (*9*). The result is a micron-scale doubly clamped beam or cantilever clamped to the SiO_2 surface by van der Waals attraction. Some devices have prepatterned gold electrodes between the trenches to make electrical contact (Fig. 1, A and D).

A noncontact mode atomic force microscope (AFM) was used to quantitatively measure the thickness of the sheets on the substrate next to the trench, as shown in the inset in Fig. 1D. However, for sheets thinner than 2 to 3 nm, such measurements are unreliable (*10*, *12*). For these we used spatially resolved Raman spectroscopy to determine the number of layers (Fig. 1C) (*10*, *12*). The graphene sheet in Fig. 1B has an AFM-determined height of 0.9 nm. By comparison with previous results (*10*, *12*), the shape of the Raman peak near 2700 cm^{-1} suggests the sheet is two layers thick over the area lying on the SiO_2 substrate (Fig. 1C), whereas the section suspended over the trench is a single graphene layer.

All resonator measurements are performed at room temperature and a pressure of $<10^{-6}$ torr unless otherwise indicated. The resonators are actuated by using either electrical (Fig. 1A) or optical modulation. In the case of electrical modulation, a time-varying radio frequency (rf)

[1]Cornell Center for Materials Research, Cornell University, Ithaca, NY 14853, USA. [2]Pomona College, Department of Physics, Claremont, CA 91711, USA.

*To whom correspondence should be addressed. E-mail: mceuen@ccmr.cornell.edu

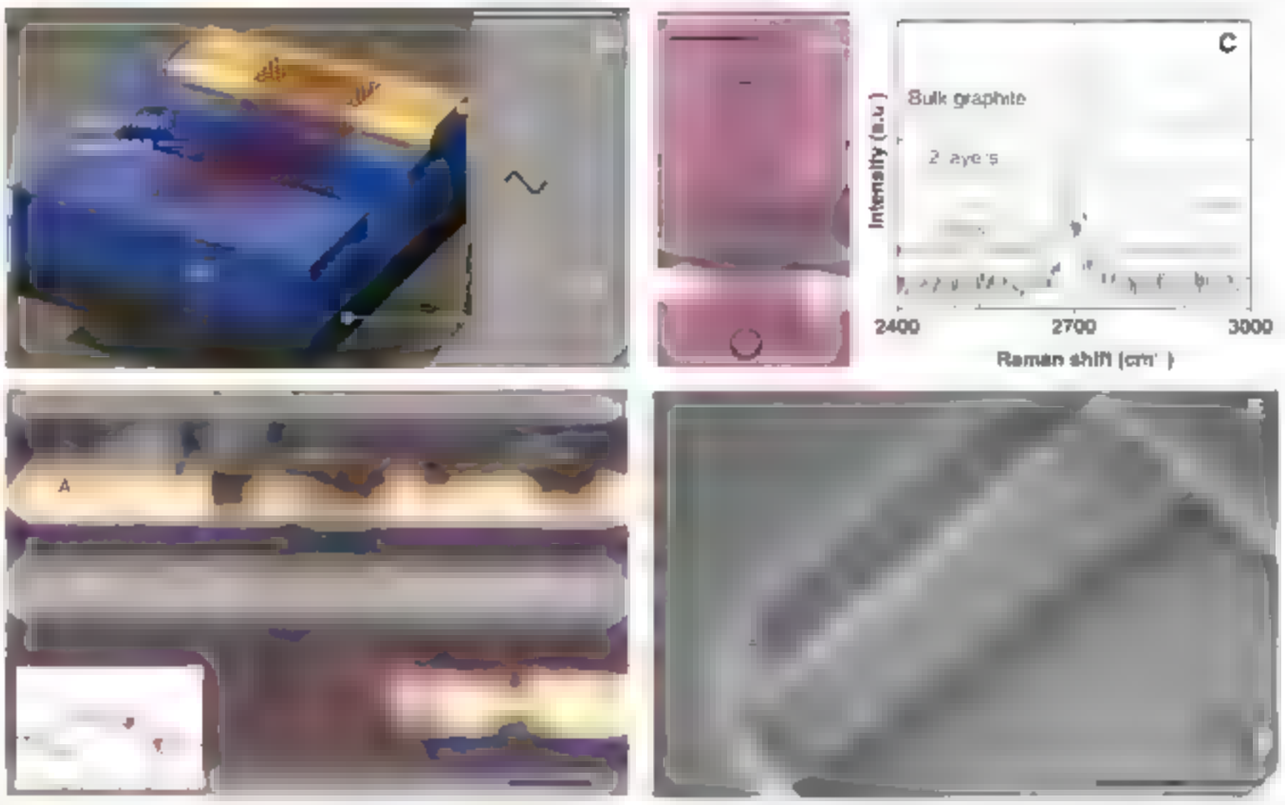

Fig. 1. (**A**) Schematic of a suspended graphene resonator. (**B**) An optical image of a double-layer graphene sheet that becomes a single suspended layer over the trench. Scale bar, 2 μm. Each colored circle corresponds to a point where a Raman spectrum was measured. (**C**) Raman signal from a scan on the graphene piece. Each colored scan is data taken at each of the matching colored circles. The top scan is used as a reference and corresponds to the Raman shift of bulk graphite. (**D**) An optical image of few-layer (~4) graphene suspended over a trench and contacting a gold electrode. Scale bar, 1 μm. (Inset) A line scan from tapping mode AFM corresponding to the dashed line in the optical image. It shows a step height of 1.5 nm. (**E**) A scanning electron microscope image of a few-layer (~2) graphene resonator. Scale bar, 1 μm.

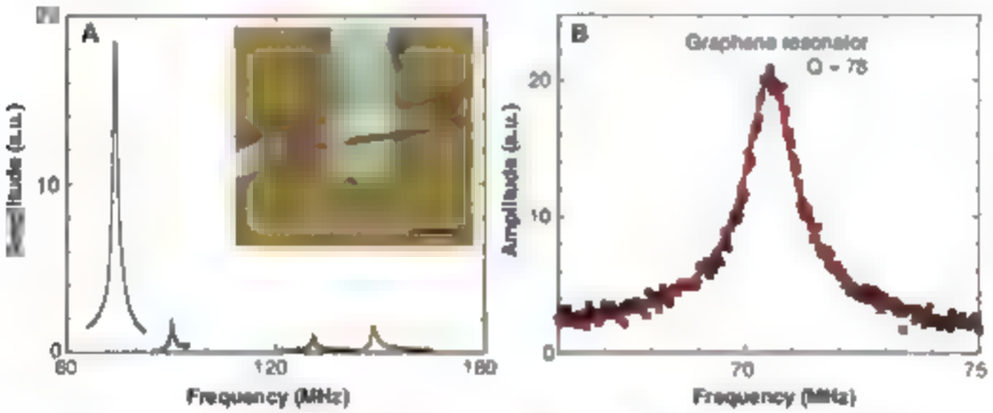

Fig. 2. (**A**) Amplitude versus frequency for a 15-nm-thick multilayer graphene resonator taken with optical drive. (Inset) An optical image of the resonator. Scale bar, 5 μm. (**B**) Amplitude versus frequency taken with optical drive for the fundamental mode of the single-layer graphene resonator shown in Fig. 1B. A Lorentzian fit of the data is shown in red.

voltage δV_g at frequency f is superimposed on top of a constant voltage and applied to the graphene sheet. The result is an electrostatic force between the suspended graphene sheet and the substrate

$$F_{es} = 1/2\, C_g'(V_g^{dc})^2 + C_g' V_g^{dc} \delta V_g \cos \omega t + \ldots \quad (1)$$

where C_g' is the derivative of the gate capacitance with respect to the distance to the gate, and V_g^{dc} and δV_g are, respectively, the dc and time-varying rf voltages applied to the gate (*13*). For optical actuation, the intensity of a diode laser focused on the sheet is modulated at frequency f, causing a periodic contraction/expansion of the layer that leads to motion. In both cases, the motion is detected by monitoring the reflected light intensity from a second laser with a fast photodiode (*9*).

Figure 2A shows the measured amplitude versus frequency for a 15-nm-thick sheet suspended over a 5-μm trench. Multiple resonances are observed, the most prominent one at the lowest frequency. We associate this dominant peak with the fundamental vibrational mode: its detected intensity is largest when the motion is in-phase across the entire suspended section. We will limit our discussion primarily to this fundamental mode. A fit to a Lorentzian yields a resonant frequency f_0 = 42 MHz and a quality factor Q = 210. Figure 2B shows similar results for the single-layer graphene resonator from Fig. 1B, f_0 = 70.5 MHz and Q = 78. Figure 3 shows the results of measurements of 33 resonators with thicknesses varying from a single atomic layer to sheets 75 nm thick. The frequency f_0 of the fundamental modes varies from 1 MHz to 170 MHz, with quality factor Q of 20 to 850.

For mechanical resonators under tension, the fundamental resonance mode f_0 is given by

$$f_0 = \frac{1}{2L}\sqrt{\frac{T}{\rho}} + \frac{\alpha}{L^2}\sqrt{\frac{E}{\rho}} \quad (2)$$

where E is the Young's modulus, ρ is the mass density, t, w, and L are the dimensions of the suspended graphene sheet, and the coupling coefficient, α, is 1.03 for doubly clamped beams and 0.162 for cantilevers (*14*). In the limit of small tension, Eq. 2 predicts that the resonance frequency f_0 scales as t/L^2. Figure 3A shows the resonant frequency of the fundamental mode for resonators with t > 7 nm as a function of t/L^2 plotted as filled squares. Also plotted is the theoretical prediction, Eq. 2, in the limit of zero tension, for both cantilevers and beams, where we have used the known values for bulk graphite ρ = 2200 kg·m^{-3} and E = 1.0 TPa (*3*). This is a valid comparison considering the extensive theoretical and experimental work that shows the basal plane of graphite to have a similar value for E as graphene and carbon nanotubes (*3*, *15*). To account for possible errors in E, we plot

dashed lines that correspond to values of E = 0.5 TPa and 2 TPa. The data follow the predictions reasonably accurately, indicating that thicker resonators are in the bending-dominated limit with a modulus E characteristic of the bulk material. This is among the highest modulus resonators to date, greater than 53 to 170 GPa in ~2- to 300-nm-thick Si cantilevers and similar to single-walled carbon nanotubes and diamond NEMS (*13*, *16*, *17*). In contrast to ultrathin Si cantilevers, the graphene resonators show no degradation in Young's modulus with decreasing thickness (*17*).

The resonant frequencies versus t/L^2 for the resonators with t < 7 nm are shown as open squares in Fig. 3A. The frequencies of these thinner resonators show more scatter, with the majority having resonant frequencies higher than predicted by bending alone. A likely explanation for this is that many of the resonators are under tension, which increases f_0 (see supporting online text). The tension likely results from the fabrication process, where the friction between the graphite and the oxide surface during mechanical exfoliation stretches the graphene sheets across the trench.

The single-layer graphene resonator shown in Fig. 1B illustrates the importance of tension in the thinnest resonators. It has a fundamental frequency f_0 = 70.5 MHz, much higher than the 5.4 MHz frequency expected for a tension-free beam with t = 0.3 nm, L = 1.1 μm, and w = 1.93 μm. From Eq. 2, this implies that the graphene resonator has a built-in tension of T = 13 nN. From the expression $\Delta L/L = T/(E A)$, this corresponds to a strain of 2.2×10^{-3}.

An important measure of any resonator is the normalized width of the resonance peak characterized by the quality factor $Q = f_0/\Delta f$. A high Q is essential for most applications because it increases the sensitivity of the resonator to external perturbation. A plot of the Q versus the thickness for all the graphene resonators (Fig. 3B) shows that there is no clear dependence of Q on thickness. This contrasts with results on thicker NEMS resonators fabricated from silicon (*18*). The quality factors at room temperature are lower than diamond NEMS (2500 to 3000) of similar volume and significantly lower than high-stress Si_3N_4 nanostrings (200,000), yet similar to those reported in single-walled carbon nanotubes (50 to 100) (*13*, *16*, *19*). Preliminary studies on a 20-nm-thick resonator found a dramatic increase in Q with decreasing temperature (Q = 100 at 300 K to Q = 1800 at 50 K). This suggests that high Q operation of graphene resonators should be possible at low temperatures.

Even when a resonator is not being driven, it will still oscillate due to thermal excitation by a root mean square (RMS) amount $v_{th} = [k_B T/\kappa_{eff}]^{1/2}$, where $\kappa_{eff} = m_{eff}\,\omega_0^2 = 0.7375\,\rho w t \omega_0^2$ is the effective spring constant of the mode (*2*). An example is shown in Fig. 4A, where a 5-nm-thick resonator with f_0 = 35.8 MHz and κ_{eff} = 0.7 N/m has a room-temperature thermal RMS motion of v_{th} = 76 pm. For resonators for which the thermal vibrations can be measured, we use this thermal RMS motion to scale the measured photodetector voltage with resonator displacement (see supporting online text). Figure 4B shows such a rescaled plot of the displacement amplitude versus rf drive voltage. The resonator is linear up to displacements of 3 nm, or on the order of its thickness, where nonlinearities associated with additional tension are known to set in (*2*). This nonlinearity is characterized as a deviation from a linear increase in amplitude with driving force and accompanied by a decrease in Q (Fig. 4B).

Two applications of nanomechanical resonators are ultralow mass detection (see supporting online text) and ultrasensitive force detection. The ultimate limit on the force sensitivity is set by the thermal fluctuations in the resonator

$$dF^f = [4\,\kappa_{eff}(k_B T/Q\,\omega_0)]^{1/2} \qquad (3)$$

For the resonator in Fig. 4A, this results in a force sensitivity of 0.9 fN/Hz$^{1/2}$. From Eq. 1, this corresponds to a charge sensitivity of $dQ^f = dF^f d\,[\partial C_g/\partial z]^{-1} = 8 \times 10^{-4}$ e/Hz$^{1/2}$, where d is the distance between the graphene sheet and the gate electrodes. This is a high sensitivity demonstrated at room temperature; at low temperatures, with the onset of higher quality factors, it could rival those of rf single-electron transistor electrometers (1×10^{-5} e/Hz$^{1/2}$) (*20*, *21*). The high Young's modulus, extremely low mass, and large surface area make these resonators ideally suited

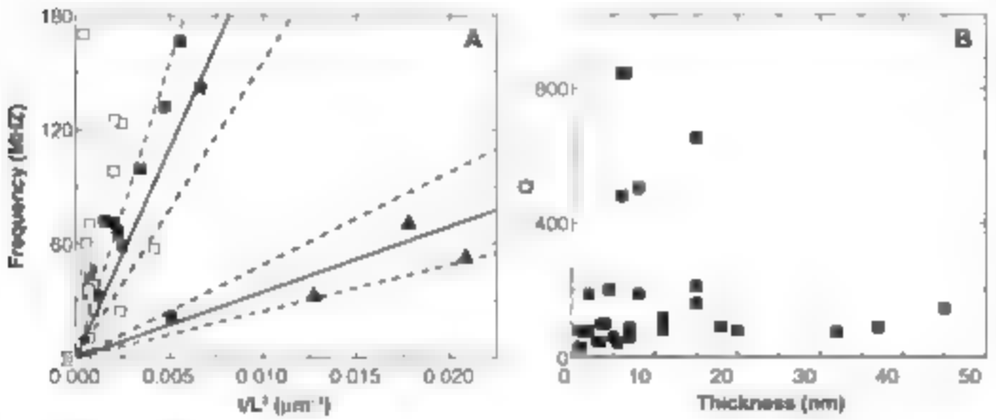

Fig. 3. (**A**) A plot showing the frequency of the fundamental mode of all the doubly clamped beams and cantilevers versus t/L^2. Cantilevers, triangles; doubly clamped beams with t > 7 nm, filled squares; doubly clamped beams with t < 7 nm, open squares. All thicknesses are determined by AFM. The solid line is the theoretical prediction with no tension and E = 1 TPa. The dashed lines correspond to E = 0.5 TPa and 2 TPa. (**B**) The quality factor of the fundamental mode versus thickness for all resonators measured.

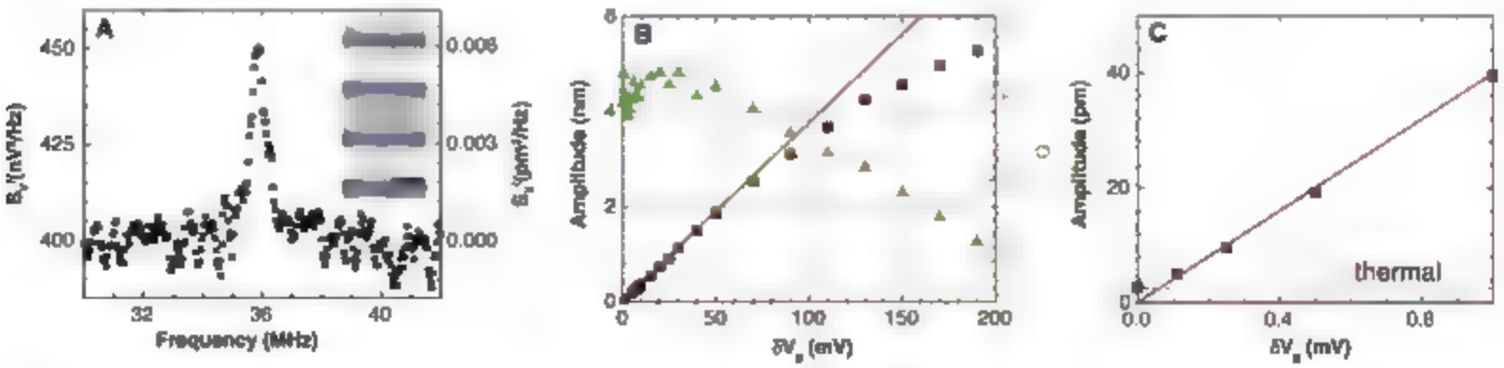

Fig. 4. (**A**) Noise power density versus frequency taken at a resolution bandwidth of 1 kHz. (Inset) An optical image of the resonator. The resonator has dimensions t = 5 nm, L = 2.7 μm, and w = 630 nm. Scale bar, 2 μm. (**B**) Amplitude of resonance and quality factor versus δV_g for $V_g^{dc} = 2$ V. (**C**) Expanded view of (B) for small δV_g.

for use as mass, force, and charge sensors (22–29). The application of graphene NEMS extends beyond just mechanical resonators. This robust conducting membrane can act as a nanoscale supporting structure or atomically thin membrane separating two disparate environments.

References and Notes

1. M. G. Craighead, *Science* **290**, 1532 (2000).
2. K. L. Ekinci, M. L. Roukes, *Rev. Sci. Instrum.* **76**, 061101 (2005).
3. B. T. Kelly, *Physics of Graphite* (Applied Science, London; Englewood, N.J., 1981).
4. M. Wilson, *Phys. Today* **59**, 21 (2006).
5. K. S. Novoselov *et al.*, *Proc. Natl. Acad. Sci. U.S.A.* **102**, 10451 (2005).
6. K. S. Novoselov *et al.*, *Nature* **438**, 197 (2005).
7. Y. B. Zhang, Y. W. Tan, H. L. Stormer, P. Kim, *Nature* **438**, 201 (2005).
8. J. S. Bunch, Y. Yaish, M. Brink, K. Bolotin, P. L. McEuen, *Nano Lett.* **5**, 287 (2005).
9. Materials and methods are available as supporting material on *Science* Online.
10. A. C. Ferrari *et al.*, *Phys. Rev. Lett.* **97**, 187401 (2006).
11. A. Gupta, G. Chen, P. Joshi, S. Tadigadapa, P. C. Eklund, *Nano Lett.* **6**, 2667 (2006).
12. D. Graf *et al.*, http://arxiv.org/PS_cache/cond-mat/pdf/0607/0607562.pdf (2006).
13. V. Sazonova *et al.*, *Nature* **431**, 284 (2004).
14. S. Timoshenko, D. H. Young, W. Weaver, *Vibration Problems in Engineering*, (Wiley, New York, ed. 4, 1974), pp. 425–427.
15. D. Qian, G. J. Wagner, W. K. Liu, M. F. Yu, R. S. Ruoff, *Appl. Mech. Rev.* **55**, 495 (2002).
16. L. Sekaric *et al.*, *Appl. Phys. Lett.* **81**, 4455 (2002).
17. X. X. Li, T. Ono, Y. L. Wang, M. Esashi, *Appl. Phys. Lett.* **83**, 3081 (2003).
18. K. Y. Yasumura *et al.*, *J. Microelectromech. Syst.* **9**, 117 (2000).
19. S. S. Verbridge, J. M. Parpia, R. B. Reichenbach, L. M. Bellan, H. G. Craighead, *J. Appl. Phys.* **99**, 124304 (2006).
20. R. J. Schoelkopf, P. Wahlgren, A. A. Kozhevnikov, P. Delsing, D. E. Prober, *Science* **280**, 1238 (1998).
21. M. D. LaHaye, O. Buu, B. Camarota, K. C. Schwab, *Science* **304**, 74 (2004).
22. B. Ilic *et al.*, *J. Appl. Phys.* **95**, 3694 (2004).
23. M. V. Lavrik, P. G. Datskos, *Appl. Phys. Lett.* **82**, 2697 (2003).
24. K. L. Ekinci, X. M. H. Huang, M. L. Roukes, *Appl. Phys. Lett.* **84**, 4469 (2004).
25. T. Kenny, *IEEE Sensors J.* **1**, 148 (2001).
26. A. N. Cleland, M. L. Roukes, *Nature* **392**, 160 (1998).
27. R. G. Knobel, A. N. Cleland, *Nature* **424**, 291 (2003).
28. F. P. Burg, S. R. Manalis, *Appl. Phys. Lett.* **83**, 2698 (2003).

29. We thank C. Urbach and L. Bellan for help with Raman spectroscopy; R. Reichenbach for help with the laser setup and the schematic in the Supporting Online Material, and P. Kim, Y. Zhang, B. Ilic, and K. Schwab for useful discussions. This work was supported by the NSF through the Center for Nanoscale Systems and the Cornell Center for Materials Research, and by the Microelectronics Advanced Research Corporation Focused Research Center on Materials, Structures, and Devices. Sample fabrication was performed at the Cornell Nanoscale Science and Technology Facility, a National Nanotechnology Infrastructure Network node funded by NSF.

Supporting Online Material

www.sciencemag.org/cgi/content/full/315/5811/490/DC1
Materials and Methods
SOM Text
Figs. S1 to S3
References

27 October 2006; accepted 11 December 2006
10.1126/science.1136836

Improved Oxygen Reduction Activity on $Pt_3Ni(111)$ via Increased Surface Site Availability

Vojislav R. Stamenkovic,[1,2]* Ben Fowler,[3] Bongjin Simon Mun,[2] Guofeng Wang,[4] Philip N. Ross,[2] Christopher A. Lucas,[3] Nenad M. Marković[1]*

The slow rate of the oxygen reduction reaction (ORR) in the polymer electrolyte membrane fuel cell (PEMFC) is the main limitation for automotive applications. We demonstrated that the $Pt_3Ni(111)$ surface is 10-fold more active for the ORR than the corresponding Pt(111) surface and 90-fold more active than the current state-of-the-art Pt/C catalysts for PEMFC. The $Pt_3Ni(111)$ surface has an unusual electronic structure (*d* band center position) and arrangement of surface atoms in the near-surface region. Under operating conditions relevant to fuel cells, its near-surface layer exhibits a highly structured compositional oscillation in the outermost and third layers, which are Pt-rich, and in the second atomic layer, which is Ni-rich. The weak interaction between the Pt surface atoms and nonreactive oxygenated species increases the number of active sites for O_2 adsorption.

When a polymer electrolyte membrane fuel cell (PEMFC) is used in demanding applications such as automobiles, it must overcome kinetic limitations of the oxygen reduction reaction (ORR), which have led to three fundamental problems (*1*–*5*). First, the substantial overpotential for the ORR (*6*–*10*) at practical operating current densities reduces the thermal efficiency well below the thermodynamic limits, typically to about 43% at 0.7 V [versus the theoretical thermal efficiency of 83% at the reversible potential for the ORR (1.23 V)]. Second, an approximately five-fold reduction of the amount of Pt (platinum-loading) in current PEMFC stacks is needed to meet the cost requirements for large-scale automotive applications (*10*). Finally, the dissolution and/or loss of Pt surface area in the cathode must be greatly reduced.

These limitations could be eliminated if stable cathode catalysts, with an order of magnitude increase in the specific activity over that of state-of-the-art Pt/C catalysts, can be developed (*10*). In the hope that a combination of different metals would have improved catalytic activity and stability relative to those of a pure metal, the ORR has been studied on numerous bi- or multimetallic alloys (*6*, *8*, *11*–*17*). These studies have led to incremental improvements to catalyst performance, but large increases in activity have yet to be realized.

Rather than use a trial-and-error or combinatorial approach, we have examined selected cathode materials with well-characterized surfaces so that the mechanism of action can be attributed to a specific property (at the atomic and molecular level) of the surface under study. In this way, we can determine (i) whether the kinetics of the ORR are structure-sensitive, (ii) the composition of the topmost surface atomic layers (the segregation profile), and (iii) how alloying [usually described in terms of the ligand effect or/and ensemble effect (*18*, *19*)] alters the chemical properties of the surfaces. Similar approaches are commonly used in gas-phase catalysis (*21*) under ultrahigh vacuum (UHV) and near-ambient conditions, but alloy surface chemistry on single-crystal surfaces at electrochemical interfaces is relatively unexplored. These aqueous interfaces are more complex in that they necessarily contain solvent and electronic/ionic charge and (experimentally) it is very challenging but still tractable to use in situ surface-sensitive methods to characterize potential-induced changes in the surface properties and reactivity.

We have used a combination of ex situ and in situ surface-sensitive probes and density functional theory (DFT) calculations to study the ORR on $Pt_3Ni(hkl)$ single-crystal surfaces, identify which surface properties govern the variations in reactivity of Pt$_3$Ni catalysts, and determine how surface structures, surface segregation, and intermetallic bonding affect the ORR kinetics. Well-characterized Pt$_3$Ni single-crystal electrode surfaces were formed and characterized with UHV methods for surface preparation and surface analysis. These surfaces were transferred into the electrochemical environment without airborne contamination, and the stability of the UHV-prepared

[1]Materials Science Division, Argonne National Laboratory, Argonne, IL 60439, USA. [2]Materials Sciences Division, Lawrence Berkeley National Laboratory, University of California, Berkeley, CA 94720, USA. [3]Oliver Lodge Laboratory, Department of Physics, University of Liverpool, Liverpool, L69 7ZE, UK. [4]Department of Chemistry and Physics, University of South Carolina, Aiken, SC 29801, USA.

*To whom correspondence should be addressed. E-mail: vrstamenkovic@anl.gov (V.R.S.); nmmarkovic@anl.gov (N.M.M.)

surface was determined with a combination of in situ surface-sensitive probes with electrochemical methods so that activity relationships could be obtained in real time.

The results of the preparation and characterization of $Pt_3Ni(hkl)$ alloy surfaces in UHV are summarized (Fig. 1). The surface-sensitive techniques that were used included low-energy electron diffraction (LEED), Auger electron spectroscopy (AES), low-energy ion scattering (LEIS), and synchrotron-based high-resolution ultraviolet photoemission spectroscopy (UPS) (see methods in the supporting online material). Each of these methods has certain advantages, and they yield complementary information. The surface symmetry obtained from LEED analysis shows that, whereas the $Pt_3Ni(111)$ surface exhibits a (1×1) pattern (Fig. 1D) (i.e. that of the bulk termination), the atomically less dense $Pt_3Ni(100)$ surface shows a (1×5) reconstruction pattern (the so-called "hex" phase) in both the [01] and [0,-1] directions (Fig. 1E). Analysis of the $Pt_3Ni(110)$ LEED data (Fig. 1F) indicates that this surface may exhibit a mixture of (1×1) and (1×2) periodicities, the latter being known as the (1×2) missing-row structure (*22*).

The composition of the outermost atomic layer was obtained with LEIS, as previously shown for Pt_3Ni polycrystalline alloys (*15*, *23*) after a final anneal the surface atomic layer of all three $Pt_3Ni(hkl)$ crystals is pure Pt (Fig. 1B) (i.e. all four the so-called Pt-skin structures (*17*, *20*). Previous studies of PtNi single-crystal surfaces in UHV had indicated that this surface enrichment of Pt in the first layer is counterbalanced by its depletion in the next two to three atomic layers, so that the concentration profile oscillates around the bulk value (*24*, *25*). We demonstrated that segregation-driven near-surface compositional changes result in distinctive electronic properties of the $PtNi(hkl)$ alloys.

The surface electronic structures were obtained from the background-corrected UPS spectra (*26*). As summarized in Fig. 1C, the *d*-band density of states (DOS) is structure-sensitive and the position of the *d*-band center shifts from −2.70 eV on $Pt_3Ni(110)$ to −3.10 eV on $Pt_3Ni(111)$ to −3.14 eV on $Pt_3Ni(100)$. Furthermore, the DOS of the alloy surfaces is quite different from that of corresponding pure Pt single crystals, that is, on the (110), (100), and (111) alloy surfaces, the *d*-band center is downshifted by about 0.16, 0.24, and 0.34 eV, respectively. An important yet largely unexplored issue in surface electrochemistry on alloys is understanding how chemisorption energies correlate with the average energy of the *d*-states on the surface atoms to which the adsorbate bonds (i.e., the Hammer-Nørskov effect). To do this, we compared the results on the (111) surfaces with the same composition and arrangement of surface atoms but with a different *d*-band center position. Although we are highlighting how the difference between the electronic surface structures of Pt(111) and $Pt_3Ni(111)$ can affect the adsorption of spectator species and the kinetics of the ORR, the findings are generally applicable to other single-crystal alloy surfaces.

We next determined the stability of a surface after transfer from UHV into the electrochemical environment. Surface x-ray scattering (SXS) was used to characterize both the potential range of stability as well as the near-surface composition of the alloy in situ. Only results for $Pt_3Ni(111)$ are presented because they provide the most useful information about the potential-induced changes in the surface structure and segregation profile; a brief description of results for (110) and (100) can be found in (*27*). The termination of the $Pt_3Ni(111)$ lattice at the surface in terms of elemental composition and surface relaxation was determined by measurement and analysis of the crystal truncation rods (CTRs) (*28*). $Pt_3Ni(111)$ has the face-centered cubic (fcc) lattice with random occupation of sites by Pt and Ni, and this lattice gives rise to SXS similar to that obtained from a monocrystalline fcc lattice. Sensitivity to atomic layer composition is enhanced by the use of anomalous x-ray scattering techniques in which the incident x-ray energy is tuned to an atomic adsorption edge of the material (*29*). Thus, from SXS, we obtained information about the positions and compositions, both in the surface and subsurface layers. The CTR analysis shows that, at 0.05 V, the first layer is composed entirely of Pt and, whereas the second atomic layer is Ni-rich (52 ± 10% Ni as com-

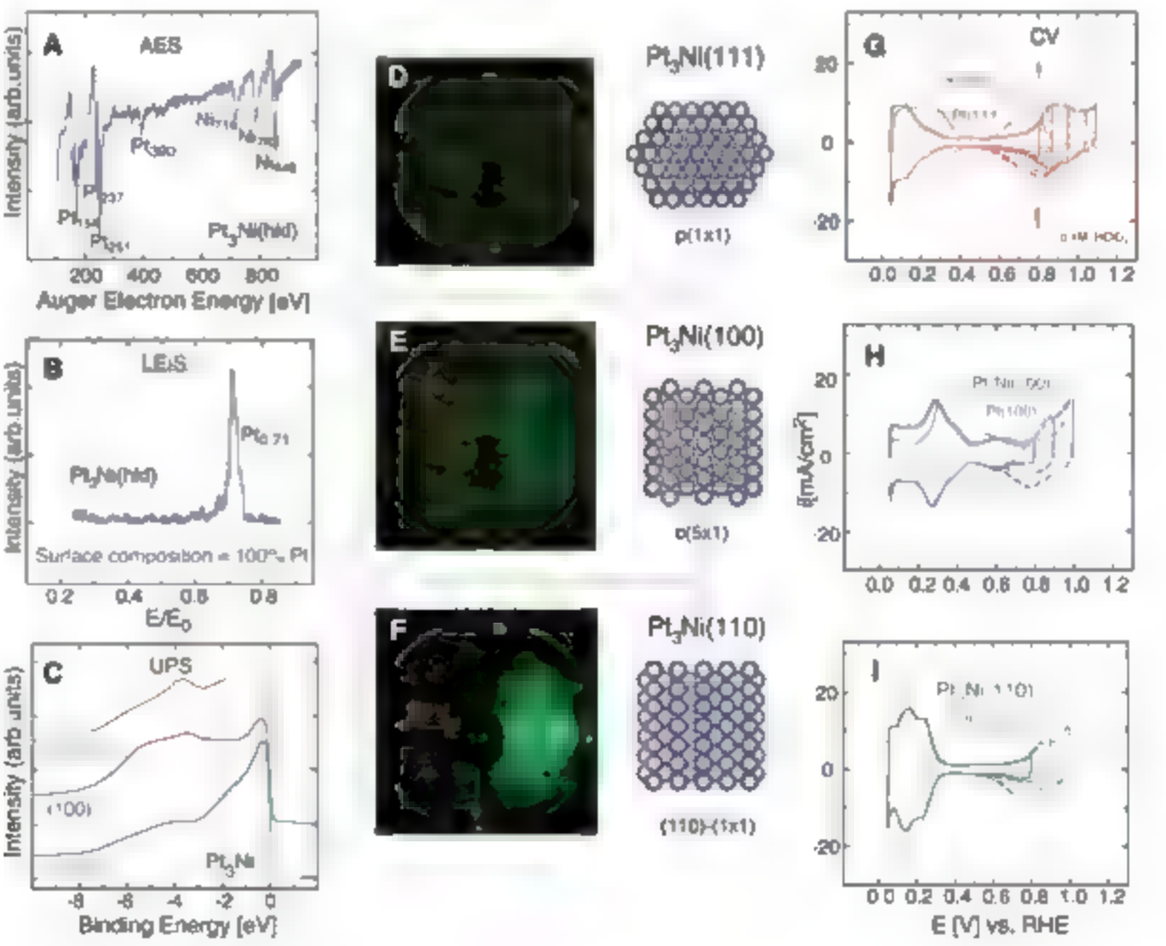

Fig. 1. Surface characterization of the Pt_3Ni single crystals in UHV and electrochemical environments. (**A**) AES spectra. (**B**) LEIS spectra. E/E_0, where E is energy of scattered electrons, and E_0 is the energy of the incident ion beam. (**C**) UPS spectra. (**D** to **F**) LEED patterns with corresponding ball models. (**G** to **I**) Cyclic voltammetry (CV) in $HClO_4$ (0.1 M) as compared to the voltammetry of the corresponding Pt single crystal (gray curves). RHE, reversible hydrogen electrode.

pared to 25% of Ni in the bulk), the third layer is again Pt-enriched (87%) (Fig. 2A). Having determined the near-surface structure at 0.05 V, the potential was cycled while the scattered x-ray intensity was measured at a CTR position that is sensitive to surface relaxation and surface roughness (Fig. 2A). We find that both the $Pt_3Ni(111)$ surface structure as well as the segregation profile are completely stable over this potential range because the changes in the x-ray scattering signal are fully reversible, and we find that the decrease in intensity at positive potential is consistent with an inward relaxation (contraction) of the surface atomic layer (this result is confirmed by similar measurements at other reciprocal lattice positions). The contraction of Pt surface atoms is induced by the adsorption of oxygenated species, which is determined by the Ni-induced modification of the Pt-skin electronic structure. A direct consequence of contraction of the topmost layer of Pt-skin at the potentials higher than 0.8 V is the increased stability of this surface over corresponding pure Pt(111), which was additionally confirmed by prolonged cycling in the designated potential range.

The relations between the surface electronic properties and the potential-dependent surface coverage by adsorbing species (the adsorption isotherms in Fig. 2C) were established by comparing the experimentally determined position of the *d*-band centers to the fractional coverages of adsorbed hydrogen ($H^+ + e^- = H_{upd}$, where H_{upd} refers to the underpotentially deposited hydrogen) between $0.05 < E < 0.4$ V, where E is the applied potential, and hydroxyl species ($2H_2O$ $OH_{ad} + H_3O^+ + e^-$, where OH_{ad} is the adsorbed hydroxyl layer) above 0.6 V (Fig. 2C). Careful inspection of the voltammograms in Fig. 2B revealed that on Pt(111)-skin, which consists of the same surface density of Pt atoms as Pt(111), a dramatic negative shift (~0.15 V) in H_{upd} formation and positive shift (~0.1 V) in OH_{ad} formation occurred relative to Pt(111). In agreement with the onset of adsorption on $Pt_3Ni(111)$, the fractional coverages by H_{upd} and OH_{ad} (Θ_{Hupd} and Θ_{OHad}) were dramatically reduced by 50% relative to Pt(111), which is in agreement with the large downshift (0.34 eV) of the *d*-band center position on the Pt-skin structure. As shown in Fig. 1, II and I, similar changes occurred for the other two single-crystal surfaces. On the Pt(100)-skin, Θ_{Hupd} was reduced by ~15% relative to Pt(100), and Θ_{OHad} was reduced by ~25%. On $Pt_3Ni(110)$, small but clearly discernable decreases in Θ_{Hupd} (~10%) and the fractional coverage by OH_{ad} (Θ_{OH}) (~20%) were observed relative to Pt(110).

To describe these effects quantitatively, we performed DFT calculations, using pseudopotentials and a plane-wave basis set, on the adsorption of OH and H_2O at 0.25 monolayer coverage on modeled Pt(111) surfaces, with second atomic layers containing 0 or 50% Ni atoms. In acid solutions, OH_{ad} would react with H^+ and form H_2O on the catalyst surface. The change in the reversible potential ΔU° of the above reaction on Pt(111) resulting from sublayer Ni atoms is

$$\Delta U^\circ = E_{ads}(OH)_{Pt} - E_{ads}(OH)_{PtNi} + E_{ads}(H_2O)_{Pt} - E_{ads}(H_2O)_{PtNi} / F$$

Here, $E_{ads}(OH)_{Pt}$, $E_{ads}(H_2O)_{Pt}$, $E_{ads}(OH)_{PtNi}$, and $E_{ads}(H_2O)_{PtNi}$ are the adsorption energies of OH and H_2O on Pt(111) with or without sublayer Ni atoms, respectively, and F is the Faraday constant. The DFT calculations show a positive shift of $\Delta U^\circ = 0.10$ V when the sublayer has 50% Ni atoms. The experiment and theory thus reach an excellent and quantitative agreement in this case and clearly establish an electronic effect of subsurface Ni on the Pt-OH chemical bonding.

The ORR is a multielectron reaction ($\frac{1}{2}O_2 + 2H^+ + 2e^- = H_2O$) that may include a number of elementary steps involving different reaction intermediates (*7*, *30*). We proposed that the rate of the ORR can be expressed as

$$i = nFAc_{O_2}(1 - \Theta_{ad})^k \exp(-\beta FE/RT) \exp(-\gamma \Delta G_{ad}/RT) \quad (2$$

where i is the measured current, n, F, A, E, x, β, γ, and R are constants [(*3*), for definitions, see (*31*)], c_{O_2} is the concentration of O_2 in the solution, Θ_{ad} is the total surface coverage by adsorbed spectator species (hydroxyl and anions, for example, OH_{ad} (Θ_{OH}) and specifically adsorbed anions (Θ_{Anad})]; ΔG_{ad} is the Gibbs energy of adsorption of reactive intermediates, and T is temperature. In the derivation of Eq. 2, it is assumed that (i) the ORR takes place on electrodes that are modified by OH_{ad} anions, etc., and (ii) the reactive intermediates (O_2 and H_2O_2) are adsorbed to low coverage (i.e., they are not a substantial part of Θ_{ad}).

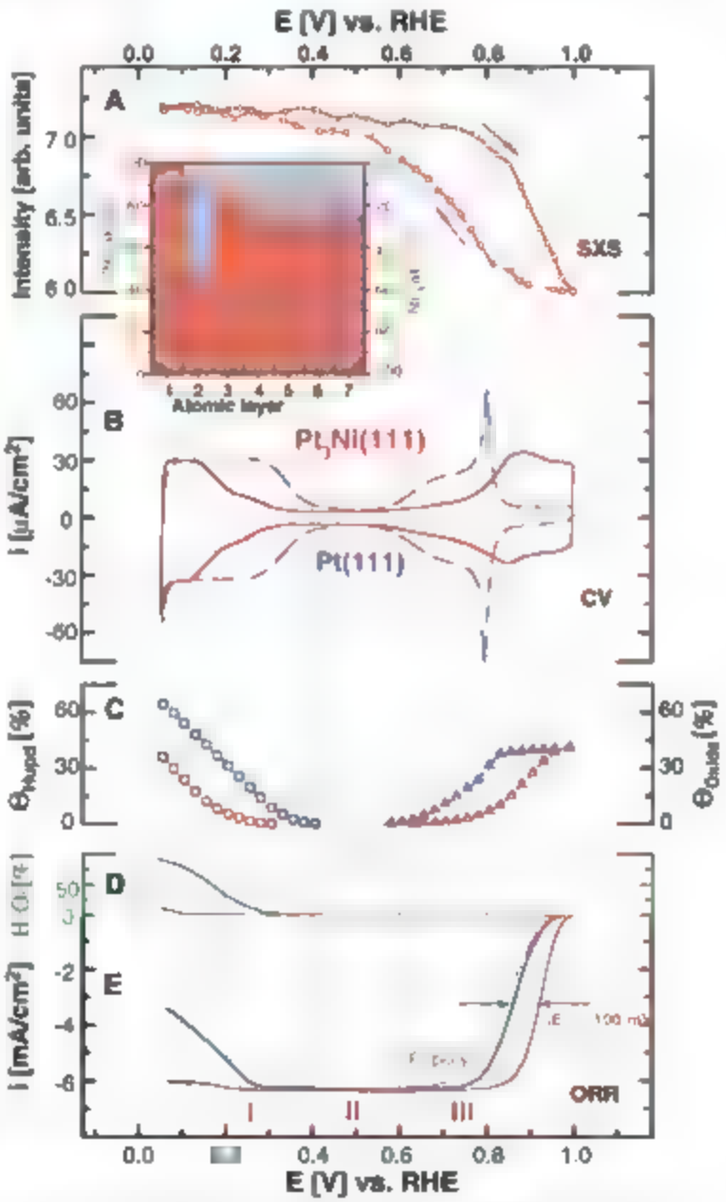

Fig. 2. In situ characterization of the $Pt_3Ni(111)$ surface in $HClO_4$ (0.1 M) at 333 K. (**A**) SXS data and (**A′**) concentration profile revealed from SXS measurements. at. %, atomic %. (**B**) Cyclic voltammetry in designated potential region (red curve) as compared to the voltammetry obtained from Pt(111) surface (blue curve). (**C**) Surface coverage calculated from cyclic voltammograms of $Pt_3Ni(111)$ (red curve) and Pt(111) (blue curve); polarization curves obtained from rotating ring disk electrode (RRDE) measurements. Θ_{OHad}, surface coverage by adsorbed spectator oxygenated species. (**D**) Green scale refers to hydrogen peroxide production in designated potential region and (**E**) ORR currents measured on $Pt_3Ni(111)$ (red curve), Pt(111) (blue curve), and polycrystalline Pt (gray curve) surfaces. The arrows are showing the positive potential shift of 100 mV in electrode half-potential ($\Delta E_{1/2}$) between ORR polarization curves measured on Pt-poly and $Pt_3Ni(111)$ surfaces. I, II, and III represent potential region of H_{upd} adsorption/desorption processes, double-layer region, and region of OH_{ad} layer formation respectively.

Based on these assumptions, the kinetics of O_2 reduction are determined by the number of free Pt sites available for the adsorption of O_2 (the $(1 - \Theta_{ad})$ term in Eq. 2) and by the ΔG_{ad} of O_2 and reaction intermediates (the ΔG_{ad} term in Eq. 3) on metal surfaces precovered by OH_{ad}. We used this reaction pathway and rate expression first to analyze the effects of electronic properties on the kinetics of the ORR on $Pt_3Ni(111)$ and Pt(111) and then, by comparing activities on different Pt_3N (*hkl*) surfaces, to establish structure sensitivity.

A characteristic set of polarization curves (the relation of i versus E) for the ORR on Pt-poly, Pt(111), and $Pt_3Ni(111)$ surfaces in $HClO_4$ (0.1 M) at 333 K is summarized in Fig. 2D. For all three surfaces, the polarization curves exhibit two distinguishable potential regions. By starting at 0.05 V and scanning the electrode potential positively, well-defined diffusion-limiting currents from 0.2 to 0.7 V are followed by a mixed kinetic-diffusion control region between 0.8 < E < 1.0 V. Further inspection of Fig. 2D reveals that the ORR kinetics is accelerated on the Pt(111)-skin relative to Pt(111), causing the positive shift of 100 mV in the half-wave potential. Given that $\Theta_{OH,ad}$ is attenuated on the Pt-skin structure, the key parameter that determines the unusually catalytic activity of $Pt_3Ni(111)$ is the low coverage by OH_{ad} [i.e., the $(1 - \Theta_{OH,ad})$ term in the kinetic equation for the ORR]. Additional confirmation that the fractional coverages by spectator species are indeed controlling the kinetics of the ORR was found by analyzing the results in the potential region where the adsorption of hydrogen is taking place (E < 0.2 V). Because of the lower coverage by H_{upd}, the production of peroxide is substantially attenuated on the Pt-skin surface. At the fuel cell relevant potentials (E > 0.8 V), the observed catalytic activity for the ORR on $Pt_3Ni(111)$ is the highest that has ever been observed on cathode catalysts, including the $Pt_3Ni(100)$ and $Pt_3Ni(110)$ surfaces.

Synergy between surface geometry and surface electronic structure for the ORR is illustrated in Fig. 3. As summarized, the different low-index surfaces have markedly different activity for this reaction [that is, $Pt_3Ni(100)$-skin < $Pt_3Ni(110)$-skin <<< $Pt_3Ni(111)$-skin, with the change in activity between the least active (100) and the most active (111) surfaces being greater than an order of magnitude]. Structure sensitivity of the ORR on the Pt low-index single-crystal surfaces in perchloric acid has been well established (*6*), with activities increasing in the order Pt(100) < Pt(111) < Pt(110) (Fig. 3). These differences have been attributed to the structure-sensitive adsorption of OH_{ad} on Pt(*hkl*) and its inhibiting (site blocking) effect on O_2 adsorption. In the potential region of OH adsorption, the structure sensitivity of the $Pt_3Ni(hkl)$-skin surfaces has the same origin.

In order to reveal the role of the electronic structure onto ORR kinetic, we compared electrodes with the same surface morphology. The most pronounced effect was observed on the (111) surfaces. For the same p(1 × 1) arrangement of the topmost layer, the same surface atomic density, and the same surface composition (100% Pt) but for a different electronic structure ($\Delta d_{[111]}$ = 0.34 eV, where $\Delta d_{[hkl]}$ is the *d*-band center shift), the ORR is being enhanced by factor of 10 on Pt(111)-skin relative to that on Pt(111). Given that extended Pt surfaces have 5 to 10 times the activity per surface Pt atoms than the state-of-the-art Pt/C catalysts that are currently used in the PEMFC (~0.2 mA/cm² at 0.9 V) (*10*, *14*), a total 90-fold enhancement of Pt(111)-skin versus that of Pt/C has been achieved.

Considering that the $Pt_3Ni(111)$-skin surface exhibits the highest catalytic activity that has ever been detected, the challenge would be to create a nanocatalyst with electronic and morphological properties that mimic the $Pt_3Ni(111)$ surface. Therefore in the future, a way to reduce the current value (~1.0g of Pt per kW) of Pt-specific power density in a PEMFC without a loss in cell voltage, while also maintaining the maximum power density (W/cm²), would be the engineering of $Pt_3Ni(111)$-skin like nanocatalysts.

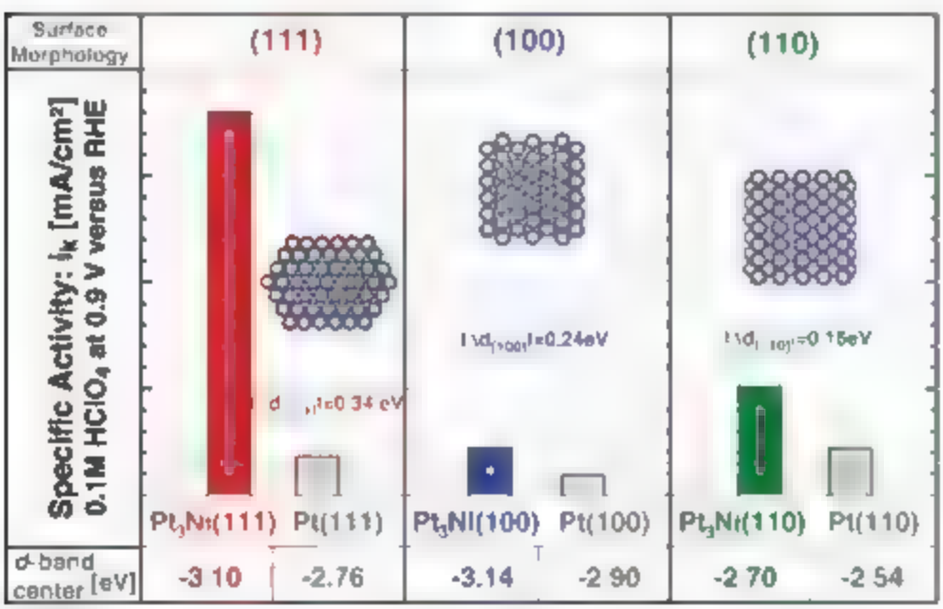

Fig. 3. Influence of the surface morphology and electronic surface properties on the kinetics of ORR. RRDE measurements for ORR in $HClO_4$ (0.1 M) at 333 K with 1600 revolutions per minute on $Pt_3Ni(hkl)$ surfaces as compared to the corresponding Pt(*hkl*) surfaces (a horizontal dashed gray line marks specific activity of polycrystalline Pt). Are shown. Specific activity is given as a kinetic current density i_k, measured at 0.9 V versus RHE. Values of *d*-band center position obtained from UPS spectra are listed for each surface morphology and compared between corresponding $Pt_3Ni(hkl)$ and Pt(*hkl*) surfaces.

References and Notes

1. S. Gottesfeld, T. A. Zawodzinski, *in Advances in Electrochemical Science and Engineering*, R. C. Alkire, H. Gerischer, D. M. Kolb, C. W. Tobias, Eds. (Wiley-VCH, Weinheim, Germany, 1997), vol. 5.
2. F. Besenbacher *et al.*, *Science* **279**, 1913 (1998).
3. N. M. Markovic, P. N. Ross, *Surf. Sci. Rep.* **45**, 117 (2002).
4. W. Vielstich, A. Lamm, H. A. Gasteiger, *Handbook of Fuel Cells: Fundamentals, Technology, and Application* (Wiley, West Sussex, UK, ed. 1, 2003).
5. J. K. Norskov, C. H. Christensen, *Science* **312**, 1322 (2006).
6. A. J. Appleby, *Catal. Rev.* **4**, 221 (1970).
7. M. R. Tarasevich, A. Sadkowski, E. Yeager, *in Comprehensive Treatise in Electrochemistry*, J. O. M. Bockris, B. E. Conway, E. Yeager, S. U. M. Khan, R. E. White, Eds. (Plenum, New York, 1983), chap. 6.
8. K. Kinoshita, *Electrochemical Oxygen Technology* (Wiley, New York, 1992).
9. N. R. Adzic, *in Electrocatalysis*, J. Lipkowski, P. N. Ross, Eds. (Wiley-VCH, New York, 1998).
10. H. A. Gasteiger, S. Kocha, B. Sompalli, F. T. Wagner, *Appl. Catal. B* **56**, 9 (2005).
11. F. J. Luczak, D. A. Landsman, U.S. Patent 4,711,829 (1987).
12. S. Mukerjee, S. Srinivasan, *J. Electroanal. Chem.* **357**, 201 (1993).
13. T. Toda, H. Igarashi, H. Uchida, M. Watanabe, *J. Electrochem. Soc.* **146**, 3750 (1999).
14. U. A. Paulus *et al.*, *J. Phys. Chem. B* **106**, 4181 (2002).
15. V. Stamenkovic, T. J. Schmidt, N. M. Markovic, P. N. Ross Jr., *J. Phys. Chem. B* **106**, 11970 (2002).
16. J. Zhang, M. B. Vukmirovic, Y. Xu, M. Mavrikakis, R. R. Adzic, *Angew. Chem.* **117**, 2170 (2005).
17. V. R. Stamenkovic, B. S. Mun, K. J. J. Mayrhofer, P. N. Ross, N. M. Markovic, *J. Am. Chem. Soc.* **128**, 8813 (2006).
18. B. Hammer, J. K. Norskov, *in Advances in Catalysis* (Elsevier, Amsterdam, 2000), vol. 45, pp. 71–129.
19. J. Greeley, J. K. Norskov, M. Mavrikakis, *Annu. Rev. Phys. Chem.* **53**, 319 (2002).
20. V. Stamenkovic *et al.*, *Angew. Chem.* **45**, 2897 (2006).
21. C. T. Campbell, *Annu. Rev. Phys. Chem.* **41**, 775 (1990).
22. P. A. Thiel, P. J. Estrup, *in The Handbook of Surface Imaging and Visualization*, A. T. Hubbard, Ed. (CRC Press, Boca Raton, FL, 1995).
23. V. Stamenkovic, T. J. Schmidt, P. N. Ross, N. M. Markovic, *J. Electroanal. Chem.* **554 555**, 191 (2003).
24. Y. Gauthier, R. Baudoing, J. Rundgren, *Phys. Rev. B* **31**, 6216 (1985).
25. Y. Gauthier, *Surf. Rev. Lett.* **3**, 1663 (1996).
26. B. S. Mun, C. Lee, V. Stamenkovic, N. M. Markovic, P. N. Ross, *Phys. Rev. B* **71**, 115420 (2005).
27. For the other two single-crystal surfaces, we have also found that the Pt-skin layer that formed in UHV is stable in an electrochemical cell. Unlike the Pt_3Ni(100)/vacuum interface, however, the electrolyte interface was found to be unreconstructed at all potentials because of anion-induced adsorption. The SXS results for the $Pt_3Ni(110)$

surface are ambiguous [i.e., it was not clear whether the (1 × 2) phase was indeed transferred from UHV into an electrochemical cell]. Nevertheless, the SXS results clearly show that the surface is relatively smooth and stable, and thus reliable electrochemical results can be obtained on both electrodes.

28. I. K. Robinson, E. Vlieg, K. Kern, *Phys. Rev. Lett.* **63**, 2578 (1989).
29. C. A. Lucas, N. M. Marković, in *Advances in Electrochemical Science and Engineering*, R. C. Alkire, D. M. Kolb, J. Lipkowski, P. N. Ross, Eds. (Wiley-VCH, Weinheim, Germany, 2006), vol. 9.
30. N. M. Marković, H. A. Gasteiger, P. N. Ross, *J. Phys. Chem.* **99**, 3411 (1995).
31. In Eq. 2, n is the number of electrons; R is the rate constant; a is the order of active Pt sites; β and γ are the symmetry factors (which are assumed to be ½); and R is the universal gas constant.
32. N.M.M. and V.R.S. acknowledge the support from the contract (DE-AC02-06CH11357) between the University of Chicago Argonne, LLC, and the U.S. Department of Energy. We acknowledge the support of General Motors and helpful discussions with H. A. Gasteiger and F. T. Wagner. C.A.L. and B.F. acknowledge the support of the UK Engineering and Physical Sciences Research Council. V.R.S. thanks M. West for support in experimental design.

Supporting Online Material

www.sciencemag.org/cgi/content/full/1135941/DC1
Materials and Methods

5 October 2006; accepted 7 December 2006
Published online 11 January 2007
10.1126/science.1135941
Include this information when citing this paper.

Water Catalysis of a Radical-Molecule Gas-Phase Reaction

E. Vöhringer-Martinez,[1] B. Hansmann,[1] H. Hernandez,[2] J. S. Francisco,[2] J. Troe,[1] B. Abel[1]*

There has been considerable speculation about the role of water and water complexes in chemical gas phase reactions, including the conjecture that water may act as a molecular catalyst through its ability to form hydrogen bonds. Here, we present kinetic studies in which the effect of water on the rate of the reaction between hydroxyl radicals and acetaldehyde has been measured directly in Laval nozzle expansions at low temperatures. An increasing enhancement of the reaction rate by added water was found with decreasing temperatures between 300 and 60 kelvin. Quantum chemical calculations and statistical rate theory support the conclusions that this observation is due to the reduction of an intrinsic reaction barrier caused by specific water aggregation. The results suggest that even single water molecules can act as catalysts in radical-molecule reactions.

Water introduces many unusual features into the kinetics and energetics of chemical and biological reaction systems, which are difficult to rationalize on a molecular level (*1*, *2*). Beyond the well-known properties of bulk water, there is evidence that even single confined water molecules in molecular aggregates may have a decisive influence on gas phase chemistry (*3*). An intriguing question is whether water molecules can even act as true catalysts in chemical reactions, for example, through their ability to form hydrogen bonds. A number of molecule-water complexes have evidenced photochemistry distinct from that of the isolated molecules (*4*). Complexes of water with ozone (*5*), sulfuric acid (*6*), nitric acid (*7*), nitrous oxide (*8*), and chlorine dioxide (*9*, *10*) are examples of water aggregates that may be important in atmospheric photochemistry.

Beyond its ability to influence photochemistry, water is known to form complexes with active species such as radicals and polar molecules in thermal reactions (*4*, *12*, *13*), and such complexation may alter intrinsic reaction barriers in bimolecular reactions. In addition, the radical-complex mechanism (*14*) is well known to have a characteristic impact on recombination processes, which could be enhanced by water molecules. Last, water may act as a particularly efficient collision partner to collisionally stabilize intermediates of such reactions. Unfortunately, all these effects (hereafter referred to as the catalysis, the radical-complex, and the energy transfer mechanisms) may influence overall reaction yields and rates in bimolecular reactions (*14*) and are often difficult to distinguish.

For example, there is experimental (*15*) and theoretical (*4*) evidence that the hydroperoxy radical (HO_2) forms a hydrogen-bonded complex with a water molecule, which has the potential to affect the kinetics of HO_2 reactions. Along these lines, the rate constant for the self reaction of HO_2 to yield H_2O_2 and O_2, which proceeds via a long-lived intermediate is somewhat faster in the presence of water than in its absence (*4*, *16*, *17*). A similar effect has been observed for the reaction of hydroperoxy radicals with nitrogen dioxide in the presence of water (*18*). However, the origin of the documented impact of water on the kinetics in general remains unclear. Although "prereaction complexes of water in chemical reactions have been suggested in the past (*16*), a conclusive mechanism and a detailed kinetic analysis of the systems were not given. The general problem for an understanding of such kinetic systems is that they depend upon temperature, pressure, and specific molecular parameters and so require a detailed kinetic analysis using reaction rate theory and high-level quantum chemistry (*14*).

Following up on a long-standing conjecture that even single or few water molecules may alter energetics in general and reaction barriers in particular or favor reaction sites, the goal of this study was to investigate the role of water as a real catalyst in chemical gas-phase reactions potentially relevant for atmospheric chemistry and, in particular, to provide a clear example for a water-catalyzed radical-molecule reaction. The fast H-atom abstraction reaction of OH with acetaldehyde proved to be a good system for studying the effect of water aggregation on the kinetics. The reaction does not involve long-lived, strongly bound intermediates such as those found in other complex-forming bimolecular reactions, for example, in the reaction of OH with CO proceeding via HOCO complexes (*14*).

Recent experimental and theoretical work has provided evidence for the assumption that the reaction proceeds predominantly through abstraction of the aldehydic hydrogen atom (*19*–*22*). The addition of the OH radical to the double bond does not take place because its activation energy is much larger than that for hydrogen abstraction (*23*, *24*). In addition, the aldehydic hydrogen atom has a relatively small binding energy compared with that of hydrogen atoms in the methyl group. A prereactive complex $CH_3C(HO)\cdots HO$ has been postulated by D'Anna *et al.* (*24*) and Alvarez-Idaboy *et al.* (*23*), and its binding energy was estimated to be 18 kJ mol^{-1}. Although transient prereactive complexes have not been directly characterized experimentally, their presence has been identified indirectly in several radical-molecule reactions and associated with a negative temperature dependence of the reaction rate (*25*, *26*). Nielsen and co-workers calculated barriers (relative to the reactant energy) to aldehydic H abstraction, methyl H abstraction, and OH addition to the carbonyl bond of −14.2 kJ mol^{-1}, 12.1 kJ mol^{-1}, and 30.9 kJ mol^{-1}, respectively (*24*). A negative temperature dependence of the reaction rate at higher temperatures has also been reported (*22*) without a theoretical analysis of the effect.

We measured rates and rate constants for the OH + CH_3CHO reaction in the presence and absence of water vapor by using a pulsed Laval nozzle expansion (*25*, *27*) (Fig. 1A). The reaction was followed by laser-induced fluorescence (LIF) to monitor the decay of OH radical concentration. The rate constants were determined over a temperature range of 58 to 300 K. The decay profiles can be fitted well by an exponential time law (Fig. 1B). Plots of pseudo-first-order

[1]Institut für Physikalische Chemie der Universität Göttingen, Tammannstrasse 6, 37077 Göttingen, Germany. [2]Department of Chemistry and Department of Earth and Atmospheric Sciences, Purdue University, West Lafayette, IN 47907-2084, USA.

*To whom correspondence should be addressed. E-mail: babel@gwdg.de

rate constants versus acetaldehyde concentrations (in nitrogen buffer gas) at a constant total density yield the second-order rate constants. Two experiments are shown for a temperature (T) of 77 K with and without added water vapor (Fig. 1C). From the slopes of the plots, rate constants of 4.6×10^{-11} cm^3-molecule^{-1}s^{-1} and 9.0×10^{-11} cm^3-molecule^{-1}s^{-1} were determined. Several experiments were averaged for a particular temperature (27). Averaged second-order rate constants of the reaction of OH with acetaldehyde alone and in the presence of water vapor at temperatures between 300 K and 60 K are shown in Fig. 2.

Deviation of the plot format in Fig. 2 from a normal Arrhenius-type plot (log k versus $1/T$) is somewhat arbitrary, and there is no reason to expect a linearization of the data. Nevertheless, the chosen plot is often used in cases where bimolecular rate constants increase with decreasing temperature. The origin of the so-called negative temperature dependence depends strongly on the molecular system. As shown below, one reason for the effect may be a "reef"-type barrier below the energy of the reactants in the entrance channel of the reaction, as opposed to a much larger barrier in other cases that would yield the typical Arrhenius behavior.

The water content of the beam was measured with off-line infrared spectroscopy and determined to be ~3%. The shaded area between the dashed lines connecting the data points marks the difference between the two data sets and illustrates the effect of added water. Experiments of the reaction without added water in the range between 500 and 700 K measured by Crowley *et al.* (22) and Michael *et al.* (19) are shown and compared with our data point at 300 K (this work). In our study, we significantly extended the temperature range and confirmed the negative dependence on temperature of the reaction rate down to 58 K. In addition, small amounts of added water accelerated the reaction (Fig. 2). Although the effect is small at 300 K, it becomes prominent at lower temperatures. The effect also depends on the water content of the buffer gas. If the concentration of water is significantly below 3%, no significant acceleration is seen. On the other hand, a water content of more than 8% increases aggregation in such a way that the intensity of the OH signal is significantly reduced, and the reaction becomes difficult to measure because of an overall quenching of LIF. From the dependence of the reaction rate on water and acetaldehyde concentrations and the density range in which we find a linearity of the rate versus reactant and water concentrations, as well as the experimental observation that larger clusters (acetaldehyde and acetaldehyde-water) are much less reactive, tending to decrease the actual reactant concentration (and in turn the rate constant), the experiments suggest that small acetaldehyde-water clusters as reactants are responsible for the observed effect.

We note that we did not measure "pure" rate constants. Instead, the observed temperature-dependent rate constant $k(T)$ in the presence of water is the sum of two contributions from the unclustered and clustered species, respectively. Both fractions f_0 and f_{aggr} are associated with their rate constants k_0 and k_{aggr}. This situation can be symbolically expressed by

$$k(T) = f_0 k_0 + f_{aggr} k_{aggr} \quad (1)$$

In order to rationalize the effect of water-acetaldehyde clusters on the reaction rate, we performed quantum chemical calculations [coupled-cluster with single and double and perturbative triple excitations, CCSD(T)] to elucidate the energetics and structure of the intermediate species of the reaction (Fig. 3). Because the acceleration effect has been seen only for small water concentrations, we posited a significant role of single water molecules in complexes with acetaldehyde. For comparison, calculations were also carried out for the reaction without water. We refer to two kinds of complex, the hydrogen-bonded one between acetaldehyde and water, which acts as a reagent (with OH) in the experiments with H_2O present, and the transient prereaction complexes for the OH

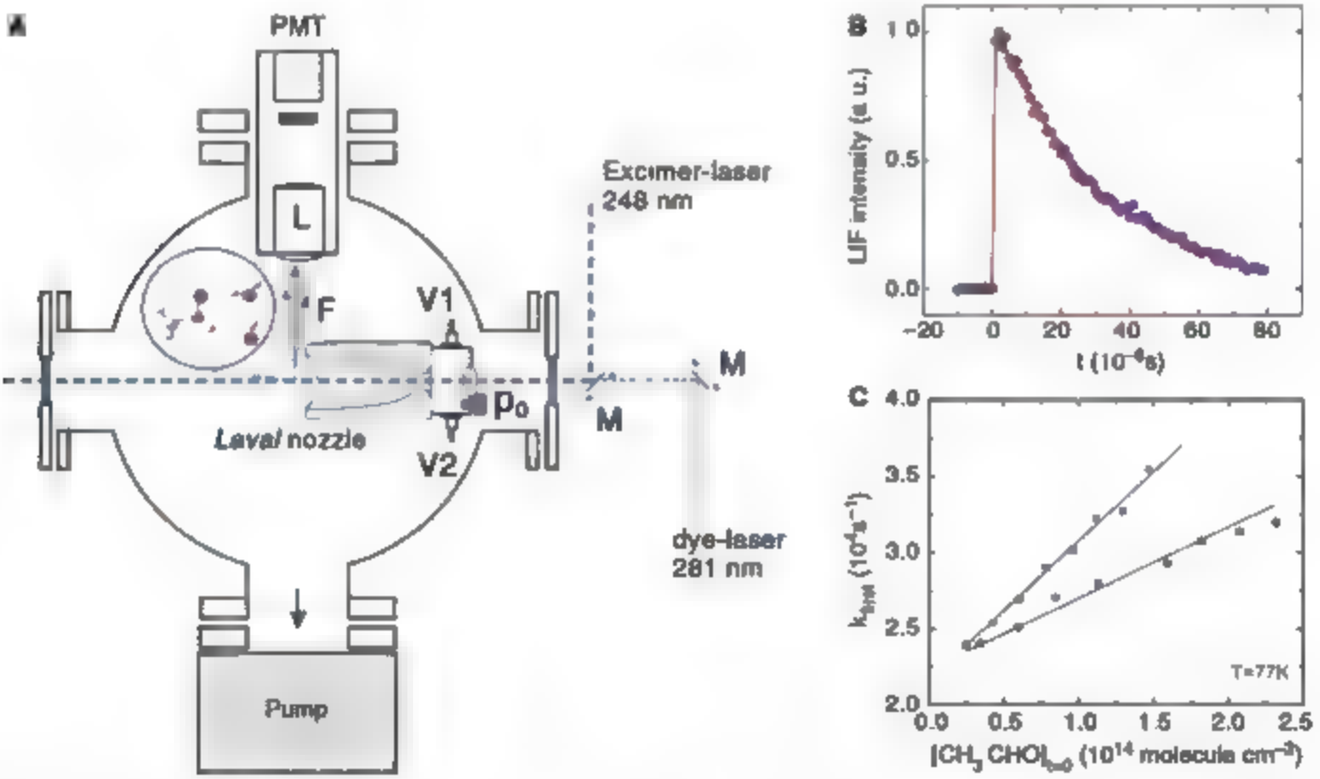

Fig. 1. (**A**) Laval nozzle expansion apparatus used here. p_0 represents the pressure in front of the Laval nozzle; V1 and V2, valves feeding the nozzle reservoir; F, fluorescence; L, lens system for the collection of fluorescence; M, mirrors; and PMT, photomultiplier. (**B**) LIF profiles of OH in the reaction between acetaldehyde and OH radicals (T = 77 K, ρ_{tot} = 8.5 × 10^{16} molecule cm^{-3}, $\rho_{acetaldehyde}$ = 1.6 × 10^{14} molecule cm^{-3}, ρ_{OH} = 1.5 × 10^{11} molecule cm^{-3}). (**C**) Pseudo-first-order rate constants k as a function of acetaldehyde concentration (buffer gas N_2, T = 77 K, ρ_{tot} = 8.5 × 10^{16} molecule cm^{-3}). Circles, reaction without water; squares, reaction with water (single experiments).

plus CH_3CHO reaction and for the reaction between OH and $CH_3CHO \cdot H_2O$ hydrogen-bonded complexes. Optimized structures for complexes and transition states with and without water are shown in Fig. 4. Calculated structures for the prereaction complex (Fig. 4A) and the transition state (Fig. 4B) in the absence of water are in agreement with previous work (*24*).

According to quantum chemical calculations (Fig. 3A), the H-abstraction reaction is governed by a shallow well and a small barrier separating the prereaction complex and the products (H_2O and CH_3CO). The barrier considered here may be described as a submerged barrier or reef on the path of maximum energy of the reaction, one whose energy maximum lies below the asymptotic reagent energy but above the earlier energy minimum associated with the prereaction complex. This situation corresponds to a loose entrance rigid exit complex-forming bimolecular reaction, as characterized in (*14*), with an overall rate constant expressed as

$$k = k_{\infty}\left(\frac{k_{forw}}{k_{back} + k_{forw}}\right) \quad (2)$$

k_{∞}, k_{forw}, and k_{back} are specific rate constants (*27*) and depend upon the energy and the angular momentum of the intermediate complex. Specific rate constants k_{forw} and k_{back} were calculated first as a function of energy and the angular momentum. A simplified statistical adiabatic channel model (*14*) was applied by using energies and calculated vibrational frequencies of the reactants, the precomplex, and the transition state from our quantum chemistry calculations. The determined rate constants at the energies relevant for the temperatures of this experiment showed that lifetimes of the complexes are in the low picosecond range because of the shallow potential well. A comparison of the sum of k_{forw} and k_{back} with Lennard-Jones collision frequencies for acetaldehyde-N_2 collisions unambiguously showed that the intermediate, even up to pressures of 1 bar, cannot be collisionally stabilized and that the reaction is in its low-pressure limit. These findings explain why no pressure dependence has been found for this reaction (*22*).

One could argue that the situation changes when water replaces nitrogen as a collision partner. Although the collision frequency for water is about 10 times that for nitrogen (*28*), the average energy transferred in a collision is about 5 times larger (*28*) for water collisions. However, water diluted to about 3% in nitrogen should not be more efficient than nitrogen alone in stabilizing the reaction complexes. The large energy transfer efficiency of water relative to the nitrogen buffer gas is compensated by its small concentration in the system and thus cannot be responsible for the observed enhancement of the reaction rate.

We have also used statistical unimolecular rate theory (*27*) to calculate the overall thermal rate constant as a function of temperature (*14*). Results from the calculation for the overall reaction without added water explicitly took into account the energy and the angular momentum dependence of the rate constants for the formation of the prereaction complex, as well as the competition between forward reaction over the barrier and backward dissociation according to the formalism given in (*14*) (Fig. 2). The observed negative temperature dependence was well reproduced, confirming the presence of the prereaction complex. The observed negative temperature dependence can be rationalized in terms of the different energy and angular momentum dependences of the specific rate constants k_{forw} and k_{back} of the intermediate complex and the resulting vibrational and rotational channel switchings (*14*). This result shows that a reef-type barrier and the corresponding transition state can be rate-determining despite their potential energy lying below the energy of the reagents.

Our quantum chemical calculations shed light on the origin of water's accelerating effect

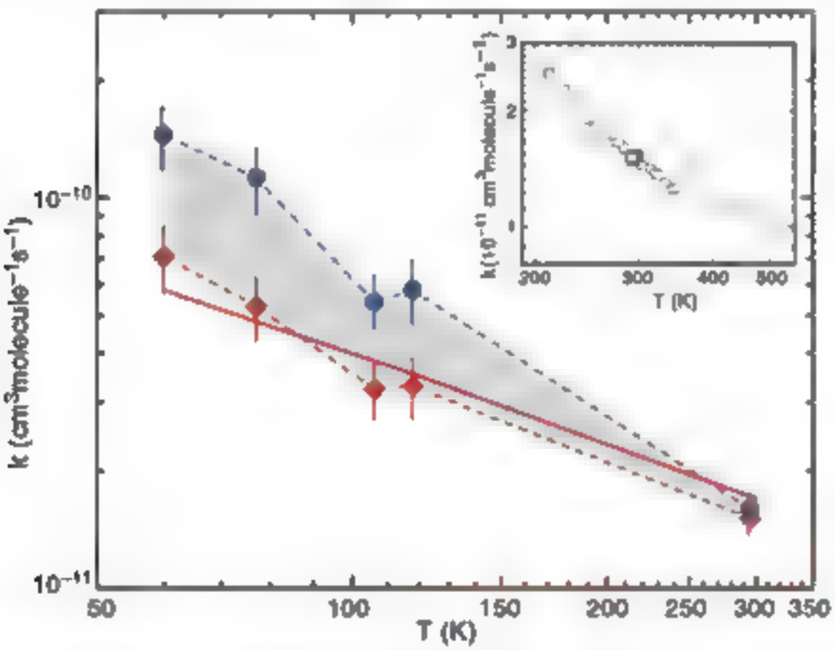

Fig. 2. Rate constants k for the reaction $OH + CH_3CHO \cdot (H_2O)_n \rightarrow 2\,H_2O + CH_3CO$ measured here with (solid circles) and without (solid diamonds) added water. (**Inset**) Data from (*22*) (open squares), (*19*) (open circles), and this work (solid square) for the reaction without water. Solid line indicates simplified SACM calculation.

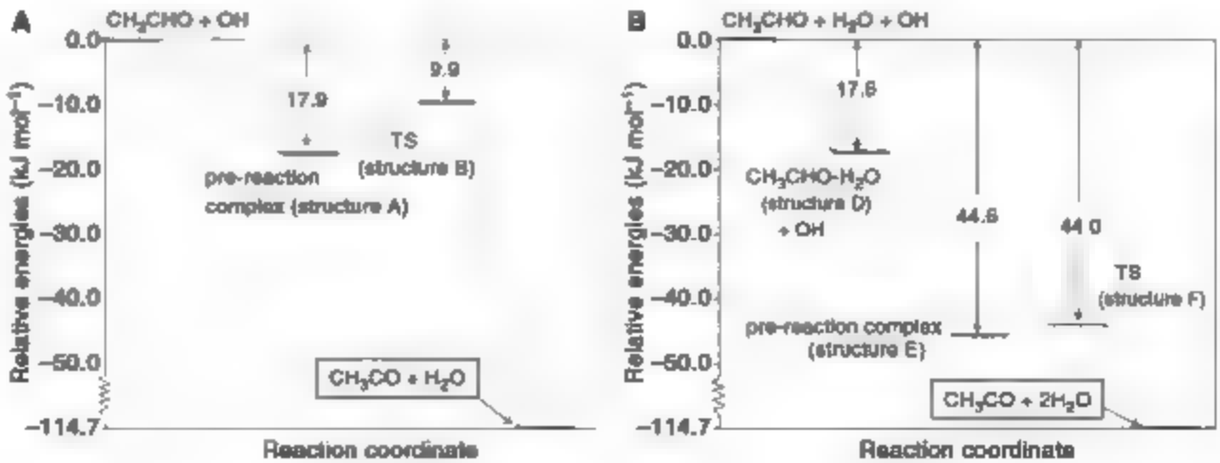

Fig. 3. Relative energies for the reaction in the absence (**A**) and the presence (**B**) of water. The energies are calculated at the CCSD(T) level of theory with the correlation consistent polarized triple-zeta (cc-pVTZ) basis set.

on this H-atom abstraction reaction. First, we calculated energies and structures for the reaction in the absence of water (Figs. 3 and 4, A and B). The 8 kJ mol^{-1} barrier, i.e., the difference in energy between the prereaction complex (structure 4A) and the transition state (structure 4B), is consistent with previous results (*29*). Next, we optimized the geometries of prospective 1:1 water-acetaldehyde complexes and found two nearly isoenergetic structures, with water top-bound in one (Fig. 4C) and side-bound in the other (Fig. 4D). The top-bound cluster reacts with OH via a transition state (TS) similar in energy to that calculated for the naked acetaldehyde, with no significant impact on the reaction barrier. In contrast, the side-bound species can form a cyclic prereaction complex with OH at a substantially lower energy (Fig. 4E), leading also to a substantial reduction of the energy of the TS (Fig. 4F) and thus the barrier of the reaction. Quantum chemical calculations at the CCSD(T) level of theory that include zero-point energy correction yield an 8 kJ mol^{-1} barrier separating the prereaction complex from the TS in the absence of water, but only a 0.6 kJ mol^{-1} barrier involving the side-bound acetaldehyde-water complex. Thus, the calculations show that even a single water molecule can accelerate the reaction by significant barrier lowering.

If the water enhancement of the reaction rate is due to a lowering or even a removal of the intrinsic reaction barrier of the prereaction water complexes, Eq. 2 helps in understanding that this effect in turn increases the rate constant, k_{forw}, for the forward reaction while lowering k_{back} due to the larger number of molecular degrees of freedom of the complex (Fig. 4F). In the extreme, this effect could increase the overall rate constant for clustered reactants to the association-limited value, $k \approx k_{coll}$, corresponding to the maximal observable catalytic effect.

As noted above and expressed in Eq. 1, the measured temperature-dependent rate constant $k(T)$ in the presence of water is the sum of two contributions, namely, from the clustered and unclustered species. k_0 is given by the red line in Fig. 2, whereas k_{aggr}, because of the near absence of an intrinsic barrier, is expected to be close to k_{coll} and therefore only weakly temperature-dependent. The marked negative temperature dependence of $k(T)$ in the presence of water is therefore attributed to that of f_{aggr} and not of k_{aggr}. For temperatures close to 300 K, the degree of clustering f_{aggr} is small, and the reaction is not much enhanced. With decreasing temperature, the degree of clustering f_{aggr} increases, which increases the rate. Together with the energetics of the reaction, thus, f_{aggr} controls the catalytic effect.

From the argumentation above, an important quantity is the concentration of $CH_3CHO \cdot H_2O$ hydrogen-bonded complexes in the experiments where ~3% of H_2O is present in the gas mixtures. Unfortunately, this quantity cannot be measured nor easily calculated, because it may depend upon the kinetics of the $CH_3CHO \cdot H_2O$ complexing process. Estimations of f_{aggr} from equilibrium constants and equilibrium concentrations for the 1:1 complexes (which are an upper limit to their actual concentration) using our ab initio data show that the temperature dependence of the rate constant qualitatively correlates with f_{aggr} for 1:1 complexes and that f_{aggr} may approach unity for temperatures well below 100 K.

Although the kinetic data and our quantum chemical calculations strongly suggest that the rate enhancement is due to specific water clusters and that even single water molecules may lower reaction barriers, the question about the role of larger clusters arises. At the lowest temperatures in principle, larger clusters such as clusters of acetaldehyde and larger water-acetaldehyde complexes may also exist to some extent. A significant impact of acetaldehyde clusters can be more or less excluded, because this manifests itself in a pronounced curvature of plots like those in Fig. 1B. Our experience is that larger clustering of the reactants obviously decreases the active reactant concentration. The same argumentation holds for acetaldehyde-water clusters; larger clusters will also decrease the effective reactant concentration. In general, working in concentration and density regions, where a linear dependence of the rate constant as a function of concentration is observed, avoids these complications. It is also known that water forms complexes with the hydroxyl radical and pure water clusters. In the present experiment, however, we were not sensitive to these types of complexation, because the rate constants were recorded for constant OH and water concentrations.

The catalytic effect that manifests itself in an increase of the overall bimolecular reaction rate is due to clustering of the reactant at specific sites and in turn a reduction of an intrinsic reaction barrier through the formation of specific hydrogen bonds. The water molecules are not actively involved in the reaction (e.g., through bond breaking) other than forming hydrogen bonds. We are aware that any general conclusions about radical-molecule reactions involving hydrates may be premature. In other related studies of potential water catalysis, it was found that, although barriers are lowered upon hydration, the dynamics and residual barriers may still be unfavorable for reaction (*29*). However, we do anticipate that this effect is not restricted to the HO-CH_3CHO system but a general low-temperature feature of a larger class of reactions of potential relevance in atmospheric chemistry. Lastly, we note that a catalytic role of water in (condensed phase) organic reactions has been reported before. However, the effect described here should be clearly distinguished from effects of microsolvation (causing ionic dissociation), classical acid-base catalysis of organic reactions, and cases in which water is actively involved as a reactive partner (e.g., as a proton donor or acceptor).

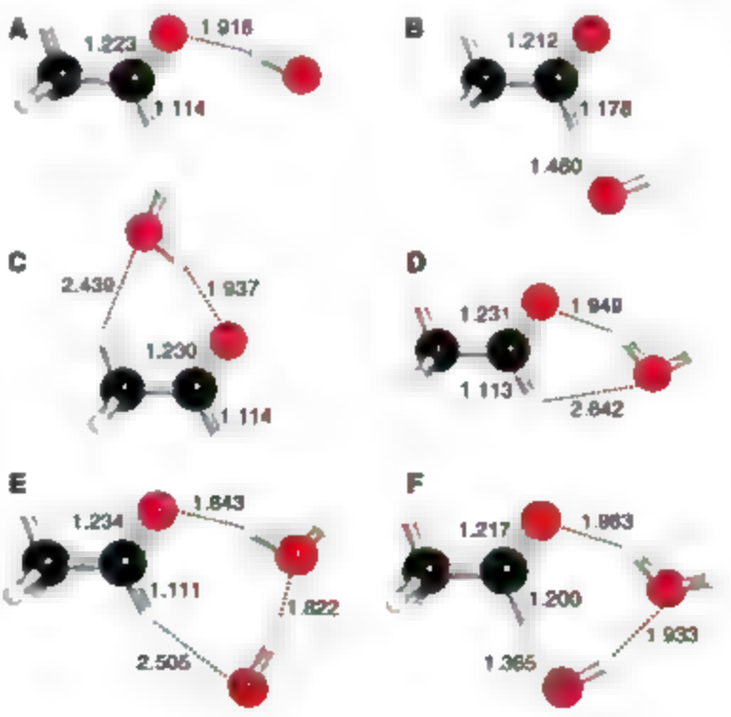

Fig. 4. Calculated structures (**A** to **F**) of reactant complexes, prereaction complexes, and transition states. Structures (bond lengths in Å) are at characteristic points along the reaction coordinates (Fig. 3) using the MP2 level of theory with the aug-cc-pVDZ basis set. (**A**) and (**B**) are the prereaction complex and the transition state without water, respectively. (**C**) and (**D**) are prospective water-acetaldehyde clusters from which (**D**) was identified to be relevant for the reaction. (**E**) is the prereaction complex, and (**F**) is the transition state for the reaction in the presence of water.

References and Notes

1. B. C. Garrett, *Science* **303**, 1146 (2004).
2. M. J. Tait, F. Franks, *Nature* **230**, 91 (1971).
3. M. L. Chabinyc, S. L. Craig, C. K. Regan, J. R. Brauman, *Science* **279**, 1882 (1998).
4. S. Alonso, J. S. Francisco, *Acc. Chem. Res.* **33**, 825 (2000).
5. G. Frost, V. Vaida, *J. Geophys. Res.* **100**, 18803 (1995).
6. V. Vaida, H. G. Kjaergaard, P. E. Hintze, D. J. Donaldson, *Science* **299**, 1566 (2003).
7. F. M. Tao, K. Higgins, W. Klemperer, D. D. Nelson, *Geophys. Res. Lett.* **23**, 1797 (1996).
8. M. Tanaka, U. Nagashima, M. Takayanagi, H. L. Kim, I. Hanazaki, *J. Phys. Chem. A* **101**, 507 (1997).
9. V. Vaida *et al.*, *Ber. Bunsenges. Phys. Chem.* **96**, 391 (1992).
10. R. C. Dunn, J. D. Simon, *J. Am. Chem. Soc.* **114**, 4856 (1992).
11. E. Johnson, A. Engdahl, P. Ovis, B. A. Nelander, *J. Phys. Chem.* **96**, 5878 (1992).

12. I. W. M. Smith, A. R. Ravishankara, *J. Phys. Chem. A* **106**, 4798 (2002).
13. J. C. Hansen, J. S. Francisco, *ChemPhysChem* **3**, 833 (2002).
14. J. Troe, *J. Chem. Soc. Faraday Trans.* **90**, 2303 (1994).
15. K. Sumi, Y. Sumiyoshi, Y. Endo, *Science* **311**, 1278 (2006).
16. E. J. Hamilton, *J. Chem. Phys.* **63**, 3682 (1975).
17. W. B. Demore, *J. Phys. Chem.* **83**, 1113 (1979).
18. S. P. Sander, M. E. Peterson, *J. Phys. Chem.* **88**, 1566 (1984).
19. J. V. Michael, D. G. Keil, R. B. Klemm, *J. Phys. Chem.* **83**, 1630 (1985).
20. P.-H. Taylor, M. S. Rahman, M. Arif, B. Dellinger, P. Marshall, *Proc. Comb. Inst.* **26**, 497 (1996).
21. R. Atkinson, *J. Phys. Chem. Ref. Data* **2**, 61 (1994).
22. J. M. Crowley, V. Sivakumaran, *Phys. Chem. Chem. Phys.* **5**, 106 (2003).
23. J. R. Alvarez-Idaboy, M. Mora-Diez, R. J. Boyd, A. Vivier-Bunge, *J. Am. Chem. Soc.* **123**, 2018 (2001).
24. B. D'Anna *et al.*, *Phys. Chem. Chem. Phys.* **5**, 1790 (2003).
25. E. Spangenberg, S. Kohler, B. Hansmann, U. Wachsmuth, B. Abel, *J. Phys. Chem. A* **108**, 7527 (2004).
26. D. L. Singleton, R. J. Cvetanovic, *J. Am. Chem. Soc.* **98**, 6812 (1976).
27. Materials and Methods are available on Science Online.
28. A. F. Wagner, *Proc. Comb. Inst.* **29**, 1173 (2002).
29. Y. Miller, R. B. Gerber, *J. Am. Chem. Soc.* **128**, 9594 (2006).

30. Support from the Deutsche Forschungsgemeinschaft (DFG) within the Sonderforschungsbereich 357 and the DFG-Graduiertenkolleg 782, as well as the Fonds der Chemischen Industrie, is gratefully acknowledged.

Supporting Online Material

www.sciencemag.org/cgi/content/full/315/5811/497/DC1
Materials and Methods
Figs. S1 and S2
Tables S1 to S3
References

29 August 2006; accepted 4 December 2006
10.1126/science.1134494

Martian Atmospheric Erosion Rates

Stas Barabash,[1]* Andrei Fedorov,[2] Rickard Lundin,[1] Jean-Andre Sauvaud[2]

Mars was once wet but is now dry, and the fate of its ancient carbon dioxide atmosphere is one of the biggest puzzles in martian planetology. We have measured the current loss rate due to the solar wind interaction for different species. $Q(O^+) = 1.6 \cdot 10^{25}$ per second = 4 grams per second (g s^{-1}), $Q(O_2^+) = 1.5 \cdot 10^{25}$ s^{-1} = 8 g s^{-1}, and $Q(CO_2^+) = 8 \cdot 10^{24}$ s^{-1} = 6 g s^{-1} in the energy range of 30 to 30 000 electron volts per charge. These rates can be propagated backward over a period of 3.5 billion years, resulting in the total removal of 0.2 to 4 millibar of carbon dioxide and a few centimeters of water. The escape rate is low, and thus one has to continue searching for water reservoirs and carbon dioxide stores on or beneath the planetary surface and investigate other escape channels.

How is the solar wind erosion of the martian atmosphere related to the history of this planet? The "warm and wet early Mars" model suggests that flowing liquid water caused the surface erosion features, such as out flow channels. The water was sustained in the liquid state because of a much higher atmospheric temperature in the past caused by a strong greenhouse effect. The amount of water needed to produce the observed geomorphologic features is about 600 m to 1 km of the equivalent water layer (*1*). The amount of atmospheric pressure needed to maintain the required greenhouse effect would be a few bars of CO_2 (*2*). The inventory of the present amounts of water and carbon dioxide [the most recent "nondiscovery" of carbonates by Mars Express (*3*)] cannot yet identify any appreciable amounts of these materials comparable with the amount present on ancient Mars, although the presence of the water in the past is unambiguously confirmed by Mars Exploration Rovers (*4*). What happened to the martian water and carbon dioxide? Apart from catastrophic removal of the ancient atmosphere by an impact at the end of the Noachian and still-to-be-discovered hidden reservoirs, the solar wind erosion is a plausible idea to explain the absence of notable amounts of water and carbon dioxide on Mars today.

When the solar wind encounters a non-magnetized atmospheric planet, a void of the solar wind is formed. The void created by the magnetic field resulting from the currents induced in the ionosphere is called an induced magnetosphere (*5*). It is separated from the solar wind by an induced magnetosphere boundary. Previous investigations (*6*) based on the magnetic field measurements revealed in the same region a boundary termed the magnetic-pile-up boundary (MPB). The identity of these two boundaries is still to be confirmed. The void is filled by escaping or accelerated ions, which are the ions from the martian atmosphere with energy exceeding the escape energy (2.1 eV for O^+). At least two processes of the acceleration are established. Those are the pick-up process (*7*) and acceleration resulting from charge separation due to the electric field (*8*). Other mechanisms are probably also active. Carlsson *et al.* (*9*) have established the mass composition of the escaping plasma. They found that the flux ratios of O_2^+/O^+ and CO_2^+/O^+ are 0.9 and 0.2, respectively. Apart from the escape due to the accelerated ions, the martian atmosphere erodes due to thermal plasma removal, sputtering, and loss of fast atoms (mostly oxygen) resulting from the exogenic dissociative recombination.

This study reports the escape rates of ions accelerated to energies in the range of 30 to 30,000 eV per charge. The earlier measurements of the escape rate in the similar energy range were attempted by the Phobos-2 mission. The obtained O^+ escape rates were $3 \cdot 10^{25}$ s^{-1} (*10*) and $\leq 10^{24}$ s^{-1} (*11*). The rate in (*10*) is in the energy range of 0.5 to 24,000 eV (the lower limit is uncertain because of the absence of the spacecraft potential control).

The total escape rates reported here are based on the measurements by the ion mass analyzer (IMA) of ASPERA-3 (Analyzer of Space Plasmas and Energetic Atoms), an instrument onboard the Mars Express mission (*12*, *13*). The IMA does not resolve directly O^+, O_2^+, CO^+, and CO_2^+, but the mass composition can be obtained by fitting of the wide mass peak by Gaussian peaks corresponding to the individual masses. The position of the peaks as a function of energy and mass, as well as their width, were obtained in laboratory and in-flight calibrations (*9*). The technique works reliably except for CO^+, which cannot be separated from O_2^+. However, the ionospheric models (*14*) predict the CO^+ density to be at least a factor of 100 lower than that of O_2^+ at 300-km height, where the ionosphere starts to interact with the solar wind (*5*). We thus assume that the whole flux associated with the O_2^+/CO^+ peak is attributed to molecular oxygen. The observational period in question is from 1 May 2004 to 30 May 2006, which corresponds to approximately one martian year. The spatial coverage is regarded as dense and statistically sufficient (supporting online text).

The total escape rate is calculated by mapping the planetary ion flux distribution in the plane perpendicular to the Sun-planet line. The ion distribution function measured for three ions, O^+, O_2^+, and CO_2^+, along the spacecraft trajectory is integrated over energy and solid angle. The obtained integral flux (cm $^{-2}$ s^{-1}) is assigned to the orbit interval corresponding to 192-s IMA accumulation time in the frame of reference related to the interplanetary electric field. In this Cartesian coordinate system, MSE (Mars Sun Electric field), centered at Mars, the x axis points toward the Sun, z coaligns with the interplanetary electric field plane, and y completes the right-hand system. The direction of the electric field, E, is calculated from the Mars Global Surveyor measurements (*15*). As shown most recently by (*15*), the ion-escape fluxes are organized by the E-field due to specific topology of the magnetic field in the wake region (where main variations of the magnetic field lie in the plane perpendicular to E) and due to finite gyroradius of the planetary ions comparable with the planetary size. The planetary ions fill the whole downtail region inside the MPB up to

[1]Swedish Institute of Space Physics, Box 812, 98128 Kiruna, Sweden. [2]Centre d'Etude Spatiale des Rayonnements, BP-4346, F-31028 Toulouse, France.

*To whom correspondence should be addressed. E-mail: stas@irf.se

the $X_{MSE} < -4$ (Fig. 1). The flux distribution correlates well with the E-field direction (Figs. 1 and 2). The escape takes place predominantly through the plasma sheet and adjacent region inside the MPB with the maximum escape rate deep inside the eclipse. The escape area is rather limited and is approximately $2R_M \times 2R_M = 4R_M^2$, where R_M is the radius of Mars (Fig. 2). It is worth noting that although the maximum averaged flux in the plasma sheet region is about 5×10^6 cm^{-2} s^{-1}, the instant flux can reach 5×10^7 cm^{-2} s^{-1}, which corresponds to a planetary ion number density of 20 cm^{-3}. Integrating the maps shown in Fig. 2 over the area, we obtain the total averaged escape rates for three species

$$Q(O^+) = 1.6 \times 10^{23}\ s^{-1} \text{ or } 4\ g\ s^{-1}\ (135\ \text{ton year}^{-1})$$
$$Q(O_2^+) = 1.5 \times 10^{23}\ s^{-1} \text{ or } 8\ g\ s^{-1}\ (250\ \text{ton year}^{-1})$$
$$Q(CO_2^+) = 8 \times 10^{22}\ s^{-1} \text{ or } 6\ g\ s^{-1}\ (185\ \text{ton year}^{-1})$$

The ratios of the total escape rates relative to oxygen are $Q(O_2^+)/Q(O^+) = 0.9$ and $Q(CO_2^+)/Q(O^+) = 0.5$. The main constituents of the escaping plasma are O_2^+ and O^+ with a small admixture of CO_2^+. Although the ratio $Q(O_2^+)/Q(O^+)$ is in agreement with the ratio reported by (9), $Q(CO_2^+)/Q(O^+)$ is a factor of 2.5 higher. This is related to a less accurate mass separation (only between O_2^+ and CO_2^+) performed automatically, whereas in (9) it was made manually. The numbers obtained are almost a factor of 100 lower than those from Phobos-2. The current escape is extremely weak.

The occurrence per spatial bin is high [at least five samples per ZY bin (Fig. 2)], and thus the statistical uncertainty related to spatial sampling is considered low. The uncertainty factors related to the instrument performance and assumptions are (i) not full coverage over solid angle, (ii) no mass separation between O_2^+ and CO, (iii) not full mass separation between O_2^+ and CO_2^+, (iv) deviation of the flux direction from the X axis, and (v) uncertainties in the geometrical factor for low energies (<300 eV). The overall uncertainties in the measured escape rates do not exceed 50% (supporting online text), which is considered low in the context of such studies.

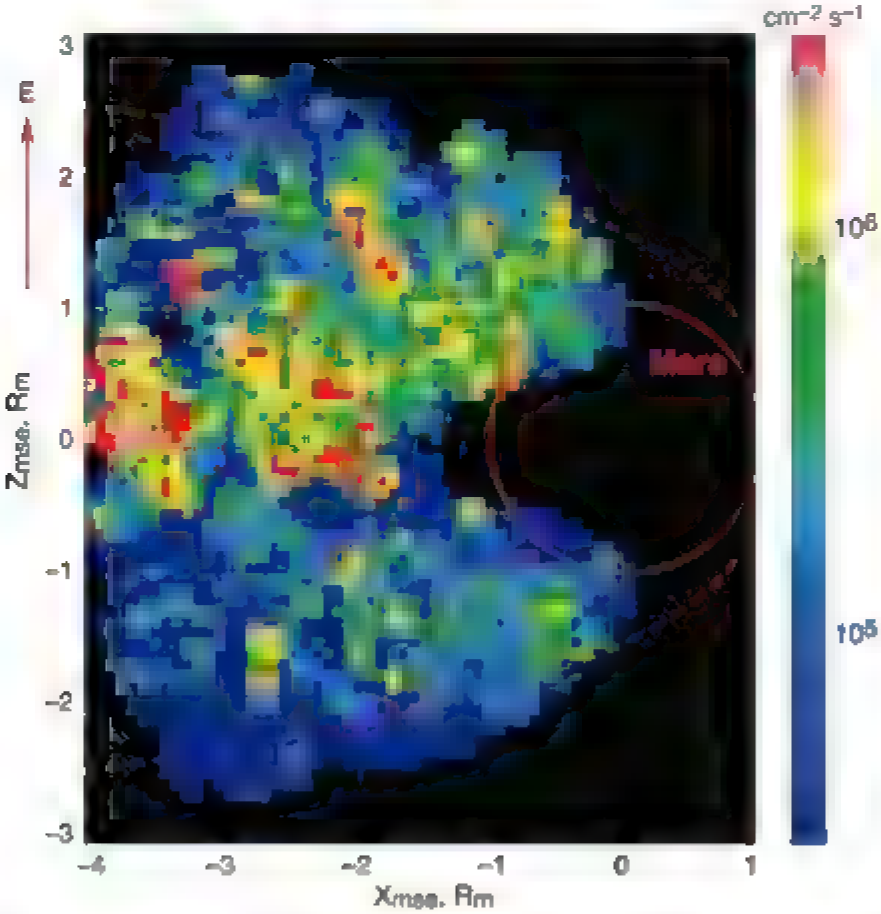

Fig. 1. The integral fluxes (cm^{-2} s^{-1}) for all three ions (O^+, O_2^+, CO_2^+) together averaged over the range $-0.8R_M < Y < 0.8R_M$ in the ZX plane of the E-related coordinate system (MSE). For reference, also shown are Mars (red circle), the eclipse region, and the MPB (red dashed line) as given by the model of (19). The white dashed lines show approximate streamlines used for averaging to get maps in the ZY plane. The slope of the streamlines is a simple linear interpolation between the slope of the MPB and the horizontal edge of the eclipse. The vertical red dashed line displays the position of the mapping plane.

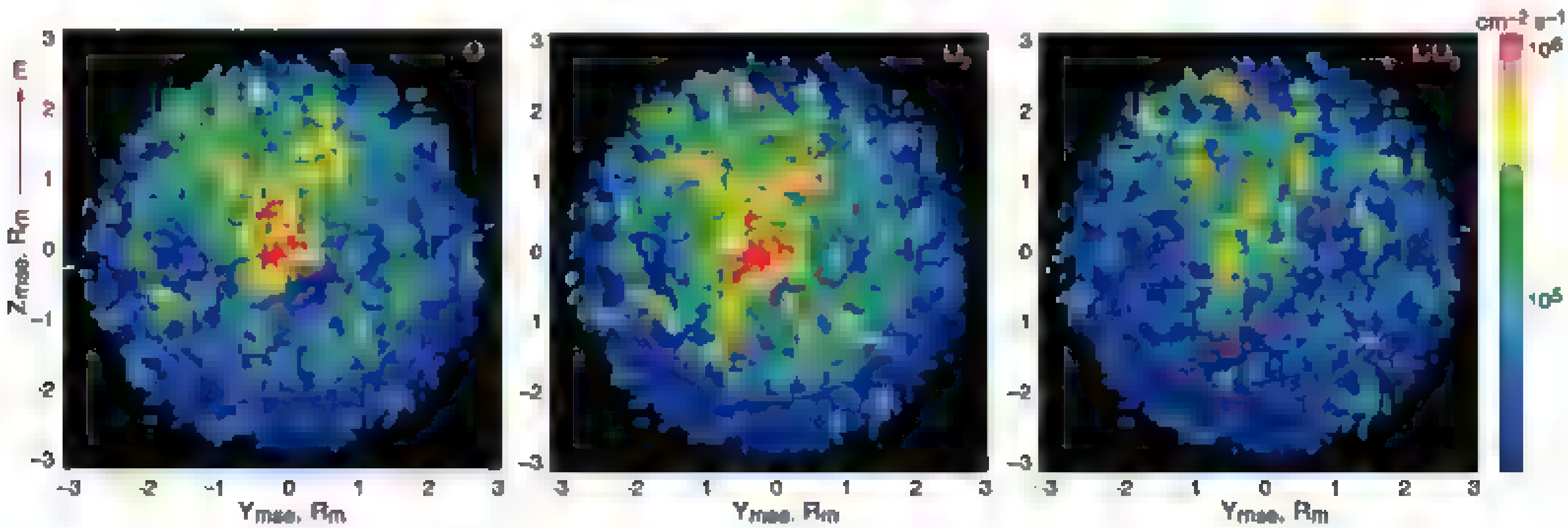

Fig. 2. ZY maps of the integral fluxes (cm^{-2} s^{-1}) of O^+ (**left**), O_2^+ (**middle**), and CO_2^+ (**right**). The fluxes are averaged over streamlines outside the eclipse and along the X_{MSE} direction inside the eclipse (Fig. 1). The average flux distribution is mapped onto the plane $X_{MSE} = -2R_M$ and collected in the $0.08R_M \times 0.08R_M$ pixel array. For the final distribution, only pixels that have been sampled at least five times were taken into account. All bins with fewer crossings were disregarded. For reference, we also show the Mars limb, the MPB cross section at the distance $x = -2R_M$. The direction of the interplanetary electric field is shown by the red vector.

Propagating the measured rates backward in time one can estimate the total amount of carbon dioxide and water $\Delta M(CO_2)$ and $\Delta M(H_2O)$, lost through this particular channel over 3.5 gigayears (Gy) (supporting online text)

$\Delta M(CO_2) \approx 0.2$ – 4 mbar over 3.5 Gy
$\Delta M(H_2O) <$ few cm over 3.5 Gy

Using a hybrid code, Modolo *et al.* (*16*) calculated the escape rates for O^+ and O_2^+ for different solar conditions. The calculated total escape rate for the heavy ions (O^+ and O_2^+) is 5.7×10^{23} s^{-1}, compared to 3.1×10^{23} s^{-1} in this study; i.e., the calculated and measured rates are in very good agreement. Also, the measured escape rates are in very good agreement with MHD (magnetohydrodynamics) simulations by (*17*). They provide the rates $Q(O^+) = 2.5 \times 10^{25}$ s^{-1}, $Q(O_2^+) = 2.9 \times 10^{25}$ s^{-1}, $Q(CO_2^+) = 3.1 \times 10^{22}$ s^{-1} for the solar maximum conditions. As can be seen even mass composition is quite well reproduced.

Because the calculated escape rates are in good agreement with the measured ones at the solar maximum conditions, we can thus rely on the calculated factor of the escape increase for the solar maximum conditions. Modolo *et al.* (*16*) predicted the factor to be 4.56 for the O^+ escape-rate increase, and Ma *et al.* (*17*) predicted the same factor to be 4.58. Scaling the measured rates on this factor brings the total escaped amount of carbon dioxide to 0.8 to 4.3 mbar, and the upper limits for water to 4 to 70 cm. Thus, we conclude that the solar-activity variations cannot increase the estimated total escape on a factor of 100 needed for evolutionary relevant numbers.

The estimated total losses of carbon dioxide and water are much lower than the few hundred meters of H_2O and 1 to 5 bar of CO_2 required for the "wet and warm early Mars" model. Therefore, either other escape channels were or are operational, e.g., impact atmospheric removal, photochemical or cold plasma bulk escape, or water and carbon dioxide are stored in nonidentified reservoirs.

We emphasize that this study considers only one channel for the escape to space. The determination of the escape rates in the form of cold plasma clouds (bulk escape) or via sputtering and photochemical reactions is beyond the scope of the ASPERA-3 experiment capabilities. To compare the measured escape rates with the other escape channels, we determined logarithmic-averaged oxygen escape rates over all available models given in the review (*18*). The photochemical O^+ escape rates are estimated to be 2×10^{25} s^{-1} on average; the sputtering, 7×10^{23} s^{-1}; and the bulk cold plasma escape, 1×10^{26} s^{-1} (Phobos-2 database (*18*)). As can be seen, at least in simulations, estimated photochemical or cold plasma escape rates are substantially higher than the reported numbers. Precise measurements of the cold plasma, photochemical, and sputtering escape rates must await future missions.

References and Notes

1. C. P. McKay, C. R. Stoker, *Rev. Geophys.* **27**, 189 (1989).
2. J. F. Kasting, *Icarus* **94**, 1 (1991).
3. J.-P. Bibring *et al.*, *Science* **307**, 1576 (2005).
4. S. W. Squyres *et al.*, *Science* **306**, 1709 (2004).
5. R. Lundin *et al.*, *Science* **305**, 1933 (2004).
6. M. H. Acuña *et al.*, *Science* **279**, 1676 (1998).
7. E. Dubinin *et al.*, *Icarus* **182**, 343 (2006).
8. E. Dubinin, R. Lundin, O. Norberg, N. Pissarenko, *J. Geophys. Res.* **98**, 3991 (1993).
9. E. Carlsson *et al.*, *Icarus* **182**, 320 (2006).
10. R. Lundin *et al.*, *Geophys. Res. Lett.* **17**, 873 (1990).
11. M. Verigin *et al.*, *Planet. Space Sci.* **39**, 131 (1991).
12. S. Barabash *et al.*, in *Mars Express: The Scientific Payload*, A. Wilson, Ed. (ESA Special Publication SP 1240, 2004), pp. 121–139.
13. A short summary of the IMA sensor is available as supporting material on *Science* Online.
14. J. L. Fox, *Geophys. Res. Lett.* **24**, 2901 (1997).
15. A. Fedorov *et al.*, *Icarus* **182**, 329 (2006).
16. R. Modolo, G. M. Chanteur, E. Dubinin, A. P. Matthews, *Ann. Geophysicae* **23**, 433 (2005).
17. Y. Ma, A. F. Nagy, I. V. Sokolov, K. C. Hansen, *J. Geophys. Res.* **109**, A07211 (2004).
18. H. Lammer *et al.*, *Icarus* **165**, 9 (2003).
19. E. Kallio, *J. Geophys. Res.* **101**, 11133 (1996).

20. The ASPERA-3 experiment on the ESA Mars Express is a joint effort of 15 laboratories from 10 countries, all supported by their national agencies. We thank all involved agencies and the department and institutes hosting the efforts. We particularly thank the Swedish National Space Board for supporting the main Principle Investigator institute, and CNES for supporting the IMA calibrations at Centre d'Etude Spatiale des Rayonnements, Toulouse, France. We are indebted to members of the European Space Agency (ESA) for their courage to embark on a mission like Mars Express and for rapidly developing a space probe to Mars, the first ESA mission to the red planet. The interplanetary electric field pulses were based on the Mars Global Surveyor MAG/ER (Magnetometer/Electron Reflectometer) measurements (Principal Investigator M. Acuna, NASA Goddard Space Flight Center, Greenbelt, MD, USA).

Supporting Online Material

www.sciencemag.org/cgi/content/full/315/5811/503/DC1
Materials and Methods
Figs. S1 and S2
References and Notes

25 August 2006; accepted 4 December 2006
10.1126/science.1134358

Slow Earthquakes Coincident with Episodic Tremors and Slow Slip Events

Yoshihiro Ito,* Kazushige Obara, Katsuhiko Shiomi, Shutaro Sekine, Hitoshi Hirose

We report on the very-low-frequency earthquakes occurring in the transition zone of the subducting plate interface along the Nankai subduction zone in southwest Japan. Seismic waves generated by very-low-frequency earthquakes with seismic moment magnitudes of 3.1 to 3.5 predominantly show a long period of about 20 seconds. The seismicity of very-low-frequency earthquakes accompanies and migrates with the activity of deep low-frequency tremors and slow slip events. The coincidence of these three phenomena improves the detection and characterization of slow earthquakes, which are thought to increase the stress on updip megathrust earthquake rupture zones.

Nonvolcanic deep low-frequency (*1*) tremors and slow slip events (*2*–*4*) occur simultaneously in the transition zone (*5*) from locked to aseismic slips at the downdip portion of the Nankai subduction zone in southwest Japan. Megathrust earthquakes with seismic moment magnitudes exceeding 8 occur in this region periodically on ~100-year time scales (*6*). There is also a large gap in the source time properties of two recently discovered mechanisms of relaxation of accumulated stress in the transition zone. Deep low-frequency tremors (*1*) predominantly show frequencies near 0.5 s, suggesting that the characteristic time scale of the rupture duration is on the order of 1 s, whereas slow slip events (*2*–*4*) do not radiate any seismic waves and cause crustal deformations that continue for 2 to 5 days.

Deep low-frequency tremors and slow slip events in Japan have been detected by the seismic network of the National Research Institute for Earth Science and Disaster Prevention (NIED), which comprises a network of ~750 high-sensitivity seismograph network (Hi-net) and 73 broadband seismograph network (F-net) stations (*7*). The Hi-net stations provide a high-level detectability for deep low-frequency tremors with small amplitude signals (*1*). The Hi-net and F-net stations also detect very-low-frequency (VLF) earthquakes within the accretionary prism at the updip portion of the Nankai subduction zone (*8*–*10*).

A two-component high-sensitivity horizontal accelerometer with a wide frequency response range from 5 Hz to direct-current component (Hi-net TILT) is installed at each Hi-net station (*11*). The accelerometers function as tiltmeters.

National Research Institute for Earth Science and Disaster Prevention, 3-1 Tennodai, Tsukuba 305-0006, Japan.

*To whom correspondence should be addressed. E-mail: yito@bosai.go.jp

they are useful in analyzing short-term slow slip events (*2*–*4*). Hi-net TILT and F-net are also useful in calculating the moment tensor solution of local earthquakes (*5*).

To understand the stress-relaxation process in the transition zone, it is important to identify all seismic and geodetic phenomena. At present, a large gap exists between the characteristic time scales for the previously identified deep low-frequency tremors and those for slow slip events. We examined the Hi-net and F-net data with the use of various bandpass filters within an overall range of 1 to 0.005 Hz in an effort to detect unidentified long-period seismic signals radiated from the transition zone. With a bandpass filter of 0.02 to 0.05 Hz, we succeed in detecting distinct, anomalous VLF signals radiated from the transition zone near the source region of deep low-frequency tremors. These signals, observed at several Hi-net TILT and F-net stations, are best identified on the radial and vertical components. The VLF signals (Fig. 1) are accompanied by wave trains of deep low-frequency tremors. The apparent velocity estimated from their arrival times at stations with an epicentral distance exceeding 50 km is ~6 km/s, which overlaps with *P*-wave velocities in this region. This value suggests that the observed VLF signals constitute body waves.

To detect VLF seismic signals and estimate their hypocenters systematically, we adopted the grid moment tensor inversion (GMT) approach (*13*–*15*), in which we assume that the target earthquake always occurs at a grid point that is arranged with respect to both space and time. Using this approach and continuous seismograms obtained from F-net, we calculated the point source moment tensor solution at 0.1° horizontal, 3 km depth, and 1 s interval grid-point spacing (fig. S1). First, we removed time periods that are potentially contaminated with seismic waves from teleseismic and ordinary regional earthquakes from all the GMT solutions. Next, using the F-net and Hi-net TILT data, we applied the centroid moment tensor inversion (CMT) approach (*12*, *15*), in which hypocenters and fault mechanisms of the target earthquakes are calculated simultaneously, to the remaining GMT solutions.

We detected many VLF seismic events coincident with the deep low-frequency tremors and slow slip events that occurred from January to May 2006 (table S1). These VLF events with seismic moment magnitudes of 3.1 to 3.5 are located on the belt-like distribution of deep low-frequency tremors along the strike of the subducting Philippine Sea plate (Fig. 2). Local ordinary earthquakes with the same seismic moment magnitude as these VLF events are not listed in any seismic catalog.

We compared a waveform of the VLF event with that of an ordinary earthquake at the F-net station UMI (fig. S2). Both events have the same moment magnitude of 3.4 and almost identical epicentral distance and depth. Both events have low-frequency components with similar amplitudes in the range of 0.02 to 0.05 Hz. However, the signal of a VLF event does not constitute any high-frequency components in the range of 2 to 8 Hz. This result suggests another type of slow earthquake, which we call a VLF earthquake. Earthquakes with similar discrepancies between amplitudes measured at low and high frequencies are observed on transform faults and are identified as slow earthquakes (*16*).

The observed waveforms of VLF earthquakes are explained by thrust faulting (Fig. 3 and fig. S3). The epicenters of VLF earthquakes are confined to a narrow band bound by the surface projection of 30- to 35-km depth contours of the plate interface (Fig. 2). Moreover, their epicenters clearly overlap with the seismicity of deep low-frequency tremors. The depths of the plate interface are based on the result of the depth variation of the oceanic Mohorovičić discontinuity (the crust-mantle boundary) calculated by receiver function analyses (*17*). The thickness of the oceanic crust in this region is assumed to be ~5 km according to an active-source seismic experiment (*18*). The focal depths of VLF earthquakes are distributed across slightly wider ranges (fig. S4); the averaged depths and standard deviations are 40 ± 8 km and 35 ± 9 km in the Kii-Tokai and Shikoku regions, respectively. This wide depth range can be attributed to the depth variation with a broad peak of variance reduction calculated by CMTI (fig. S5), which suggests that the focal depth is not well constrained. However, these focal depths are roughly consistent with the subducting

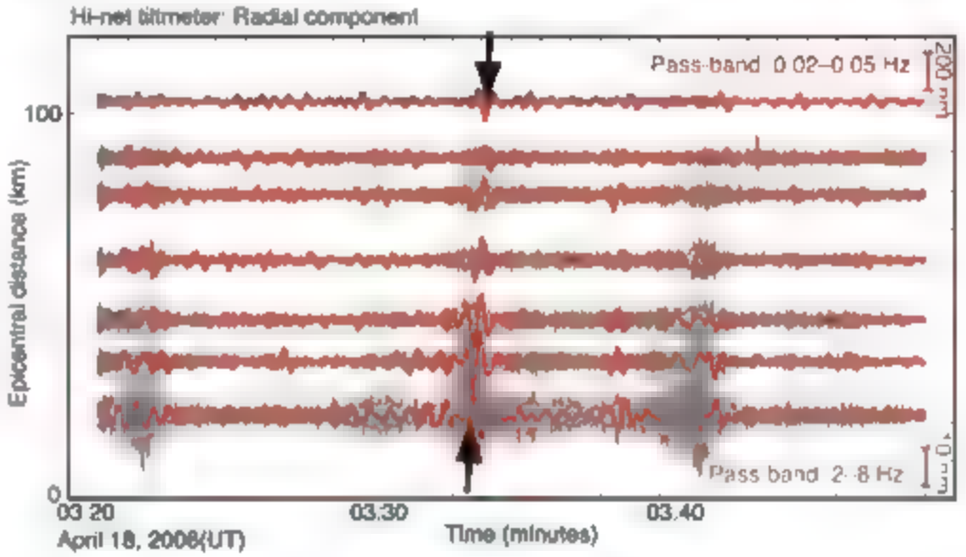

Fig. 1. Sample seismograms of a VLF earthquake at selected sites. Radial components at seven Hi-net TILT stations are shown. The observed waveforms are arranged in epicentral distance order from an estimated source location. The red and black traces represent the observed waveforms filtered for bands of 0.02 to 0.05 Hz and 2 to 8 Hz, respectively. The vertical bars on the right indicate the displacement amplitudes.

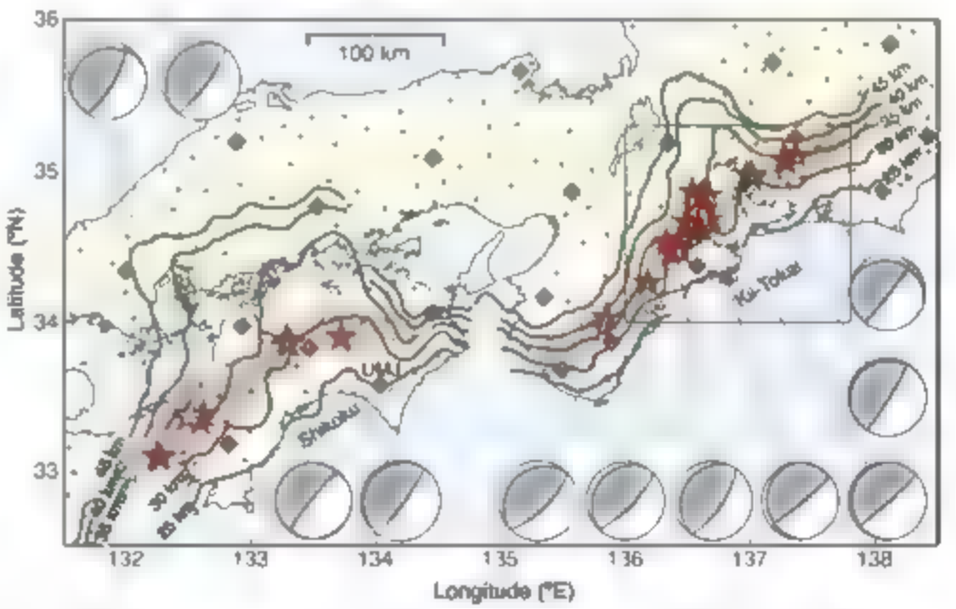

Fig. 2. VLF earthquakes (stars), deep low-frequency tremors (circles), station distribution, and moment tensor solutions of VLF earthquakes. The plus and diamond symbols represent the NIED Hi-net and F-net stations, respectively. The depth contour indicates the upper surface of the Philippine Sea plate. The rectangle indicates the area shown in Fig. 3. The yellow triangle indicates the epicenter of an ordinary earthquake with a moment magnitude of 3.4.

plate interface. The dip angles of the nodal planes dipping landward are consistent with the slope of the Philippine Sea plate; the averaged dip angles and standard deviations are 14° ± 8° in the Kii-Tokai region and 15° ± 9° in the Shikoku region. These values imply that VLF earthquakes may occur on the subducting plate interface.

The simultaneous occurrence of deep low-frequency tremors and slow slip events has been observed in southwest Japan (*2*). These activities are coincident both spatially and temporally, and they exhibit a clear migration pattern when the activity of deep low-frequency tremors is high (*4*). A clear northeastward migration of the seismicity of deep low-frequency tremors and geodetic deformations by a slow slip event were observed in the Kii-Tokai region in January 2006 (*19*). Concurrently, an identical migration of the seismicity of VLF earthquakes was observed in the same region (Fig. 3). The migration pattern of VLF earthquake seismicity is consistent with both the deep low-frequency tremor activity and the observation of the geodetic deformations. This observation indicates a close relationship between slow slip events and the activity of both VLF earthquakes and deep low-frequency tremors, thereby reflecting the stress accumulation and relaxation process in the transition zone.

The excitations of wave trains caused by VLF earthquakes appear to always overlap with the peak amplitude of wave trains caused by deep low-frequency tremors (Fig. 1). However, it should be noted that deep low-frequency tremors occur without the excitation of VLF earthquakes. This result suggests that the VLF event and the deep low-frequency tremors are two distinct phenomena.

Considering the predominance of VLF components of ~20 s (Fig. 1 and fig. S2), their response to the rupture process may correspond to a slow earthquake with a characteristic time scale of rupture duration on the order of 10 s. This rupture duration is longer than that of ordinary earthquakes and also exceeds the duration proposed for deep low-frequency tremors, ~1 s (*1*). However, this 10-s duration is obviously shorter than the 2- to 5-day duration of regionally observed slow slip events (*2*–*4*). Similar VLF earthquakes that occur within the accretionary prism are thought to represent slow earthquakes with low stress drops, low rupture velocities, and low slip velocities on the fault plane with high pore-fluid pressure (*10*). These observations suggest that three types of slow earthquakes—deep low-frequency tremors, VLF earthquakes, and slow slip events—occur simultaneously in the transition zone of the subducting plate interface.

Tomography studies that image seismic velocity structure show that a high Poisson's ratio exists around the source region of the deep low-frequency tremor (*20*). A recent precise study in the Nankai subduction zone proposes a linear distribution of low-frequency earthquakes, similar to the classification of deep low-frequency tremors with slightly obvious *P* and *S* phases, at 35 to 40 km around the plate interface and corresponding to a zone of high Poisson's ratio in the vicinity of the transition zone. This suggests the following two interpretations: (i) generation of low-frequency earthquakes by shear slip, and (ii) formation of a region of high pore-fluid pressure due to the fluid released from the dehydration of the subducted oceanic crust (*21*). Considering that three types of slow earthquakes including low-frequency earthquakes occur in the transition zone (Fig. 4), the existence of a zone of high pore-fluid pressure may play an important role in the occurrence of these slow earthquakes. One possible scenario of the stress-relaxation process in the transition zone is based on an asperity model (*22*, *23*), in which stronger coupled patches of VLF earthquakes are surrounded by aseismic slow slip regions. The fault shear strength of the slow slip segment is weaker than that of the asperity of a megathrust earthquake because the high pore-fluid pressure causes a reduction in the normal stress on the plate interface. If the shear stress loaded by the subducting plate reaches the yield stress of the bulk for the slow slip segment, the slow slip event starts in the transition zone. When the shear stress increases on the patches of VLF earthquakes due to the occurrence of the slow slip event, these patches eventually rupture after the cumulative stress reaches the yield stress reduced by the high pore-fluid pressure. This rupture results in a low stress drop and possibly induces the behavior of a VLF earthquake. Many new microcracks, with shear strength weaker than that of ordinary microearthquakes and source size smaller than that of VLF earthquakes, may rupture in the transition zone as a result of the local stress change around the plate interface, induced by the

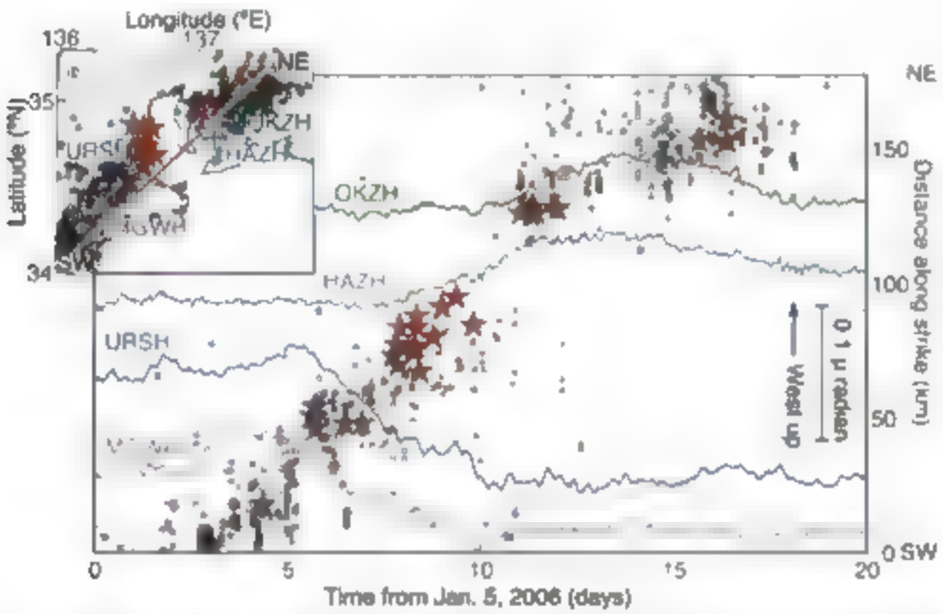

Fig. 3. Migration of seismicity of both VLF earthquakes and deep low-frequency tremors and tilt change at four Hi-net stations (OKZH, HAZH, URSH, and MGWH) between 5 January and 25 January 2006. The temporal variation of VLF earthquakes (red stars) and deep low-frequency tremors (circles) is shown along the southwest-northeast line in the inset representing the strike of the subducting plate interface. The four colored lines are records of the east-west component of the tilt changes observed at Hi-net stations. The inset shows the distribution of the VLF earthquakes and deep low-frequency tremors during the same period, as well as the Hi-net TILT station locations (plus symbols).

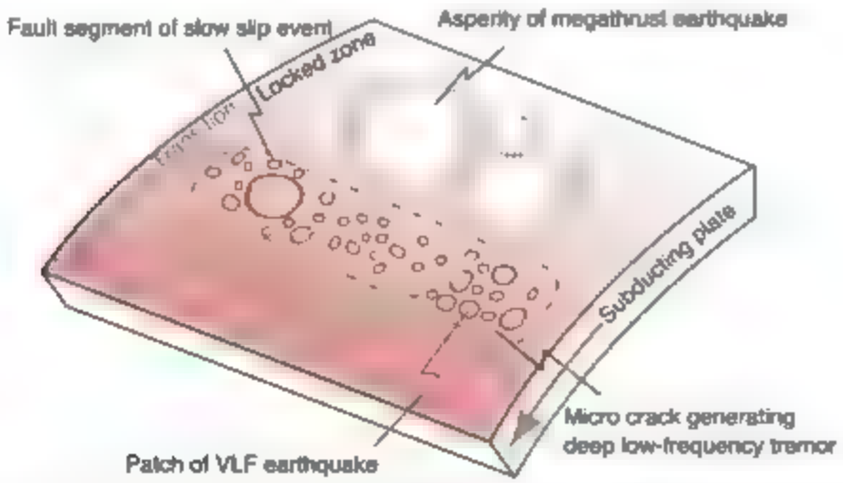

Fig. 4. Schematic of the seismic source distribution for VLF earthquakes, deep low-frequency tremors, and slow slip events at the downdip portion of the subduction zone in southwest Japan.

migration slow slip. The superposition of a seismic signal from each small failure yields the observed sequence of deep low-frequency tremors. Low-frequency tremors in the Cascadia subduction zone have an extensive depth distribution from 10 to 40 km, where there are strong seismic reflectors, suggesting the existence of fluid (24). These tremors also may be caused by the stress change outside the transition zone due to a slow slip event, because a similar migration of the tremor seismicity and slow slip is observed in the Cascadia subduction zone (25).

The monitoring of not only deep low-frequency tremors but also VLF earthquakes may be useful to assess the stress on the rupture zone of a megathrust earthquake. This is because the shear stress on the asperity of the megathrust earthquake may increase as a result of slow earthquakes of all sizes occurring at the downdip portion of the subduction zone. VLF earthquakes are also useful indicators for estimating the stress condition of the rupture zone of an anticipated megathrust earthquake.

References and Notes

1. K. Obara, *Science* **296**, 1679 (2002).
2. K. Obara, H. Hirose, F. Yamamizu, K. Kasahara, *Geophys. Res. Lett.* **31**, L10602, doi:10.1029/2004GL020848 (2004).
3. H. Hirose, K. Obara, *Earth Planets Space* **57**, 961 (2005).
4. K. Obara, H. Hirose, *Tectonophysics* **417**, 33 (2006).
5. R. D. Hyndman, K. Wang, M. Yamano, *J. Geophys. Res.* **100**, 15373 (1995).
6. M. Ando, *Tectonophysics* **25**, 69 (1975).
7. Y. Ohzeki *et al.*, *Earth Planets Space* **56**, xx (2004).
8. K. Obara, Y. Ito, *Earth Planets Space* **57**, 321 (2005).
9. Y. Ito, K. Obara, *Geophys. Res. Lett.* **33**, L10311, doi:10.1029/2005GL025270 (2006).
10. Y. Ito, K. Obara, *Geophys. Res. Lett.* **33**, L02311, doi:10.1029/2006GL025883 (2006).
11. K. Obara *et al.*, *Rev. Sci. Instrum.* **76**, 10.1063/1.1854197 (2005).
12. Y. Ito *et al.*, *Geophys. J. Int.* **167**, 1317 (2006).
13. H. Kawakatsu, *Bull. Earthq. Res. Inst.* **73**, 267 (1998).
14. F. Tajima, C. Megnin, D. S. Dreger, B. Romanowicz, *Bull. Seismol. Soc. Am.* **92**, 739 (2002).
15. See supporting material on *Science* Online.
16. E. A. Okal, L. M. Stewart, *Earth Planet. Sci. Lett.* **57**, 75 (1982).
17. K. Shiomi, H. Sato, K. Obara, M. Ohtake, *J. Geophys. Res.* **109**, B10307, doi:10.1029/2003JB002774 (2004).
18. S. Kodaira *et al.*, *Science* **304**, 1295 (2004).
19. S. Sekine, K. Obara, H. Hirose, paper presented at the Japan Geoscience Union Meeting 2006, Chiba, Japan, 14 May 2006.
20. K. Shiomi, K. Obara, H. Sato, *Tectonophysics* **420**, 205 (2006).
21. D. R. Shelly, G. C. Beroza, S. Ide, S. Nakamula, *Nature* **442**, 188 (2006).
22. T. Lay, H. Kanamori, in *Earthquake Prediction*, D. Simpson, P. Richards, Eds. (American Geophysical Union, Washington, DC, 1981), pp. 579–592.
23. R. L. Wesson, W. L. Ellsworth, *J. Geophys. Res.* **78**, 8527 (1973).
24. H. Kao *et al.*, *Nature* **436**, 841 (2005).
25. G. Rogers, H. Dragert, *Science* **300**, 1942 (2003); published online 8 May 2003 (10.1126/science.1084783).

26. We thank T. Maeda, A. Hutko, and J. Rokosky for their extensive comments and discussion.

Supporting Online Material

www.sciencemag.org/cgi/content/full/1134454/DC1
Materials and Methods
Figs. S1 to S5
Table S1
References

28 August 2006; accepted 3 November 2006
Published online 30 November 2006
10.1126/science.1134454
Include this information when citing this paper.

Strong Relationship Between DMS and the Solar Radiation Dose over the Global Surface Ocean

Sergio M. Vallina and Rafel Simó

Marine biogenic dimethylsulfide (DMS) is the main natural source of tropospheric sulfur which may play a key role in cloud formation and albedo over the remote ocean. Through a global data analysis, we found that DMS concentrations are highly positively correlated with the solar radiation dose in the upper mixed layer of the open ocean, irrespective of latitude, plankton biomass, or temperature. This is a necessary condition for the feasibility of a negative feedback in which light attenuating DMS emissions are in turn driven by the light dose received by the pelagic ecosystem.

Oceanic biota influence climate in the long term by shaping the biogeochemical cycles of elements essential for Earth-system functioning (such as C, O, N, P, Si, and S) (*1*–*3*) and in the short term by exchanging climate-active gases with the atmosphere (greenhouse gases, oxidant and light scavengers, and free-radical and aerosol precursors) (*4*–*8*). One of these gases is dimethylsulfide (DMS), which represents the largest natural source of atmospheric sulfur and a major precursor of hygroscopic (i.e., cloud-forming) particles in clean air over the remote oceans (*4*, *9*), thereby acting to reduce the amount of solar radiation that crosses the atmosphere and is absorbed by the ocean. A 20-year-old hypothesis (*10*) postulated that marine plankton, cloud albedo, and solar radiation can be connected through DMS production, ventilation, and oxidation in a feedback interaction. whether this feedback would be positive or negative was uncertain.

We wanted to explore whether DMS concentrations are linked to epipelagic ecosystem exposure to solar radiation. A monthly sampling of surface DMS concentrations, as well as biological and physical variables, was conducted during 2003 and part of 2004 at the Blanes Bay Microbial Observatory, located at 41°30′N, 2°48′E in the coastal northwest Mediterranean. We noted that the light exposure of an idealized seawater particle (and its associated dissolved substances and buoyant organisms) depends not only on the surface irradiance and its underwater attenuation but also on the depth of the mixed layer within which the particle is confined. Thus, we estimated the daily-averaged solar radiation received in the upper mixed layer (UML), or UML solar radiation dose (SRD), from measured data of the daily-averaged surface irradiance, the underwater light extinction coefficient, and the mixed layer depth (MLD) (*11*). A linear regression analysis revealed that, during the period examined, the SRD accounted for 94% of the variance of monthly surface DMS concentrations (Fig. 1).

Application of this analysis to a triannual (1992 to 1994) time series of DMS concentrations at Hydrostation S in the Sargasso Sea (*12*) (32°10′N, 64°30′W) produced similar results. Daily surface irradiances measured in Bermuda as well as MLD and extinction coefficients

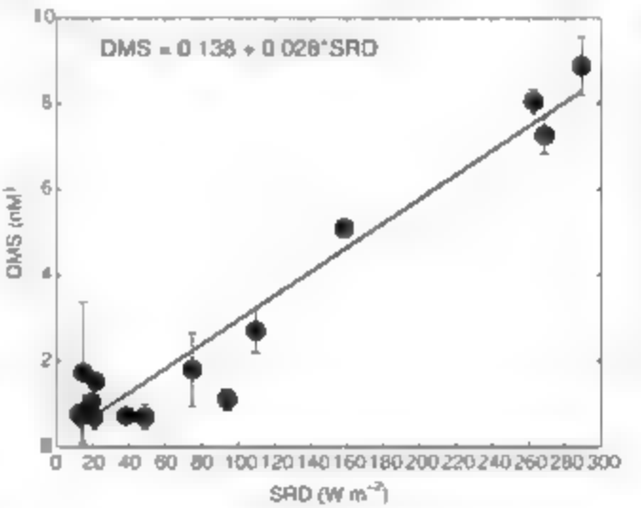

Fig. 1. Linear regression ($n = 15$, $r^2 = 0.94$) of surface DMS concentrations versus SRD in Blanes Bay (coastal northwest Mediterranean). Dots are monthly data during the period from January 2003 to April 2004. Error bars represent standard deviations of two consecutive sampling days each month. A Spearman correlation analysis of the same data gives a significant positive coefficient $\rho = 0.75$ ($P << 0.01$).

Institut de Ciències del Mar (CSIC), Passeig Marítim de la Barceloneta 37-49, 08003 Barcelona, Catalonia, Spain. E-mail: sergio.vallina@icm.csic.es (S.M.V.); rsimo@icm.csic.es (R.S.)

measured at the Bermuda Atlantic Time Series Study station nearby (*11*) were used to estimate daily MLD solar radiation dose on the same days as DMS was measured. The variation in the SRD explained 81% of the variance of monthly surface DMS concentrations (Fig. 2). This is consistent with a recent work (*13*) showing that the biological production and concentration of DMS in the MLD was highly correlated with the ultraviolet radiation (UVR) dose at this same study site.

The original plankton-sulfur-climate hypothesis postulated that a regulatory (negative) feedback would occur if positive changes in sunlight and/or temperature caused increases in primary production and associated changes in DMS, particularly at low latitudes (*10*). However, monthly DMS and chlorophyll a (chl-a) concentrations (one commonly used measure of biomass) were not positively correlated but rather showed opposite patterns in both the coastal Mediterranean ($\rho = -0.51$) and the Sargasso Sea ($\rho = -0.61$) (*13*) sampling sites. This is not a particular case of these two stations. Away from the equatorial region, surface DMS concentrations usually peak in summer. In subtropical and low temperate waters, this summertime DMS coincides with the increase of phytoplankton biomass. This feature has been called the "DMS summer paradox" (*14*). At high latitudes and over areas of the Southern Ocean, on the other hand, the summertime surface DMS maximum co-occurs with a chl-a minimum, and both variables look strongly correlated (*14*). Such a heterogeneous behavior results in very weak global correlations between DMS and chl-a (*15, 16*).

To assess whether global DMS distributions better follow those of solar radiation or sea surface temperature (SST) than those of plankton biomass, we compiled monthly global maps of available DMS concentrations from the Global Surface Seawater (GSS) DMS database (*17*). This database includes about 30,000 individual data points collected from 1972 to 2003. No information about the corresponding in situ MLD, surface irradiances, or light extinction coefficients is available directly from the database. Bover-Montegut *et al.* (*18*) recently constructed a comprehensive climatology of global MLD based on more than 4,000,000 temperature profiles obtained between 1941 and 2002. We made use of this climatology with a modification of the detection criterion (*11*). The daily averaged solar irradiance at the top-of-the-atmosphere was calculated (*19*) and converted into ocean-surface irradiance (I_0) considering a transmission coefficient of 0.5—that is, an atmospheric reduction by a half (*20*). Monthly global maps of SRD were obtained from the aforementioned variables in the same way as for the local studies (*11*). For chl-a concentrations and SST, we used satellite-derived climatologies (*11*). Monthly latitudinal distributions of DMS, chl-a, SST, and SRD show that DMS follows solar radiation dose much more closely than it follows plankton biomass or temperature (Fig. 3).

We divided the surface of the globe into 324 boxes of 10° latitude by 20° longitude. Available DMS measurements and calculated SRD values were averaged for each month and each box. Next, we subdivided the range of SRD values (from 0 to 210 W m^{-2}) into spaced intervals of 14 W m^{-2}, and mean ± standard deviation was calculated for the box-averaged DMS concentrations corresponding to each of the intervals. Data from different latitudes and months were averaged together as long as they had a similar solar radiation dose. The highest 5% of the DMS box means were purposely not taken into account in order to exclude high DMS values associated with eutrophic coastal systems and local blooms of algae that produce very high amounts of dimethylsulfoniopropionate (DMSP), which are well-documented short-term sources of DMS that would have a disproportionately high weight on the averages. This cut-off criterion roughly corresponded to an upper limit of 10 nM (fig. S1). The final number of box-month combinations used was 545, and the total number of GSS DMS data points included was about 26,400 (i.e., nearly 90% of the original data).

Consistent with the local time series, a significant positive correlation was found between averaged surface DMS concentrations and the SRD along the radiation dose range (Fig. 4). Notably, there is a strong similarity between the slope and the intercept of the globally derived linear equation and those obtained in the Sargasso Sea (Fig. 2). Even though the data scatter for the

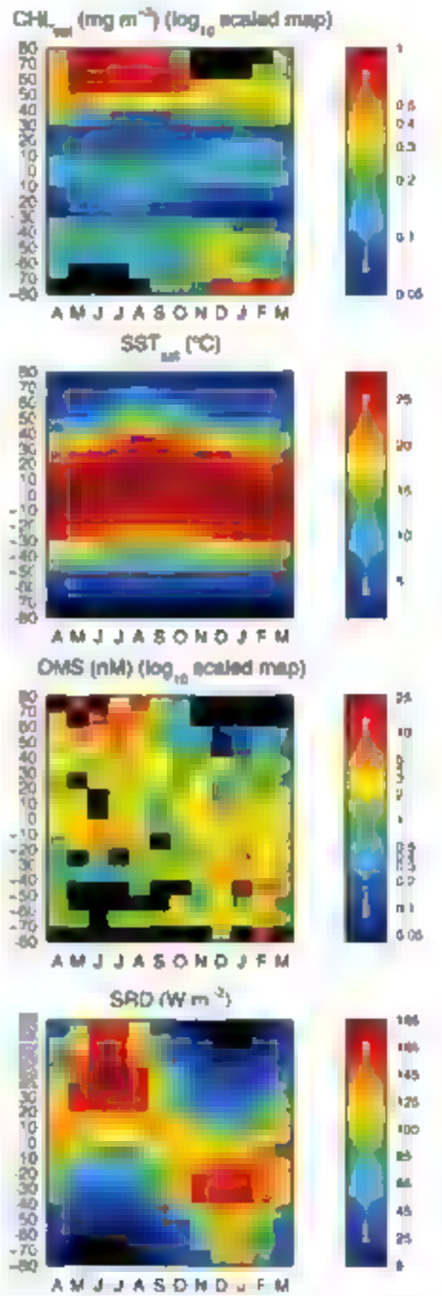

Fig. 3. Month (April through March) by latitude plots of climatological global distributions of satellite-derived chl-a concentrations (CHL_{sat}, Sea-Viewing Wide Field-of-View Sensor, 2002 to 2004), satellite-derived sea surface temperature (SST_{sat}, Climate Diagnostics Center, 1971 to 2000), surface DMS concentrations (GSS DMS database), and the SRD (calculated). All variables are monthly averaged by 10° latitude bands. Spearman coefficients (ρ) for the correlations between the latitude-month distributions of DMS and the other variables are DMS versus CHL_{sat}, 0.08; DMS versus SST_{sat}, 0.16; DMS versus SRD, 0.56 ($n = 155$).

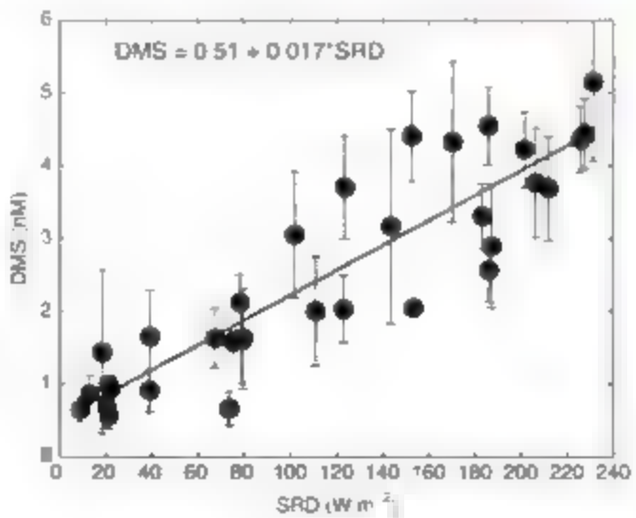

Fig. 2. Linear regression ($n = 33$, $r^2 = 0.81$) of surface DMS concentrations versus the SRD in Hydrostation S (Sargasso Sea). Dots are monthly data during the period from January 1992 to November 1994. Error bars represent standard deviations of multiple sampling days each month. A Spearman correlation analysis of the same data gives a significant positive coefficient $\rho = 0.89$ ($P << 0.01$). DMS data are from (*12*).

global relationship is quite large (shaded areas in Fig. 4), the upper and lower contours of the scatter still show clear proportionality between DMS and the SRD.

Although upper-ocean DMS dynamics have been the object of extensive research, definitive conclusions about the main factors controlling DMS concentrations have remained elusive, and this has prevented giving an unequivocal sign for any feedback link between climate and DMS. Experimental work (*9*, *12*) has unveiled the interaction of multiple biotic and abiotic players (e.g., phytoplankton composition and physiological state, zooplankton grazing, bacterial activity and diversity, and photolysis), and solar radiation (and especially UVR) exerts a substantial but not straightforward influence on many of them (*21*–*23*). A particularly relevant, recent hypothesis suggests that DMS leakage from the algal cell is the by-product of a sulfur-based antioxidant mechanism (*21*). Given that high light (high UVR) doses induce oxidative stress (i.e., DMS release) and inhibit bacterial DMS consumption as well (*23*), DMS may accumulate in seawater. Phytoplankton succession to higher-DMSP producers in summer stratified waters, oxidative stress on these producers, and oxidative damage on DMS consumers may be concurrent reasons why DMS concentrations are higher in high-light conditions.

A recent analysis of the DMS time series in the Sargasso Sea revealed that the temporal DMS variation emerging from such a complex cycle resembles that of the local UVR, and the latter was suggested as the major driving force (*13*). Whether this very same quantitative DMS-UVR relationship would be applicable to most of the global ocean was unknown but unlikely because other local factors such as plankton abundance and community structure would be expected to have a large complementary influence. Nonetheless, a pioneering work by Bates *et al.* (*24*) showed, with the few data available at the time, that the seasonally averaged DMS emission flux covaried with the seasonally averaged surface solar irradiance at different latitudes. More recently, the depth of the UML was seen to have a regulatory influence on DMS production and concentration on a global scale and it was hypothesized that such regulation would partly occur through the effects of the MLD on plankton exposure to solar radiation (*14*, *25*). Using the most comprehensive data set available today, we show that surface DMS concentrations respond positively to the UML solar radiation dose, and this response follows the same proportionality over the global open ocean, irrespective of latitude and the large variability of, for example, temperature and trophic status.

One of the challenges of today's Earth-system science is to elucidate how the biosphere responds to climate in ways that in turn influence climate (*26*), determine their operation time scale, and clarify whether these responses confer stability to the climate system in front of perturbations such as anthropogenic global environmental change. The tight coupling of DMS concentrations to the solar radiation dose that we observed is a necessary condition for the occurrence of a negative feedback between plankton and climate through the influence of the former on the radiative energy budget (*10*). Notably, it also provides a clue on the time scale of such feedback. The solar radiation dose of the surface ocean varies strongly over the seasonal cycle as a consequence of the coupled variation of surface irradiance and the MLD. Our data indicate that it is at this seasonal scale that the epipelagic ecosystems respond to temporal and latitudinal changes in solar radiation by changing the production of light-attenuating volatile sulfur. Exploration of responses at time scales shorter than a month should be carried out with high-resolution measurements of DMS and solar radiation in coherent water masses. Whether this feedback will also operate efficiently at the longer time scale of anthropogenic global warming will depend on induced changes in global cloudiness, aerosol light scattering, and, most important, mixing depths in the ocean.

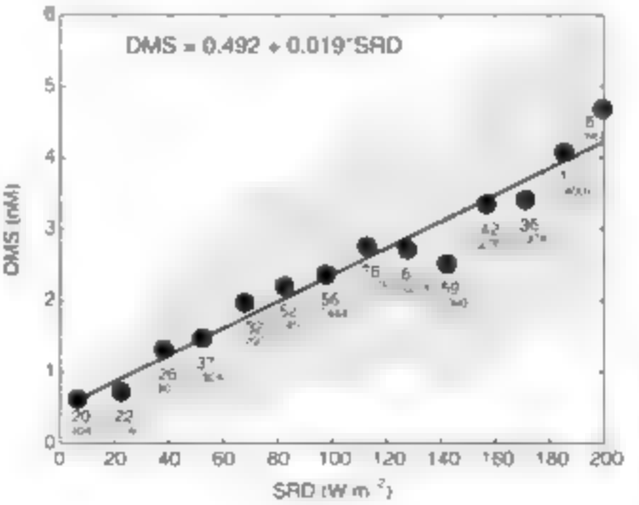

Fig. 4. Linear regression (n = 14, r^2 = 0.95) of surface DMS concentrations versus the SRD in the global open ocean. Dots are averages of 10° by 20° (latitude by longitude) box mean DMS concentrations grouped by intervals of 15 W m^{-2} of SRD. The shaded area represents the standard deviation of the averages. The numbers by the data points indicate the amount of DMS box means used for each average (upper number) and the amount of original data included (number in parentheses). A Spearman correlation analysis of the 545 box means gives a significant positive coefficient ρ = 0.47 ($P \ll 0.01$).

References and Notes

1. P. G. Falkowski, *Nature* **387**, 272 (1997).
2. P. G. Falkowski, R. T. Barber, V. Smetacek, *Science* **281**, 200 (1998).
3. T. M. Lenton, A. J. Watson, *Global Biogeochem. Cycles* **14**, 225 (2000).
4. M. O. Andreae, P. J. Crutzen, *Science* **276**, 1052 (1997).
5. H. Singh *et al.*, *Nature* **410**, 1078 (2001).
6. A. L. Chuck, S. M. Turner, P. S. Liss, *Science* **297**, 1151 (2002).
7. C. D. O'Dowd *et al.*, *Nature* **417**, 632 (2002).
8. A. I. Hirsch *et al.*, *Global Biogeochem. Cycles* **20**, GB1008, 10.1029/2004GB002443 (2006).
9. R. Simó, *Trends Ecol. Evol.* **16**, 287 (2001).
10. R. J. Charlson, J. E. Lovelock, M. O. Andreae, S. G. Warren, *Nature* **326**, 655 (1987).
11. Materials and methods are available as supporting material on *Science* Online.
12. J. W. Dacey, F. A. Howse, A. F. Michaels, S. G. Wakeham, *Deep-Sea Res. I* **45**, 2085 (1998).
13. D. A. Toole, D. A. Siegel, *Geophys. Res. Lett.* **31**, L09308, 10.1029/2004GL019581 (2004).
14. R. Simó, C. Pedrós-Alio, *Nature* **402**, 396 (1999).
15. S. M. Vallina, R. Simó, S. Gassó, *Global Biogeochem. Cycles* **20**, GB1014, 10.1029/2005GB002597 (2006).
16. A. J. Kettle *et al.*, *Global Biogeochem. Cycles* **13**, 399 (1999).
17. Global Surface Seawater Dimethylsulfide Database (http://saga.pmel.noaa.gov/dms/).
18. C. de Boyer Montégut *et al.*, *J. Geophys. Res.* **109**, 10.1029/2004JC002378 (2004).
19. F. D. Brock, *Ecol. Model.* **14**, 1 (1981).
20. J. T. Kiehl, E. Trenberth, *Bull. Am. Meteorol. Soc.* **78**, 197 (1997).
21. W. Sunda, D. J. Kieber, R. P. Kiene, S. Huntsman, *Nature* **418**, 317 (2002).
22. R. Simó, *Can. J. Fish. Aquat. Sci.* **61**, 673 (2004).
23. D. A. Toole *et al.*, *Deep-Sea Res. I* **53**, 136 (2006).
24. T. S. Bates, R. J. Charlson, R. H. Gammon, *Nature* **329**, 319 (1987).
25. R. Simó, J. Dachs, *Global Biogeochem. Cycles* **16**, 1018, 10.1029/2001GB001829 (2002).
26. P. Meir, P. Cox, J. Grace, *Trends Ecol. Evol.* **21**, 254 (2006).

27. We thank M. Vila-Costa and F. Unrein for sharing some sulfur and light data, C. de Boyer-Montégut for providing the MLD climatology; J. M. Gasol and the Blanes Bay Microbial Observatory study team for sampling assistance and coordination; J. Dacey, A. Michaels, and S. Wakeham for the use of the Bermuda DMS data set; J. Johnson for the maintenance of the GSS DMS database, and the SeaWiFS Project team at the Goddard Space Flight Center (NASA), the National Oceanic and Atmospheric Administration, the Bermuda Atlantic Time-Series Study, the Bermuda Bio-Optics Project, and the Baseline Surface Radiation Network (WRMC) for making data available online. This work was supported by the Spanish Ministry of Education and Science through the project "Modeling matter exchanges between the surface ocean and the atmosphere" (contract CTM2005-06513 to R.S.) and a Ph.D. studentship to S.M.V., by the Catalan government through grant 2005SGR00021 (to R.S.), and by the NSF through grant OPP-0083078 (to P. Matrai). This is a contribution to the objectives of the International program Surface Ocean Lower Atmosphere Study (SOLAS) and the Network of Excellence EUR-OCEANS of the European Union's Sixth Framework Program.

Supporting Online Material

www.sciencemag.org/cgi/content/full/315/5811/506/DC1
Materials and Methods
Fig. S1
References

9 August 2006; accepted 6 December 2006
10.1126/science.1133680

A Plasminogen-Activating Protease Specifically Controls the Development of Primary Pneumonic Plague

Wyndham W. Lathem,[1] Paul A. Price,[1] Virginia L. Miller,[1,2] William E. Goldman[1]*

Primary pneumonic plague is transmitted easily, progresses rapidly, and causes high mortality, but the mechanisms by which *Yersinia pestis* overwhelms the lungs are largely unknown. We show that the plasminogen activator Pla is essential for *Y. pestis* to cause primary pneumonic plague but is less important for dissemination during pneumonic plague than during bubonic plague. Experiments manipulating its temporal expression showed that Pla allows *Y. pestis* to replicate rapidly in the airways, causing a lethal fulminant pneumonia; if unexpressed, inflammation is aborted, and lung repair is activated. Inhibition of Pla expression prolonged the survival of animals with the disease, offering a therapeutic option to extend the period during which antibiotics are effective.

Of the three species of *Yersinia* pathogenic to humans, *Y. pestis* is the most virulent owing to its ability to cause plague. Although usually transmitted by an arthropod vector, it is during cases of secondary pneumonic plague that *Y. pestis* can be spread from person to person through the inhalation of respiratory droplets carrying the bacteria (*1*). This method of transmission may initiate an epidemic of primary pneumonic plague, which is fatal if not treated early. Pneumonic plague is the most likely form to result in the event of a bioweapon attack with aerosolized *Y. pestis* (*2*).

Yersinia virulence in mammals requires the Ysc type III secretion system (T3SS), which is shared among all three pathogenic species (*3*). Unlike *Y. pestis*, *Y. enterocolitica* and *Y. pseudotuberculosis* are foodborne pathogens and usually result in self-limiting gastrointestinal infections (*4*–*6*). Thus, the presence of the Ysc T3SS alone is not sufficient to cause a rapidly progressing respiratory infection.

Y. pestis also carries pPCP1, a 9.6-kb plasmid that encodes the plasminogen activator Pla, a surface protease that is thought to promote plasmin degradation of fibrin clots (*1*, *7*). In models of bubonic plague, Pla promotes the invasion of *Y. pestis* from subcutaneous sites of inoculation into the lymphatic system and deeper tissues but is dispensable for growth at the site of inoculation (*8*, *9*). When introduced by aerosol, *Y. pestis* lacking Pla was reported to be equivalent or near equivalent in virulence to wild-type by median lethal dose (LD_{50}) analysis (*10*, *11*), but the progression of lung and systemic disease has never been evaluated in a model of primary pneumonic plague. On the basis of these studies, we predicted that respiratory infection with a strain of *Y. pestis* lacking Pla would proceed normally in the lungs and result in a lethal pneumonia but that fibrin deposition would restrict the ability of bacteria to escape the respiratory system.

We infected C57BL/6 mice intranasally with wild-type *Y. pestis* CO92, an isogenic *Y. pestis* strain lacking Pla (CO92 Δ*pla*), or the Δ*pla* strain complemented with the coding sequence for Pla. Mice given wild-type *Y. pestis* CO92, a strain isolated from a fatal case of pneumonic plague (*12*), succumbed to the infection in a highly synchronous manner. In contrast, only 50% of the mice infected with the Δ*pla* strain developed terminal plague after 7 days, and the rate at which the mice died was less synchronous than the rate of those infected with the wild-type strain (Fig. 1A). Complementation of the mutant with the coding sequence for Pla fully restored virulence. Thus, the lack of Pla substantially delayed the time to death resulting from respiratory infection.

Although the kinetics of bacterial growth during infection with CO92 proceeded as expected (*13*), bacterial outgrowth in the Δ*pla*-infected mice was significantly altered (Fig. 1, B and C). After 24 hours, 100- to 1000-fold fewer bacteria were recovered from the lungs of Δ*pla*-infected mice compared with the lungs with wild-type infection. Over the next 2 days, the numbers of Δ*pla* bacteria in the lungs did not substantially change, whereas wild-type bacteria increased by almost 6 logs. In contrast, we detected bacteria in the spleens of all mice by 72 hours, indicating that escape of the Δ*pla* strain from the lungs to distal organs still occurred (Fig. 1C). Indeed, at later times, mice [illegible] had a bacterial burden approaching 10^8 to 10^9 colony-forming units (CFU) in the spleen. This corresponds with [illegible]

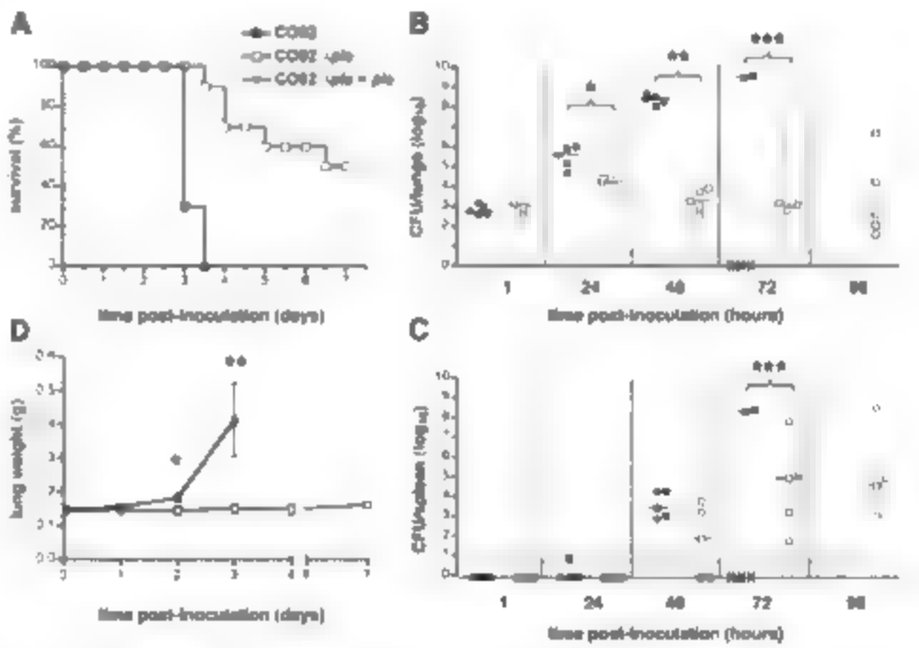

Fig. 1. Pla is required for *Y. pestis* to cause a fulminant infection of the lungs. (**A**) Survival of C57BL/6 mice infected intranasally with *Y. pestis* CO92 (black squares), CO92 Δ*pla* (white squares), or CO92 Δ*pla* complemented with *pla* (white diamonds). (**B** and **C**) Kinetics of infection with *Y. pestis* CO92 (black) or CO92 Δ*pla* (white). Bacteria were introduced intranasally, and at various times CFU per organ in the lungs (B) and spleen (C) were determined. Each point represents the numbers recovered from a single mouse. The limit of detection is indicated by a dashed line. Symbols below the limit of detection represent mice that survived but did not have detectable numbers of bacteria; an "X" indicates a mouse that succumbed to the infection. A solid line indicates the median of CFU recovered. $^*P = 0.037$, $^{**}P = 0.002$, and $^{***}P < 0.001$ (unpaired *t* test). (**D**) Gross weight of lungs from mice infected with *Y. pestis* CO92 (black) or CO92 Δ*pla* (white). C57BL/6 mice were infected as above, and at various times, lungs were excised and weighed. $^*P = 0.01$ and $^{**}P < 0.001$. Each experiment was repeated twice. Error bars represent standard deviation.

[1]Department of Molecular Microbiology, Washington University School of Medicine, St. Louis, MO 63110, USA. [2]Department of Pediatrics, Washington University School of Medicine, St. Louis, MO 63110, USA.

*To whom correspondence should be addressed. E-mail: goldman@wustl.edu

teria in the lungs, however this is likely due to the recirculation of systemic organisms back into the lungs (*13*) rather than outgrowth of bacteria in this organ.

These data show that Pla controls the proliferation of *Y. pestis* in the lungs but is not essential for bacteria to disseminate. This is a distinct phenotype from that attributed to Pla in models of bubonic plague. When Pla-negative *Y. pestis* is introduced subcutaneously, dissemination is dramatically reduced, but bacterial outgrowth at the local site of infection is unaffected (*8, 9*). Indeed, we show that rates of dissemination from the initial site of colonization to the spleen were substantially increased when Pla-negative bacteria were introduced intranasally compared with the subcutaneous route (table S2). This may be due to the highly vascularized nature of the lung, allowing escape of a few Pla-negative bacteria through an alveolar capillary and thus initiating systemic infection.

A hallmark of fatal bacterial pneumonia is the development of edema in the lungs, which can be measured by a change in gross lung weight as fluid and cells contribute to increased mass of the organ. Although mouse lungs infected with wild-type *Y. pestis* weighed significantly more than uninfected lungs, the lungs of mice infected with the Δ*pla* strain of *Y. pestis* showed no change in weight, even after 7 days (Fig. 1D), suggesting that the death of mice infected with this strain is not due to pneumonia but rather is caused by systemic infection. Our results, therefore, may explain the similar LD_{50} values for wild-type and Pla-negative strains when inhaled, even though *Y. pestis* requires Pla to cause a severe pneumonia.

We also examined lung histology of wild-type and mutant *Y. pestis*–infected mice to resolve an existing controversy regarding pathology and inflammation at the site of infection (*8, 9, 13*). An influx of inflammatory cells was detected in the lungs in both wild-type and Δ*pla* infections 36 hours after inoculation; in both cases, the predominant infiltrating cell type was polymorphonuclear (Fig. 2). Although the size of the pulmonary lesions in the wild-type infection increased over time, resulting in tissue destruction and hemorrhage, the foci of inflammation in mice infected with CO92 Δ*pla* remained relatively constant and restricted. In addition, we examined infected lung sections by using immunofluorescence with an antibody against *Y. pestis*. Numerous extracellular bacteria were associated with inflammation in the lungs of wild-type infected mice, but relatively few bacteria were detected in the Δ*pla* infection and were restricted to the much smaller inflammatory lesions (Fig. 2). Thus, both bacterial outgrowth and subsequent inflammation in the lungs were dependent on the Pla surface protease.

These results suggest that host immunity controls the pulmonary infection without developing an overwhelming inflammatory reaction to Pla-negative bacteria. Therefore, we assessed the amount of immune activation in the lungs by using quantitative reverse-transcription polymerase chain reaction (qRT-PCR) to determine changes in transcript quantities of multiple inflammatory mediators. Consistent with our previous observations (*13*), mice infected with CO92 remained unresponsive early in the infection but showed significant cytokine up-regulation by 48 hours (Fig. 3A). Similarly, the cytokine transcript numbers in the lungs of mice infected with Δ*pla* were also relatively unchanged early in the infection. After 48 hours, however, cytokine transcript numbers in response to Δ*pla* were unchanged or only slightly increased, and by the following day of infection transcript numbers for most cytokines decreased, suggesting down-regulation of the inflammatory response to Δ*pla*. Thus, the data reveal that, in the absence of Pla, an anti-inflammatory state is maintained in the lungs and the infection is unable to progress to the pro-inflammatory phase that we described previously (*13*).

That cytokine transcript amounts appeared to stabilize and then decrease in the Δ*pla*-infected mice suggested the pulmonary inflammatory lesions were resolving. We immunostained infected lungs for the proliferating cell nuclear antigen (PCNA), a marker for host cellular

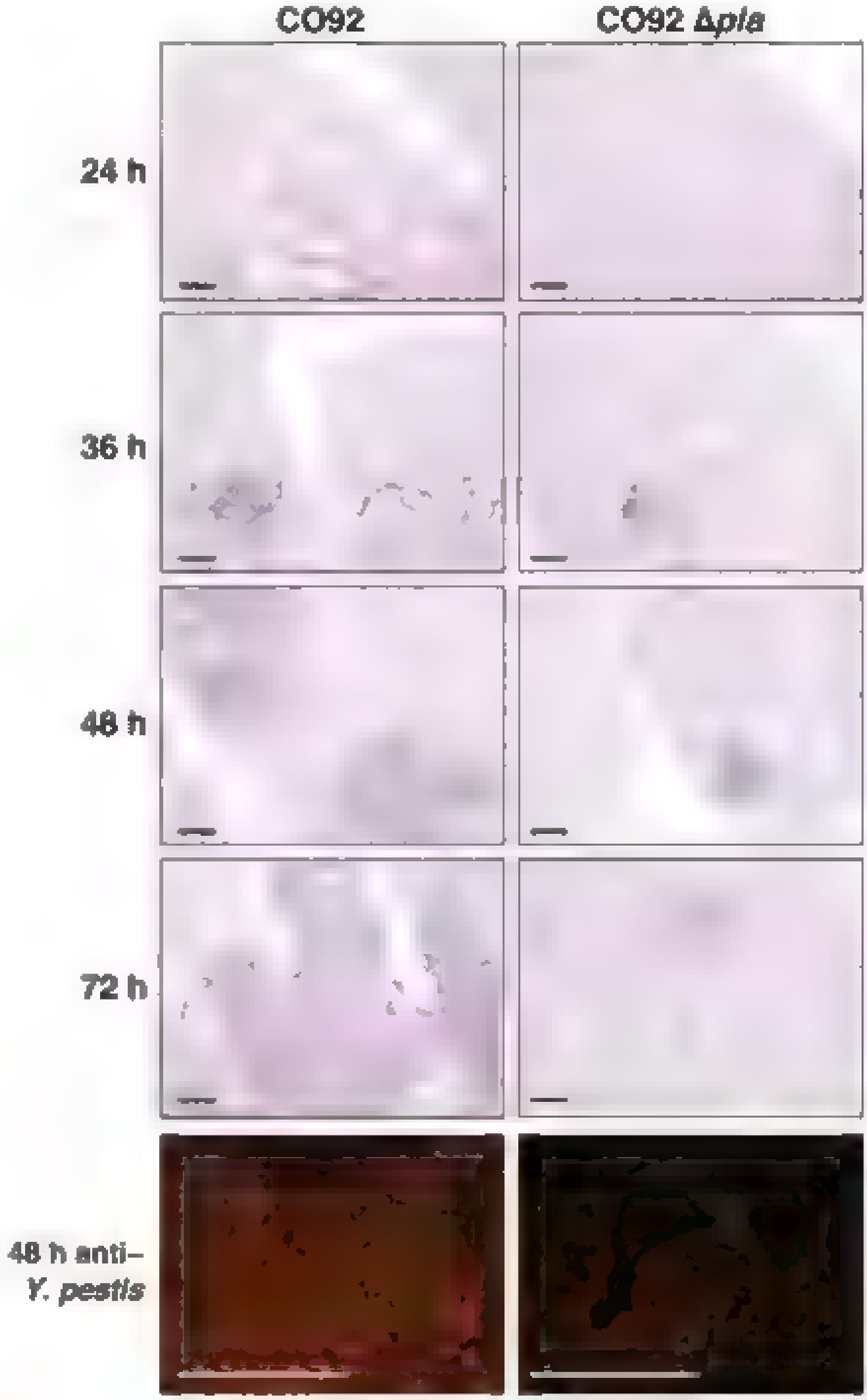

Fig. 2. Histology and presence of bacteria in the lungs of mice during the progression of pneumonic plague. Mice were infected intranasally; at various times, lungs were inflated and fixed with 10% neutral buffered formalin and embedded in paraffin, and 5 μm sections were stained with hematoxylin and eosin or a *Y. pestis* antibody. The images shown are representative of experiments repeated twice. Scale bars indicate 200 μm.

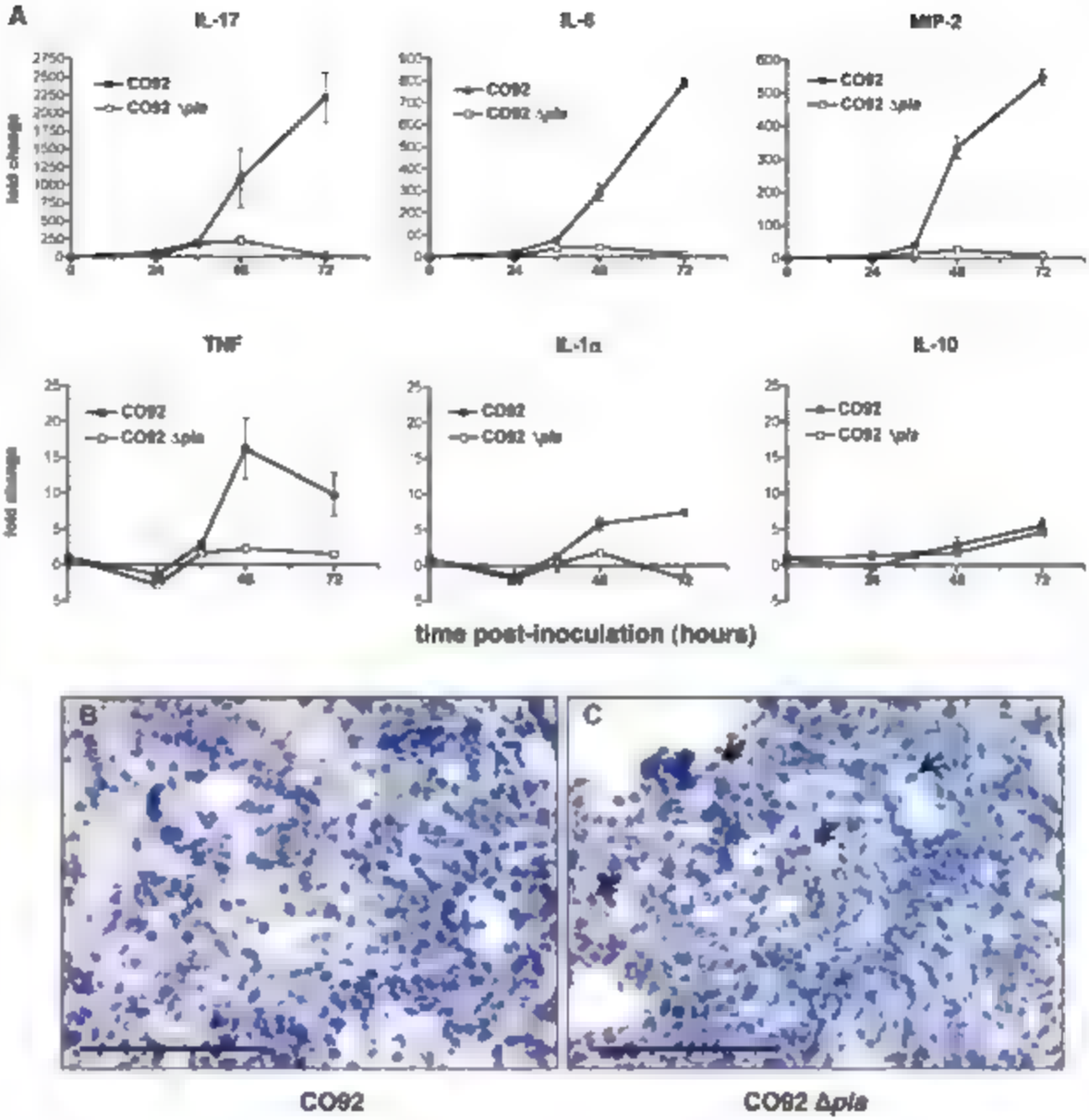

Fig. 3. Progression of the inflammatory response to *Y. pestis* CO92 or CO92 Δ*pla*. (**A**) Mice were uninfected or infected intranasally, and at various times lungs were removed and immersed in RNAlater (Ambion, Woodward, TX). RNA was extracted and reverse-transcribed, and relative cytokine transcript quantities compared with those of uninfected mice were determined by qRT-PCR using the $\Delta\Delta C_t$ method (*22*) and normalized to glyceraldehyde-3-phosphate dehydrogenase for *Y. pestis* CO92 (black) or Δ*pla*-infected mice (white). IL, interleukin; MIP, macrophage inflammatory protein; and TNF, tumor necrosis factor. (**B** and **C**) PCNA antibody stain and hematoxylin counterstain of lungs infected with *Y. pestis* CO92 or CO92 Δ*pla* after 48 hours. PCNA-positive cells (arrows) are present in the lungs of Δ*pla*-infected mice but largely absent in the wild-type infection. Extranuclear granular staining in the CO92-infected lungs correlates with the presence of bacteria. Scale bars, 50 μm.

DNA synthesis (*14*). Whereas the cells of wild-type infected lungs were almost uniformly PCNA-negative (Fig. 3B), large numbers of PCNA-positive cells were present in Δ*pla*-infected mice (Fig. 3C), indicating active cell proliferation and regeneration of tissue in the lungs. Lung repair at this stage of the infection is further evidence that fatalities among Δ*pla*-infected mice are not a consequence of airway inflammation or damage but instead are the result of systemic spread of the bacteria.

If Pla alone controls the ability of *Y. pestis* to cause pneumonic plague, we hypothesized that experimental induction of *pla* expression midway during the aborted pulmonary disease would be sufficient to turn the nonpneumonic infection into a pneumonic one. To test this, we adapted the tetracycline-responsive promoter system (*15*) to exogenously control gene expression in *Y. pestis* during infection (Materials and Methods and figs. S1 and S2). We cultured the Δ*pla* strain of *Y. pestis* carrying *pla* under control of the tetracycline-responsive promoter (*Y. pestis* CO92 Δ*pla* P_{tet}-*pla*, strain YP138) in *pla*-repressing conditions (i.e., absence of anhydrotetracycline, or ATC). Thirty-six hours after intranasal inoculation, we induced *pla* expression by injecting ATC and then followed the progression of the infection. Bacteria in the *pla*-repressed state established a nonprogressive lung infection in a manner similar to that of the Δ*pla*-infected mice. However, once ATC was administered and Pla expression was up-regulated, the condition of these mice quickly converted to a disease with all the features of pneumonic plague: rapid proliferation of bacteria with development of visible microcolonies (Fig. 4, A and B), unrestricted inflammatory infiltrate tissue damage (Fig. 4C), and shortened time to death. Thus, the absence of Pla stalls the development of disease in the early anti-inflammatory phase but does not eliminate the potential of these organisms to cause pneumonic plague. Ultimately, the block in the progression of infection by the respiratory route is completely reversible by the expression of Pla.

One hypothesis of the mechanism by which Pla facilitates the invasive nature of *Y. pestis* is that the protease converts host plasminogen into plasmin while degrading the plasmin inhibitor α$_2$-antiplasmin, releasing bacteria from the entrapment of fibrin clots (*16*, *17*). Indeed, recent evidence has shown that fibrin deposition is an important means of immune control for a variety of pathogens (*18*–*20*), and thus the subversion of the coagulation cascade may be a notable virulence mechanism. Consistent with this, we show that the plasminogen-activating activity of Pla is essential to *Y. pestis* virulence in the pulmonary system (Materials and Methods and fig. S3). Additionally, fibrin(ogen) deposition can be detected in the lungs of mice infected with either the wild-type or the Δ*pla* strain, but the pattern and extent of fibrin(ogen) immunostaining is substantially altered (fig. S4). We cannot exclude, however, the possibility that other targets of Pla activity may also contribute to the development of primary pneumonic plague. Nonetheless, the role of Pla during pneumonic

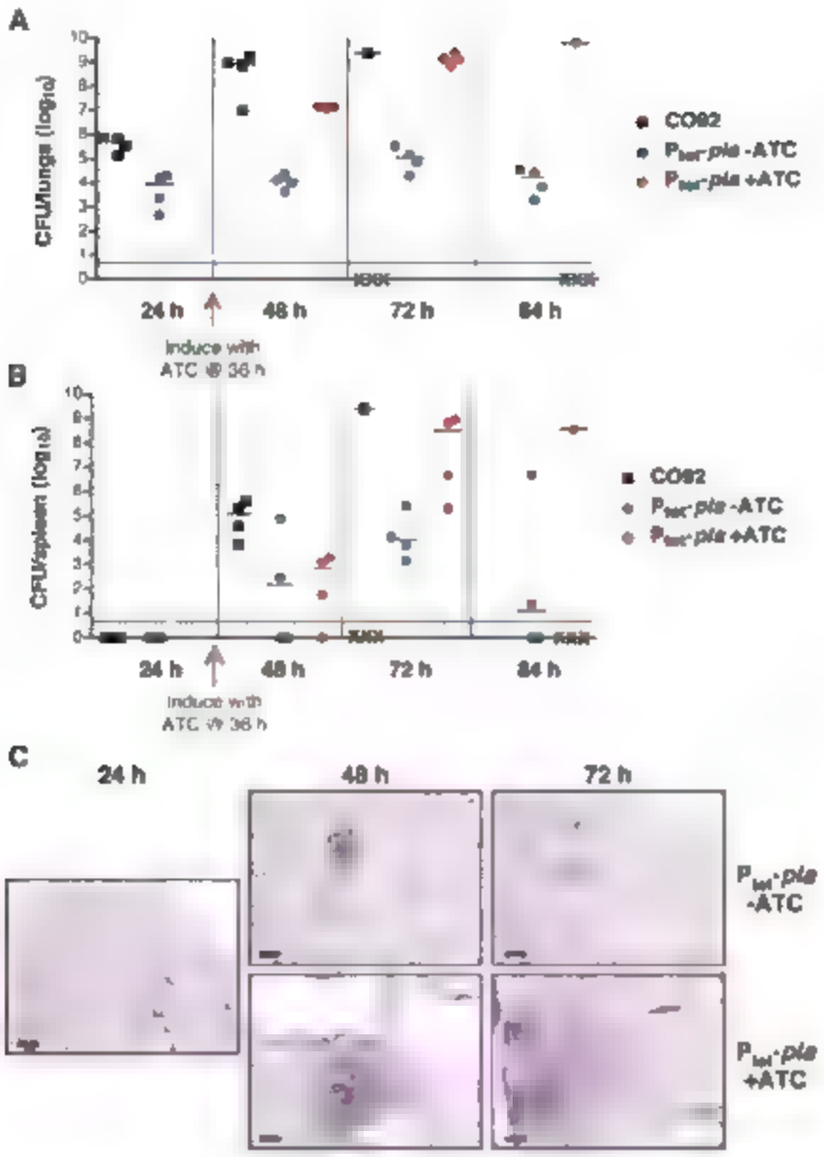

Fig. 4. Control of primary pneumonic plague progression by the tetracycline-responsive promoter system in *Y. pestis*. (**A** and **B**) Induction of Pla during intranasal infection. Mice were infected intranasally with *Y. pestis* CO92 (black) or CO92 Δ*pla* + P_{tet}-*pla* prepared in the absence of ATC (repressed state). After 36 hours, mice infected with the P_{tet}-*pla* strain were administered phosphate-buffered solution (PBS) (blue) or ATC (red) by intraperitoneal injection bid. CFU in the lungs (A) and spleen (B) were determined at various times. Symbols and lines as in Fig. 1. (**C**) Lung histology of mice infected with the P_{tet}-*pla* strain and treated with PBS or ATC. Lungs were prepared as for Fig. 2. Scale bars, 200 μm. (**D**) Repression of *pla* expression midway through pneumonic plague infection. Survival of mice infected with CO92 Δ*pla* plus P_{tet}-*pla* in the *pla*-induced state for the duration of the experiment (black) [mean time to death (MTD) = 3.1 days], in the *pla*-repressed state for the duration (blue) (MTD = 5.1 days), or in the *pla*-induced state for the first day followed by the *pla*-repressed state for the remainder of the experiment (red) (MTD = 4.6 days). See Materials and Methods for details. The bar beneath the graph approximates the period at which *pla* induction ends and repression begins.

plague may help explain how *Y. pestis* acquired the ability to cause a rapid, severe respiratory infection and be transmitted from person to person by the aerosol route, whereas *Y. pseudotuberculosis* and *Y. enterocolitica* did not. Interestingly, the altered syndrome we observed with Pla-negative strain is similar to case descriptions from the early 20th-century Manchurian epidemics in which aerosol-acquired plague resulted in fatal sepsis before a local lung disease could develop (*21*).

The critical role for Pla suggests that its inhibition could offer a therapeutic advantage, particularly because the rapid progression of pneumonic plague leaves little time for effective treatment. We tested this experimentally by infecting mice with the Pla-inducible *Y. pestis* strain YP138 prepared in the presence of ATC. We then provided ATC to the animals for only the first day of the infection, allowing the ATC to be cleared and *pla* expression to be repressed for the remainder of the experiment. The time until death was delayed when the Pla-induced state was switched to a Pla-repressed state during the infection (Fig. 4D); in fact, the kinetics more closely resemble those of a Δ*pla* infection. This suggests that exogenous inhibition of Pla during primary pneumonic plague may indeed prolong the survival of the affected individual, expanding the window during which antibiotics could be successfully administered to treat the disease.

References and Notes

1. R. D. Perry, J. D. Fetherston, *Clin. Microbiol. Rev.* **10**, 35 (1997).
2. T. V. Inglesby *et al.*, *JAMA* **283**, 2281 (2000).
3. G. L. Viboud, J. B. Bliska, *Annu. Rev. Microbiol.* **59**, 69 (2005).
4. X. Z. Huang, M. P. Nikolich, L. E. Lindler, *Clin. Med. Res.* **4**, 189 (2006).
5. L. E. Lindler, in *Encyclopedia of Medical Genomics and Proteomics*, J. Fuchs, M. Podda, Eds. (Taylor & Francis, New York, 2004), pp. 1355–1359.
6. T. L. Cover, R. C. Aber, *N. Engl. J. Med.* **321**, 16 (1989).
7. J. Parkhill *et al.*, *Nature* **413**, 523 (2001).
8. O. A. Sodeinde *et al.*, *Science* **258**, 1004 (1992).
9. S. L. Welkos, A. M. Friedlander, K. J. Davis, *Microb. Pathog.* **23**, 211 (1997).
10. S. Welkos *et al.*, *Vaccine* **20**, 2206 (2002).
11. S. V. Samoilova, L. V. Samoilova, I. N. Yezhov, I. G. Drozdov, A. P. Anisimov, *J. Med. Microbiol.* **45**, 440 (1996).
12. J. M. Ostl *et al.*, *Am. J. Trop. Med. Hyg.* **51**, 109 (1994).
13. W. W. Lathem, S. D. Crosby, V. L. Miller, W. E. Goldman, *Proc. Natl. Acad. Sci. U.S.A.* **102**, 17786 (2005).
14. J. E. Cells, P. Madsen, A. Celis, H. V. Nielsen, B. Gesser, *FEBS Lett.* **220**, 1 (1987).
15. R. Lutz, H. Bujard, *Nucleic Acids Res.* **25**, 1203 (1997).
16. M. Kukkonen *et al.*, *Mol. Microbiol.* **40**, 1097 (2001).
17. O. A. Sodeinde, J. D. Goguen, *Infect. Immun.* **57**, 1517 (1989).
18. I. K. Mullarky *et al.*, *Infect. Immun.* **73**, 3888 (2005).
19. L. L. Johnson, K. N. Berggren, F. M. Szaba, W. Chen, S. T. Smiley, *J. Exp. Med.* **197**, 801 (2003).
20. M. J. Flick *et al.*, *J. Clin. Invest.* **113**, 1596 (2004).
21. L-T. Wu, *A Treatise on Pneumonic Plague* (League of Nations, Geneva, 1926), p. 466.
22. Applied Biosystems, in *ABI Prism 7700 Sequence Detection System User Bulletin 2* (Applied Biosystems, Foster City, CA, 1997).

23. We thank K. Wright, J. Fischer, and I. Vogel for helpful discussions; J. Hinnebusch for the *Y. pestis* antibody; and the Washington University Digestive Diseases Research Core (DDRCC) for histological sections. This work was supported by NIH grant U54 AI057160.

to the Midwest Regional Center of Excellence for Biodefense and Emerging Infectious Disease Research (MRCE) and by NIH grant AI53298. The ODRCC is supported by NIH grant RR52574. W.W.L was supported by the Clinical/Translational Fellowship Program of the MRCE, the W.M. Keck Foundation, and the NIH National Research Service Award (NRSA) F32 AI069688-01. P.A.P was supported by the NIH institutional NRSA T32 GM07067 to the Washington University School of Medicine.

Supporting Online Material

www.sciencemag.org/cgi/content/full/315/5811/509/DC1
Materials and Methods
SOM Text
Figs. S1 to S4
Tables S1 and S2
References

6 November 2006; accepted 14 December 2006
10.1126/science.1137195

A Virus in a Fungus in a Plant: Three-Way Symbiosis Required for Thermal Tolerance

Luis M. Marquez,[1] Regina S. Redman,[2,3] Russell J. Rodriguez,[2,4] Marilyn J. Roossinck[1]*

A mutualistic association between a fungal endophyte and a tropical panic grass allows both organisms to grow at high soil temperatures. We characterized a virus from this fungus that is involved in the mutualistic interaction. Fungal isolates cured of the virus are unable to confer heat tolerance, but heat tolerance is restored after the virus is reintroduced. The virus-infected fungus confers heat tolerance not only to its native monocot host but also to a eudicot host, which suggests that the underlying mechanism involves pathways conserved between these two groups of plants.

Endophytic fungi commonly grow within plant tissues and can be mutualistic in some cases, as they allow plant adaptation to extreme environments (*1*). A plant-fungal symbiosis between a tropical panic grass from geothermal soils, *Dichanthelium lanuginosum*, and the fungus *Curvularia protuberata* allows both organisms to grow at high soil temperatures in Yellowstone National Park (YNP) (*2*). Field and laboratory experiments have shown that when root zones are heated up to 65°C, nonsymbiotic plants either become shriveled and chlorotic or simply die, whereas symbiotic plants tolerate and survive the heat regime. When grown separately, neither the fungus nor the plant alone is able to grow at temperatures above 38°C, but symbiotically they are able to tolerate elevated temperatures. In the absence of heat stress, symbiotic plants have enhanced growth rates compared with nonsymbiotic plants and also show significant drought tolerance (*3*).

Fungal viruses or mycoviruses can modulate plant-fungal symbioses. The best known example of this is the hypovirus that attenuates the virulence (hypovirulence) of the chestnut blight fungus, *Cryphonectria parasitica* (*4*). Virus regulation of hypovirulence has been demonstrated experimentally in several other pathogenic fungi (*5*–*8*). However, the effect of mycoviruses on mutualistic fungal endophytes is unknown. There is only one report of a mycovirus from the well-known mutualistic endophyte, *Epichloë festucae*, but no phenotype has been associated with this virus (*9*).

Fungal virus genomes are commonly composed of double-stranded RNA (dsRNA) (*10*). Large molecules of dsRNA do not normally occur in uninfected cells and therefore, their presence is a sign of a viral infection (*9*). Using a protocol for nucleic acid extraction with enrichment for dsRNA (*11*), we detected the presence of a virus in *C. protuberata*. The dsRNA banding pattern consists of two segments of about 2.2 and 1.8 kb. A smaller segment, less than 1 kb in length, was variable in presence and size in the isolates analyzed and, later, was confirmed to be a subgenomic element most likely a defective RNA (fig. S1 and Fig. 1, A and B). Using arbitrary random hexamer primers, we transcribed the virus with reverse transcriptase (RT) followed by amplification and cloning. Sequence analysis revealed that each of the two RNA segments contains two open reading frames (ORFs) (fig. S2). The 2.2-kb fragment (RNA 1) is involved in virus replication, as both of its ORFs are similar to viral replicases. The first, ORF1a, has 29% amino acid sequence identity with a putative RNA-dependent RNA polymerase (RdRp) from the rabbit hemorrhagic disease virus. The amino acid sequence of the second, ORF1b, has 35% identity with the RdRp of a virus of the fungal pathogen *Discula destructiva*. These two ORFs overlap and could be expressed as a single protein by frameshifting, a common expression strategy of viral replicases. The two ORFs of RNA 2 have no similarity to any protein with known function. As in most dsRNA mycoviruses, the 5′ ends (21 bp) of both RNAs are conserved. Virus particles purified from *C. protuberata* are similar to those of other fungal viruses, spherical and ~27 nm in diameter (fig. S3). This virus is transmitted vertically in the conidiospores. We propose naming this virus *Curvularia* thermal tolerance virus (CThTV) to reflect its host of origin and its phenotype.

The ability of the fungus to confer heat tolerance to its host plant is related to the presence of CThTV. Wild-type isolates of *C. protuberata* contained the virus in high titers, as evidenced by their high concentration of dsRNA (~2 μg g of lyophilized mycelium). However, an isolate obtained from sectoring (change in morphology) of a wild-type colony contained a very low titer of the virus, as indicated by a low concentration of dsRNA (~0.02 μg g of lyophilized mycelium). These two isolates were identical by simple sequence repeat (SSR) analysis with two single-primer polymerase chain reaction (PCR) reactions and by sequence analysis of the rDNA ITS1-5.8S-ITS2 region (figs. S4 and S5). Desiccation and freezing-thawing cycles are known to disrupt virus particles (*12*); thus, mycelium of the isolate obtained by sectoring, was

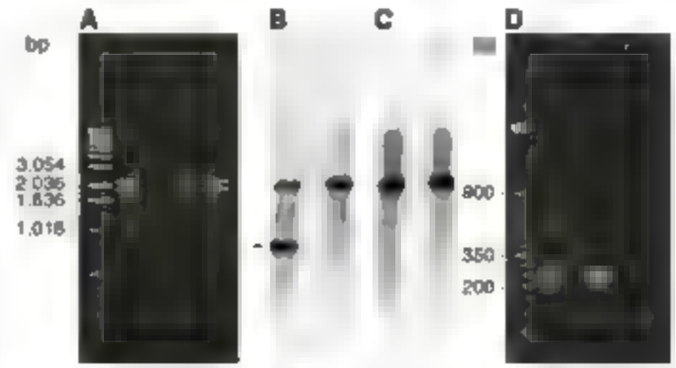

Fig. 1. Presence or absence of CThTV in different strains of *C. protuberata*, detected by ethidium bromide staining (**A**). Northern blot using RNA 1 (**B**) and RNA 2 (**C**) transcripts of the virus as probes, and RT-PCR using primers specific for a section of the RNA 2 (**D**). The isolate of the fungus obtained by sectoring was made virus-free (VF) by freezing-thawing. The virus was reintroduced into the virus-free isolate through hyphal anastomosis (An) with the wild type (Wt). The wild-type isolate of the fungus sometimes contains a subgenomic fragment of the virus that hybridizes to the RNA 1 probe (arrow).

[1]Plant Biology Division, Samuel Roberts Noble Foundation, Post Office Box 2180, Ardmore, OK 73402, USA. [2]Department of Botany, University of Washington, Seattle, WA 98195, USA. [3]Department of Microbiology, Montana State University, Bozeman, MT 59717, USA. [4]U.S. Geological Survey, Seattle, WA 98115, USA.

*To whom correspondence should be addressed. E-mail: mroossinck@noble.org

ly sporulated, frozen at −80°C, and subcultured to cure it completely of the virus. The complete absence of CThTV in this isolate was confirmed by dsRNA extraction, Northern blotting, RT-PCR (Fig. 1), and electron microscopy (no particles were observed in four grids). We assessed experimentally the ability of the wild-type and virus-free isolates to confer heat tolerance by using thermal soil simulators (*13*). Plants inoculated with the virus-infected wild-type isolate of the fungus tolerated intermittent soil temperatures as high as 65°C for 2 weeks (10 hours of heat per day), whereas both nonsymbiotic plants and plants inoculated with the virus-free isolate of the fungus became shriveled and chlorotic and died (Fig. 2).

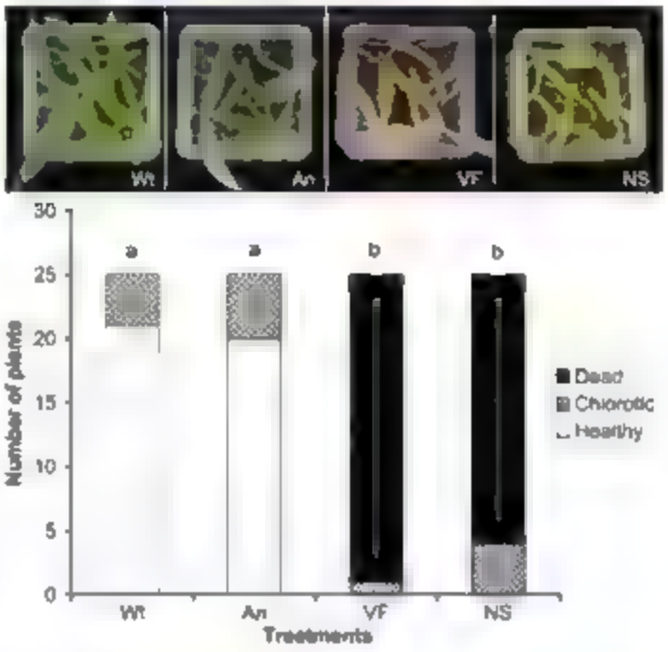

Fig. 2. (Top) Representative *D. tanuginosum* plants after the heat stress experiment with thermal soil simulators. Rhizosphere temperature was maintained at 65°C for 10 hours and 37°C for 14 hours/day for 14 days under greenhouse conditions. Plants were nonsymbiotic (NS) and symbiotic with the wild-type virus-infected isolate of *C. protuberata* (Wt), the hygromycin-resistant isolate newly infected with the virus through hyphal anastomosis (An), or the virus-free hygromycin-resistant isolate (VF). **(Bottom)** The histogram presents the number of plants chlorotic, dead, and alive at the end of the experiment. The small letters on top of the bars indicate statistical differences or similarities (chi-square test, $P < 0.01$).

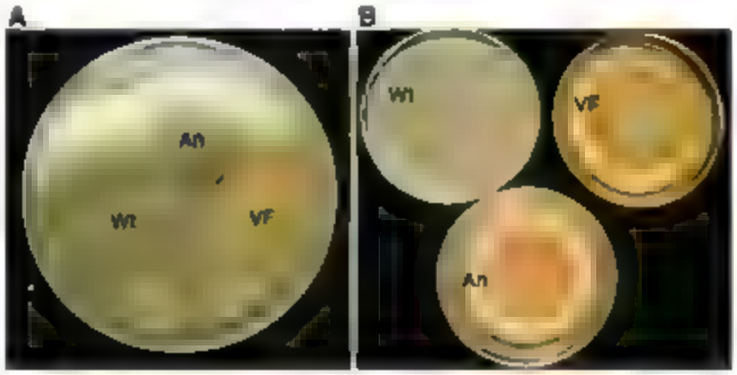

Fig. 3. (**A**) Anastomosis of the wild-type virus-infected isolate of *C. protuberata* (Wt) and the virus-free hygromycin-resistant isolate (VF) to produce a virus-infected hygromycin-resistant isolate (An). (**B**) After single-spore isolation to produce pure cultures, the isolate newly infected with the virus (An) retained the hygromycin-resistance and the morphology of the VF isolate.

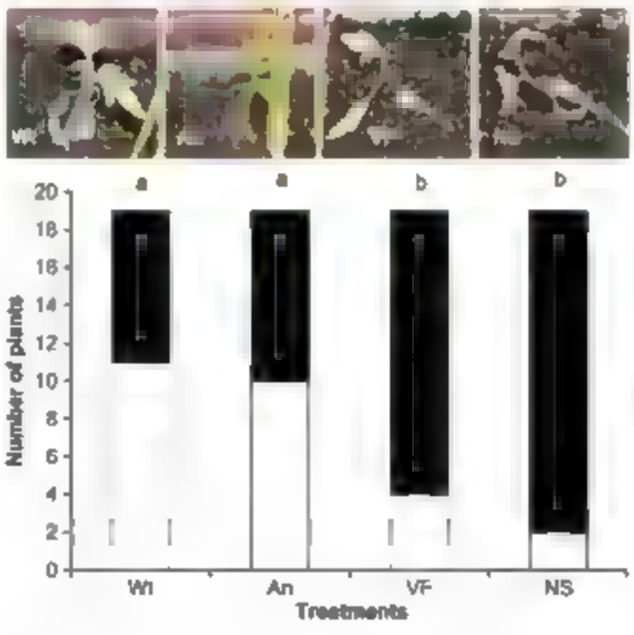

Fig. 4. (Top) Representative tomato (*Solanum lycopersicon*, var. Rutgers) plants after the heat-stress experiment. Plants were nonsymbiotic (NS) and symbiotic with the wild-type virus-infected isolate of *C. protuberata* (Wt), the hygromycin-resistant isolate newly infected with the virus through hyphal anastomosis (An) or the virus-free hygromycin-resistant isolate (VF). Rhizosphere temperature was maintained at 65°C for 10 hours and ambient temperature (26°C) for 14 hours/day for 14 days under greenhouse conditions. **(Bottom)** The histogram presents the number of plants dead (white) and alive (black) at the end of the experiment. The small letters on top of the bars indicate statistical differences or similarities (Fisher's exact test, $P < 0.05$).

To confirm that CThTV was involved in heat tolerance in the plant-fungal symbiosis, we reintroduced the virus into the virus-free fungal isolate and tested its ability to confer heat tolerance. To provide a selectable marker, the virus-free isolate was transformed with a pCT74 vector containing a hygromycin-resistance gene (*13*) by restriction enzyme mediated integration (REMI) transformation (*14*). Virus-containing wild-type hygromycin-sensitive (Wt) and virus-free hygromycin-resistant (VF) isolates of *C. protuberata* were cultured on single Petri dishes and allowed to undergo hyphal fusion or anastomosis (Fig. 3A). The mycelium from the area of anastomosis was subcultured twice with single conidiospores grown on hygromycin-containing plates. Thirty-five hygromycin-resistant isolates obtained in this way were screened for their dsRNA profiles, but only one was found to have acquired the virus (Figs. 1 and 3B). This fungal isolate, newly infected by hyphal anastomosis with CThTV (An), was tested for its ability to confer heat tolerance by the same experimental approach indicated above. The heat-stress experiment confirmed that the isolate newly infected with CThTV confers the same level of heat tolerance as that conferred by the wild-type isolate (Fig. 2).

Previously, we found that some beneficial endophytes selected from nonsymbiotic roots can be considered to endosymbionts that have evolved as mutualists (*3*). Thus, we tested the ability of the *C. protuberata* isolates to confer heat tolerance to tomato (*Solanum lycopersicon*). Using a slightly modified protocol for the heat-stress experiment (*13*), we obtained similar results to those obtained with *D. tanuginosum* (Fig. 4). However, it was not possible to attain 100% fungal colonization of tomato plants (*13*), and this may explain the higher proportion of dead plants colonized with the Wt or An fungus, compared with the experiments using *D. tanuginosum*. Given that *C. protuberata* when infected with CThTV provides similar mutualistic benefits to both a monocot and a dicot, it is possible that the underlying mechanism is conserved between these two groups of plants.

Plants inoculated with *C. protuberata* infected with CThTV do not activate the heat-stress response system as the usual way. For example, the osmolyte concentration in these plants does not increase as a response to heat stress, although the levels are consistently higher than in plants colonized with the virus-free isolate or the nonsymbiotic plants (Fig. S6). It has been hypoth-

esized that endophytes may protect their host plants by scavenging the damaging reactive oxygen species (ROS) generated by the plant defense mechanisms in response to environmental stress (*19*). The leaves of nonsymbiotic plants generated detectable ROS when stressed with heat, whereas those of symbiotically colonized plants did not (table S1). However, there was no difference in the ROS response to heat between plants inoculated with the virus-free and the CThTV-infected isolates of *C. proliferatum*.

Complex tripartite symbioses have been found among arthropods, bacteria, and mutualistic bacteriophages (*16*, *17*). This study reports a three-way mutualistic symbiosis involving a virus, a fungal endophyte, and either a monocot or eudicot plant.

References and Notes

1. R. J. Rodriguez, R. S. Redman, J. M. Henson, *Mitig. Adapt Strategies Global Change* **9**, 261 (2004).
2. R. S. Redman, K. B. Sheehan, R. G. Stout, R. J. Rodriguez, J. M. Henson, *Science* **298**, 1581 (2002).
3. R. J. Rodriguez, R. S. Redman, J. M. Henson, in *The Fungal Community: Its Organization and Role in the Ecosystem*, J. Dighton, J. F. White Jr., P. Oudemans, Eds. (CRC Press, Boca Raton FL, 2004), pp. 683–695.
4. A. L. Dawe, D. L. Nuss, *Annu. Rev. Genet.* **35**, 1 (2001).
5. S. L. Anagnostakis, P. B. Day, *Phytopathology* **69**, 1226 (1979).
6. F. Zhou, G. J. Boland, *Phytopathology* **87**, 147 (1997).
7. I. P. Ahn, Y. H. Lee, *Mol. Plant Microbe Interact.* **14**, 496 (2001).
8. Y. M. Cho *et al.*, *Appl. Environ. Microbiol.* **68**, 2529 (2002).
9. I. Zabalgogeazcoa, E. P. Benito, A. G. Ciudad, B. G. Criado, A. P. Eslava, *Mycol. Res.* **102**, 914 (1998).
10. S. A. Ghabrial, *Adv. Virus Res.* **43**, 303 (1994).
11. Materials and methods are available as supporting material on *Science* Online.
12. Y. G. Kuznetsov, A. McPherson, *Virology* **352**, 329 (2006).
13. J. M. Lorang *et al.*, *Appl. Environ. Microbiol.* **67**, 1987 (2001).
14. R. S. Redman, J. C. Ranson, R. J. Rodriguez, *Mol. Plant-Microbe Interact.* **12**, 969 (1999).
15. R. Rodriguez, R. Redman, *Proc. Natl. Acad. Sci. U.S.A.* **102**, 3175 (2005).
16. S. R. Bordenstein, J. J. Wernegreen, *Mol. Biol. Evol.* **21**, 1981 (2004).
17. M. A. Moran, P. H. Degnan, S. R. Santos, H. E. Dunbar, H. Ochman, *Proc. Natl. Acad. Sci. U.S.A.* **102**, 16919 (2005).

18. We thank F. Coker, M. Hoy, Y. Chen, and R. Pescador for technical assistance and P. Xu, J. Pita, K. Craven, F. Feldmann, A. Ali, G. Shen, R. Lippapalli, and C. Bastidas for providing comments and suggestions that improved the manuscript. This project was made possible by the permission, assistance, and guidelines of YNP. This work was supported by The Samuel Roberts Noble Foundation, the MSU Thermal Biology Institute, and grants from the U.S. Geological Survey, the NSF (9977922 and 0414463), and the U.S. Army Research Office (DAAH04-96-1-01194). Sequences were deposited in GenBank under accession numbers EF120984 (RNA 1) and EF120985 (RNA 2). The CThTV description was deposited in the ICTVdB—The Universal Virus Database version 4 (www.ncbi.nlm.nih.gov/ICTVdb/ICTVdB/), with the virus accession number 00000040020.

Supporting Online Material

www.sciencemag.org/cgi/content/full/315/5811/513/DC1
Materials and Methods
Figs. S1 to S5
Table S1
References

12 October 2006; accepted 12 December 2006
10.1126/science.1136237

The Neural Basis of Loss Aversion in Decision-Making Under Risk

Sabrina M. Tom,[1] Craig R. Fox,[1,2] Christopher Trepel,[2] Russell A. Poldrack[2,3,4]*

People typically exhibit greater sensitivity to losses than to equivalent gains when making decisions. We investigated neural correlates of loss aversion while individuals decided whether to accept or reject gambles that offered a 50/50 chance of gaining or losing money. A broad set of areas (including midbrain dopaminergic regions and their targets) showed increasing activity as potential gains increased. Potential losses were represented by decreasing activity in several of these same gain-sensitive areas. Finally, individual differences in behavioral loss aversion were predicted by a measure of neural loss aversion in several regions, including the ventral striatum and prefrontal cortex.

Many decisions, such as whether to invest in the stock market or to accept a new job, involve the possibility of gaining or losing relative to the status quo. When faced with such decisions, most people are markedly risk averse. For instance, people typically reject gambles that offer a 50/50 chance of gaining or losing money, unless the amount that could be gained is at least twice the amount that could be lost (e.g., a 50/50 chance to either gain $ 100 or lose $50) (*1*). Prospect theory, the most successful behavioral model of decision-making under risk and uncertainty (*1*, *2*), explains risk aversion for "mixed" (gain-loss) gambles using the concept of loss aversion. People are more sensitive to the possibility of losing objects or money than they are to the possibility of gaining the same objects or amounts of money (*1*, *3*–*5*). Thus, people typically require a potential gain of at least $100 to make up for exposure to a potential loss of $50 because the subjective impact of losses is roughly twice that of gains. Similarly, people demand substantially more money to part with objects that they have been given than what they would have been willing to pay to acquire those objects in the first place (*6*). Loss aversion also has been used to explain a wide range of economic behaviors outside the laboratory (*7*, *8*). Further, loss aversion is seen in trading behavior of both children as young as age five (*9*) and capuchin monkeys (*10*), which suggests that it may reflect a fundamental feature of how potential outcomes are assessed by the primate brain.

Previous neuroimaging studies of responses to monetary gains or losses have focused on activity associated with the anticipation of immediate outcomes ("anticipated" utility) (*11*, *12*) or the actual experience of gaining or losing money ("experienced" utility) (*11*, *13*, *14*) rather than specifically investigating which brain systems represent potential losses versus gains when a decision is being made ("decision" utility). Behavioral researchers have shown that anticipated, experienced, and decision utilities often diverge in dramatic ways, which raises the possibility that the corresponding brain systems involved may also differ (*15*). In the current study, we aimed to isolate activity associated with the evaluation of a gamble when choosing whether or not to accept it (i.e., decision utility) without the expectation that the gamble would be immediately resolved. This allowed us to test whether neural responses during the evaluation of potential outcomes are similar to patterns previously reported in studies of anticipated and experienced outcomes.

One fundamental question for the study of decision-making is whether loss aversion reflects the engagement of distinct emotional processes when potential losses are considered. It has been suggested that enhanced sensitivity to losses is driven by negative emotions, such as fear or anxiety (*16*). This notion predicts that exposure to increasing potential losses should be associated with increased activity in brain structures thought to mediate negative emotions in decision-making [such as the amygdala or anterior insula; compare with (*17*, *18*)]. Alternatively, loss aversion could reflect an asymmetric response to losses versus gains within a single system that codes for the subjective value of the potential gamble, such as ventromedial prefrontal cortex (VMPFC)/orbitofrontal cortex (OFC) and ventral striatum (*11*, *19*, *20*).

To examine the neural systems that process decision utility, we collected functional magnetic resonance imaging (fMRI) data while partici-

[1]Department of Psychology, University of California, Los Angeles (UCLA), Franz Hall, Box 951563, Los Angeles, CA 90095–1563, USA. [2]Anderson School of Management, UCLA, 110 Westwood Plaza, Los Angeles, CA 90095–1481, USA. [3]Brain Research Institute, UCLA, Los Angeles, CA 90095, USA. [4]Department of Psychiatry and Biobehavioral Sciences, UCLA, Los Angeles, CA 90095, USA.

*To whom correspondence should be addressed. E-mail: poldrack@ucla.edu

pants decided whether to accept or reject mixed gambles that offered a 50/50 chance of either gaining one amount of money or losing another amount (Fig. 1A) (27). To encourage participants to reflect on the subjective attractiveness of each gamble rather than to rely on a fixed decision rule, we asked them to indicate one of four responses to each gamble (strongly accept, weakly accept, weakly reject, and strongly reject). In order to allow for separate estimates of neural responses to gains and losses, the sizes of the potential gain and loss were manipulated independently, with gains ranging from $10 to $40 (increments of $2) and losses ranging from $5 to $20 (in increments of $1). We chose these ranges because previous studies indicate that people are, on average, roughly twice as sensitive to losses as to gains (1, 5); thus, we expected that, for most participants, this range of gambles would elicit a wide range of attitudes, from strong acceptance to indifference to strong rejection. To introduce incentive-compatible payoffs, we endowed participants with $30 one week before scanning and told participants that one decision from each of three scanning runs would be honored for real money.

We assessed behavioral sensitivity to gains and losses by fitting a logistic regression to each participant's acceptability judgments collected during scanning, using the size of the gain and loss as independent variables. Based on this analysis, we computed a measure of behavioral loss aversion (λ) as the ratio of the (absolute) loss response to the gain response, which yielded a median λ = 1.93 (range: 0.99 to 6.75). This finding is consistent with the observations that participants were, on average, indifferent to gambles in which the potential gain was twice the amount of the potential loss (Fig. 1B) and that participants were slower to decide whether or not to accept these gambles (Fig. 1C). These behavioral data also accord well with previous studies (1, 5).

We first analyzed the imaging data to identify brain regions whose activation correlated with the size of the potential gain or loss, using parametric regressors (27). This analysis isolated a set of regions responsive to the size of potential gains when evaluating gambles (averaging over levels of loss) (Fig. 2 and fig. S2). The gain-responsive network included regions previously shown to be associated with the anticipation and receipt of monetary rewards, including the dorsal and ventral striatum, VMPFC, ventrolateral PFC, anterior cingulate cortex (ACC), OFC, and dopaminergic midbrain regions. There were no regions that showed decreasing activation as gains increased.

If loss aversion is driven by a negative affective response (e.g., fear, vigilance, discomfort), then one would expect increasing activity in brain regions associated with these emotions as the size of the potential loss increases. Contrary to this prediction, no brain regions showed significantly increasing activation during evaluation of gambles as the size of the potential loss increased (averaging over levels of gain). Instead, a group of brain regions including the striatum, VMPFC, ventral ACC, and medial OFC (most of which also coded for gains) showed decreasing activity as the size of the potential loss increased (Fig. 2 and fig. S3). A conjunction analysis between increasing activity for gains and decreasing activity for losses demonstrated joint sensitivity to both gains and losses in a set of regions including the dorsal and ventral striatum and VMPFC (Fig. 3 and table S4).

In order to ensure that potential loss-related responses were not being obscured by the overall positive expected value of the gambles, we compared activity evoked by the worst possible gambles (gain: $10 to $16; loss: $17 to $20) and the best possible gambles (gain: $34 to $40; loss: $5 to $8). In a whole-brain analysis, there were no regions that showed significantly more activity for the worst gambles as compared to that for the best gambles (corrected $P < 0.05$ for all voxels by means of randomization tests). Given the specific prediction regarding loss-related activity in the amygdala and insula based on previous studies of experienced utility and risk aversion (13–15), we performed further analyses that focused on these areas. Even at a very liberal uncorrected threshold of $P < 0.01$, there were no significant voxels in the amygdala and only two single unconnected voxels in the insula. By comparison, at the same threshold, there were large clusters of activation for the best versus the worst

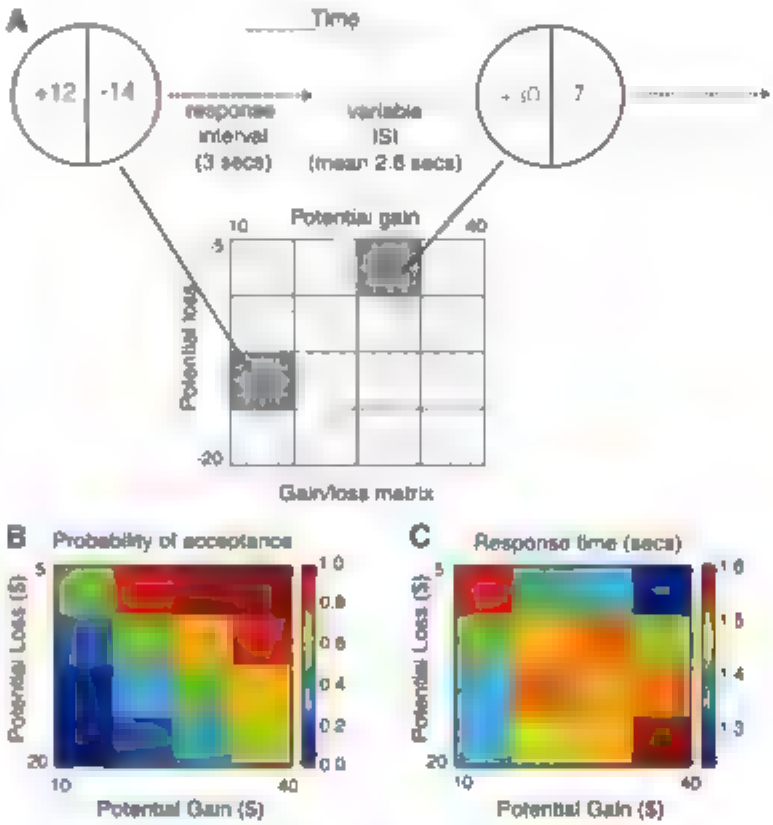

Fig. 1. (**A**) An illustration of the event-related task design. During each trial, the participant was presented for 3 s with a display showing the size of the potential gain (in green) and loss (in red). After the accept or reject response, a variable interval was presented to allow for optimal deconvolution of fMRI responses to each trial (27). Gambles were not resolved during scanning. The values of gain and loss for each trial were sampled from the gain/loss matrix, as shown here for two example gambles; a gamble from each cell in this 16 × 16 matrix was presented during scanning, but the data were collapsed into a 4 × 4 matrix for analysis. All combinations of gains and losses were presented. ISI, interstimulus interval. (**B**) Color-coded heatmap of probability of gamble acceptance at each level of gain/loss (red indicates high willingness to accept the gamble, and blue indicates low willingness to accept the gamble). (**C**) Color-coded heatmap of response times (red indicates slower response times, and blue indicates faster response times).

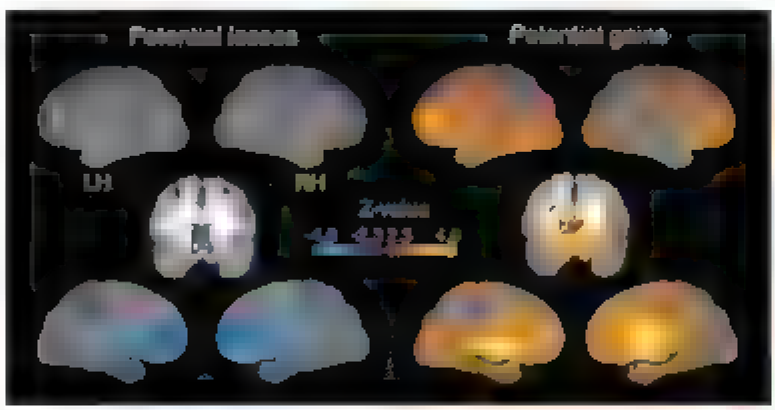

Fig. 2. Whole-brain analysis of parametric responses to size of potential loss (left) or gain (right). Statistical maps were projected onto an average cortical surface with the use of multifiducial mapping in CARET software (28); coronal slices (y = 10) are included to show ventral striatal activation. All maps are corrected for multiple comparisons at the whole-brain level by means of cluster-based Gaussian random field correction (29) at $P < 0.05$. LH, left hemisphere; RH, right hemisphere.

gambles in the ventral striatum and VMPFC. Although null results in fMRI must be interpreted with caution, these results are consistent with the conclusion that losses and gains are coded by the same mechanism rather than by two separate mechanisms. Moreover, this aggregate representation of decision utility appears to be represented by the same neural circuitry that is engaged by a range of experienced rewards (*17*). These results support previous studies showing increased and decreased activity in the striatum for experienced monetary gains and losses, respectively (*7*, *8*).

We next investigated whether individual differences in brain activity during decision-making were related to individual differences in behavior using whole-brain analyses to identify regions where the neural response to gains or losses was correlated with behavioral loss aversion. Unexpectedly, greater behavioral loss aversion was associated with greater neural sensitivity not only to losses but also to gains. For increasing gains, we observed a significant correlation with behavioral loss aversion in the sensorimotor cortex and superior frontal cortex (fig. S4). On the other hand, as potential losses increased, an extensive set of areas showed a more rapidly decreasing response to monetary losses among individuals who were more loss averse (fig. S5). Notably, these regions encompassed many of the areas that showed a parallel decrease in activity with increasing potential loss. The association of decreased behavioral loss aversion with decreased neural responses to both losses and gains during decision-making is consistent with the long-standing notion that some forms of risk taking may have their roots in sensation seeking by individuals who have a diminished physiological response to stimulation (*22*).

Examination of regions of interest in the striatum and VMPFC from the gain-loss conjunction analysis (Fig. 3) revealed that these regions exhibited a pattern of "neural loss aversion": that is, the (negative) slope of the decrease in activity for increasing losses was greater than the slope of the increase in activity for increasing gains in a majority of participants (striatum: loss > gain for 14 out of 16 participants, $P = 0.004$; VMPFC: loss > gain for 13 out of 16 participants, $P = 0.021$). In order to more directly assess the relationship between neural loss aversion and behavioral loss aversion, we performed a whole-brain robust regression analysis with these measures (*23*). This analysis revealed significant correlations between behavioral and neural loss aversion in several regions, including bilateral ventral striatum (Fig. 4), bilateral lateral and superior PFC (pre-supplementary motor area), and right inferior parietal cortex (figs. S6 and S7 and table S2). These results demonstrate that differences in behavior were strongly predicted by differences in neural responses.

The present study replicates the common behavioral pattern of risk aversion for mixed gambles that offer a 50/50 chance of gaining or losing money and shows that this pattern of behavior is directly tied to the brain's greater sensitivity to potential losses than gains. These results provide evidence in favor of one of the fundamental claims of prospect theory (*1*, *2*), namely that the function that maps money to subjective value is markedly steeper for losses than gains [see also (*4*)]. Moreover, mediation analysis (*23*) suggests that individual differences in behavioral loss aversion (as inferred by willingness to accept mixed gambles) are driven primarily by individual differences in neural sensitivity to potential losses. Although the present study focuses on loss aversion in the context of mixed gambles, recent work has found that the coefficient of loss aversion (λ), the ratio of sensitivity to losses versus gains, is highly correlated across risky and riskless contexts (*23*). Therefore, we surmise that a similar mechanism may contribute to other manifestations of loss aversion.

Previous studies have shown that anticipated or experienced losses give rise to activation in regions that have been associated with negative emotions, such as the amygdala or anterior insula (*11*, *17*, *18*). In contrast, the present study demonstrates that, in the context of decision-making, potential losses are represented by decreasing activity in regions that seem to code for subjective value rather than by increasing activity in regions associated with negative emotions. This difference between present and previous results reinforces the importance of distinguishing among experienced, anticipated, and decision utility as economic theories of choice (*15*). It is possible that amygdala engagement for experienced losses reflects negative prediction errors (*11*, *24*) rather than negative value, whereas the lack of immediate outcomes in the present study (which was designed to isolate decision utility) precludes the computation of prediction errors.

The neural basis of decision under risk was investigated in a recent study by De Martino *et al.* (*25*), who found that amygdala activity correlated with choices of risky gambles framed as losses and sure outcomes framed as gains. However, the reflection in risk attitudes when moderate-probability gambles are framed as losses versus gains has been attributed in prospect theory primarily to the reflection in curvature of the value function for losses versus gains (*2*) and secondarily to distortions in probability weighting rather than to loss aversion. In contrast, we asked participants in the present study to evaluate balanced (50/50) gain-loss gambles, which allowed us to isolate the role of loss aversion. Thus, although amygdala activation may play a role in some decisions under risk, it does not appear to be a necessary component in loss aversion.

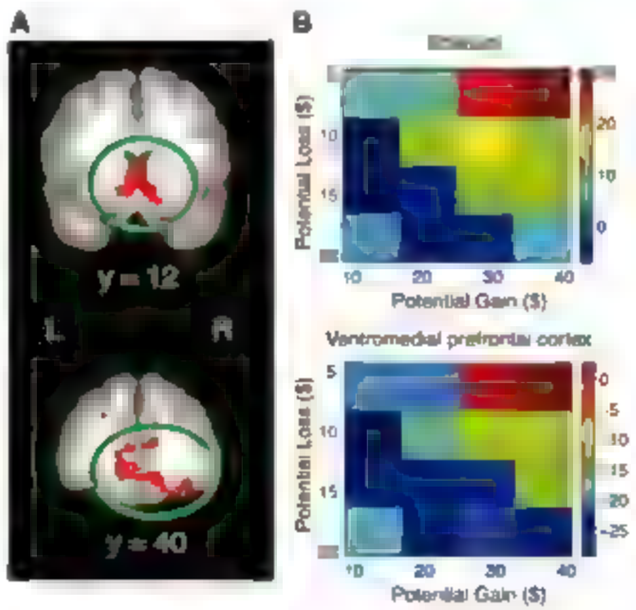

Fig. 3. Conjunction analysis results. (**A**) Map showing regions with conjointly significant positive gain response and negative loss response ($P < 0.05$, whole-brain corrected, in each individual map) (see also table S1). Red pixels indicate regions showing significant conjunction; green circles highlight clusters included in the respective heatmaps to the right. L, left; R, right. (**B**) Heatmaps were created by averaging parameter estimates versus baseline within each cluster in the conjunction map for each of the 16 cells (of 16 gambles each) in the gain/loss matrix; color coding reflects strength of neural response for each condition, such that dark red represents the strongest activation and dark blue represents the strongest deactivation.

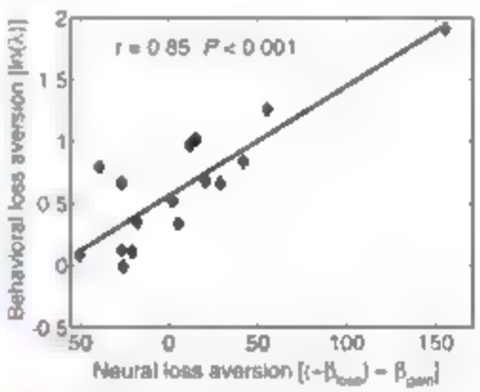

Fig. 4. Scatterplot of correspondence between neural loss aversion and behavioral loss aversion in ventral striatum [Montreal Neurological Institute coordinates (*x*, *y*, *z*): 3.6, 6.3, 3.9; center of gravity in millimeters]. Regression line and *P* value were computed with the use of robust regression by iteratively reweighted least squares to prevent the influence of outliers; however, this regression also remained highly significant ($P = 0.004$) when the extreme data point (top right-hand corner) was removed from the analysis. β_{loss} and β_{gain} are the unstandardized regression coefficients for the loss and gain variables, respectively.

The present results illustrate how neuroimaging can be used to directly test predictions stemming from behavioral theories: in this case, the prediction from prospect theory that risk aversion for mixed gambles can be attributed to enhanced sensitivity to losses. Neural loss aversion was observed throughout, though not strictly limited to, the targets of the mesolimbic and mesocortical dopamine (DA) systems. It is tempting to speculate that individual differences in behavioral and neural loss aversion observed in the present study may be related to naturally occurring differences in DA function. Though the relationship between genetic variation in the DA system and personality traits such as impulsivity and risk taking remains largely unknown (26). Further, the diminished neural sensitivity to losses among individuals who were less loss averse (i.e., more risk seeking) may shed light on a number of neuropsychiatric and behavioral disorders, such as substance abuse, pathological gambling, and antisocial personality disorder that are associated with increased risk taking and impulsive behavior. This suggests that studies integrating methods from behavioral economics and cognitive neuroscience may provide greater insight into the nature of these disorders.

References and Notes

1. A. Tversky, D. Kahneman, *J. Risk Uncert.* **5**, 297 (1992).
2. D. Kahneman, A. Tversky, *Econometrica* **47**, 263 (1979).
3. N. Novemsky, D. Kahneman, *J. Market. Res.* **42**, 119 (2005).
4. M. Rabin, *Econometrica* **68**, 1281 (2000).
5. M. Abdellaoui, H. Bleichrodt, C. Paraschiv, *Management Sci.*, in press; available at http://papers.ssrn.com/sol3/papers.cfm?abstract_id=956613.
6. D. Kahneman, J. Knetsch, R. H. Thaler, *J. Polit. Econ.* **98**, 1325 (1990).
7. S. Benartzi, R. H. Thaler, *Q. J. Econ.* **110**, 73 (1995).
8. B. Hardie, E. Johnson, P. Fader, *Marketing Sci.* **12**, 378 (1993).
9. W. T. Harbaugh, K. Krause, L. Vesterlund, *Econ. Lett.* **70**, 175 (2001).
10. M. K. Chen, V. Lakshminarayanan, L. R. Santos, *J. Polit. Econ.* **114**, 517 (2006).
11. H. C. Breiter, I. Aharon, D. Kahneman, A. Dale, P. Shizgal, *Neuron* **30**, 619 (2001).
12. B. Knutson, C. M. Adams, G. W. Fong, D. Hommer, *J. Neurosci.* **21**, RC159 (2001).
13. M. R. Delgado, H. M. Locke, V. A. Stenger, J. A. Fiez, *Cogn. Affect. Behav. Neurosci.* **3**, 27 (2003).
14. B. Knutson, G. W. Fong, C. M. Adams, J. L. Varner, D. Hommer, *Neuroreport* **12**, 3683 (2001).
15. D. Kahneman, P. P. Wakker, R. Sarin, *Q. J. Econ.* **112**, 375 (1997).
16. C. F. Camerer, *J. Market. Res.* **42**, 129 (2005).
17. I. Kahn *et al.*, *Neuron* **33**, 983 (2002).
18. C. M. Kuhnen, B. Knutson, *Neuron* **47**, 763 (2005).
19. B. Knutson, G. W. Fong, S. M. Bennett, C. M. Adams, D. Hommer, *Neuroimage* **18**, 263 (2003).
20. S. M. McClure *et al.*, *Neuron* **44**, 379 (2004).
21. Materials and methods are available as supporting material on *Science* Online.
22. M. Zuckerman, D. M. Kuhlman, *J. Pers.* **68**, 999 (2000).
23. E. Johnson, S. Gächter, A. Herrmann, "Exploring the nature of loss aversion" [Institute for the Study of Labor (IZA) Discussion Paper No. 2015, Social Science Research Network, 2006]; http://ssrn.com/abstract=897336.
24. J. Yacubian *et al.*, *J. Neurosci.* **26**, 9530 (2006).
25. B. De Martino, D. Kumaran, B. Seymour, R. J. Dolan, *Science* **313**, 684 (2006).
26. E. Congdon, T. Canli, *Behav. Cognit. Neurosci. Rev.* **4**, 262 (2005).
27. A. M. Dale, *Hum. Brain Mapp.* **8**, 109 (1999).
28. D. C. Van Essen, *Neuroimage* **28**, 635 (2005).
29. K. J. Worsley, A. C. Evans, S. Marrett, P. Neelin, *J. Cereb. Blood Flow Metab.* **12**, 900 (1992).

30. This work was supported by NSF DMU-0433693 [R. Poldrack and C. Fox, principal investigators (PIs)] and by NIH P20 R80020750 (R. Bilder, PI). The authors thank A. Aron, R. Bilder, M. Frank, A. Galvan, M. Geoghegan, E. Johnson, M. Lieberman, R. Razzada, and E. Stover for helpful comments; K. Preacher for assistance with mediation analysis; and A. Satpute and J. Cohen for assistance in data collection.

Supporting Online Material

www.sciencemag.org/cgi/content/full/315/5811/515/DC1
Materials and Methods
Figs. S1 to S7
Tables S1 and S2
References

23 August 2006; accepted 12 December 2006
10.1126/science.1134239

Asymmetric Inheritance of Mother Versus Daughter Centrosome in Stem Cell Division

Yukiko M. Yamashita,[1]*† Anthony P. Mahowald,[2] Julie R. Perlin,[1] Margaret T. Fuller[1,3]†

Adult stem cells often divide asymmetrically to produce one self-renewed stem cell and one differentiating cell, thus maintaining both populations. The asymmetric outcome of stem cell divisions can be specified by an oriented spindle and local self-renewal signals from the stem cell niche. Here we show that developmentally programmed asymmetric behavior and inheritance of mother and daughter centrosomes underlies the stereotyped spindle orientation and asymmetric outcome of stem cell divisions in the *Drosophila* male germ line. The mother centrosome remains anchored near the niche while the daughter centrosome migrates to the opposite side of the cell before spindle formation.

Adult stem cells maintain populations of highly differentiated but short-lived cells throughout the life of the organism. To maintain the critical balance between stem cell and differentiating cell populations, stem cells have a potential to divide asymmetrically, producing one stem and one differentiating cell (*1*). The asymmetric outcome of stem cell divisions can be specified by regulated spindle orientation, such that the two daughter cells are placed in different microenvironments that either specify stem cell identity (stem cell niche) or allow differentiation (*2*, *3*).

Drosophila male germline stem cells (GSCs) are maintained through attachment to somatic hub cells, which constitute the stem cell niche. Hub cells secrete the signaling ligand Upd, which activates the Janus kinase signal transducer and activator of transcription (JAK-STAT) pathway in the neighboring germ cells to specify stem cell identity (*4*, *5*). *Drosophila* male GSCs normally divide asymmetrically, producing one stem cell which remains attached to the hub, and one gonialblast, which initiates differentiation. This stereotyped asymmetric outcome is controlled by the orientation of the mitotic spindle in GSCs. The spindle lies perpendicular to the hub so that one daughter cell inherits the attachment to the hub, whereas the other is displaced away (*6*).

The stereotyped orientation of the mitotic spindle is set up by the positioning of centrosomes during interphase (Fig. 1A) (*6*). GSCs remain oriented toward the niche throughout the cell cycle. In G_1 phase, the single centrosome is located near the interface with the hub. When the duplicated centrosomes separate in G_2 phase, one stays next to the hub, whereas the other migrates to the opposite side of the cell. Centrosomes in the GSCs separate unusually early in interphase, rather than at the G_2-prophase transition, so it is common to see GSCs with fully separated centrosomes without a spindle (of >500 GSCs in the 0- to 3-day-old males counted, ~40% of the GSCs had two centrosomes that were separated to opposite sides of the cell, but no spindle was yet assembled) (*6*).

Differences between the mother and daughter centrosomes underlie the stereotyped behavior of the centrosomes in *Drosophila* male GSCs. The mother centrosome normally remains anchored to the hub-GSC interface and is inherited by the GSC, whereas the daughter centrosome moves away from the hub and is inherited by the cell that commits to differentiation. Mother and daughter centrosomes were differentially

[1]Department of Developmental Biology, Stanford University School of Medicine, Stanford, CA 94305–5329, USA. [2]Department of Molecular Genetics and Cell Biology, University of Chicago, Chicago, IL 60637, USA. [3]Department of Genetics, Stanford University School of Medicine, Stanford, CA 94305–5329, USA.

*Present address: Life Sciences Institute, Room 5403, University of Michigan, Ann Arbor, 210 Washtenaw Avenue, Ann Arbor, MI 48183-2216, USA.

†To whom correspondence should be addressed. E-mail: yukikomy@umich.edu (Y.M.Y.); fuller@stanford.edu (M.T.F.)

labeled by transient expression of green fluorescent protein pericentrin-AKAP450 C-terminus (GFP-PACT) from the *Drosophila* pericentrin-like protein (7) under heat shock Gal4 control (8). The PACT domain, which is necessary and sufficient for centriolar localization, is incorporated into centrioles only during centrosome duplication and does not exchange with the cytoplasmic pool (7). Both the mother and daughter centrosomes are labeled by GFP-PACT in the first cell cycle after heat shock (fig. 1B). In the second cell cycle, the daughter centrosome retains GFP-PACT, whereas the mother centrosome is not labeled, thus distinguishing the mother and daughter centrosomes (fig. 1B). After a short burst of GFP-PACT expression induced by a 2.5-hour heat shock, 70 to 80% of the GSCs had GFP-labeled centrosomes, indicating the duplication of centrosomes during the window of GFP-PACT expression. By 2 hours after heat shock, ~90% of the labeled GSCs had two GFP-positive centrosomes, indicating that they had progressed to the G_2 phase of the first cell cycle after GFP-PACT incorporation (fig. 1, C and E).

By 18 to 24 hours after heat shock, the number of GSCs with two GFP-positive centrosomes had decreased, whereas the number of GSCs with one GFP-positive and one GFP-negative centrosome had increased, suggesting progression into the second cell cycle. Generally, the centrosome distal to the hub was labeled, whereas the centrosome proximal to the hub was GFP-negative. GSCs in the second cell cycle (fig. 1, D and E), indicating that the daughter centrosomes migrate away from the hub-GSC interface during asymmetric GSC divisions.

Labeling the mother rather than the daughter centrosomes confirmed that stem GSCs in the niche preferentially retain mother centrosomes over time. Centrioles assembled during early embryogenesis were labeled using the NGT40 Gal4 driver to drive the expression of GFP-PACT in [illegible] stage embryos, shortly after germband extension (9). In the first cell cycle after the depletion of the cytoplasmic pool of GFP-PACT in the GSCs, both the mother and daughter centrosomes should be labeled. In subsequent cell cycles, only the mother centrosomes should be labeled (fig. 2A).

In most GSCs in the second or later cell cycle after the depletion of cytoplasmic GFP-PACT, the labeled centrosome was positioned next to the hub-GSC interface, and the unlabeled centrosome had moved away from the hub (fig. 2, B and C). The frequency of GSCs that had the proximal, but not distal, centrosome labeled remained constant over time (at 0 days (L3 larvae) to day 7 adults), suggesting that the mother centrosomes are reliably retained by the GSCs, even through multiple rounds of GSC divisions. Some GSCs maintained cytoplasmic GFP-PACT, especially in L3 larvae, suggesting that the GFP-PACT had not yet been diluted out (fig. 2C, green column). We also observed some GSCs with two labeled centrosomes, suggesting that they are in the first cell cycle after the depletion of cytoplasmic GFP-PACT (fig. 2C, red columns).

The mother centrosomes in GSCs appeared to maintain robust interphase microtubule arrays. Ultrastructural analysis of the GSCs revealed that the centrosome proximal to the hub was commonly associated with many microtubules throughout the cell cycle. Nineteen centrosomes in GSCs were scored in serial sections of the apical tips of five wild-type testes. Eleven centrosomes were localized close to the adherens junctions between the hub and the GSCs. Nine of these proximal centrosomes appeared to be in interphase cells, based on nuclear morphology and microtubule arrangement. Typically, these interphase centrosomes proximal to the hub were associated with numerous microtubules (fig. 3A and fig. S4A). In some samples, microtubules appeared to extend from centrosomes toward the adherens junctions (fig. 3A, arrowheads). One of the two proximal centrosomes appeared to be in cells in mitotic prophase (fig. S1B), based on

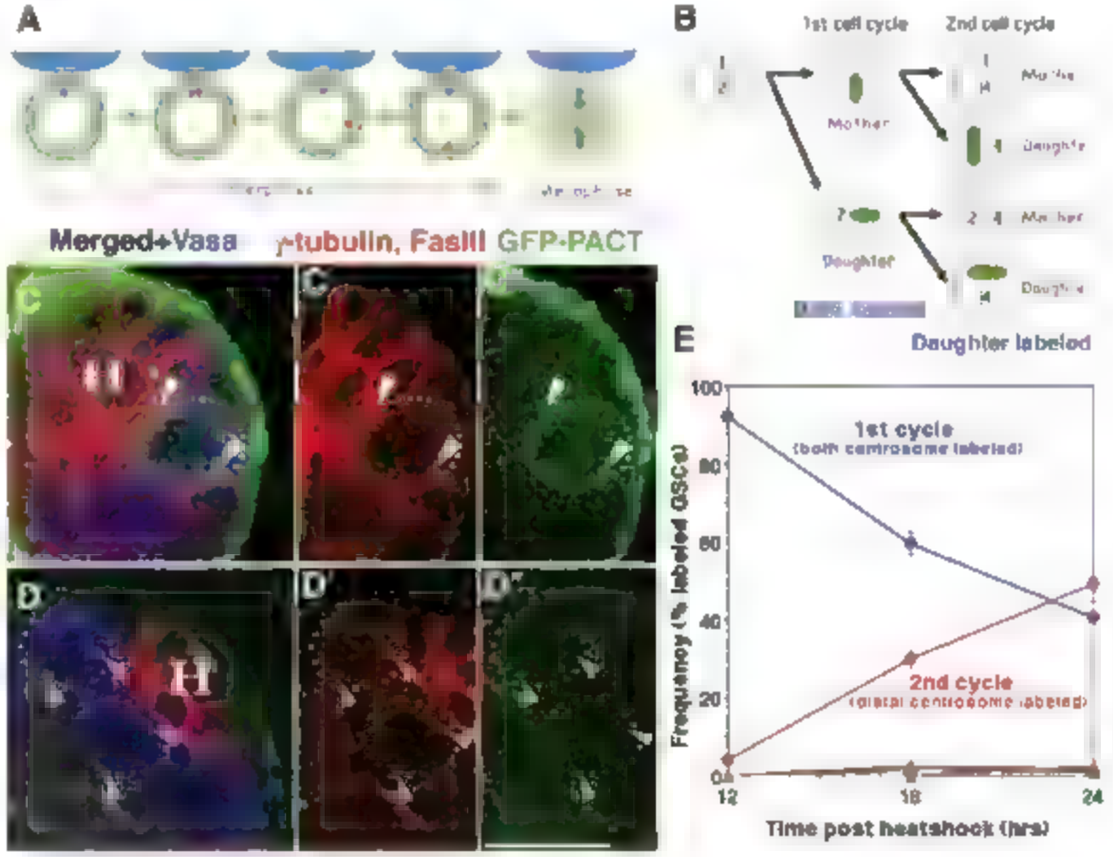

Fig. 1. GFP-labeled daughter centrosomes migrate away from the niche. **(A)** Stereotyped positioning of centrosomes in male GSC during interphase sets up the orientation of the mitotic spindle [adapted from (6)]. Red, centrosome; blue, hub; green, tubulin. **(B)** Pulse-chase strategy to label the daughter centrosome. Each centrosome (circle) contains two centrioles (ovals numbered in order of generation). Transient expression of GFP-PACT labels newly assembled centrioles (3). In the first cell cycle after the GFP-PACT pulse, both the mother (1+3) and daughter (2+3) centrosomes are GFP-positive. In the second cell cycle, the mother centrosomes (1+4 or 2+4) are GFP-negative whereas the daughter centrosomes (3+4) are GFP-positive. **(C** and **D)** Testis tips with labeled GSCs (dotted outline) in the G_2 phase of the first cell cycle after the GFP-PACT pulse [(C), 12 hours after heat shock] or the second cell cycle [(D), 24 hours after heat shock]. Green, GFP-PACT; red, γ-tubulin (centrosomes are shown with arrowheads) and Fas III (hub, H); blue, Vasa (germ cells). Scale bar, 10 μm. **(E)** Frequency of label outcomes over time after heat shock. Blue, GSCs in the first cell cycle (two labeled, oriented centrosomes); red, GSCs in the second cell cycle (one labeled and one unlabeled centrosome) with the labeled (daughter) centrosome distal from the hub. Rarely observed outcomes were pink, the first cell cycle, with neither centrosome next to the hub; black, the second cell cycle, with the mother centrosome distal to the hub; green, the second cell cycle, with neither centrosome next to the hub. Only those GSCs that had two centrosomes, with one or both centrosomes labeled with GFP-PACT, were counted.

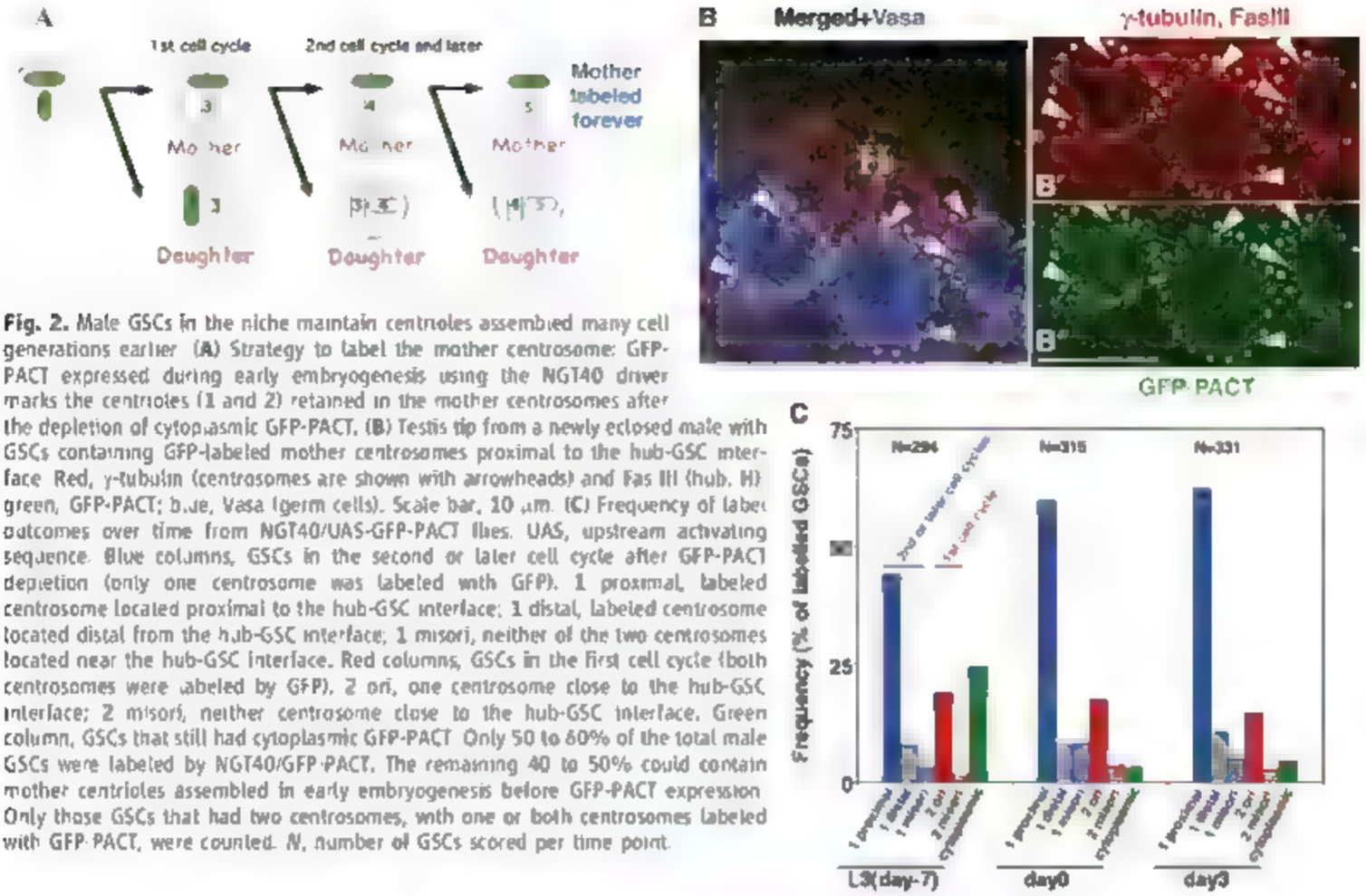

Fig. 2. Male GSCs in the niche maintain centrioles assembled many cell generations earlier. (**A**) Strategy to label the mother centrosome: GFP-PACT expressed during early embryogenesis using the NGT40 driver marks the centrioles (1 and 2) retained in the mother centrosomes after the depletion of cytoplasmic GFP-PACT. (**B**) Testis tip from a newly eclosed male with GSCs containing GFP-labeled mother centrosomes proximal to the hub-GSC interface. Red, γ-tubulin (centrosomes are shown with arrowheads) and Fas III (hub, H); green, GFP-PACT; blue, Vasa (germ cells). Scale bar, 10 μm. (**C**) Frequency of label outcomes over time from NGT40/UAS-GFP-PACT flies. UAS, upstream activating sequence. Blue columns, GSCs in the second or later cell cycle after GFP-PACT depletion (only one centrosome was labeled with GFP). 1 proximal, labeled centrosome located proximal to the hub-GSC interface; 1 distal, labeled centrosome located distal from the hub-GSC interface; 1 misori, neither of the two centrosomes located near the hub-GSC interface. Red columns, GSCs in the first cell cycle (both centrosomes were labeled by GFP). 2 ori, one centrosome close to the hub-GSC interface; 2 misori, neither centrosome close to the hub-GSC interface. Green column, GSCs that still had cytoplasmic GFP-PACT. Only 50 to 60% of the total male GSCs were labeled by NGT40/GFP-PACT. The remaining 40 to 50% could contain mother centrioles assembled in early embryogenesis before GFP-PACT expression. Only those GSCs that had two centrosomes, with one or both centrosomes labeled with GFP-PACT, were counted. *N*, number of GSCs scored per time point.

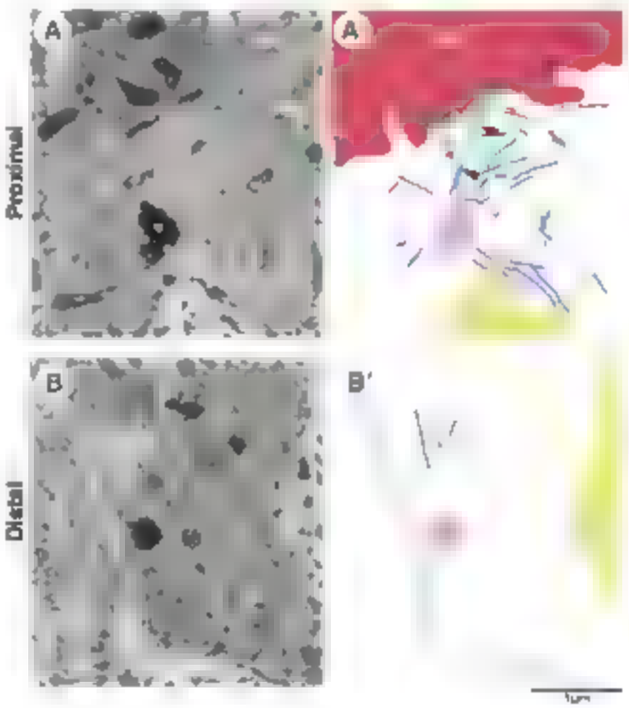

Fig. 3. Centrosomes next to the hub harbor robust microtubule arrays. (**A**) Electron micrograph and (**A'**) summary diagram of a proximal centrosome in a GSC. Arrowheads in (A') show a microtubule that runs from the centrosome to the adherens junction. (**B**) Electron micrograph and (**B'**) summary diagram of a distal centrosome in a GSC. Red, hub; blue, microtubules; green, adherens junctions; yellow, nucleus; pink, centriole; gray in (B'), plasma membrane. Scale bar, 1 μm.

their robust microtubule arrays containing bundled microtubules running parallel to or piercing the nuclear surface.

In contrast, of the five distal centrosomes in the apparently interphase cells that were scored, four had few associated microtubules (Fig. 3B and fig. S1C). The remaining three distal centrosomes appeared to be in cells in mitotic prophase based on microtubule arrays containing bundled microtubules (fig. S1D). Thus, the mother centrosomes may maintain interphase microtubule arrays that anchor them to the hub-GSC interface, whereas the daughter centrosomes may initially have few associated microtubules and be free to move, establishing a robust microtubule array only later in the cell cycle.

Consistent with the idea that astral microtubules anchor the mother centrosomes to the hub-GSC interface, mother- versus daughter centrosome positioning was randomized in GSCs that were homozygous mutant for *centrosomin* (*cnn*) (*8*), an integral centrosomal protein required to anchor astral microtubules to centrosomes (*10*, *12*). Analysis of mother and daughter centrosomes after transient expression of GFP-PACT revealed that, in *cnn* homozygous mutant GSCs where one of the two centrosomes was positioned next to the hub, it was essentially random whether the mother or the daughter centrosome stayed next to the hub (Fig. 4). In addition, in ~25% of total labeled GSCs, neither of the two centrosomes was next to the hub, which is consistent with our previous observations (Fig. 4) (*6*).

Our results indicate that the two centrosomes in *Drosophila* male GSCs have different characters and fates. The mother centrosome stays next to the junction with the niche and is associated by the cell that self-renews stem cell fate. Thus, GSCs can maintain an old centriole

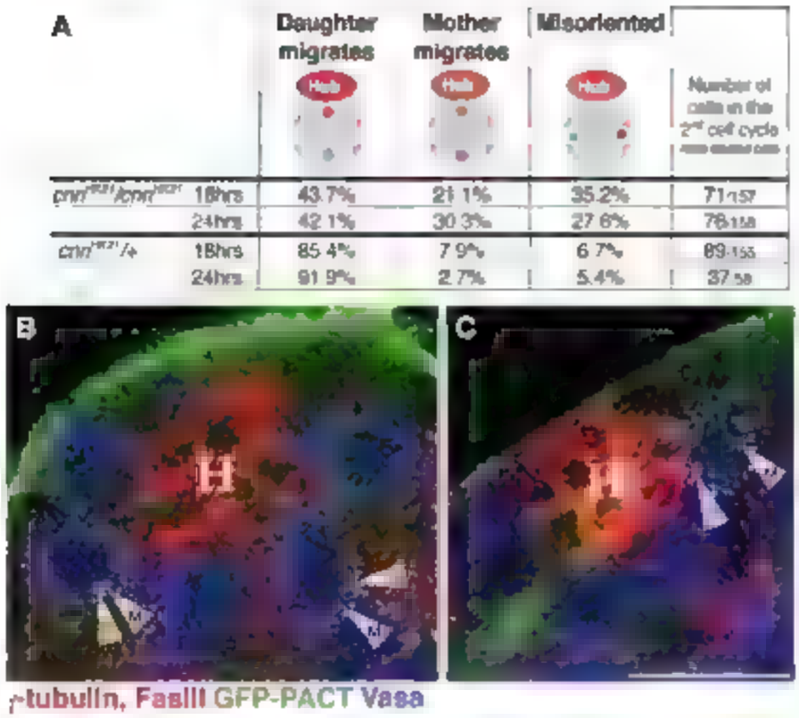

Fig. 4. *cnn* is required for nonrandom segregation of mother and daughter centrosomes. (**A**) Summary of the centrosome-positioning pattern in cnn^{HK21} homozygous mutant and control cnn^{HK21}/+ GSCs. Daughter centrosomes were labeled by a pulse of GFP-PACT as in Fig. 1B. Only counts of cells in the second cell cycle are shown. (**B** and **C**) Testis tips from *cnn* mutants with GSCs in the second cell cycle with misoriented centrosomes (B) or with the mother rather than the daughter centrosome segregated to the opposite side of the GSC (C). Red, γ-tubulin [centrosomes are shown with arrowheads (M, mother; D, daughter)] and Fas III (hub; H); green, GFP-PACT; blue, Vasa (germ cells). Scale bar, 10 μm.

assembled many cell generations earlier. In contrast, the daughter centrosome migrates away from the niche and is inherited by the cell that will initiate differentiation. We postulate that the mother centrosomes in male GSCs may remain anchored to the GSC-niche interface throughout the cell cycle by attachment to astral microtubules connected to the adherens junction, whereas the daughter centrosomes may initially have few associated microtubules and thus can move away from the niche. Microtubule-dependent differential segregation of mother and daughter spindle-pole bodies (equivalent to centrosomes in higher organisms) is observed in budding yeast (*17*). In cultured vertebrate cells, the centrioles mature slowly over the cell cycle, and the mother centrosomes [containing a mature centriole] attach astral microtubules more effectively and are more stationary than daughter centrosomes in interphase (*14*). The unusually early separation of centrosomes in interphase male GSCs may provide a way to move the daughter centrosome out of range of the stabilizing influence of the adherens junction complex before it becomes competent to hold a robust microtubule array.

Developmentally programmed anchoring of the mother centrosome may provide a key mechanism to ensure the stereotyped orientation of the mitotic spindle and thus the reliably asymmetric outcome of the male GSC divisions. Although it is tempting to speculate that determinants associated with the mother or daughter centrosome may play a role in specifying stem cell or differentiating-cell fates, such determinants are yet to be identified. Rather, the asymmetric inheritance of mother and daughter centrosomes in male GSCs may be a consequence of the cytoskeletal mechanisms that are imposed as part of the stem cell program to anchor one centrosome next to the niche throughout the interphase, ensuring a properly oriented spindle.

References and Notes

1. S. J. Morrison, J. Kimble, *Nature* **441**, 1068 (2006).
2. A. Spradling, D. Drummond-Barbosa, T. Kai, *Nature* **414**, 98 (2001).
3. F. M. Watt, B. L. M. Hogan, *Science* **287**, 1427 (2000).
4. A. A. Kiger, D. L. Jones, C. Schulz, M. B. Rogers, M. T. Fuller, *Science* **294**, 2542 (2001).
5. N. Tulina, E. Matunis, *Science* **294**, 2546 (2001).
6. Y. M. Yamashita, D. L. Jones, M. T. Fuller, *Science* **301**, 1547 (2003).
7. M. Martinez-Campos, R. Basto, J. Baker, M. Kernan, J. W. Raff, *J. Cell Biol.* **165**, 673 (2004).
8. Materials and methods are available as supporting material on *Science* Online.
9. W. D. Tracey Jr., X. Ning, M. Klingler, S. G. Kramer, J. P. Gergen, *Genetics* **154**, 273 (2000).
10. E. L. Megraw, L. R. Kao, T. C. Kaufman, *Curr. Biol.* **11**, 116 (2001).
11. D. Vazquez-Ohayon, E. D. Schejter, *Curr. Biol.* **9**, 889 (1999).
12. E. L. Megraw, K. Li, L. R. Kao, T. C. Kaufman, *Development* **126**, 2829 (1999).
13. G. Pereira, T. U. Tanaka, K. Nasmyth, E. Schiebel, *EMBO J.* **20**, 6359 (2001).
14. M. Piel, P. Meyer, A. Khodjakov, C. L. Rieder, M. Bornens, *J. Cell Biol.* **149**, 317 (2000).

15. We thank the Bloomington Stock Center, the Developmental Studies Hybridoma Bank, and R. Lehmann for reagents; the Stanford Cell Science Imaging Facility for assistance in microscopy; Fuller lab members for comments; the Jose Carreras International Leukemia Foundation for a fellowship to Y.M.Y.; and NIH for grant R01 DK53074 to M.T.F.

Supporting Online Material

www.sciencemag.org/cgi/content/full/315/5811/518/DC1
Materials and Methods
Fig. S1
References

8 September 2006; accepted 22 November 2006
10.1126/science.1134910

Kinetics of Morphogen Gradient Formation

Anna Kicheva,[1,2]* Periklis Pantazis,[1]*† Tobias Bollenbach,[3]*‡ Yannis Kalaidzidis,[1,4] Thomas Bittig,[3] Frank Jülicher,[3]§ Marcos González-Gaitán[1,2]§

In the developing fly wing, secreted morphogens such as Decapentaplegic (Dpp) and Wingless (Wg) form gradients of concentration providing positional information. Dpp forms a longer-range gradient than Wg. To understand how the range is controlled, we measured the four key kinetic parameters governing morphogen spreading: the production rate, the effective diffusion coefficient, the degradation rate, and the immobile fraction. The four parameters had different values for Dpp versus Wg. In addition, Dynamin-dependent endocytosis was required for spreading of Dpp, but not Wg. Thus, the cellular mechanisms of Dpp and Wingless spreading are different. Dpp spreading requires endocytic, intracellular trafficking.

Although the molecular and cellular mechanisms controlling morphogen transport have received much attention, many questions remain open (*1*–*3*). This might be due in part to the existence of only a few quantitative studies of the steady-state gradients and the kinetics of morphogen transport. To address this, we studied quantitatively two key morphogens during development of the fly wing: Decapentaplegic (Dpp) and Wingless (Wg).

Dpp is produced at the anterior-posterior compartment boundary in the center of the wing imaginal disc of *Drosophila* (*8*) (Fig. 1, A and B). Dpp spreads nondirectionally, is degraded while spreading, and forms a gradient of concentration in the plane of the wing epithelium (*2*, *7*). Regardless of the actual transport mechanism, these facts imply that Dpp spreading can be captured by the physics of molecules that are produced in a localized source, which generates a current J_0 [molecules/(μm × s)] at the source boundary, that are degraded with a rate k (s^{-1}), and that spread in a nondirectional manner with an effective diffusion coefficient D ($\mu m^2/s$). Thus, the rate of change of Dpp concentration in the x-y plane, $C(x,y,t)$, is described by the equation

$$\partial C/\partial t = D\nabla^2 C - kC + 2J_0\delta(x) \quad (1)$$

where x is linear distance to the source in the target tissue, ∇^2 is the Laplace operator, and $\delta(x)$ is the Dirac delta function [see supporting online material (SOM)].

The steady-state solution for Eq. 1 is a single exponential gradient

$$C(x) = C_0 e^{-x/\lambda} \quad (2)$$

where the Dpp concentration $C(x)$ depends only on the distance x from the source, the concentration C_0 at the source boundary, and the decay length λ. The decay length corresponds to the distance at which the concentration decays by a factor $1/e$ of C_0 [$C(x) = C_0(1/e)$ at $x = \lambda$]. The shape of the gradient therefore depends on two key parameters, λ and C_0, which are determined by D, k, and J_0.

In the scenario of nondirectional morphogen spreading with degradation, λ in the steady state is related to the diffusion coefficient and the degradation rate by the expression

$$\lambda = \sqrt{D/k} \quad (3)$$

In turn, C_0 depends on the current J_0 and on diffusion and degradation, which occur both in the receiving tissue and in the source

$$C_0 = J_0\sqrt{D/k} \quad (4)$$

Indeed, the experimental Dpp distribution in the target tissue was well described by a single exponential (Fig. 1C) [correlation index R^2 = 0.97 ± 0.05 (n = 76) with a decay length λ = 29.2 ± 5.7 μm, corresponding to 7.7 ± 2.1 cells (see materials and methods section in SOM)].

To measure the kinetic parameters (D, k, and J_0) that determine the steady-state shape (characterized by λ and C_0) of the Dpp gradient, we developed an experimental strategy based on imaging a functional green fluorescent protein Dpp fusion (GFP-Dpp) produced at the endogenous wing source (*2*) and fluorescence recovery after photobleaching (FRAP) (*9*, *10*). The FRAP assay consisted of irreversibly photobleaching the GFP-Dpp fluorescence in a rectangular region of interest (ROI) with dimensions 10 μm by 200 μm adjacent to the source (Fig. 1, D to K). Subsequently, we monitored the fluorescence recovery in the ROI for about 60 min, which occurred at the expense of the nonbleached GFP-Dpp molecules in the neighboring areas, until the fluorescence intensity was close to a steady state (Fig. 1L). To quantify the recoveries, we imaged and projected five confocal planes encompassing the most apical 5 μm of the epithelium and measured the average fluorescence intensity of GFP-Dpp in the ROI (see materials and methods and fig. S3).

We first controlled several conditions: (i) we limited photodamage and photobleaching during imaging so that they were negligible, (ii) we imaged most of the GFP-Dpp molecules in the tissue, (iii) we estimated the detection inaccuracy, and (iv) we calibrated detection of fluorescence intensity to GFP-Dpp concentration by using GFP-tagged nanotrap particles (*11*). These important controls are summarized in section 2 of the supporting online material and in figs. S1 and S2. After verification of these conditions, we

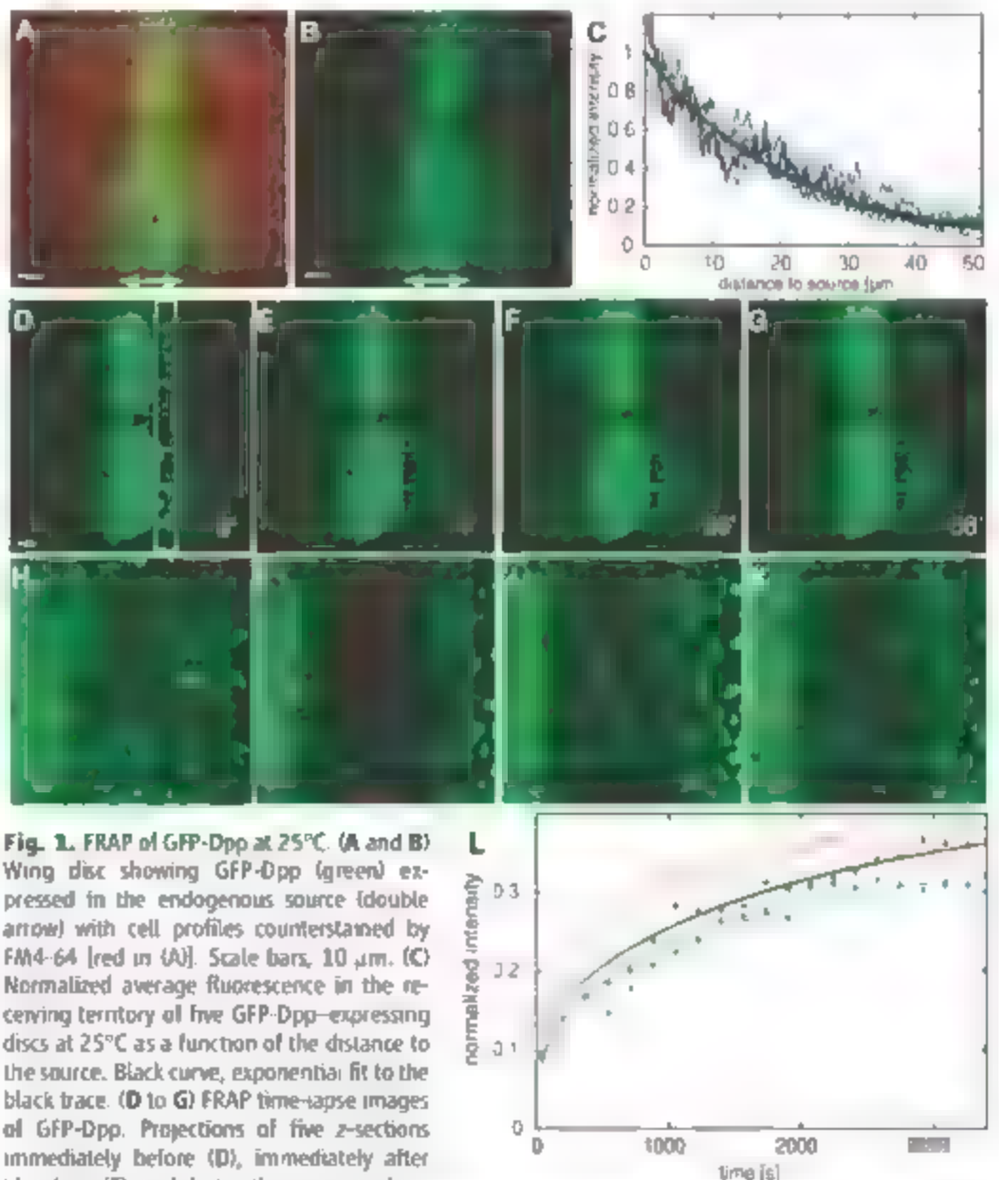

Fig. 1. FRAP of GFP-Dpp at 25°C. (**A** and **B**) Wing disc showing GFP-Dpp (green) expressed in the endogenous source (double arrow) with cell profiles counterstained by FM4-64 [red in (A)]. Scale bars, 10 μm. (**C**) Normalized average fluorescence in the receiving territory of five GFP-Dpp–expressing discs at 25°C as a function of the distance to the source. Black curve, exponential fit to the black trace. (**D** to **G**) FRAP time-lapse images of GFP-Dpp. Projections of five z-sections immediately before (D), immediately after bleaching (E), and during the recovery phase (F and G). Scale bar, 10 μm. Times (1, 26, 58) indicate minutes after the start of the experiment. White box, ROI. Blue boxes are magnified in (H to K). (**L**) FRAP recovery curves for four GFP-Dpp experiments at 25°C. Theoretical curves (solid lines) are fit to normalized average fluorescence intensities in the ROI (squares and crosses). Anterior, left. Genotype: *dppGal4::UAS-GFP-Dpp/+*

*Max Planck Institute of Molecular Cell Biology and Genetics, Pfotenhauer Strasse 108, 01307 Dresden, Germany. †Department of Biochemistry and Department of Molecular Biology, Geneva University Sciences II, Quai Ernest-Ansermet 30, 1211 Geneva 4, Switzerland. ‡Max Planck Institute for the Physics of Complex Systems, Nöthnitzer Strasse 38, 01187 Dresden, Germany. §A. N. Belozersky Institute for Physico-Chemical Biology, Moscow State University, Moscow 119899, Russia.

¶These authors contributed equally to this work.
#Present address: California Institute of Technology, Pasadena, CA 91125, USA.
‡Present address: Department of Systems Biology, Harvard Medical School, Boston, MA 02115, USA.
§To whom correspondence should be addressed. E-mail: pfeutcher@pks.mpg.de (F.J.); marcos.gonzalez@biochem.unige.ch (M.G.-G.)

used our calibrations to estimate the concentration of GFP-Dpp at the source boundary C_0 (802 ± 312 molecules/μm² (n = 8 discs), which corresponds to 4379 ± 1741 molecules per cell (see materials and methods). In addition, we estimated the fraction of "extracellular" GFP-Dpp, which was equal to or smaller than 15 ± 4% (n = 8 discs) of the total pool. The latter measurement, together with the fact that our detection inaccuracy was less than 2%, showed that the extracellular pool was not a dominant pool (section 2 of SOM).

We then studied the recovery profiles in the FRAP experiments to determine D, k, v_0, as well as the immobile fraction w. w is the fraction of molecules that did not recover in the ROI during the experiment. The standard procedure (*12*) to solve the diffusion equation, which neglects production and degradation and is commonly used in FRAP studies of single cells (*13*), is not suitable for our FRAP assay in tissues. The time span of recovery in tissue FRAP was 30 to 90 min (Fig. 1L), so that production and degradation could not be neglected. Thus, we solved Eq. 1 for the particular geometry and conditions of our FRAP experiments in the tissue (SOM, fig. S3D).

From the resulting time-dependent concentration profile $C(x,t)$ (fig. S3D), we calculated the average concentration $I(t)$ in the ROI as a function of time. We optimized the two parameters D and v_0, which determine the shape of this theoretical recovery curve, to obtain the best agreement with the experimental curves (see SOM). The parameters k and v_0 were not independent, because we measured two key quantities before bleaching that impose further constraints: (i) the decay length λ, which allows us to determine k from the fitted D via Eq. 3, $\lambda = \sqrt{D/k}$, and (ii) the concentration at the source boundary C_0, which enabled us to determine j_0 via Eq. 4, $C_0 = j_0\sqrt{D/k}$. The resulting theoretical curves were in excellent agreement with the experimental recovery data (R^2 = 0.95 ± 0.03) (see also table S1), which provided sufficient constraints to confidently determine the actual values of D and w. Thus, analysis of the experimental recovery curves, together with Eqs. 3 and 4, allowed us to determine the kinetic parameters D, k, j_0, and v of morphogen spreading.

The effective diffusion coefficient of GFP-Dpp was D = 0.10 ± 0.05 μm²/s (n = 8 experiments). This number is about three orders of magnitude less than the coefficient of free diffusion in water of molecules with the size of the mature Dpp homodimer [similar to that of GFP, which has D = 87 μm²/s (*14*)], but consistent with a restricted diffusion of Dpp in the extracellular space [e.g., hindered by binding to immobile extracellular matrix molecules or membrane receptors (*15*–*17*)] and/or endocytosis plus recycling of Dpp through a fast recycling pathway (*18*). Dpp was degraded at a rate k = 2.3 × 10⁻⁴ s⁻¹ (*19*), or 10⁻³ s⁻¹ corresponding to a GFP-Dpp half-life of about 45 min, which is consistent with the turnover time of Dpp molecules in the developing wing determined biochemically (*7*). In addition, the majority of the GFP-Dpp molecules in the target tissue were immobile or moved very slowly (v = 62 ± 5 nm/s, i.e., with recovery kinetics too slow compared with the 60-min time scale of the FRAP experiments. Thus immobile pool was stored in intracellular compartments, because the extracellular pool was equal to or smaller than 15% of the total pool. We found j_0 = 3.98 ± 2.34 molecules/(μm × s), which implies that the Gal4-driven GFP-Dpp production rate from the endogenous source was v = 2.69 ± 1.58 molecules per cell per second. The effective production rate v per cell with diameter a can be obtained from j_0 by $v \approx 2a^2 j_0/w$ for small values of the width of the source w (μm) (*3*).

We tested the validity of the diffusion and degradation description for the FRAP recoveries by performing FRAP experiments in different geometries (fig. S4 and table S1). The results of these experiments were consistent with the independence of the four kinetic parameters on position in the tissue (see SOM).

After studying the GFP-Dpp kinetics, we analyzed the dependence of gradient formation on endocytosis by performing the FRAP assay in animals where the target tissue was mutant for the thermosensitive *shibire*^{ts1} allele and in which the source was rescued by a functional *shibire* transgene ["shibire-rescue" animals, see materials and methods and (*21*)]. The role of endocytosis has previously been studied using shibire-rescue animals in qualitative assays (*1*, *3*) (SOM and fig. S5). The FRAP assay allowed us to determine separately D, k, v, and w in each experimental condition and to measure sensitively the kinetic effects in conditions of partial or complete endocytic block in the wing. *shibire*^{ts1} is a tight temperature-sensitive mutant at 34°C but leaky at 32°C (*2*) (fig. S5). In addition, during the FRAP experiment, the effects could be detected immediately after only a few minutes of block. In control animals, D, k, v, and w were not significantly different at 25°C, 32°C, and 34°C (figs. S6 and S7). In shibire-rescue animals, which were raised at the permissive temperature, the

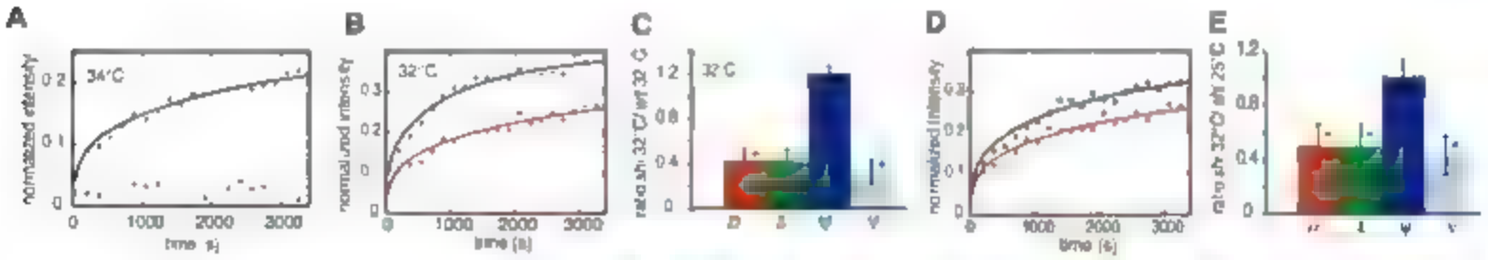

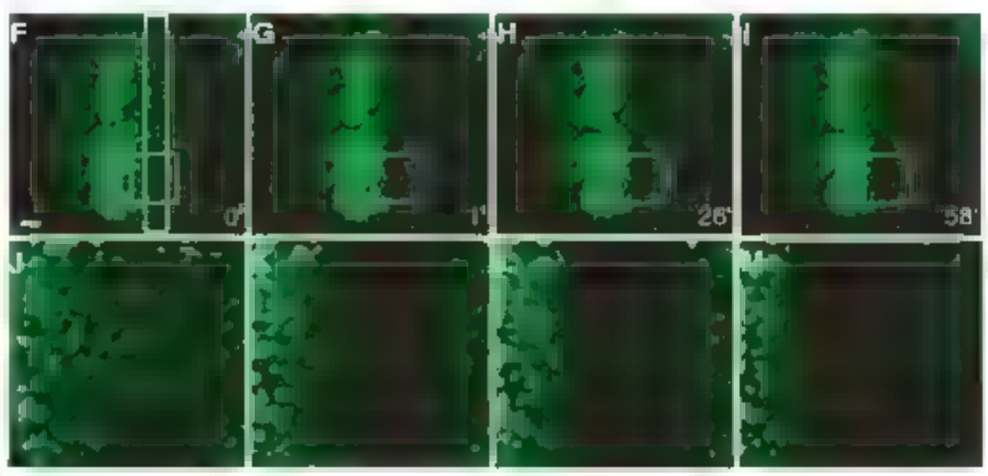

Fig. 2. GFP-Dpp shibire-rescue FRAP assay at 32°C and 34°C. (**A** and **B**) FRAP recovery curves of GFP-Dpp (black) and GFP-Dpp shibire rescue (red) at 34°C (A) and 32°C (B). Genotypes: *dppGal4/+;UAS-GFP-Dpp/+* and *shi*^{ts1}*; UAS-Dynamin*$^{+}$*/+; UAS-GFP-Dpp/ dppGal4*. (**C**) Average D, k, v_0, and v from seven GFP-Dpp shibire-rescue experiments at 32°C normalized to the respective averages at 32°C in GFP-Dpp (wild-type control). Error bars, SEM. Asterisks, statistically significant differences between shibire rescue and wild-type at 32°C (double-sided $P < 0.05$). (**D**) GFP-Dpp shibire rescue at 25°C (black) and 32°C (red). (**E**) Average D, k, v_0, and v from eight GFP-Dpp shibire-rescue experiments at 32°C normalized to the respective average in GFP-Dpp shibire rescue at 25°C. Asterisks, statistically significant differences. (**F** to **M**) FRAP time-lapse images of GFP-Dpp shibire rescue at 34°C as in Fig. 1, D to K.

tight endocytic block at 34°C during the FRAP experiment impaired Dpp spreading completely, and no recovery could be detected into the ROI (Fig. 2, A and F to M). When the block was released by shifting the temperature down to 25°C, fluorescence recovered into the ROI which indicated that the effect was reversible and that the lack of recovery was not due to unspecific tissue damage (fig. S8).

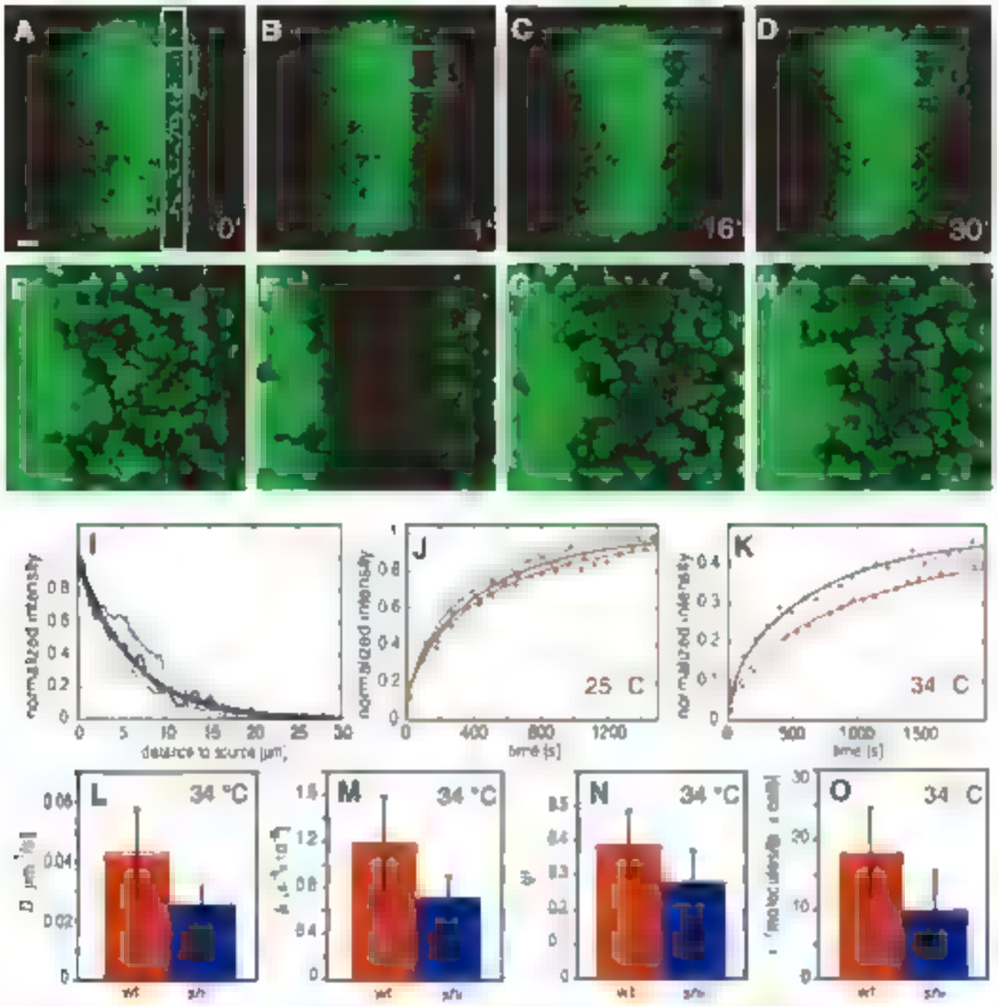

Fig. 3. FRAP of GFP-Wingless and GFP-Wingless shibire rescue. (**A** to **H**) FRAP time-lapse images of GFP-Wg expressed in the wing Dpp domain. Boxes and times as in Fig. 1, D to K. Genotype: *UAS-GFP-wingless/+; dppGal4/+*. Scale bar, 10 µm. (**I**) Normalized average fluorescence in the receiving territory of five Wg expressing discs at 25°C as a function of the distance to the source. Black curve, exponential fit to the black trace. (**J**) Four FRAP recovery traces of GFP-Wingless at 25°C. (**K**) GFP-Wingless (black) and GFP-Wingless shibire-rescue at 34°C (red). Genotypes: *UAS GFP-wingless/+; dppGal4/+* and shi^{ts1}; *UAS-Dynamin*$^{+}$; *UAS GFP-wingless; dppGal4/+*. (**L** to **O**) Average *D*, *k*, ω, and ν from GFP-Wingless (red; $n = 9$) and GFP-Wingless shibire-rescue experiments at 34°C (blue; $n = 10$). Error bars, SEM. The differences are not statistically significant for any of the four parameters considered.

which indicated that the effect was reversible and that the lack of recovery was not due to unspecific tissue damage (fig. S8).

This lack of recovery after blocking endocytic uptake was imposed could be due to decreased diffusion or increased degradation rate. Because no recovery was observed, a theoretical curve could not be fitted to determine the actual values of the kinetic parameters. Thus, we studied the recoveries under conditions of partial block of endocytosis at 32°C. At 32°C, the diffusion coefficient in shibire-rescued animals decreased by a factor of more than 2 compared with that of control animals at 32°C (Fig. 2, B and C) and with shibire-rescued animals at the permissive temperature 25°C (Fig. 2, D and E, and table S1). The degradation rate was not increased, but decreased by a factor of about 2. Finally, the production rate was also affected, whereas ω was not (see materials and methods). Thus endocytosis is required not only for Dpp degradation, but also for Dpp movement.

It is worth noting here that (i) given our imprecision of measurement (2%; see SOM), the minimal recovery we would have been able to detect is 2% of the total pool (fig. S2, E to G), excluding the possibility that we might have missed a significant extracellular recovery, (ii) other morphogens did recover in this FRAP shibire-rescue assay, which excludes an artifact of the treatment as causing the lack of recovery (see below), (iii) the observed effects of endocytic block were acute because the lack of recovery was observed after a few minutes of block, and (iv) the endocytic block was reversible.

To explore whether this kinetic description of Dpp applied to other morphogens, we performed the same FRAP analysis for another secreted ligand, Wingless (Wg) (Fig. 3, A to H, and J). In order to compare Wg and Dpp, we expressed a functional GFP-Wingless fusion (*19*) at the endogenous Dpp source, instead of the endogenous source region of Wg in wild type (Fig. 3, A to D). Wg also moves in the tissue nondirectionally and is degraded, but had a different profile (Fig. 3I). The Dpp gradient is a long-range gra-

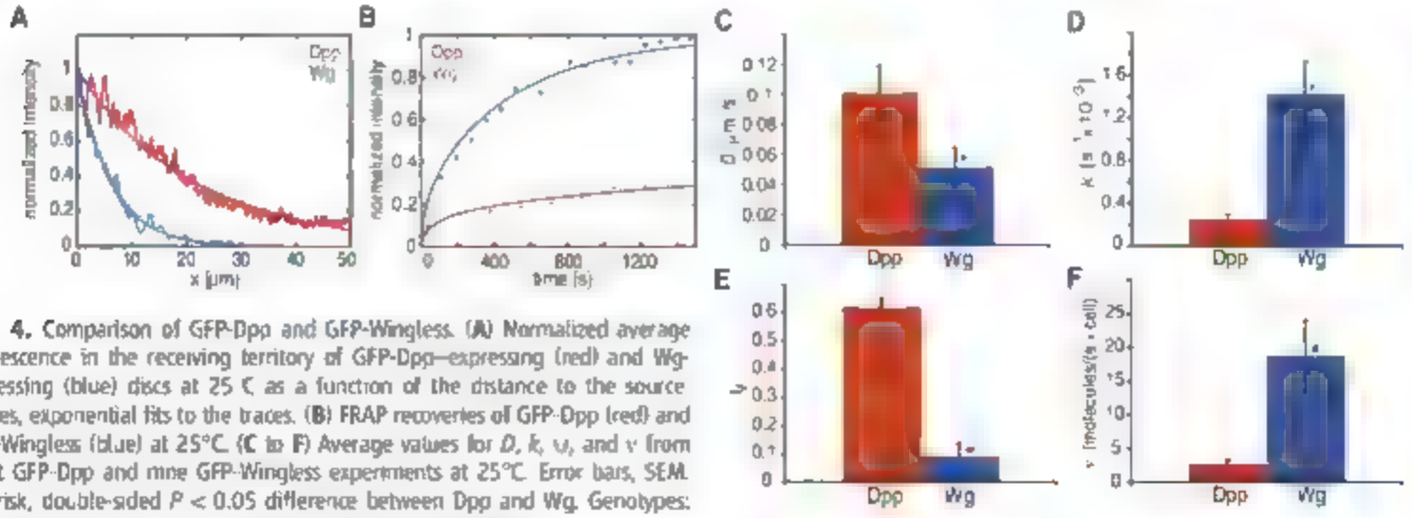

Fig. 4. Comparison of GFP-Dpp and GFP-Wingless. (**A**) Normalized average fluorescence in the receiving territory of GFP-Dpp–expressing (red) and Wg-expressing (blue) discs at 25°C as a function of the distance to the source. Curves, exponential fits to the traces. (**B**) FRAP recoveries of GFP-Dpp (red) and GFP-Wingless (blue) at 25°C. (**C** to **F**) Average values for *D*, *k*, ω, and ν from eight GFP-Dpp and nine GFP-Wingless experiments at 25°C. Error bars, SEM. Asterisk, double-sided $P < 0.05$ difference between Dpp and Wg. Genotypes: *dppGal4::UAS-GFP-Dpp/+* and *UAS-GFP-wingless/+; dppGal4/+*.

dient with decay length $\lambda = 20.2$ μm, whereas, in these in vivo conditions, Wg made a short-range gradient with $\lambda = 5.8 \pm 2.04$ μm (Figs. 3I and 4A). Which kinetic parameter could account for this difference? Because Dpp and Wg have inherently different properties—Wg is a lipid-modified molecule (*20*); Dpp is not (*21*)—they are likely to display different mechanisms and kinetics of spreading through the epithelium.

The shorter decay length of the Wingless gradient was due to a higher degradation rate of GFP-Wingless, by a factor of 5, and to a lesser extent its smaller diffusion coefficient (Fig. 4). Although the Gal4 driver was the same in the Dpp and Wg experiments, the production rate of Wg was about seven times that of Dpp, which implied that their maturation and secretion were controlled differently. In addition, while 62% of the Dpp molecules were immobile, the Wg pool was almost fully mobile at 25°C ($\psi = 9.2 \pm 13\%$), although, unlike Dpp, a significant immobile fraction appeared at higher experimental temperatures (Fig. 3, K and N). The different immobile fractions of Dpp and Wg at 25°C validated the specificity of the Dpp immobile fraction. Thus, the immobile fraction was not an artifact of incomplete recovery in sick cells. Finally, in contrast to Dpp, Wg transport and degradation were independent of Dynamin endocytosis (Fig. 3, K to O). Indeed, Wg movement has been suggested to be Dynamin-independent (*6*, *22*). In addition, expression of dominant-negative Dynamin and of long-term thermosensitive *shibire* block caused an extension of the gradient in the wing ($\lambda = 22 \pm 3$ μm), which was attributed to decreased degradation (*5*, *22*). Our FRAP approach studying the results of an acute block suggests that endocytosis is not required for Wg transport and degradation or, alternatively, that endocytosis of Wg is Dynamin-independent.

Altogether, the GFP-Wingless FRAP experiments (i) validated our FRAP assay and shibire^{ts} rescue experiment, (ii) indicated that different morphogen gradients can be generated by independently fine-tuning D, k, v, and ψ, and (iii) showed that different morphogens may use different mechanisms of transport and cellular machineries (e.g., Dynamin-dependent versus Dynamin-independent transport) to achieve the formation of morphogen gradients.

References and Notes

1. F. Y. Belenkaya *et al.*, *Cell* **119**, 231 (2004).
2. E. V. Entchev, A. Schwabedissen, M. González-Gaitán, *Cell* **103**, 981 (2000).
3. K. Kruse, P. Pantazis, T. Bollenbach, F. Jülicher, M. González-Gaitán, *Development* **131**, 4843 (2004).
4. A. D. Lander, Q. Nie, F. Y. Wan, *Dev. Cell* **2**, 785 (2002).
5. E. Piddini, F. Marshall, L. Dubois, E. Hirst, J.-P. Vincent, *Development* **132**, 5479 (2005).
6. M. Strigini, S. M. Cohen, *Curr. Biol.* **10**, 293 (2000).
7. A. A. Teleman, S. M. Cohen, *Cell* **103**, 971 (2000).
8. K. Basler, G. Struhl, *Trends Genet.* **10**, 187 (1994).
9. J. Lippincott-Schwartz, N. Altan-Bonnet, G. H. Patterson, *Nat. Cell Biol.* **5** (suppl.), 57 (2003).
10. G. Carrero, D. McDonald, E. Crawford, G. de Vries, M. J. Hendzel, *Methods* **29**, 14 (2003).
11. A. Charpilienne *et al.*, *J. Biol. Chem.* **276**, 29361 (2001).
12. D. Axelrod, D. E. Koppel, J. Schlessinger, E. Elson, W. W. Webb, *Biophys. J.* **16**, 1055 (1976).
13. J. Ellenberg, J. Lippincott-Schwartz, *Methods* **19**, 362 (1999).
14. R. Swaminathan, C. P. Hoang, A. S. Verkman, *Biophys. J.* **72**, 1900 (1997).
15. G.-H. Baeg, E. M. Selva, R. M. Goodman, R. Dasgupta, N. Perrimon, *Dev. Biol.* **276**, 89 (2004).
16. C. Han, D. Yan, T. Y. Belenkaya, X. Lin, *Development* **132**, 667 (2005).
17. T. Lecuit, S. M. Cohen, *Development* **125**, 4901 (1998).
18. J. Klingauf, E. T. Kavalali, R. W. Tsien, *Nature* **394**, 581 (1998).
19. S. Pfeiffer, S. Ricardo, J. B. Manneville, C. Alexandre, J. P. Vincent, *Curr. Biol.* **12**, 957 (2002).
20. K. Willert *et al.*, *Nature* **423**, 448 (2003).
21. J. Greppe *et al.*, *J. Biol. Chem.* **273**, 29052 (1998).
22. E. S. Seto, H. J. Bellen, *J. Cell Biol.* **173**, 95 (2006).
23. A. F. Ames, K. M. Rochlin, M. Wehrli, S. L. Schwartz, S. DiNardo, *Dev. Biol.* **293**, 268 (2006).

24. We thank J.-P. Vincent and A. Charpilienne for reagents, C. P. Heisenberg and E. Entchev for critical reading of the manuscript, as well as all members of the M.G.-G. and F.J. groups. This work was supported by the Max Planck Society, Deutsche Forschungsgemeinschaft, Volkswagen Stiftung, the European Union, and the Human Frontier Science Program.

Supporting Online Material

www.sciencemag.org/cgi/content/full/315/5811/521/DC1
Materials and Methods
SOM Text
Figs. S1 to S8
Table S1
Movies S1 to S3

2 October 2006; accepted 6 December 2006
10.1126/science.1135774

A "Silent" Polymorphism in the *MDR1* Gene Changes Substrate Specificity

Chava Kimchi-Sarfaty,*† Jung Mi Oh,†‡ In-Wha Kim, Zuben E. Sauna, Anna Maria Calcagno, Suresh V. Ambudkar, Michael M. Gottesman†

Synonymous single-nucleotide polymorphisms (SNPs) do not produce altered coding sequences, and therefore they are not expected to change the function of the protein in which they occur. We report that a synonymous SNP in the *Multidrug Resistance* 1 (*MDR1*) gene, part of a haplotype previously linked to altered function of the *MDR1* gene product P-glycoprotein (P-gp), nonetheless results in P-gp with altered drug and inhibitor interactions. Similar mRNA and protein levels, but altered conformations, were found for wild-type and polymorphic P-gp. We hypothesize that the presence of a rare codon, marked by the synonymous polymorphism, affects the timing of cotranslational folding and insertion of P-gp into the membrane, thereby altering the structure of substrate and inhibitor interaction sites.

The *MDR1* gene product, the adenosine triphosphate (ATP) binding cassette (ABC) transporter ABCB1 or P-gp, is an ATP-driven efflux pump contributing to the pharmacokinetics of drugs that are P-gp substrates and to the multidrug resistance of cancer cells (*1*, *2*). To date, more than 50 single-nucleotide polymorphisms (SNPs) have been reported for *MDR1* (www.ncbi.nlm.nih.gov/SNP/GetHtmlSnp.cgi?geneId=5243). One of these, a synonymous SNP in exon 26 (C3435T), was sometimes found to be associated with altered P-gp activity (*3*–*6*) and, when it appears in a haplotype, with reduced functionality (*7*). This association may be explained in different ways. Perhaps it is because C3435T is in linkage disequilibrium with other common functional nonsynonymous polymorphisms such as G2677T. In fact, the C1236T (a synonymous SNP), G2677T, and C3435T polymorphisms are part of a common haplotype (*8*, *9*). Another possible explanation is that allele-specific differences in mRNA folding could influence splicing, processing, or translational control and regulation (*10*, *11*). A third possibility is that the effect of the C3435T polymorphism on the levels of cell surface P-gp activity or its function is rather modest or drug-specific. Finally, numerous environmental factors are known to affect the expression and phenotypic activity of P-gp (*12*).

To determine whether the C3435T polymorphism actually does affect P-gp activity, we expressed wild-type and polymorphic P-gps in HeLa cells with the use of a transient expression system (*13*). The same experiments were carried out on BSC-1 (epithelial cells of African green monkey kidney origin), Vero-76 (monkey kidney cells), and 12E1 (CEM human cells) cell lines (*14*), with similar results, indicating that this phenomenon is not specific to HeLa cells.

Laboratory of Cell Biology, Center for Cancer Research, National Cancer Institute, Bethesda, MD 20892, USA.

*Present address: Center for Biologics Evaluation and Research, Food and Drug Administration, 29 Lincoln Drive, Room 316, Bethesda, MD 20892, USA.

†To whom correspondence should be addressed. E-mail: mgottesman@nih.gov (M.M.G.); jmoh@snu.ac.kr (J.M.O.); kimi@cber.fda.gov (C.K.-S.)

‡Present address: College of Pharmacy, Seoul National University, Seoul 151-742, South Korea.

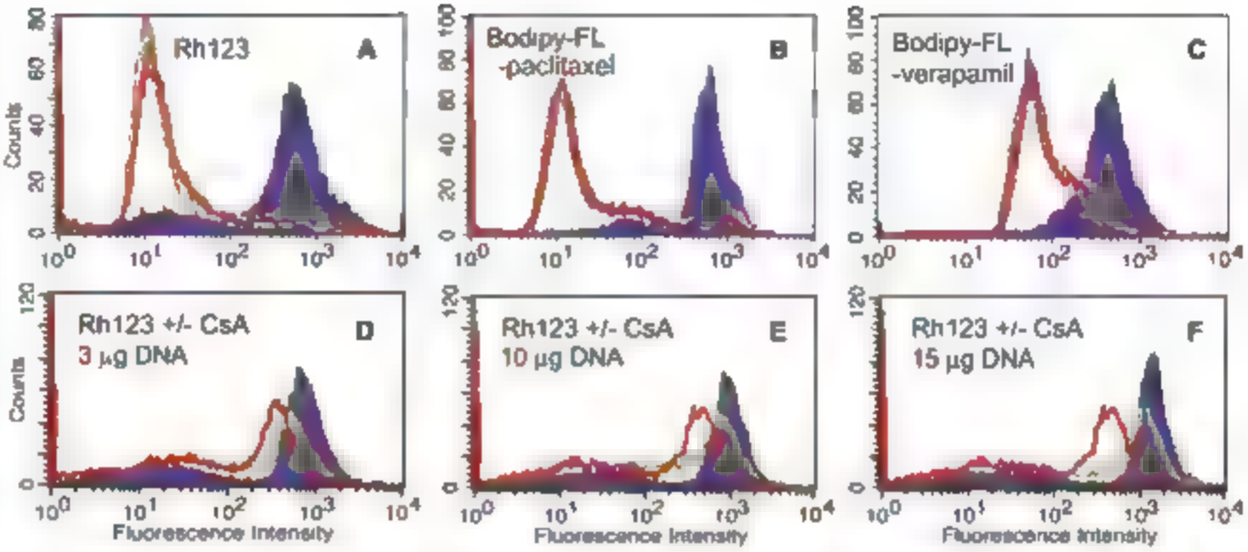

Fig. 1. Drug transport function of wild-type MDR1 and seven MDR1 SNPs and haplotypes. The drug efflux from vaccinia virus infected-transfected HeLa cells was determined by FACS analysis. Cells were transfected with pTM1 (control, purple) pTM1-*MDR1* (wild-type P-gp; green), C1236T (pink), G2677T (lavender), C3435T (orange), C1236T-G2677T (blue), C1236T-C3435T (yellow), G2677T-C3435T (light blue), and C1236T-G2677T-C3435T (red) (**A**, 0.5 μM Rh123; (**B**) 0.1 μM bodipy-FL-paclitaxel; (**C**) 0.5 μM bodipy-FL-verapamil. (**D** to **F**) Effect of plasmid DNA concentration during infection/transfection on Rh123 efflux (0.5 μM) in the presence of an inhibitor (10 μM CsA, infected/transfected DNA; (D) 3 μg; (E) 10 μg; (F) 15 μg.

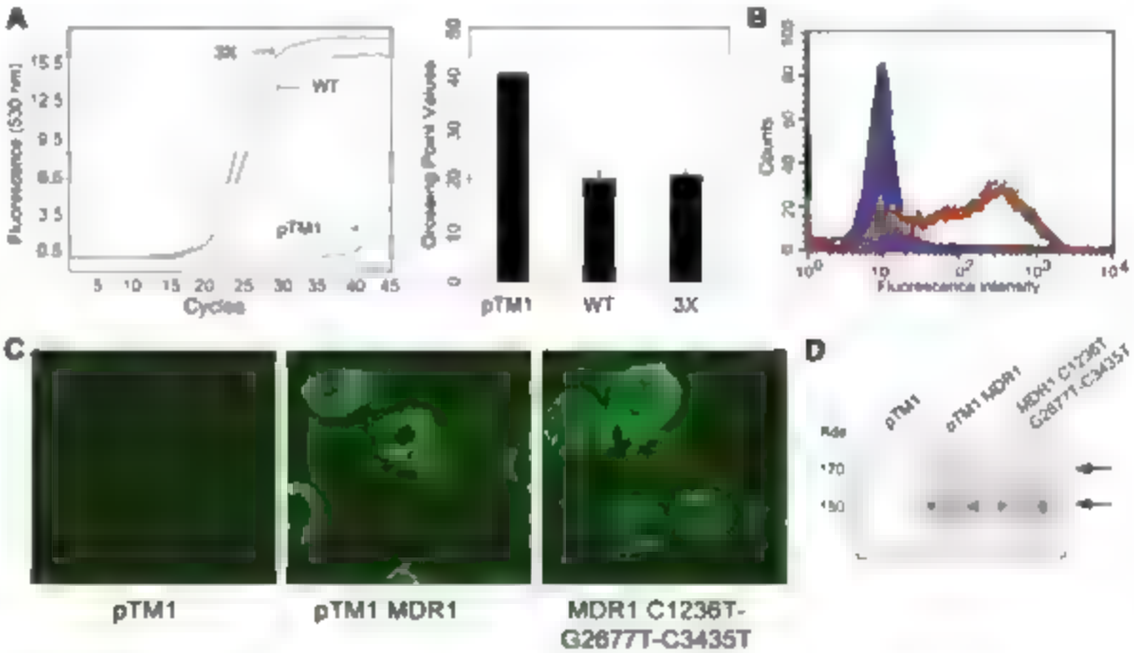

Fig. 2. mRNA levels and P-gp expression in the vaccinia expression system. (**A**) Analysis of pTM1 only, wild-type *MDR1*, and the haplotype C1236T-G2677T-C3435T (3X) with real-time quantitative RT-PCR. Crossing-point values for the graph on the left are plotted in the histogram. (**B**) Assessment of cell surface expression, using MRK16 mAb of all nine constructs as described in Fig. 1. (**C**) Confocal assessment of MDR1 expression, using MRK16 mAb with fluorescein isothiocyanate–conjugated secondary antibody of pTM1 (control, left panel), pTM1-MDR1 (wild-type P-gp; middle panel), and C1236T-G2677T-C3435T (right panel). (**D**) Immunoblot analysis of pTM1 only, wild-type MDR1, and the haplotype C1236T-G2677T-C3435T (2 μg protein/lane) with C219 mAb (*14*). The mature fully glycosylated (~170 kD) and immature P-gp bands (~150 kD) are marked by arrows (*19*).

Assays for P-gp's transport function with the fluorescent substrates Rhodamine 123 (Rh123), bodipy-FL-paclitaxel, bodipy-FL-verapamil, daunorubicin, bodipy-FL-prazosin, and calcein-AM (*13*, *15*) were performed on HeLa cells expressing the MDR1 wild-type, polymorphisms (C1236T, G2677T, or C3435T), and haplotypes consisting of these polymorphisms in various combinations (C1236T-G2677T, C1236T-C3435T, G2677T-C3435T, and C1236T-G2677T-C3435T). The functions of P-gp for all single-nucleotide polymorphisms as well as for wild-type MDR1 as measured by intracellular accumulation of efflux of fluorescent compounds were not significantly altered under substrate concentrations (*13*). HeLa cells expressing double and triple haplotypes' mutants also revealed results similar to those for the single mutants (fig. S1A) (*13*). However, the P-gp inhibitors cyclosporin A (CsA) and verapamil (fig. S1) were less effective against all the substrates in cells expressing the double or triple haplotypes carrying C3435T relative to the wild-type, the SNP-only or the haplotype that does not carry C3435T. This is not the presence of the nonsynonymous polymorphism G2677T that results in the phenotype, but rather the presence of C3435T in combination with one or two of the other polymorphisms.

We next tested to see whether these differences correlated with the concentrations of transfected plasmid DNA. The expression and function of all transfected cells were measured by fluorescence-activated cell sorter (FACS) with MRK16 monoclonal antibody (mAb) staining and by Rh123 in the presence of CsA, respectively (*14*). The differences in inhibition by CsA and Rh123 between the cells expressing wild-type MDR1 and the haplotype (C1236T-G2677T-C3435T) were more distinct as the concentration of the DNA increased (Fig. 1, D to F). These data suggest that the differences were more pronounced at higher levels of mRNA where more P-gp was being translated in the cells. The expression levels of P-gp from the various plasmid-transfected vaccinia cells or human adrenal glands were found to be comparable (fig. S2).

Figure S1, C to F, shows that the haplotypes including C3435T have altered susceptibility to verapamil but not to rhodamine (fig. S1, C to F). When the cells were incubated with the inhibitors before adding the fluorescent substrates, as opposed to simultaneous incubation with the drugs, the same pattern was observed. Bodipy-FL-verapamil is a substrate for P-gp, and the haplotype (C1236T-G2677T-C3435T) exhibited different

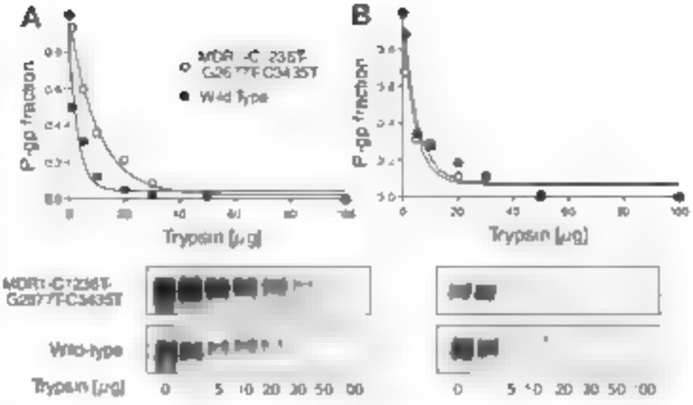

Fig. 3. Determining the sensitivity of wild-type and the haplotype C1236T-G2677T-C3435T P-gp to trypsin. Crude membranes prepared from vTF7-3 infected/transfected HeLa cells expressing wild-type MDR1 or the haplotype C1236T G2677T C3435T were treated with increasing concentrations of trypsin and the disappearance of the P-gp band was quantified as described above. (**A**) Experiment performed in the absence of verapamil; IC_{50} = 2.1 μg (wild type), 7.1 μg (C1236T-G2677T-C3435T). The mature (170 kD) and immature (150 kD) P-gp bands were also analyzed separately. IC_{50} = 0.68 μg (wild-type immature), 2.9 μg (haplotype immature), 2.8 μg (wild-type mature), 10.8 μg (haplotype mature). (**B**) Same experiment in the presence of 30 μM verapamil; IC_{50} = 3.7 μg (wild type), 3.3 μg (C1236T-G2677T-C3435T). Values for the mature and immature P-gp bands. (IC_{50} = 2.5 μg (wild-type immature), 2.5 μg (haplotype immature), 3.6 μg (wild-type mature), 3.2 μg (haplotype mature). Immunoblots with C219 mAb are shown at the bottom.

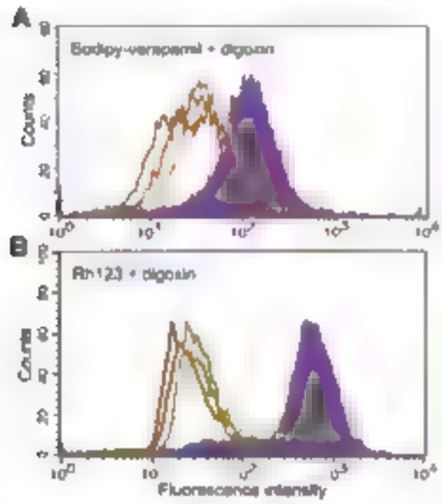

Fig. 4. Drug transport function of wild-type and two MDR1 haplotypes. The drug efflux of vaccinia infected/transfected HeLa cells was determined by FACS analysis (*14*). Cells were transfected with pTM1 (control, purple), MDR1, (wild-type P-gp, green), C1236T-G2677T-C3435T (red), and C1236T-G2677T-C3435A (brown). (**A**) 0.5 μM bodipy-FL-verapamil in the presence of 500 μM digoxin; (**B**) 0.5 μM Rh123 in the presence of 150 μM digoxin.

accumulations in a concentration-dependent manner, suggesting a change in affinity (fig. S3).

Synonymous SNPs or mutations can cause inactivation of the native splicing donor site which results in a premature stop codon (*16*) or exon skipping, yielding a shorter mRNA. A previous report indicated that the polymorphism C3435T resulted in decreased levels of mRNA expression (*17*). We therefore compared mRNA levels (*14*) in the wild-type and haplotype (C1236T-G2677T-C3435T) with the use of real-time quantitative reverse transcription polymerase chain reaction (RT-PCR), which revealed equivalent mRNA levels (Fig. 2A). Western blots using C219 mAb showed comparable total cell expression of P-gp, and the infected transfected cells expressed the same levels of P-gp as determined by FACS assays and immunohistochemical staining with MRK16 mAb (Fig. 2, B and C). This result was reproduced in different cell lines including BSC-1, Vero-76, and 12E1 (fig. S4). The complete amino acid sequence of MDR1 haplotype C1236T-G2677T-C3435T protein was identical to the predicted sequence.

We hypothesized that a conformation difference between wild-type and haplotype P-gp might explain these results. Indeed, UIC2 (*18*), a conformation-sensitive mAb, alone or in combination with CsA or vinblastine at 37°C, revealed pronounced differences in binding consistent with altered conformations in the haplotype (fig. S5) (*18*). To determine whether there are subtle differences in the folding of wild-type and haplotype P-gp, we compared their relative susceptibility to trypsin. Figure 3 shows the disappearance of the P-gp band as a function of trypsin concentration. The concentration required for 50% degradation (IC_{50}, here expressed as μg trypsin) was greater for haplotype P-gp than for wild-type P-gp by a factor of about 3.4, this result implies that the two have slightly different tertiary structures. Both wild-type and haplotype P-gps had comparable IC_{50} (μg trypsin) values in the presence of verapamil, which suggests that the altered conformation can be corrected by drug interaction with P-gp. The immature, core-glycosylated form of P-gp (150-kD band) was more sensitive to trypsin than the mature, glycosylated form, consistent with (*19*), by a factor of 5. However, the ratios (wild-type/haplotype) of the IC_{50} (μg trypsin) values were comparable for the mature and immature bands (3.86 μg versus 4.4 μg). Thus, it is unlikely that altered glycosylation is responsible for the functional differences observed.

The use of rare codons appears to influence the translation rate, which in turn affects protein folding (*20*–*25*), with the third base in the codon having the largest effect (*26*). We hypothesize that as the cell produces more P-gp (Fig. 1, D to F), the role of codon usage may become more critical when certain tRNA species become depleted. The codon usage for the SNP at position 12 1236 with GGC changed to GGT (both encode Gly) changes from 34% [relative synonymous codon usage (RSCU), 22.4] to 16% (RSCU, 10.8). The SNP at position 21 2677 that changes GCT (Ala) to TCT (Ser) also uses a less common codon (26% to 18%, RSCU values change from 18.5 to 15.1). The SNP at position 26 3435 that changes the codon from ATC (Ile) to ATT (Ile) reduces the codon usage from 47% to 35% (RSCU values change from 20.9 to 15.8). Clusters of rare codon usage (table S1) occur both upstream and downstream of each of these SNPs. Codon usage rates are similar in humans and monkeys, which explains the similarity in the results with all transduced cells (*27*).

To test whether codon usage compromises P-gp function, we introduced C3435A (isoleucine codon usage for ATA is 18%, RSCU, 7.4) to produce the haplotype C1236T-G2677T-C3435A. Functional assays using bodipy-verapamil or Rh123 in the presence of digoxin (Fig. 4, A and B) showed even larger decreases in inhibitor effects between this haplotype and the common haplotype C1236T-G2677T-C3435T. Moreover, use of Rh123 in the presence of fexofenadine revealed median fluorescence of 26.9 for the wild-type, 24.3 for C1236T-G2677T-C3435T, and 20.3 for C1236T-G2677T-C3435A. The median fluorescence in the presence of pachysandra and fexofenadine was 38.2 for the wild type, 28.6 for C1236T-G2677T-C3435T, and 22.9 for C1236T-G2677T-C3435A.

The amino acid sequence of proteins is generally believed to determine protein expression, folding, and function; mutations that alter the primary structure of a protein can affect these properties. The important question addressed by this study is the role of silent mutations (i.e., those that do not affect amino acid sequence) in protein folding and function. Recent theoretical studies have suggested that codon usage is not random, and experimental studies in prokaryotes suggest that this may be so (*28*). Here we show that a silent mutation in a complex, mammalian membrane transport protein alters the substrate specificity. We hypothesize that when frequent codons are changed to rare codons in a cluster of infrequently used codons, the timing of cotranslational folding is affected (*29*) and may result in altered function. This finding may be clinically important. For example, mutations in the *MRP6* (*ABCC6*) gene cause the disease pseudoxanthoma elasticum, but missense and nonsense mutations are found in only about 60% of cases (*30*), raising the possibility that mutations that do not change coding sequence may contribute to disease by a similar mechanism.

References and Notes

1. M. M. Gottesman, T. Fojo, S. E. Bates, *Nat. Rev. Cancer* **2**, 48 (2002).
2. C. Cordon-Cardo *et al.*, *J. Histochem. Cytochem.* **38**, 1277 (1990).

3. S. Hoffmeyer *et al.*, *Proc. Natl. Acad. Sci. U.S.A.* **97**, 3473 (2000).
4. S. Oscarson *et al.*, *Br. J. Clin. Pharmacol.* **53**, 526 (2002).
5. M. Goto *et al.*, *Pharmacogenetics* **12**, 451 (2002).
6. S. V. Ambudkar, C. Kimchi-Sarfaty, E. Z. Sauna, M. M. Gottesman, *Oncogene* **22**, 7468 (2003).
7. H. H. Salama, Z. Yang, T. Bun, R. J. Y. Ho, *J. Pharm. Sci.* **95**, 2293 (2006).
8. K. Tang *et al.*, *Pharmacogenetics* **12**, 437 (2002).
9. M. Horinouchi *et al.*, *Pharm. Res.* **19**, 1581 (2002).
10. L. X. Shen, J. P. Basilion, V. P. Stanton Jr., *Proc. Natl. Acad. Sci. U.S.A.* **96**, 7871 (1999).
11. L. Fritsche *et al.*, *Diabetes* **50**, 1952 (2001).
12. M. D. Perloff, L. L. von Moltke, E. Stormer, R. L. Shader, D. J. Greenblatt, *Br. J. Pharmacol.* **134**, 1601 (2001).
13. J. J. Gribar, M. Ramachandra, C. A. Hrycyna, S. Dey, S. V. Ambudkar, *J. Membr. Biol.* **173**, 203 (2000).
14. See supporting material on *Science* Online.
15. C. Kimchi-Sarfaty, J. J. Gribar, M. M. Gottesman, *Mol. Pharmacol.* **62**, 1 (2002).
16. N. T. Th. Tran *et al.*, *Mol. Genet. Metab.* **85**, 213 (2005).
17. D. Wang, A. D. Johnson, A. C. Papp, O. L. Kroetz, W. Sadee, *Pharmacogenet. Genomics* **15**, 693 (2005).
18. A. Ruth, W. D. Stein, E. Rose, I. B. Rosenson, *Biochemistry* **40**, 4332 (2001).
19. E. W. Lee, D. M. Clarke, *J. Biol. Chem.* **273**, 14671 (1998).
20. L. Z. Sherman, P. J. Sherman, *Biosystems* **33**, 139 (1994).
21. S. Brunak, J. Engelbrecht, *Proteins* **25**, 237 (1996).
22. A. A. Adzhubei, L. A. Adzhubei, E. A. Krasheninnikov, S. Nendle, *FEBS Lett.* **399**, 78 (1996).
23. S. K. Gupta, S. Majumdar, T. K. Bhattacharya, T. C. Ghosh, *Biochem. Biophys. Res. Commun.* **269**, 692 (2000).
24. P. Cortazzo *et al.*, *Biochem. Biophys. Res. Commun.* **293**, 537 (2002).
25. A. A. Komar, T. Lesnik, C. Reiss, *FEBS Lett.* **462**, 387 (1999).
26. T. Xie, D. Ding, *FEBS Lett.* **434**, 93 (1998).
27. P. M. Sharp, W. H. Li, *Nucleic Acids Res.* **15**, 1281 (1987).
28. F. Supek, K. Vlahovicek, *BMC Bioinformatics* **6**, 182 (2005).
29. V. Anthony, W. R. Slack, *Curr. Protein Pept. Sci.* **3**, 485 (2002).
30. L. Bercovitch, P. Terry, *J. Am. Acad. Dermatol.* **51**, 513 (2004).

31. We thank W. Stein for fruitful discussions, R. Kincaid for a discussion that led to the idea that substitution of rare codons could affect folding of complex transmembrane proteins, G. Lesman for valuable editorial assistance, P. FitzGerald, who assisted us with codon usage rates; and S. Garfield for help with confocal images. Supported by the National Institute of General Medical Sciences Pharmacology Research Associate (PRAT) program (A.M.C.) and by the Intramural Research Program of the Center for Cancer Research, National Cancer Institute.

Supporting Online Material

www.sciencemag.org/cgi/content/full/1135308/DC1
Materials and Methods
Figs. S1 to S5
Table S1
References

19 September 2006; accepted 28 November 2006
Published online 21 December 2006
10.1126/science.1135308
Include this information when citing this paper.

Imaging of Germinal Center Selection Events During Affinity Maturation

Christopher D. C. Allen,*† Takaharu Okada,*† H. Lucy Tang,‡ Jason G. Cyster†

The germinal center (GC) is an important site for the generation and selection of B cells bearing high-affinity antibodies, yet GC cell migration and interaction dynamics have not been directly observed. Using two-photon microscopy of mouse lymph nodes, we revealed that GC B cells are highly motile and extend long cell processes. They transited between GC dark and light zones and divided in both regions, although these B cells resided for only several hours in the light zone where antigen is displayed. GC B cells formed few stable contacts with GC T cells despite frequent encounters, and T cells were seen to carry dead B cell blebs. On the basis of these observations, we propose a model in which competition for T cell help plays a more dominant role in the selection of GC B cells than previously appreciated.

Germinal centers (GC) represent critical sites within organized lymphoid tissues in which B cell responses to antigens are amplified and refined in specificity. A classical model of GC function holds that B cells in the dark zone undergo rapid rounds of proliferation and somatic hypermutation of their antibody genes, followed by exit from the cell cycle and migration to the light zone, where the B cells undergo selection based on the affinity of their cell-surface antibodies for antigen (*1*–*4*). The selection process is thought to involve competition between GC B cells for capture of antigen in the form of immune complexes displayed on the processes of follicular dendritic cells (FDCs) (*1*, *3*, *5*, *6*). However, recent experimental evidence and computer simulations have contradicted aspects of this classical model (*3*, *7*–*9*).

Howard Hughes Medical Institute and Department of Microbiology and Immunology, University of California, San Francisco, CA 94143, USA.

*These authors contributed equally to this work.
†To whom correspondence should be addressed. E-mail: Takaharu.Okada@ucsf.edu (T.O.), Jason.Cyster@ucsf.edu (J.G.C.)
‡Present address: Amgen Inc., 1120 Veterans Boulevard, South San Francisco, CA 94080, USA.

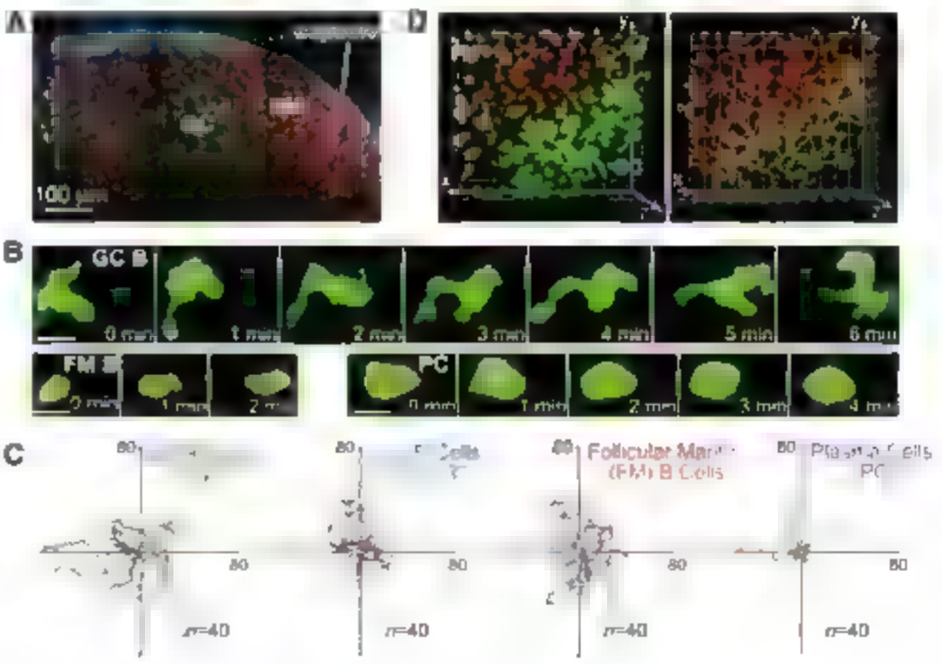

Fig. 1. Dynamics and motility of GC B cells compared with follicular mantle (FM) B cells and plasma cells (PC). (**A**) An 18-μm maximum intensity *z*-projection from two-photon microscopy image stacks of a GC and FM in an intact LN. A time-lapse recording corresponding to the center of this region is shown in movie S1. (**B**) Representative time-lapse images from two-photon microscopy showing the morphology of a GC B cell, FM B cell, and PC. The FM B cells in this experiment were naïve GFP$^+$ cells that were also labeled with CMTMR (*10*), and only the GFP channel is shown in the images. Scale bars, 10 μm. (**C**) Superimposed 15-min tracks of 40 randomly selected cells of each indicated type in the *xy* plane, setting the starting coordinates to the origin. Units are in micrometers. WT, wild type. Each color represents one cell's path. (**D**) (Left) Maximum-intensity projection of FM (red) and GC (green) B cells. (Right) Tracks of FM (red) and GC (green) B cells. The gridlines are separated by 20 μm.

and the mechanism by which selection occurs in the GC has remained elusive. One of the challenges in studying GC selection has been a lack of knowledge about the dynamics of GC B cells in their complex physiological milieu.

We developed a system to study the dynamics of GC B cells within intact mouse lymph nodes (LNs) by two-photon microscopy (the system is described in detail in the supporting online material (SOM) text) (*10*). In this system, 1 to 2% of GC B cells expressed green fluorescent protein (GFP) (Fig. 1A and figs. S1 and S2) and by our measurements were able to undergo the normal processes of class switching, somatic hypermutation, and affinity maturation (figs. S3 and S4). The dynamics of GC B cell motility in explanted LNs were compared with two other B cell populations: (i) naïve B cells (representing B cells before antigen encounter) in the follicular mantle that surrounds the GC and (ii) plasma cells (representing post-selected B cells that secrete antibodies) in the LN medulla (SOM text). GC B cells had highly dynamic shapes, extending dendritic processes resembling pseudopods as they moved (Fig. 1B and movie S1), whereas naïve follicular mantle B cells and plasma cells exhibited a more round phenotype (Fig. 1B). Similar observations were made when GC and follicular mantle B cells were imaged by intravital microscopy of intact LNs (movie S2). Tracking analysis indicated that GC B cells were highly motile, similar to follicular mantle B cells, whereas plasma cells showed little motility (Fig. 1C, fig. S5, A to I, at S6, and movie S3). GC B cell motility was partially dependent on the chemokine CXCL13 (Fig. 1C and fig. S5) that is expressed by FDCs (SOM text) (*11*).

On average, GC B cells formed separate clusters from naïve B cells in the follicular mantle (Fig. 1, A and D), giving the impression of distinct regions typically seen in static images, such as those obtained by immunohistochemistry (for an example, see fig. S2C). However, examination of the boundary between these regions revealed that the tracks of GC B cells and follicular mantle B cells were overlapping (Fig. 1D and movie S4), indicating that a physical boundary does not demarcate the GC and follicular mantle. Instead, the majority of cells turned after crossing from one region to the other, suggesting that the GC and follicular mantle are segregated by the responses of cells to attractive (or repulsive) cues.

The behavior of cells in GC dark and light zones was characterized by labeling light zone FDCs (CD21/35) immune complexes containing the fluorescent protein phycoerythrin (PE) (Fig. 2A and movie S5). B cells in dark and light zones were similarly motile (fig. S7). In 1 hour, most GC B cells appeared to stay within the dark or light zones, although a measurable proportion (5 to 8%) traveled along relatively straight paths from one zone to the other, covering substantial distances (Fig. 2, B and C, and movies S6 and

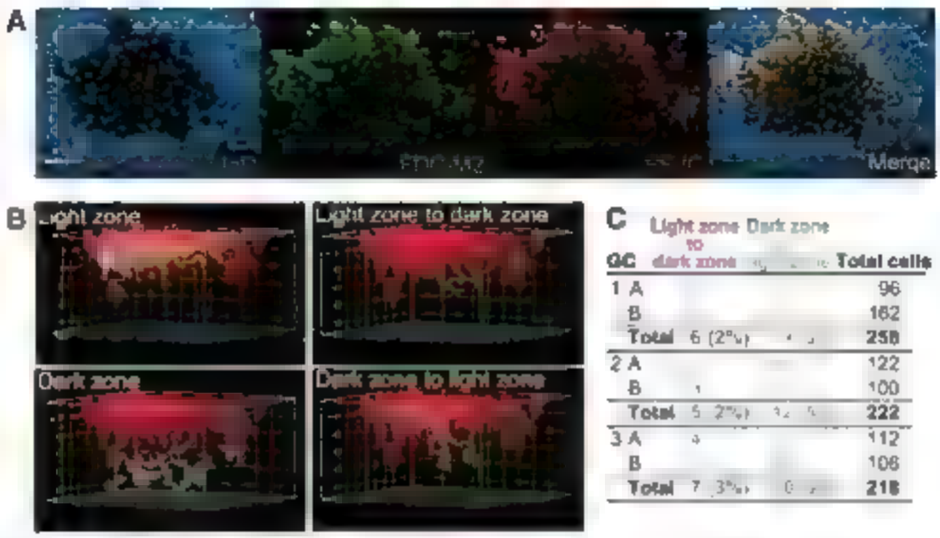

Fig. 2. GC B cell movement within and between GC dark and light zones. (**A**) Immunofluorescence of cryostat sections showing extensive overlap of in vivo deposited PE immune complexes (PE-IC) (red) with FDC-M2 antibody staining (green). The follicular mantle is shown with staining for immunoglobulin D (IgD) (blue). Scale bar, 100 μm. (**B**) Representative manual classification (*10*) of cell tracks into groups with respect to the PE⁺ light zone corresponding to GC 1A in (C). The gridlines are separated by 20 μm. (**C**) Frequency of cells traveling between the light and dark zones in three GCs imaged 7 days after immunization. Imaging sessions of 1 hour each were subdivided into two segments (A and B) to facilitate analysis.

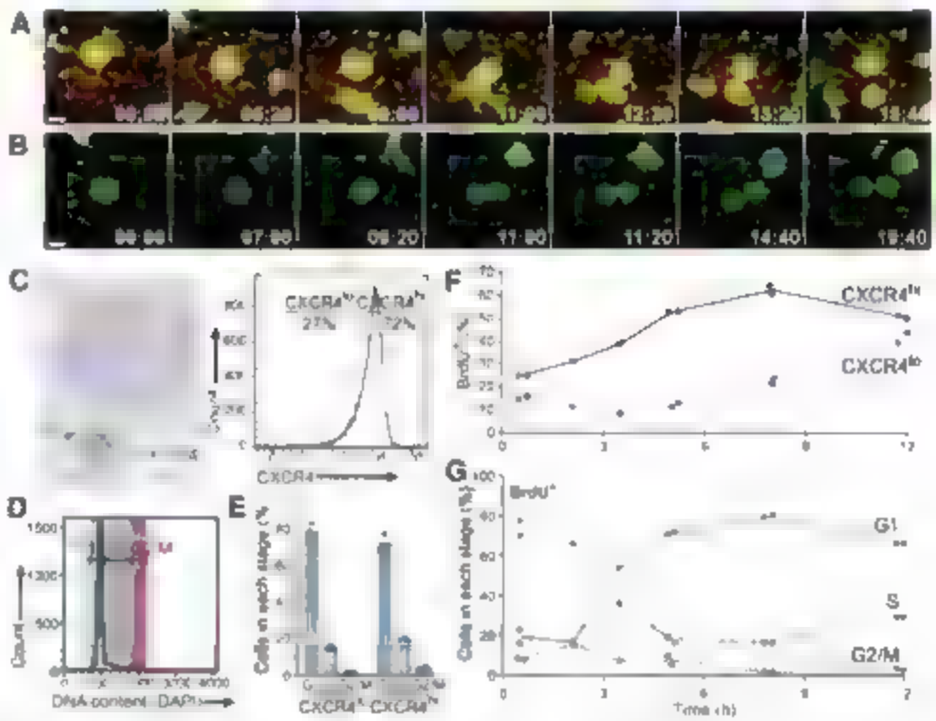

Fig. 3. Cell-cycle analysis in dark and light zones. (**A** and **B**) Single-plane time-lapse images of dividing GC B cells in the light (A) and dark (B) zones. The image sequences begin when the cells have rounded up and stopped moving. (**C**) CXCR4 is expressed more highly on GC B cells in the dark zone than in the light zone. (Left) Representative immunohistochemistry of a cryostat section of an immunized mouse LN (antibodies used for staining, bottom right). (Right) Representative gating of CXCR4^{lo} (light zone) and CXCR4^{hi} (dark zone) GC B cells by flow cytometry. (**D**) Representative cell cycle analysis of GC B cells by flow cytometric measurement of DNA content. DAPI, 4′,6-diamidino-2-phenylindole. (**E**) Frequency of cells that were in each stage of the cell cycle in the CXCR4^{lo} and CXCR4^{hi} GC B cell subsets. (**F**) Frequency of cells that were BrdU⁺ in the CXCR4^{lo} or CXCR4^{hi} GC B cell subsets after BrdU injection at 0 hours. (**G**) Frequency of cells that were in each stage of the cell cycle among BrdU⁺ GC B cells. Data points in (E) to (G) represent individual mice. Similar data were obtained in splenic GCs in other experiments. GC B cells in (C) to (G) were gated as in fig. S9A.

S7). These observations extend previous conclusions based on fixed tissue analysis (*1*) that GC B cells migrate from the dark zone to the light zone. We provide direct evidence that GC B cells return from the light zone to the dark zone. Within the light zone, FDC processes appeared to undulate, perhaps due to displacement by migrating GC B cells (movie S5). However, there was little evidence that GC B cells pause on FDC processes, in contrast to observations of the T cell DC interactions in the T cell area (*12*). GC B cells in the light zone followed straighter paths than those in the dark zone (fig. S7, B and C), which may relate to the higher concentration of CXCL13 on the FDC processes in the light zone (*1*).

During time-lapse recordings, we occasionally observed cell division in both light zones (Fig. 3A) and dark zones (Fig. 3B), consistent with other studies that have questioned the classical model that proliferation only occurs in the dark zone (*3*, *8*, *13*). We further analyzed the relationship between GC B cell position and cell cycle behavior by flow cytometry (SOM text). As the surface abundance of the chemokine receptor CXCR4 (Fig. 3C) is a marker to delineate cells in dark ($CXCR4^{hi}$) and light ($CXCR4^{lo}$) zones (*11*). Analysis of DNA content (Fig. 3D) revealed that a similar proportion of GC B cells were in S phase in both dark and light zones (Fig. 3E). A subset of cells was tracked over one complete cell cycle by pulse labeling with 5-bromo-2-deoxyuridine (BrdU), a thymidine analog that is incorporated into cells undergoing DNA synthesis (S phase) near the time of BrdU injection (*14*). A similar proportion of GC B cells in dark and light zones were labeled 30 min after BrdU injection, however after 5 hours at which time the cells had divided and returned to G_1 phase they accumulated in the dark zone and not in the light zone (Fig. 3, F and G, fig. S8, and fig. S9). These observations indicate that cells that divide in the light zone do not stay resident there—perhaps they return to the dark zone via the GC, or undergo apoptosis. From 5 to 12 hours after BrdU injection, the G_1 phase cells that had accumulated in the dark zone began to appear in the light zone, suggesting that the light zone is replenished continuously by an influx of cells from the dark zone that recently completed cell cycle (Fig. 3, F and G, fig. S8, and fig. S9). Cells were not seen reentering S phase until 12 hours after they were first labeled with BrdU in S phase (Fig. 3G and fig. S9, C and D), indicating that the average cell-cycle time is 12 hours or longer, rather than 6 to 7 hours as has been concluded in previous studies (*1*).

T cells are concentrated in the light zone (*1*), and T cell help is thought to be essential for GCs (*3*–*5*). To understand the mode of B cell–T cell interaction in GCs, we visualized the interactions between GFP$^+$ GC B cells and GC T cells expressing cyan fluorescent protein (CFP) (movie S8). Most contacts between GC B and T cells were of short duration (Fig. 4A), and only about 4% of GC B cell–T cell encounters led to the formation of stable conjugates, defined here as contacts lasting for more than 5 min (Fig. 4, B and C). In contrast, early in the immune response before GC formation, more than 50% of contacts between cognate antigen-specific B and T cells led to the formation of stable conjugates (Fig. 4C and movie S9) (*16*). Upon encounters leading to stable interactions with GC B cells, rapidly migrating GC T cells sharply decreased their motility to match B cell motility (Fig. 4D), and conjugates were led by B cells (movie S10), similar to the dynamics of stable B-T conjugates early in the immune response (*16*). The median velocity of GC T cells stably interacting with GFP$^+$ B cells was below 10 μm/min (Fig. 4E). Only 32% of total GC T cells showed a median velocity below 10 μm/min (Fig. 4E), and the motility coefficient of GC T cells was greater than that of GC B cells (Fig. 4F and fig. S5E), strongly suggesting that the majority of T cells in GCs were not engaged in stable interactions with B cells. Our analyses suggest that each GC B cell encounters as many as 50 T cells per hour and that the majority of GC B cells are capable of binding antigen (fig. S3B). It thus seems likely that T cell help is limited, not only because there are fewer T cells than B cells, but also

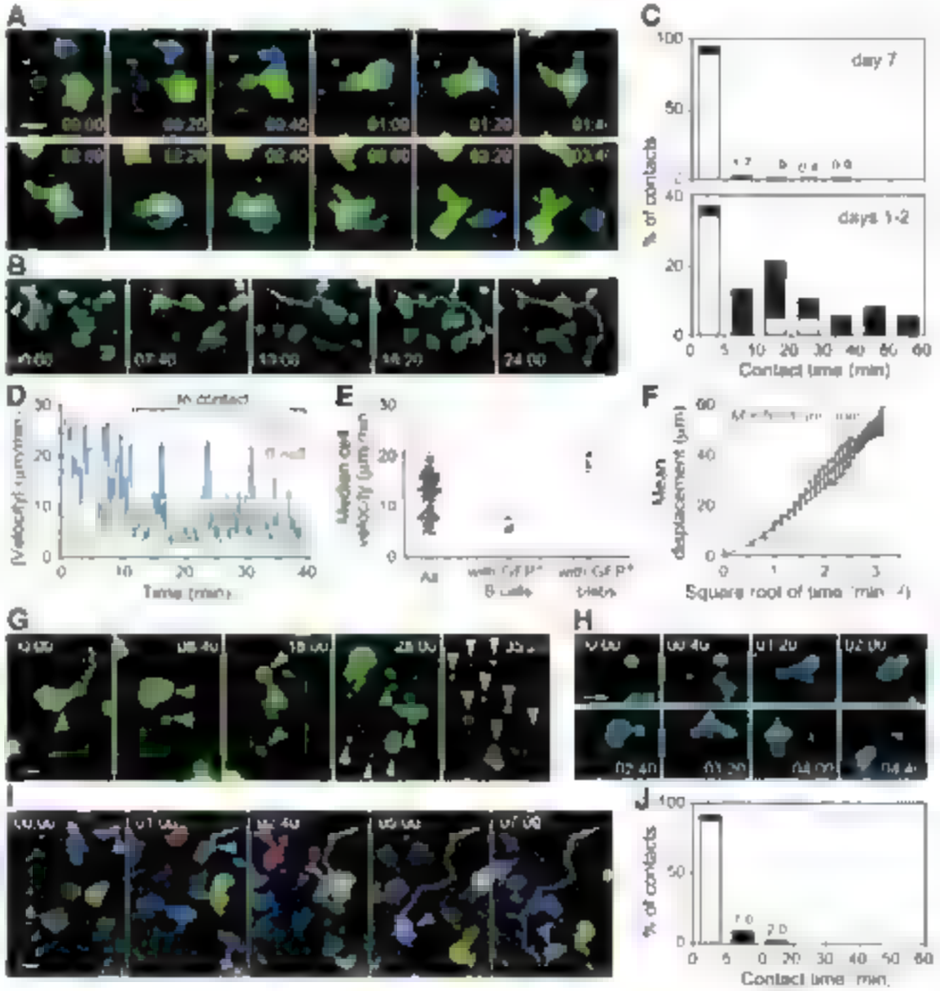

Fig. 4. Dynamics of GC T cell interactions with live GC B cells and dead B cell blebs. (**A** and **B**) Time-lapse images of a brief contact (A) and a stable conjugate (B). Arrowhead and dotted line] of a GC B cell (green) and T cell (blue). (**C**) Contact times between antigen-specific B and T cells at the indicated number of days after immunization. Black bar segments indicate conjugates that could not be tracked for their entire duration and therefore are underestimates. Data are from three independent experiments. (**D**) Magnitudes of the velocities of a GC B cell and T cell that formed a stable conjugate. (**E**) Median velocity of total GC T cells, GC T cells stably interacting with GFP$^+$ GC B cells, and GC T cells stably interacting with GFP$^+$ blebs. (**F**) Displacement of GC T cells plotted against the square root of time. Blue line, mean of four imaging data sets from four recipient mice (error bars indicate SD); red line, mean of seven T cells stably interacting with GC B cells; *M*, motility coefficient (*10*). (**G**) Image of a GC B cell undergoing cell death. Dotted line, 5 min track of migration preceding the first time point; arrowheads, fragments of the cell. (**H**) Image of a GC T cell (blue) picking up a GC B cell bleb (green). (**I**) Image of a GC T cell (blue) carrying a GC B cell bleb (green, indicated by arrowheads) over a path shown with a dotted line. Some follicular mantle cells (red) are also visible. (**J**) Contact time distribution between GC T cells and GFP$^+$ GC B cell blebs from three independent experiments. Black bar segments indicate incomplete tracking as in (C). Scale bars, 10 μm.

because of additional mechanisms suppressing stable B-T interactions in GCs.

During the selection process in GCs, many GC B cells die and are visible by histology as "tingible bodies" inside macrophages (*1*). The cell bodies of dying GFP$^+$ GC B cells were observed to undergo fragmentation (Fig. 4G), but surprisingly, this occurred outside of macrophages (movie S11). Blebs of dead GFP$^+$ GC B cells appeared to be taken up by multiple macrophages (movie S11), although some blebs moved rapidly away from the original location of cell death, as if carried by motile cells (movie S2). Indeed, some GFP$^+$ B cell blebs were attached to and carried by rapidly migrating GFP$^+$ T cells (Fig. 4, H and I, and movie S12). All T cells that carried GFP$^+$ B cell blebs had a median velocity greater than 0 μm/min (Fig. 4E), suggesting that they were not undergoing stable interactions with living B cells. The GFP$^+$ GC B cells represent only about 1 to 2% of GC B cells, and we observed about 0.5% of T cells carrying GFP$^+$ blebs; by extrapolation, at least one quarter of the GC T cells may be associated with one or more blebs from dead GC B cells. A higher frequency of bleb T cell interactions were stable compared with live B cell–T cell interactions (Fig. 4, C and J), suggesting that these dead B cell fragments may affect the availability of T cell help in GCs.

Our findings reveal that GC B cells are highly motile and exhibit a probing behavior as they travel over the antigen-bearing FDC$^+$ network. The lack of GC B cell pausing suggests that the selection mechanism does not involve competition for adhesion to FDCs, whereas the rapid movement of B cells in close proximity to each other raises the possibility that high-affinity cells remove surface-bound antigen from lower-affinity cells. The observed migration of GC B cells from light to dark zones is consistent with GC B cells undergoing repeated rounds of mutation and selection within a given GC (*17*). Our estimate that GC B cells spend only several hours in the light zone suggests a limited amount of time to access helper T cells. Given that stable interactions of GC B cells with GC T cells were infrequent, it seems possible that T cell help is a limiting factor driving selection of higher-affinity B cell clones. In vitro studies have shown that T cells responding to antigen-presenting B cells can be sensitive to variations in the affinity of the B cell receptor across several orders of magnitude (*18*). We propose a selection model in which newly arising mutated GC B cells with higher affinity for antigen obtain and process greater amounts of antigen in a given period of time and then outcompete the surrounding B cells and B cell blebs for the attention of GC T cells.

References and Notes

1. I. C. MacLennan, *Annu. Rev. Immunol.* **12**, 117 (1994).
2. G. Kelsoe, *Immunity* **4**, 107 (1996).
3. J. Mamer, *J. Immunol.* **172**, 3369 (2004).
4. L. J. McHeyzer-Williams, L. P. Malherbe, M. G. McHeyzer-Williams, *Immunol. Rev.* **211**, 255 (2006).
5. D. Tarlinton, *Nat. Rev. Immunol.* **6**, 785 (2006).
6. M. H. Kosco-Vilbois, *Nat. Rev. Immunol.* **3**, 764 (2003).
7. A. M. Haberman, M. J. Shlomchik, *Nat. Rev. Immunol.* **3**, 757 (2003).
8. Y. Wang, R. H. Carter, *Immunity* **22**, 749 (2005).
9. M. E. Meyer-Hermann, P. K. Maini, D. Iber, *Math. Med. Biol.* **23**, 255 (2006).
10. Materials and methods are available as supporting material on *Science* Online.
11. C. D. Allen *et al.*, *Nat. Immunol.* **5**, 943 (2004).
12. M. D. Cahalan, I. Parker, *Curr. Opin. Immunol.* **18**, 476 (2006).
13. S. A. Camacho, M. H. Kosco-Vilbois, E. Berek, *Immunol. Today* **19**, 511 (1998).
14. J. E. Ryser *et al.*, *Mol. Med. Biol.* **26**, 673 (1999).
15. C. G. de Vinuesa *et al.*, *J. Exp. Med.* **191**, 485 [illegible].
16. T. Okada *et al.*, *PLoS Biol.* **3**, e150 (2005).
17. T. B. Kepler, A. S. Perelson, *Immunol. Today* **14**, 412 (1993).
18. F. D. Batista, M. S. Neuberger, *Immunity* **8**, 751 (1998).

19. We thank Y. Xu for technical assistance; O. Lam for screening of mice; N. Killeen for help with gene targeting; M. Egeblad, S. Nutt, B. L. Rennhardt, and A. J. Todey for providing mice; the Mount Zion Animal Care Facility for animal husbandry; E. Passegue for advice on single-cell sorting and for use of her cell sorter; and T. G. Phan and I. S. Grigorova for helpful discussions and critical reading of the manuscript. C.D.C.A. is a predoctoral fellow and J.G.C. is an investigator of the Howard Hughes Medical Institute. This work was supported in part by grants from NIH and by a Sandler New Technology Award.

Supporting Online Material

www.sciencemag.org/cgi/content/full/1136736/DC1
Materials and Methods
SOM Text
Figs. S1 to S9
References
Movies S1 to S12

25 October 2006; accepted 15 December 2006
Published online 21 December 2006
10.1126/science.1136736
Include this information when citing this paper.

Damage to the Insula Disrupts Addiction to Cigarette Smoking

Nasir H. Naqvi,[1] David Rudrauf,[1,2] Hanna Damasio,[1,4] Antoine Bechara[1,3,4]*

A number of brain systems have been implicated in addictive behavior, but none have yet been shown to be necessary for maintaining the addiction to cigarette smoking. We found that smokers with brain damage involving the insula, a region implicated in conscious urges, were more likely than smokers with brain damage not involving the insula to undergo a disruption of smoking addiction, characterized by the ability to quit smoking easily, immediately, without relapse, and without persistence of the urge to smoke. This result suggests that the insula is a critical neural substrate in the addiction to smoking.

Cigarette smoking, the most common preventable cause of morbidity and mortality in the developed world (*1*), is an addictive behavior. Despite being aware of negative consequences, many smokers have difficulty quitting, and even those who quit experience urges to smoke and tend to relapse (*2*, *3*). These phenomena appear to arise from long-term adaptations within specific neural systems. Subcortical regions, such as the amygdala, the nucleus accumbens, and the mesotelencephalic dopamine system, have been shown in animal models to promote the self-administration of drugs of abuse (*4*, *5*). Functional imaging studies have shown that exposure to drug-associated cues activates cortical regions such as the anterior cingulate cortex, the orbitofrontal cortex, and the insula (*6*–*13*). Among these regions, the insula is of particular interest because of its potential role in conscious urges. The insula has been proposed to function in conscious emotional feelings through its role in the representation of bodily (interoceptive) states (*14*–*16*). Activity within the insula on both sides of the brain has been shown to correlate with subjective cue-induced drug urges (*7*, *8*, *11*). It has also been shown that a high amount of activity in the right insula during a simple decision-making task is associated with relapse to drug use (*17*). Given its potential role in cognitive and emotional processes that promote drug use, the question arises as to whether the insula is necessary for maintaining addiction to smoking. We hypothesized that the insula is a critical neural substrate in the addiction to smoking. We predicted, therefore, that damage to the insula would disrupt addiction to smoking.

We identified 19 cigarette smokers who had acquired brain damage that included the insula (*18*). Six of these patients had right insula damage, and 13 had left insula damage. We also

[1]Division of Cognitive Neuroscience, Department of Neurology, University of Iowa Carver College of Medicine, 200 Hawkins Drive, Iowa City, IA 52242, USA. [2]Laboratory of Computational Neuroimaging, Department of Neurology, University of Iowa Carver College of Medicine, 200 Hawkins Drive, Iowa City, IA 52242, USA. [3]Dornsife Cognitive Neuroscience Imaging Center, SGM 501, University of Southern California, Los Angeles, CA 90089, USA. [4]Brain and Creativity Institute, HNB B26, University of Southern California, Los Angeles, CA 90089, USA.

*To whom correspondence should be addressed. E-mail: bechara@usc.edu

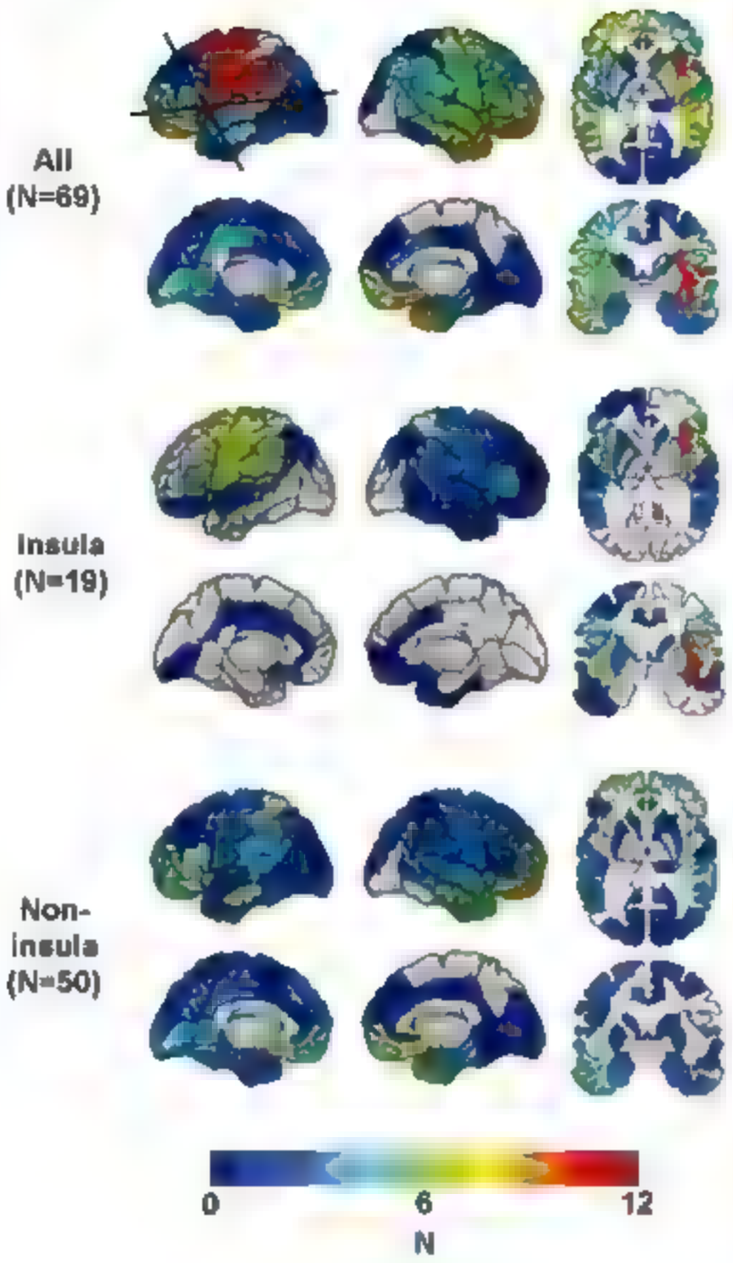

Fig. 1. Number (*N*) of patients with lesion in each of the regions identified in this study, mapped onto a reference brain. Boundaries of anatomically defined regions are drawn on the brain surface. Regions names are provided in the Materials and Methods. Regions not assigned a color contained no lesions. (**Top**) All patients. The horizontal line marks the transverse section of the brain shown in the top row. The vertical line marks the coronal section shown in the bottom row. (**Middle**) Patients with lesions that involved the insula. (**Bottom**) Patients with lesions that did not involve the insula.

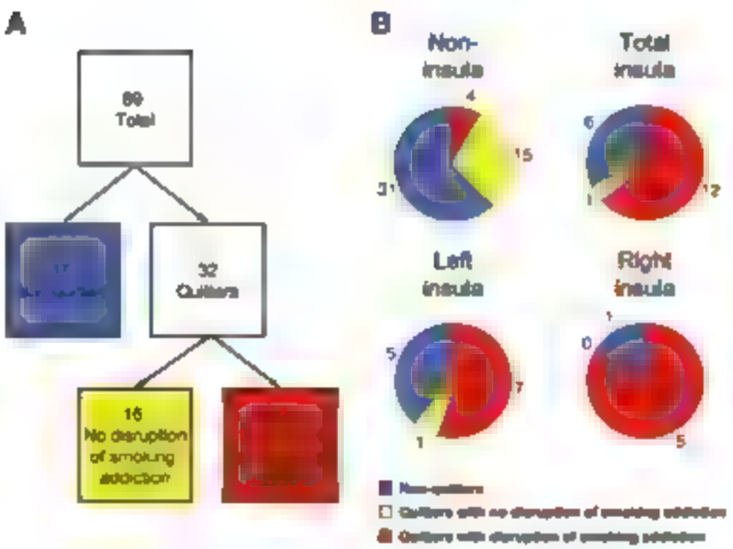

Fig. 2. Patients who quit smoking after lesion onset and patients who underwent a disruption of smoking addiction after lesion onset. (**A**) Tree diagram showing the behavioral classification of patients. (**B**) Pie charts illustrating the proportion of patients in each anatomical group who fell into each of the behavioral categories. The colors correspond to the behavioral group depicted in (A). These actual proportions are shown in the Materials and Methods. The proportion of patients with a disruption of smoking addiction was higher among both left insula–lesioned patients and right insula–lesioned patients compared with among noninsula-lesioned patients.

identified a group of 50 cigarette smokers who had acquired damage that did not include the insula. All of these patients had been smoking more than five cigarettes per day for more than 7 years at the time of lesion onset. The groups were matched with respect to several characteristics, including the number of cigarettes they were smoking at lesion onset, the total number of years they had been smoking at lesion onset, and the etiology of their brain damage (Fig. 1 and table S1).

First, we performed a logistic regression analysis in which the dependent variable was whether or not patients quit smoking some time after lesion onset (i.e., whether or not they were smoking at the time of the study). The independent variable of interest was the extent of damage in the insula on a given side. An estimate of the total extent of the lesion was entered as a nuisance covariate (Materials and Methods). We found that the likelihood of quitting smoking after a lesion in either the right or the left insula was not significantly higher than the likelihood of quitting after a noninsula lesion (odds ratio = 2.94, χ^2 = 2.74, and P = 0.10). When we examined the right and left insulae separately, we found that the likelihood of quitting smoking was not significantly higher after a right insula lesion than after a noninsula lesion (odds ratio = 2.53, χ^2 = 2.05, and P = 0.08), nor was it significantly higher after a left insula lesion compared with after a noninsula lesion (odds ratio = 1.44, χ^2 = 1.12, and P = 0.29) (Fig. 2 and table S3). One explanation of this null finding is that, whereas the insula-lesioned patients may have quit smoking due to a disruption of smoking addiction, the noninsula-lesioned patients may have quit smoking at a similar rate because they were concerned about the negative consequences of smoking. Simply determining whether the patients were smoking at the time of the study did not address this distinction.

To more specifically assess a disruption of smoking addiction, we asked all of the patients who quit smoking after lesion onset a set of questions aimed at their recollection of the experience of quitting. Patients were classified as having had a disruption of smoking addiction if they fulfilled all four of the following criteria: (i) reporting quitting smoking for less than a year after lesion onset, (ii) reporting that they did not start smoking again after they quit, (iii) rating the difficulty of quitting as less than three on a scale of one to seven, and (iv) reporting feeling no urges to smoke since quitting. According to these criteria, 16 of the patients who quit smoking after lesion onset were classified as having a disruption of smoking addiction. The 16 quitters who failed to meet all four of these criteria, along with all 37 nonquitters, were considered to have no disruption of smoking addiction (Fig. 2).

We performed a logistic regression in which the dependent variable was whether or not patients underwent a disruption of smoking addiction after lesion onset as defined by the above

criteria. As before, the independent variable of interest was the extent of damage to the insula on a given side, whereas the estimate of the total extent of the lesion was entered as a nuisance covariable. We found that the likelihood of having a disruption of smoking addiction after a lesion in either the right or the left insula was significantly higher than the likelihood of having a disruption of smoking addiction after a noninsula lesion (odds ratio = 22.05, χ^2 = 16.64, and P = 0.0005). When we examined the right and left insulae separately, we found that the likelihood of having a disruption of smoking addiction was significantly higher after a right insula lesion than after a noninsula lesion (odds ratio = 10.87, χ^2 = 12.90, and P = 0.0003) and was also significantly higher after a left insula lesion compared with after a noninsula lesion (odds ratio = 3.61, χ^2 = 10.33, and P = 0.001) (Fig. 2 and table S3). Although it appears that effects may be somewhat larger with right insula lesions compared with left insula lesions, the sample sizes were too small to confirm this statistically.

We then conducted a similar logistic regression that included only the patients in our sample who quit smoking after lesion onset (thus, we were not required to assume that patients who continued to smoke after lesion onset had an intact smoking addiction). We found that five of five of the patients who quit smoking after a right insula lesion and seven of eight of the patients who quit smoking after a left insula lesion met the criteria for having a disruption of smoking addiction, compared to 4 of 19 of the patients who quit smoking after a noninsula lesion (right insula lesioned patients versus noninsula-lesioned patients: odds ratio = 6.55, χ^2 = 7.76, and P = 0.005; left insula lesioned patients versus noninsula-lesioned patients: odds ratio = 7.19, χ^2 = 10.06, and P = 0.002). Putting the right and left sides together, 12 of 13 patients who quit smoking after a lesion in the insula did so with a disruption of smoking addiction. Relative to noninsula-lesioned patients, this translates into an odds ratio of 136.49 as estimated by the logistic regression (χ^2 = 18.48 and P = 0.00008) (Fig. 2 and table S3).

In our sample, the patients with insula lesions tended also to have damage in adjacent areas (Fig. 1). This raises the question of whether the observed effects were necessarily due to insula damage or whether they required damage in one or more areas adjacent to the insula. To address this issue, we performed a region-by-region logistic regression analysis that estimated, for each region of the brain that we sampled, the likelihood of having a disruption of smoking addiction after a lesion that included the region compared to a lesion that did not include the region. This analysis included all of the patients in the sample. We found that the only regions in which lesions were significantly associated with an increased likelihood of having a disruption of smoking addiction were the right and left insulae (Fig. 3). On the left side, there were near-significant effects in regions adjacent to the insula, such as the putamen. We cannot rule out the possibility that some of these regions independently or cumulatively play a role in smoking addiction. For example, evidence from animal studies suggests that the dorsal striatum, which includes the putamen, is involved in learning and expression of drug-use habits (*4*). However, for most of these regions the patients with lesions who had a disruption of smoking addiction also had damage in the insula (table S4), suggesting that apparent effects of lesions in these regions were due to a bystander effect. We did find four patients who had a disruption of smoking addiction after suffering from brain damage that did not involve the insula. When we examined their lesions, we found that each of them had damage in a unique set of regions (table S5). This raises the possibility that certain patients may undergo a disruption of smoking addiction as a general effect of suffering from a brain injury.

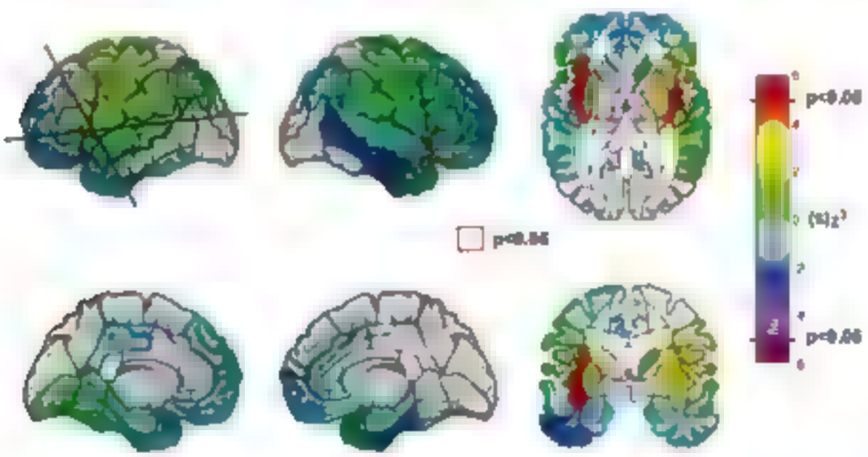

Fig. 3. Whole-brain region-by-region logistic regression analysis. The color of each region corresponds to a χ^2 statistic given the sign of regression coefficient obtained from the logistic regression analysis. The only regions that were assigned a color were those for which the number of patients was sufficient to detect a statistically significant effect (Materials and Methods). Regions for which there was a statistically significant association between a lesion and a disruption of smoking addiction (P < 0.05, uncorrected) are highlighted in red. The insula is the only region on either side of the brain where a lesion was significantly associated with a disruption of smoking addiction. There were nonsignificant effects in regions on the left side that are adjacent to the insula; however, patients with damage in these regions also tended to have damage in the insula (Materials and Methods). The likelihood of having a disruption of smoking addiction was not increased after damage in the orbitofrontal cortex.

The results indicate that smokers who acquire insula damage are very likely to quit smoking easily and immediately and to remain abstinent. In addition, smokers with insula damage are very likely to no longer experience conscious urges to smoke after quitting. These findings are consistent with previous functional imaging evidence showing that activity in the insula is correlated with subjective drug urges (*7*, *8*, *11*). Additionally, the results provide evidence that subjective urges are an important factor in maintaining smoking addiction. However, urges may not be the only factor that promotes smoking. Recent theories of addiction propose that usual drug use in addicted individuals is driven primarily by automatic or impulsive motivational processes, such as habits (*4*) and incentive salience wanting (*19*). Conscious urges come into play when there is an impediment to drug use, such as an attempt to quit or to resist relapse (*20*). The present results are consistent with this view. However, it remains to be seen whether insula damage spares the automatic tendency to smoke. It also remains to be seen whether patients with insula damage still obtain pleasure from smoking, because pleasure and urge may be dissociable facets of smoking reward (*19*).

Our sample included a number of patients with damage to the orbitofrontal cortex (Fig. 1), a region that, like the insula, has been implicated by functional imaging studies to play a role in conscious drug urges (*6*, *8*, *9*, *11*–*13*). We found no association between lesions in the orbitofrontal cortex and a disruption of smoking addiction (Fig. 3 and table S4). One explanation of this result is that smokers who acquire orbitofrontal damage experience a reduction in conscious urges but continue to smoke because their automatic tendency to smoke is still intact. At the same time, these patients may have a low likelihood of attempting to quit smoking after suffering from a brain injury, because the orbitofrontal region is critical for decisions that override the automatic tendency to obtain immediate rewards in order to avoid future negative consequences (*21*, *22*). Insula-lesioned patients, in contrast, may not have such severe decision-making deficits and thus may be likely to attempt to quit smoking after suffering from a brain injury.

The results of this study suggest that the insula is a critical neural substrate for the urge to

smoke, although they do not in themselves indicate why the insula, a region known to play a role in the representation of the bodily states (*16*), would play such an important role in urge. A clue may be provided by the account of one patient in our sample who quit smoking immediately after he suffered a stroke that damaged his left insula. He stated that he quit because his "body forgot the urge to smoke" (*23*). His experience suggests that the insula plays a role in the feeling that smoking is a bodily need. Indeed, much of the pleasure and satiety that is obtained from smoking is derived from its bodily effects, in particular its impact on the airway (*24*, *25*). In addition, nicotine withdrawal is associated with changes in autonomic and endocrine function (*26*, *27*), which may contribute to its unpleasantness. Current evidence suggests that the insula plays a role in conscious feelings by anticipating the bodily effects of emotional events (*13*, *15*). The insula may therefore function in the conscious urge to smoke by anticipating pleasure from the airway effects of smoking and/or relief from the aversive autonomic effects of nicotine withdrawal. Thus, damage to the insula could lead a smoker to feel that his or her body has "forgotten" the urge to smoke.

An important question pertains to whether insula lesions cause a disruption of motivated behaviors other than smoking. In a follow-up survey, we found that none of the patients with insula damage who had a disruption of smoking addiction committed to any reductions in their pleasure from eating, their desire to eat, or their intake of food. This does not preclude the possibility that these patients had some impairment of taste perception (*28*, *29*) or had deficits in other motivated behaviors that we did not assess. One possibility is that motivated behaviors that are fundamental to survival, such as eating, are supported by redundant neural mechanisms that are difficult to disrupt with a lesion in a single brain region. A related possibility is that the insula is critical for behaviors whose bodily effects become pleasurable through learning, although the bodily effects of eating are inherently pleasurable, the bodily effects of smoking are initially aversive and become pleasurable as addiction develops (*25*). It would be interesting to see how insula damage affects other learned pleasures.

Our findings suggest that therapies that modulate the function of the insula will be useful in helping smokers quit. For example, sensory replacements for smoking, such as denicotinized cigarettes and inhalers, are highly effective in reducing urges and promoting abstinence (*30*, *31*). Such therapies may work by engaging sensory representations of the airway within the insula, thereby satisfying the "bodily need" to smoke. Future pharmacologic therapies may target neurotransmitter receptors that are expressed within the insula. In addition, the efficacy of various smoking cessation therapies may be monitored by measuring activity within the insula with functional brain imaging. Lastly, the findings of this study demonstrate that conscious feelings, such as urges, are an important component of addiction.

References and Notes

1. R. Peto, A. D. Lopez, J. Boreham, M. Thun, C. Heath Jr., *Lancet* **339**, 1268 (1992).
2. American Psychiatric Association (A.P.A.), *Diagnostic and Statistical Manual of Mental Disorders Text Revision: DSM-IV-TR* (A.P.A., Washington, DC, ed. 4, 2000) pp. 191–296.
3. U.S. Department of Health and Human Services, *1988 Surgeon General's Report: The Health Consequences of Smoking: Nicotine Addiction* (U.S. Government Printing Office, Rockville, MD, 1988) chap. 6, pp. 377–458.
4. B. J. Everitt, T. W. Robbins, *Nat. Neurosci.* **8**, 1481 (2005).
5. F. E. Pontieri, G. Tanda, F. Orzi, G. Di Chiara, *Nature* **382**, 255 (1996).
6. S. Grant *et al.*, *Proc. Natl. Acad. Sci. U.S.A.* **93**, 12040 (1996).
7. K. R. Benson *et al.*, *Neuropsychopharmacology* **26**, 376 (2002).
8. A. L. Brody *et al.*, *Arch. Gen. Psychiatry* **59**, 1162 (2002).
9. R. Z. Goldstein, N. D. Volkow, *Am. J. Psychiatry* **159**, 1642 (2002).
10. H. Garavan *et al.*, *Am. J. Psychiatry* **157**, 1789 (2000).
11. G. J. Wang *et al.*, *Life Sci.* **64**, 775 (1999).
12. L. A. Selt *et al.*, *Drug Alcohol Depend.* **60**, 207 (2000).
13. H. Myrick *et al.*, *Neuropsychopharmacology* **29**, 393 (2004).
14. A. R. Damasio *et al.*, *Nat. Neurosci.* **3**, 1049 (2000).
15. A. R. Damasio, *The Feeling of What Happens: Body and Emotion in the Making of Consciousness* (Harcourt, Chicago, 2000).
16. A. D. Craig, *Nat. Rev. Neurosci.* **3**, 655 (2002).
17. M. P. Paulus, S. F. Tapert, M. A. Schuckit, *Arch. Gen. Psychiatry* **62**, 761 (2005).
18. All of the patients in this study were selected from the patient registry of the Division of Behavioral Neurology and Cognitive Neuroscience, Department of Neurology, University of Iowa. Selection criteria are detailed in the Materials and Methods. The insula was defined here as the region bounded anteriorly by the limen insulae and posteriorly, inferiorly, and superiorly by the circular insular sulcus. This included both anterior and posterior insular cortices and underlying white matter.
19. K. C. Berridge, T. E. Robinson, *Trends Neurosci.* **26**, 507 (2003).
20. S. T. Tiffany, *Psychol. Rev.* **97**, 147 (1990).
21. A. Bechara, *Nat. Neurosci.* **8**, 1458 (2005).
22. A. Bechara, D. Tranel, H. Damasio, *Brain* **123**, 2189 (2000).
23. Patient N. is a right-handed male who was 38 years old when we interviewed him. N. started smoking at the age of 14. At the time of his stroke, he was smoking more than 40 unfiltered cigarettes per day and was enjoying smoking very much. By his own admission, he was heavily addicted to smoking. He recalled that he used to experience frequent urges to smoke, especially upon waking, after eating, when he drank coffee or alcohol, and when he was around other people who were smoking. He often found it difficult to refrain from smoking in situations where it was inappropriate (e.g., at work or when he was sick and bedridden). He was aware of the health risks of smoking before his stroke but was not particularly concerned about those risks. Before his stroke, he had never tried to stop smoking, and he had had no intention of doing so. N. smoked his last cigarette on the evening before his stroke. When asked about his reason for quitting smoking, he stated simply "I forgot that I was a smoker." When asked to elaborate, he said that he did not forget the fact that he was a smoker but rather that "my body forgot the urge to smoke." He felt no urge to smoke during his hospital stay, even though he had the opportunity to go outside to smoke. His wife was surprised by the fact that he did not want to smoke in the hospital, given the degree of his prior addiction. N. recalled how his roommate in the hospital would frequently go outside to smoke and that he was so disgusted by the smell upon his roommate's return that he asked to change rooms. He volunteered that smoking in his dreams, which used to be pleasurable before his stroke, was now disgusting. N. stated that although he ultimately came to believe that his stroke was caused in some way by smoking, suffering a stroke was not the reason why he quit. In fact, he did not recall ever making any effort to stop smoking. Instead, it seemed to him that he had spontaneously lost all interest in smoking. When asked whether his stroke might have destroyed some part of his brain (fig. S2) that made him want to smoke, he agreed that this was likely to have been the case.
24. M. H. Maqbool, A. Bechara, *Pharmacol. Biochem. Behav.* **61**, 621 (2005).
25. J. E. Rose, *Psychopharmacol. Ser. (Berlin)* **184**, 274 (2006).
26. D. Hatsukami, J. R. Hughes, R. Pickens, *Natl. Inst. Drug Abuse Res. Monogr.* **53**, 56 (1985).
27. W. B. Pickworth, R. V. Fant, *Psychoneuroendocrinology* **23**, 131 (1998).
28. T. C. Pritchard, D. A. Macaluso, P. J. Eslinger, *Behav. Neurosci.* **113**, 663 (1999).
29. C. Cereda, J. Ghika, P. Maeder, J. Bogousslavsky, *Neurology* **59**, 1950 (2002).
30. A. R. Buchhalter, M. C. Acosta, S. E. Evans, A. B. Breland, T. Eissenberg, *Addiction* **100**, 550 (2005).
31. E. C. Westman, F. M. Behm, J. E. Rose, *Chest* **107**, 1358 (1995).

32. The authors thank A. Damasio, T. Grabowski, D. Tranel, and B. Porter for helpful comments on the manuscript and S. Mehta for expert advice on the logistic regression analyses. This research was supported by National Institute on Drug Abuse grants F30 DA016847 (N.H.N.) and R21 DA16708 (A.B.) and National Institute of Neurological Disorders and Stroke grant PO1 NS019632 (A.R. and H.D.).

Supporting Online Material

www.sciencemag.org/cgi/content/full/315/5811/531/DC1
Materials and Methods
Figs. S1 and S2
Tables S1 to S5
References

4 October 2006; accepted 15 December 2006
10.1126/science.1135926

Combo System

The OmniLog Combo System is capable of both microbial identification and kinetic characterization of cellular functions. Laboratories often pursue research projects such as strain characterization, comparisons between pathogenic and non-pathogenic strains of bacteria, or product contamination tests with access to both technologies in a single analytical system helps. The system's proprietary method for microbial identification allows laboratories to easily identify and characterize a wide range of gram negative and gram positive bacteria. With the added capabilities of Phenotype MicroArray technology for oxidation of kinetic quantitation of phenotypes, researchers are able to measure cell pathway activities and phenotypes by analyzing cells under thousands of culture conditions. This provides data essential to understanding variations among bacterial strains, correlating genotypes to phenotypes, discovering new targets for antimicrobial compounds, improving and optimizing bioprocesses, and more. Biolog microbial identification is based on the use of 95 different carbon compounds contained in a convenient pre-filled microtiter format to measure metabolic reactions. This diverse set of tests enables the system to identify microorganisms that kit-based methods do not recognize or often misidentify.

Biolog For information 510-785-2564 www.biolog.com

Sulfhydryl Group Quantification

Ellman's reagent is a versatile, water soluble compound used in the quantification of free sulfhydryl residues. Assays using this reagent allow researchers to eliminate the reduction and purification step in sulfhydryl cross linking reactions by testing if free sulfhydryls are already present. Suitable for peptide and protein coupling reactions, Ellman's reagent is a quick colorimetric assay.

G-Biosciences/Genotech For information 800-628-7730 www.GBiosciences.com

Custom Microplates

Porvair Sciences offers custom design and manufacture of microplates for life science, chromatography, environmental, and medical applications. Customers can benefit from a range of proprietary techniques used in the generation of custom microplates, including polymer ultrasonic welding, plasma surface treatment, co-sintering of polymers/silicas, and "two shot" injection molding. Porvair also offers a comprehensive range of high performance 96 well and 384 well glass bottom microplates that combine the advantages of optical properties of glass, low background, and low birefringence with the versatility of a microplate. They are available tissue culture treated to optimize cell growth or without surface modification.

Porvair Sciences For information +44 1932 240255 www.porvair-sciences.com

Multispectral Imaging System

The In Vivo Multispectral system can identify molecular abnormalities that are the origin of disease at a very early stage. In vivo molecular imaging allows noninvasive measurement of biological processes within a living organism. The new system incorporates workflow automation and advanced multispectral fluorescence, luminescence, digital x-ray, and radioisotopic imaging capabilities for in vivo imaging of small animals for drug development and life science research. The system's computer controlled multispectral tuning of excitation light allows the identification and separation of multiple fluorochromes and the removal of autofluorescence background. The In Vivo Multispectral system automatically generates and analyzes multispectral fluorochrome images with spatially co-registered x-ray and white light images for improved localization of biological markers in vivo. By combining multispectral fluorescence with digital x-ray, the system allows researchers to precisely locate, identify, and monitor changes in molecular activity of specific cells or organs within small animals, long before morphological changes can be detected.

Eastman Kodak For information 877-747-4357 www.kodak.com/go/molecular

HLA Antibody Analysis System

The DynaChip HLA Antibody Analysis system makes use of an automated microarray platform to detect antibody reaction to specific human leukocyte antigens. Up to 96 tests can be performed at the same time in a fully automated manner, with each test including an array of proteins. The system includes software for rapid analysis of results.

Invitrogen For information 800-955-6288 www.invitrogen.com

Evaporator

The Activotec Evaporator is a simple-to-use, low cost parallel evaporator and lyophilizer. Designed to be small and light enough to be used safely in conjunction with any rotary evaporator or vacuum pump fitted with a cold trap, the evaporator offers a productive means of simultaneously evaporating or lyophilizing solvent from multiple glass vials. The evaporator transforms an ordinary rotary evaporator or vacuum pump with a cold trap into a productive tool that can evaporate up to 33 samples simultaneously, accommodating a wide range of vial sizes (3 ml, 7.4 ml, 20 ml, 22 ml, and 40 ml). Using standard vials for evaporation enables direct transfer of samples from a synthesizer to the evaporator, eliminating the need for liquid transfer with its potential for contamination. Each evaporator vial incorporates a novel filter through which all solvent has to evaporate, thereby minimizing the possibility of sample loss or cross-contamination. The evaporator is manufactured from a Teflon composite material, chosen for its robustness, chemical resistivity, and high thermal conductivity.

Activotec For information +44-1223 260008 www.activotec.com

Newly offered instrumentation, apparatus, and laboratory materials of interest to researchers in all disciplines in academic, industrial, and government organizations are featured in this space. Emphasis is given to purpose, chief characteristics, and availability of products and materials. Endorsement by *Science* or AAAS of any products or materials mentioned is not implied. Additional information may be obtained from the manufacturer or supplier by visiting www.science.labvelocity.com on the Web, where you can request that the information be sent to you by e-mail, fax, mail, or telephone.

POSITIONS OPEN

FACULTY POSITION IN PROTEOMICS/MASS SPECTOMETRY. The Department of Pathology at the University of California, San Diego (UCSD), **website: http://medicine.ucsd.edu/Pathology**, seeks a Ph.D. in chemistry or biochemistry with significant experience in the use of mass spectrometry to analyze complex protein solutions. Appointment is available at the **ASSISTANT** or **ASSOCIATE PROFESSOR** level. The successful candidate will be expected to develop and direct a state-of-the-art mass spectrometry/proteomics facility and to have a strong understanding of innovative technology development in this area. Working in collaboration with biologists and biochemists in the Department of Pathology, the new appointee will build a research program in biomarker discovery. This team effort will focus on cancer, neurodegeneration, infectious diseases, and cardiovascular sciences. At least three years of postdoctoral experience, strong area-specific publications, an understanding of the use of bioinformatics in the analysis of proteomics data, outstanding communication skills, and an ability to collaborate are required. Please forward application letters addressed to: **Search Committee Co-Chairs, Drs. David Cheresh and Steve Gonias,** together with curriculum vitae and names/addresses of at least three references, c/o **Ms. Catherine Schumacher, Search Coordinator, Department of Pathology 0717, University of California San Diego School of Medicine, 9500 Gilman Drive, La Jolla, CA 92093-0717.** Applications by e-mail are acceptable to **e-mail: cschumacher@ucsd.edu.** Review of applications will begin March 2, 2007, and will continue until filled. *UCSD is an Affirmative Action/Equal Opportunity Employer with a* [illegible]

ASSISTANT PROFESSOR OF BIOLOGY. One-year sabbatical replacement position beginning September 2007. Ph.D. required. Salary competitive. Responsibilities include team-teaching the [illegible] and genetics and upper-level courses in his/her area of specialization. Preferred areas include microbiology, immunology, and developmental biology. Kalamazoo College is a highly selective, nationally known liberal arts college that takes pride in its tradition of outstanding undergraduate science education. Candidates are expected to have high aptitude and interest in undergraduate teaching and a [illegible] the liberal arts. For more information please see **website: http://www.kzoo.edu.** Completed applications received by March 15, 2007, will receive full consideration; later applications reviewed as needed until the position is filled. Send letter of application, [illegible] undergraduate and graduate transcripts (unofficial acceptable), statement of teaching philosophy and research interests, and three letters of recommendation [illegible] **Dr. James Langeland, Chair, Department of Biology, Kalamazoo College, 1200 Academy Street, Kalamazoo, MI 49006-3295.** Kalamazoo College encourages candidates who will contribute to the cultural diversity of the College to apply and to identify themselves if they wish. *Equal Opportunity Employer.*

FACULTY POSITION
Department of Biochemistry
Tulane University School of Medicine

The successful candidate will be expected to conduct a nationally competitive research program in the biochemical sciences and to play a leading role in maximizing the impact of the Department's educational activities on the medical school's doctoral (M.D. and Ph.D.) training programs. Rank, salary, startup, and tenure considerations will depend on the candidate's experience and potential for substantive contributions to our academic environment. Send curriculum vitae and a statement describing research interests and career goals to the **Biochemistry Search Committee, TUHSC SL43, 1430 Tulane Avenue, New Orleans, LA 70112-2699 or by e-mail: biochem@tulane.edu.**

Tulane University is an Affirmative Action/Equal Opportunity Employer and encourages applications from minorities [illegible]

DIRECTOR, CENTER for SCIENCE and MATHEMATICS EDUCATION

We invite applications for the position of Director of San Francisco State University's new Center for Science and Mathematics Education. The Center has been created to recruit, prepare, and support good science and mathematics teachers, foster educational research, and develop a K to 18-plus community of educators. The Director will lead and manage the Center, plan and coordinate its activities in collaboration with the faculty, and supplement its budget through external grants. Candidates should have a Ph.D. in math, science, or math or science education, and at least five years of increasingly responsible experience administering educational programs.

The Director position is a full-time, nonfaculty Administrator III management position in the College of Science and Engineering. (For more information, see **website: http://curie.sfsu.edu/csme/people/DirectorAd.pdf.**) Applications will be considered beginning March 5, 2007; the position will remain open until filled.

San Francisco State University (SFSU), **website: http://www.sfsu.edu,** a campus of the California State University system, serves a diverse student body of 30,000 undergraduate and graduate students. *SFSU is an Equal Opportunity/Americans with Disabilities Act Employer and has a strong commitment to the principles of diversity.*

The Biology Department at Clarkson University invites applications for **DIRECTOR OF FIRST YEAR BIOLOGY** at the level of **ASSISTANT PROFESSOR.** This nontenure track, full-time, renewable position is appropriate for doctoral-level professionals in the life sciences committed to excellence in teaching introductory college biology in both lecture and laboratory format. Experience and demonstrated success in teaching a broad array of topics in contemporary biology to both biology majors and nonscience majors are required. The position includes responsibility for designing and implementing laboratory exercises, training and supervising teaching assistants, and conducting an annual departmental teaching assessment. Candidates with research experience who are interested in collaborating on externally funded pedagogical or laboratory-based projects are especially encouraged to apply. Clarkson is a small private University with a mission focused on technology serving humanity. Potsdam is an educational and cultural center of northern New York located in proximity to the Adirondack Park and within two hours of Ottawa, Montreal, and Lake Placid. Applicants should submit a cover letter with curriculum vitae, a statement of teaching philosophy, and contact information for three or more references in one PDF file to **e-mail: biologysearch@clarkson.edu** or by mail to: **Biology Search Committee, P.O. Box 5805, Clarkson University, Potsdam, NY 13699.** Applications received before February 28, 2007, will receive full consideration. Position number 77-06. *Clarkson University is an Equal Opportunity/Affirmative Action Employer.*

DIRECTOR OF THE ENERGY POLICY INSTITUTE AND ASSOCIATE DIRECTOR OF CENTER OF ADVANCED ENERGY STUDIES
Boise State University

The Department of Public Policy and Administration at Boise State University is seeking qualified individuals to apply as a **SENIOR LEVEL PROFESSOR** to serve as the Director of the Energy Policy Institute. For information about the position and how to apply, please see position number AAC[illegible]2006-67 on our **website: http://hrs.boisestate.edu/joblistings/faculty/** *Boise State University is an Equal Employment Opportunity/Affirmative Action Institution.* [illegible] *preference.*

WWW.NIH.GOV
Positions NIH
THE NATIONAL INSTITUTES OF HEALTH

Tenure-Track and Tenured Investigator Positions in Systems Immunology and Infectious Disease Modeling

The National Institute of Allergy and Infectious Diseases (NIAID), Division of Intramural Research (DIR) is seeking several outstanding individuals for its new Program in Systems Immunology and Infectious Disease Modeling (PSIIM).

Modern technology allows the analysis of immune responses and host-pathogen interactions at multiple levels – from intracellular signaling networks, to individual cell behavior, to the function of a tissue, organ, or even whole organism. The challenge is not only to collect large amounts of data, but also to organize it in a manner that enhances our understanding of how the immune system operates or how an agent affects the host. To do this, we need to develop detailed quantitative models that can be used to predict the behavior of a complex biological system. These models can help to explain the mechanisms underlying physiological and pathological responses to infection or vaccination, which can then be exploited to design better therapies or vaccines.

Achieving this goal requires an interdisciplinary effort and to this end the PSIIM will be organized as an integrated team of scientists and support staff with expertise in computational biology, bioinformatics, proteomics, cell biology, immunology, and infectious diseases, rather than as a group of independent laboratories. These teams will have access to the latest technology for gene expression profiling, high-content screening of RNAi libraries for the discovery of pathway components, imaging tools, cores for the genetic manipulation of animals and/or primary cell lines, and a substantial computer infrastructure. BSL-3 facilities for working with high priority pathogens will also be available.

Although the PSIIM has been established within NIAID and has an immune system or infectious disease focus, we expect it to foster the growth of systems biology efforts at other NIH Institutes, primarily through the development of new software tools for multiscale systems modeling and methods for high-throughput screening. Thus, PSIIM team members are expected to interact extensively with other NIH scientists and with extramural groups in the U.S. and abroad who share our interest in a systems approach to biology.

The PSIIM is now recruiting for tenure-track or tenure level team leader appointments in three key areas:

Computational Biology. The incumbent will lead a group focused on the development and improvement of software tools and multiscale modeling and simulation that can be used by the PSIIM as well as by biologists interested in subjects other than immune system or infectious diseases. The ideal candidate will have a strong background in mathematics, physics, and computer programming, and a clear desire and ability to interact with and support the efforts of bench biologists. A demonstrated ability to generate computer software tools for biological modeling will be a strong plus.

Molecular/Cell Biology. The incumbent will lead a group involved in the design, implementation, and interpretation of screening experiments to identify and determine the interactions among the components in signaling networks that could then be modeled mathematically or software generated by the computational biology team or obtained from other sources. Discovery tools such as gene arrays, high-content image-based screens using RNAi methods, various protein-protein hybrid screening methodologies, and optical imaging are expected to be key elements in the toolbox of this group. A strong background in molecular biology and molecular biology with experience in analysis of protein-protein interactions, signaling, and/or gene regulation is required. Expertise in large-scale screening is highly desirable.

Infectious Diseases. The incumbent will be responsible for developing novel approaches to systems-wide analysis of the interaction of infectious agents and their hosts. These may include the use of gene expression signatures, the production of gene-modified animals, the development of methods for in vivo imaging of the interactions of models, and the use of biophysical imaging and other tools for probing the interaction of pathogens and host cells in vitro. A strong background in virology and/or bacterial infectious diseases and cell and molecular biology are necessary. Training in the immunology of infectious diseases and substantial bioinformatics experience are highly desirable.

These positions and the research activities they conduct are fully funded by the intramural research program of NIH. Each team leader is expected to build a working group consisting of postdoctoral fellows, staff scientists, collaborators, and students. The team leaders will work with the program director to help set the goals of the PSIIM and to determine how best to reach these goals as an integrated group. To ensure appropriate career trajectories for those joining the PSIIM team, the NIH has modified its tenure decision policies to encourage and account for contributions made in such a team science setting. Applicants should be seeking a difficult challenge in which creativity, technical expertise, and a strong desire to achieve in a team environment are critical for success.

Interested candidates may contact **Dr. Ronald Germain, Program Director, PSIIM, DIR, NIAID at 301-496-1904 or rgermain@niaid.nih.gov** for additional information about these positions.

To apply, submit your curriculum vitae, bibliography, and detailed statement of how you can contribute to the success of the PSIIM program to **Felicia Braunstein at braunstein@niaid.nih.gov**. In addition, three letters of reference must be sent directly from the referee to **Dr. Robert Hohman, Chair, NIAID Search Committee, c/o Ms. Felicia Braunstein, DIR Committee Management Team Lead, 10 Center Drive, MSC 1356, Building 10, Room 4A31, Bethesda, Maryland 20892-1356**. Completed applications **MUST** be received by **February 16, 2007** for computational biology, and **March 16, 2007** for Molecular/Cell Biology as well as for infectious diseases. Please refer to ad **#012 for computational biology, #013 for molecular/cell biology, and #014 for infectious diseases** in all correspondence. Further information on these positions and guidance on submitting your application are available at **http://healthresearch.niaid.nih.gov**. For more information about the NIAID systems biology program, please visit **http://www.nih.gov/catalyst/2006/06.09.01/page1.html**

Positions NIH
THE NATIONAL INSTITUTES OF HEALTH

TENURE TRACK POSITION
LABORATORY OF CELLULAR AND MOLECULAR BIOLOGY

The Laboratory of Cellular and Molecular Biology (LCMB), Center for Cancer Research, of the National Cancer Institute, National Institutes of Health (http cancer.gov/labs/lab.asp?labid=64) has a long tradition of excellence in the investigation of signal transduction pathways involved in both normal cellular function and malignant transformation. The Laboratory now invites applications for a tenure track investigator to develop an independent basic research program in cellular and molecular biology with emphasis on understanding basic signal transduction processes. Areas of potential interest include but are not restricted to the role of signaling pathways in stem cell biology, inflammation and cancer, or malignant transformation. The applicant should hold a Ph.D., M.D., or M.D., Ph.D. degrees. Salary is commensurate with education and experience. This position is supported by the Intramural Center for Cancer Research of the National Cancer Institute. A two-page statement of research interests and goals should be submitted in addition to three letters of recommendation and a curriculum vitae by March 9, 2007 to: Mrs. Erin M. Breedlove, Executive Secretary, Laboratory of Cellular and Molecular Biology, CCR, NCI, Building 37, Room 2066, Bethesda, MD 20892-4256, phone: 301-496-9683, Fax: 301-496-8479, email: breedlovee@mail.nih.gov. Candidates must be U.S. citizens or permanent residents. NIH Tenure track investigators with educational debts may be eligible for the NIH Loan Repayment Program. The NCI is an Equal Opportunity Employer.

NIEHS
National Institute of Environmental Health Sciences

Functions of Sir2 and Nuclear Receptors

Postdoctoral positions are available immediately in the Laboratory of Signal Transduction at the National Institute of Environmental Health Sciences (NIEHS), a major research institute of the NIH located in Research Triangle Park, North Carolina. NIEHS offers an outstanding research environment and has been constantly rated by The Scientist as one of the best places for post-docs to work.

Our research is focused on the roles of NAD+-dependent protein deacetylase Sir2 and corresponding post-translational modification of nuclear receptors in aging and age-associated diseases. We have shown that SIRT1, the mammalian orthology of Sir2, physically interacts and deacetylates Liver X Receptors (LXRs), thus regulates their transcriptional activity and cholesterol homeostasis. Current research areas include nuclear receptor signaling pathways regulated by SIRT1 and their roles in metabolism, aging, and metabolic diseases such as atherosclerosis and obesity.

We seek highly self-motivated individuals who have a strong background in signaling and transcriptional/translational regulation, and are interested in aging research. Experience with mouse models is a plus. To apply, please send a cover letter, CV and list of three references to Dr. Xiaoling Li at email: lix2@niehs.nih.gov.

Tenure/Tenure-Track Position
Laboratory of Persistent Viral Diseases
Rocky Mountain Laboratories, Hamilton, Montana

The Laboratory of Persistent Viral Diseases (LPVD), Rocky Mountain Laboratories, NIAID, NIH, DHHS, in Hamilton, Montana, seeks applicants for a tenured or tenure-track position (full to assistant professor equivalent) to conduct independent research on host immune or inflammatory responses in neuropathogenic viral diseases. Candidates with a background in adaptive or innate immunity, including neuroinflammation and gliosis are preferred; those interested in neurobiology, biochemistry or pathogenesis of CNS infections are also encouraged to apply. Candidates must hold a Ph.D., D.V.M. or M.D. degree and have a minimum of 3 years of relevant postdoctoral experience. Candidates must be able to develop an independent research program, supervise staff and fellows, and collaborate with other LPVD researchers working on CNS viral or prion diseases.

Rocky Mountain Laboratories' state-of-the-art facilities include an operational BSL-3 facility, a BSL-4 lab and animal facility nearing completion, and in-house core facilities for genomics, electron microscopy, and flow cytometry. Research programs focus on prions, murine retroviruses, HIV, flaviviruses, and numerous pathogenic prokaryotic organisms. The lab is located in the scenic Bitterroot Valley of western Montana with easy access to some of the finest outdoor recreational opportunities in North America. Additional information on the position may be obtained by contacting Dr. Bruce Chesebro at bchesebro@niaid.nih.gov.

Application Process: Salary depends on degree and qualifications. To apply, submit a curriculum vitae and bibliography including a list of your five most significant papers, and a 2-3-page description of a proposed research program, via e-mail to **Ms. Felicia Braunstein at braunsteinf@niaid.nih.gov**. In addition, three letters of recommendation must be sent directly from the referees to **Ms. Felicia Braunstein, Committee Manager, NIAID/NIH: 18 Crater Drive, Bldg. 18, Rm.4A31, MSC-1356, Bethesda, MD 20892-1356**. Applications must reference **AD #010** and must be received by **March 9, 2007**. Applicants will be notified when their applications are received and then completed. All information provided by applicants will remain confidential.

The NIH Director's Wednesday Afternoon Lecture Series

Biomedical scientists around the world are invited to join us on-line to hear leading investigators present their latest results to the NIH Intramural Research community. Lectures may be viewed live at 3:00 p.m. EST (20:00 GMT) on Wednesdays, from September through June. Live webcasts can be viewed under "Today's Events" at http://videocast.nih.gov >

The current schedule of lectures is available at: <http://www1.od.nih.gov/wals/schedule.htm>

Upcoming Lectures:

•January 10: Thomas J. Silhavy, Princeton University: Outer membrane Biogenesis in Gram-Negative Bacteria

•January 17: Joshua LaBaer, Harvard Medical School: Functional Proteomics for Biomarker and Target Discovery

•January 24: Robert G. Griffin, MIT, Cambridge, MA: Solid State NMR of Membrane and Amyloid Proteins

•January 31: Clara Franzini-Armstrong, University of Pennsylvania: Protein Interactions in Calcium Release Units of Skeletal and Cardiac Muscles

WWW.NIH.GOV

Department of Health and Human Services
National Institutes of Health
Clinical Center

Chief, Clinical Imaging Sciences Department

The National Institutes of Health (NIH) invites candidates with outstanding clinical leadership and scientific credentials to apply for the position of Chief, Clinical Imaging Sciences Department, Clinical Center, Bethesda, MD. The Clinical Imaging Sciences Department is a multidisciplinary program of radiologists, scientists, and support staff who provide clinical services and imaging research in the NIH Clinical Center, the world's largest hospital totally dedicated to translational clinical research.

The NIH Clinical Center Clinical Imaging Sciences Department is a unique medical environment with a diverse staff of ~30 individuals. The department has undergone an extensive multi-million dollar renovation which includes state-of-the-art multidetector CT (64 and 32) MRI units, an interventional suite with a dedicated CT, fluoro and stereotactic breast biopsy, digital fluoroscopy and radiography. A recently updated PACS system provides electronic archiving throughout the Clinical Center. The Nuclear Medicine component includes PET/CT and SPECT/CT as well as conventional gamma cameras. There are extensive opportunities for independent and collaborative clinical and imaging research with the diverse Institutes with in the NIH. The department has an extensive research infrastructure which includes a fully equipped molecular biology laboratory, cold and hot chemistry facilities, a research MR facility and access to a Molecular Imaging Laboratory which houses microCT, ultrasound and optical imaging.

The ideal candidate will be a board certified radiologist with extensive academic, clinical and managerial experience in providing radiological services. The individual should have made significant contributions to the scientific peer-reviewed imaging literature and have a track record of combining excellence in imaging services with a unique clinical and/or basic research program. The appointment (tenure/tenure track/Senior Clinician) will be commensurate with experience. The salary and benefits package will be competitive.

Candidates should submit their CV, letter of interest, and the names of six references to **Ms. Colleen McGowan, Office of the Director, CC, NIH, Bldg 10, CRC, Room 6-2551, 10 Center Dr., MSC 1504, Bethesda MD 20892 or via email at cmcgowan@cc.nih.gov**. Materials should be submitted by **February 28, 2007**.

Health Scientist Administrator
National Institute of Dental and Craniofacial Research (NIDCR)

The National Institute of Dental and Craniofacial Research (NIDCR), National Institutes of Health (NIH), Department of Health & Human Services (DHHS), is seeking applicants for a supervisory Health Scientist Administrator position in the Center for Integrative Biology and Infectious Diseases (CIBID). The position advertised is for the Chief of the Translational Genomics Research Branch. The Branch coordinates the development and implementation of the NIDCR extramural basic and translational genomics research program related to NIDCR-relevant human and microbial genetics and genomics. Includes studies of basic and applied research in the NIDCR mission to include: infectious diseases such as dental caries and periodontal diseases, microbiology, molecular and cellular neuroscience, developmental biology, mineralized tissue and salivary gland physiology, immunology and immunotherapy, epithelial cell regulation and transformation as well as biomaterials, biomimetics and tissue engineering, and behavior, health promotion and environment. In addition, there are cross-cutting programs involving clinical trials and comprehensive centers of discovery.

The incumbent will direct and oversee the administration of a portfolio of research projects employing translational genetics and genomics research strategies targeted to NIDCR-relevant diseases and will stimulate interest in and provide advice to the extramural community regarding the respective research portfolio. In addition, the incumbent will participate in funding decisions, policy development, as well as implementation and coordination with other programs both within and outside of the NIDCR.

The salary range for this position is $107,527 to $139,774 per annum, commensurate with qualifications and professional experience. A full benefits package is available, which includes retirement, Thrift Savings Plan participation, health, life and long term care insurance.

Applications will be accepted through **February 15, 2007**. For qualifications required, evaluation criteria, and application instructions, view the Vacancy announcements at **http://jobsearch.usajobs.opm.gov/a9nih.asp**. Refer to announcement # **NIDCR-07-162498-DE or NIDCR-07-162738-MP.** Please contact **Elan Ey at 301-594-2320 or eye@mail.nih.gov** if you have questions.

THE UNIVERSITY OF HONG KONG

香港大學

Founded in 1911, The University of Hong Kong is committed to the highest international standards of excellence in teaching and research, and has been at the international forefront of academic scholarship for many years. Of a number of recent indicators of the University's performance, one is its ranking at 33 among the top 200 universities in the world by the [illegible] Higher Education Supplement. The [illegible] has a total [illegible] students [illegible] graduate [illegible] undergraduate and postgraduate students from [illegible] countries, and a complement of [illegible] academic members of staff, many of whom are internationally renowned.

Tenure-Track position in Planetary/Earth Science in the Faculty of Science (Ref.: RF-2006-2007-27R)

Applications are invited for appointment as Associate Professor/Assistant Professor in Planetary/Earth Science in the Faculty of Science, [illegible] 2007 or as soon as possible thereafter. The post will initially be made on a three-year term. Appointment with tenure will be considered during the second three-year [illegible].

The Faculty seeks a person with a research background in one or more of the following areas: early history and evolution of the Earth and other planets, interactions between the geological, atmospheric, and biological evolution, influence of extraterrestrial events on [illegible] evolution. Applicants must have a [illegible] and a commitment to excellence in undergraduate and graduate teaching. Research start-up funds will be available. The appointee is expected to foster collaborative research between the disciplines of earth sciences, biological sciences, and astronomy and may be offered a joint appointment in more than one department as deemed appropriate.

Annual salaries will be in the following ranges (subject to review from time to time at the entire discretion of the University):

Associate Professor	[illegible] approximately US$ [illegible] HK$ [illegible]
Assistant Professor	[illegible]

The fixed-term appointment will attract a contract-end gratuity and University contributions to a provident fund scheme. Other fringe benefits include [illegible] and medical/dental benefits. At current rates, salaries tax does not exceed 16% of gross salary. Housing benefits will be provided as applicable.

For enquiries of the existing research activities and the specific job requirements, please write to Professor S. Kwok, Dean, Faculty of Science (e-mail: [illegible]). **Further particulars and application forms** (232.30[illegible] amended) can be obtained at http://www.hku.hk/apptunit/form.htm. Application should be sent to the Assistant Registrar (Appointments), Room [illegible], Hong Kong (fax: [illegible]; e-mail: [illegible]). **Closes February 28, 2007.**

The University is an equal opportunity employer and [illegible]

IIASA

DIRECTOR
International Institute for Applied Systems Analysis

The International Institute for Applied Systems Analysis (IIASA), located near Vienna, Austria, is seeking a highly qualified scientific leader for the position of Director beginning 1 July 2008. The successful candidate will oversee and guide a diverse research program combining natural and social science to produce scientifically based policy guidance on issues related to global change. Candidates should combine a vision for IIASA with scientific excellence, management and diplomatic skills, fundraising accomplishments, and broad experience in interdisciplinary, policy-relevant research. The Director should be an effective and active advocate to expand participation in and membership of IIASA. The Director supervises approximately 200 scientists and support staff from 30 countries.

IIASA is independent, governed by an international consortium of its National Member Organizations. Applicants should have excellent written and spoken English, the working language of the Institute. The Institute's management and staff alike are committed to a working environment that promotes equality, diversity, and tolerance. The Institute encourages applications from all qualified candidates.

The post is a 3-year position with the possibility of renewal. Salary and benefits are competitive with comparable international organizations. Review of applications will begin on **1 April 2007**. Submit letter of application, CV, bibliography, and contact information for three references, to: **Professor Pentti Vartia, Chairman of the Search Committee, c/o Irina Forsman, The Academy of Finland, Vilhonvuorenkatu 6, P.O. Box 99, FIN-00501 Helsinki, Finland.**

For more information about IIASA and this position, visit our web site at: **http://www.iiasa.ac.at**

FACULTY – TENURE TRACK
BIOLOGICAL SCIENCES

The Department of Molecular Pharmacology at the Albert Einstein College of Medicine is searching for tenure track faculty. Candidates may apply for positions at any academic level.

Key criteria include a record of excellence in research; an innovative research plan that will address fundamentally important biological problems; and a commitment to training and teaching fellows, graduate and medical students.

Specific areas of interest are: mechanisms of action of drugs, hormones, oncogenes, growth factors, and neurotransmitters; receptor functions; physiology and regulation; glycobiology relevant to receptors and specificity of protein interactions; regulatory enzymes; structure/function of plasma membrane transporters; signal transduction, second messengers and protein phosphorylation; regulation of cell functions by proteolysis; intracellular targeting and trafficking of vesicles and regulatory proteins; and drug resistance. Areas targeted for development of Molecular Pharmacology include proteomics, micro RNAs, chemical biology and regulation of multi-protein complexes.

Molecular Pharmacology is broadly interpreted and investigators employing a variety of model systems will be considered. NIH—funded centers for Cancer, Diabetes, Obesity and Liver diseases provide outstanding colleagues, collaborators and core facilities for members of the Department. Members of the Molecular Pharmacology Department will participate in creation of the Price Center for Genetics and Translational Medicine, which will open in early 2008. State-of-the-art centers for Biophotonics Imaging, Structural Biology and Chemical Biology will be expanded in the new facility. Substantial resources are committed to start and sustain laboratories of recruited faculty.

Albert Einstein College of Medicine is located in a residential area of the northeast Bronx, with close proximity to Westchester County and Manhattan. A curriculum vitae, statement of research interests, future plans and names of three references should be sent via email to **molpharm@aecom.yu.edu** or by mail to **Ms. Anna Cioffi, Administrator, Department of Molecular Pharmacology, Albert Einstein College of Medicine, Jack and Pearl Resnick Campus, 1300 Morris Park Avenue, Bronx, NY 10461. EOE**

ALBERT EINSTEIN COLLEGE OF MEDICINE
Advancing science. Building careers.

MICHIGAN STATE UNIVERSITY

Chemical Carcinogenesis or Developmental Toxicology
Tenure-Track Faculty Position at Michigan State University

The Center for Integrative Toxicology (CIT) at Michigan State University invites applications for a tenure-track academic year faculty position at the Assistant or Associate Professor level. The CIT has over 40 affiliated faculty members and administers a Superfund Program Project grant and a Training grant, both awarded by the NIH/NIEHS. We are seeking candidates with expertise in either chemical carcinogenesis or developmental toxicology to strengthen our growing interest in these areas. Candidates should have a Ph.D. degree in Toxicology or a related discipline, postdoctoral research experience and demonstrated success in obtaining extramural funding.

This position involves a joint appointment in the CIT and in a biomedical science department (e.g. Biochemistry & Molecular Biology, Food Science and Human Nutrition, Pharmacology & Toxicology, Physiology) consistent with his/her expertise and interests. In addition to contributing to the CIT the candidate will have the opportunity [illegible] interdisciplinary research and training programs including the National Food Safety and Toxicology Center, the Center for Biological Modeling, Breast Cancer and the Environment Research Centers and the Genetics and Neuroscience Programs. He/she will be expected to establish and maintain an independent and extramurally-funded research program and [illegible] the teaching and service missions of the department and the CIT.

[illegible]ed individuals should send their curriculum vitae, statement of [illegible] and future research plans, and 3 letters of recommendation [illegible] Center for Integrative Toxicology, [illegible] Biochemistry Building, Michigan State University, East [illegible], MI [illegible]. Electronic submissions may be sent to [illegible]@msu.edu. Review of applications will begin March 2007 and will continue until the position is filled.

MSU IS AN AFFIRMATIVE ACTION, EQUAL OPPORTUNITY INSTITUTION.

DEPARTMENT OF COMMUNICATIONS, MARINE AND NATURAL RESOURCES
ROINN CUMARSÁIDE, MARA AGUS ACMHAINNÍ NÁDÚRTHA

Charles Parsons Energy Research Awards

20 Researcher Posts (7 year Contracts)

34 PhD Studentships

This is an innovative scheme recently established by the Minister for Communications, Marine & Natural Resources of Ireland with the objective of developing Irish energy research capacity. The initiative also seeks to attract mobile early stage researchers from abroad to Ireland and encourage Irish researchers to visit and work in international centres of energy research.

7 Research Groups/Centres were successful in their bid for the Awards following evaluation by international experts. The research groups/centres are located in Higher Education Institutions on the island of Ireland (32 counties) and have the capacity to conduct innovative research and provide research training. The following are the research groups/centres supported under the scheme and their parent universities:

Bioresources Research Centre (BRC), University College Dublin
Contact: *Prof Shane Ward*. Email: shane.ward@ucd.ie
Tel: + 353 1 7167351. http://www.ucd.ie/bioresources/
Research Group requires – 3 Researchers, 4 PhD Students

Electrical Power & Energy Systems Research Cluster, Queen's University Belfast
Contact: *Dr Damian Flynn*. Email: d.flynn@ee.qub.ac.uk
Tel: + 44 28 9097 4268. http://www.ee.qub.ac.uk/power/
Research Group requires – 2 Researchers, 5 PhD Students

Hydraulics & Maritime Research Centre, University College Cork
Contact: *Dr Tony Lewis*. Email: t.lewis@ucc.ie
Tel: + 353 21 4250021. http://hmrc.ucc.ie
Research Group requires – 4 Researchers, 3 PhD Students

Centre for Sustainable Technologies, University of Ulster
Contact: *Dr Neil J Hewitt*. Email: nj.hewitt@ulster.ac.uk
Tel: + 44 28 9036 8566
Research Group requires – 4 Researchers, 4 PhD Students

Electricity Research Centre (ERC), University College Dublin
Contact: *Ms. Rose Mary Logue*. Email: erc@ucd.ie
Tel: + 353 1 7161858. http://ee.ucd.ie/erc/
Research Group requires – 2 Researchers, 7 PhD Students

Microbial Bioenergy Group, National University of Ireland, Galway
Contact: *Dr Vincent O' Flaherty*
Email: vincent.oflaherty@nuigalway.ie
Tel: + 353 91 493734. http://www.nuigalway.ie/biogen
Research Group requires – 2 Researchers, 4 PhD Students

Charles Parson Research Initiative & Graduate School, University of Limerick
Contact: *Dr Martin J. Leahy*. Email: martin.leahy@ul.ie
Tel: + 353 61 213056. http://www.cp.ul.ie
Research Group requires – 3 Researchers, 7 PhD Students

The research groups/centres above will be advertising shortly for the following positions.

Researchers – up to seven years funding on salary scale €55 000 to €80 486 p.a. and a significant pension contribution. Researchers should have obtained a PhD and have 3 years postdoctoral research experience. Researchers may come from relevant disciplines according to the requirements of the individual research groups/centres.

PhD Studentship – Stipend of €18,000 p.a. plus tuition fees. As part of the PhD studentship funding is available for stays in international centres of excellence. As this measure is designed to stimulate engineers into energy research, PhD students must be graduate engineers.

Interested candidates should contact individual research groups/centres directly for further information on the application process.

The Charles Parsons Energy Research Awards is an initiative under the Irish Government's 'Strategy for Science, Technology and Innovation (2006-2013)'

UNIVERSITÂT BASEL

The Faculty of Science (Philosophisch-Naturwissenschaftliche Fakultät) of the University of Basel invites applications for the position of

Professor of Chemistry

The candidate is expected to have an exceptional track record in inorganic chemistry. The University of Basel has priority research areas in Life Sciences and Nanoscale Sciences and hence we are seeking excellent candidates with internationally recognized research programmes in any area of

Bioinorganic Chemistry

The successful person will participate in teaching inorganic chemistry at all levels of the BSc-MSc- and PhD programmes. Depending on the candidate's qualifications, the appointment will be a tenured Associate or Full Professorship.

The Department of Chemistry is located near the centre of Basel, a town which provides a stimulating and attractive environment for interdisciplinary research due to the concentration of science institutes and chemical and pharmaceutical industry.
For further information see http://www.chemie.unibas.ch

It is hoped that the successful candidate will commence the appointment February 2008, or as soon as possible thereafter. Applications received by 1st April 2007 will be guaranteed full consideration. The University of Basel is an equal opportunity employer. Applications from women candidates are particularly encouraged. Applications, including a curriculum vitae, list of publications, names of four referees, outline of current and future research plans should be sent on CD (one zip file including all documents as pdf files) and on paper to the Dean of the Faculty at the following address: Prof. Dr. phil. Hans-Peter Hauri, Dekanat der Philosophisch-Naturwissenschaftlichen Fakultät, Klingelbergstrasse 70, CH-4056 Basel.
For further information please contact: Prof. Dr. Wolf-D. Woggon, Head, Department of Chemistry, Tel+FAX: +41 61 267 11 02, E-mail: Wolf-D.Woggon@unibas.ch

UNI BASEL

BOWDOIN COLLEGE

Marine Biology

The Bowdoin College Biology Department seeks applicants for a one-year visiting faculty position in marine biology. Candidates should have a Ph.D. by August 2007 and will be expected (1) to teach 3 courses during the 07/08 academic year: a majors core course in marine biology with a weekly laboratory, an advanced course in their area of expertise and a course for non-science majors, and (2) to mentor independent student research projects. The position encourages the use of an all-campus dock and running seawater marine lab for research and teaching (see **http://academic.bowdoin.edu/csc/resources/marine.shtml**).

Review of applications will begin March 1, 2007. Please send a curriculum vita, statement of teaching and research interests and expertise, and arrange for 3 letters of recommendations to be forwarded to: **Marine Biology Search, Dept of Biology, 6500 College Station, Bowdoin College, Brunswick, ME 04011.** For further information about the college, the department and the program, please see our website: **www.bowdoin.edu**

Bowdoin College is committed to equality through affirmative action. Women and minorities are encouraged to apply.

www.bowdoin.edu **Bowdoin**

TEXAS TECH UNIVERSITY
HEALTH SCIENCES CENTER
at Amarillo

Mrs. J. Avery Rush Endowed Chair in Women's Health and Oncology

The Texas Tech University Health Sciences Center (TTUHSC) Women's Health Research Institute is pleased to initiate the search for the newly established Mrs. J. Avery Rush Endowed Chair in Women's Health and Oncology. The aim of the Rush Endowed Chair is to contribute to the growth and excellence of the established TTUHSC Women's Health and Oncology research and clinical programs. Areas of high research interest for the Rush Endowed Chair include breast, ovarian and other gynecologic malignancies. This academic position includes research, clinical and teaching activities to be adapted to the successful applicant's research program and clinical skills.

Accordingly, the successful applicant will typically have attained an MD, MD PhD or an equivalent degree, have both clinical expertise, an established extramurally funded research program in women's health oncology and be eligible for Texas medical licensure. The Rush Endowed Chair will hold an academic appointment at the rank of associate or full professor in the appropriate TTUHSC SOM department(s). Dual departmental school appointments are available.

TTUHSC's campus includes Schools of Medicine, Pharmacy and Allied Health. Each academic unit offers a collaborative, collegial environment that incorporates a wide variety of research and clinical areas of expertise. TTUHSC Amarillo has focus areas of excellence in the areas of genetics, aging, women's health and cancer. Thus, there are many opportunities for cross-collaboration with established researchers.

TTUHSC SOM administration and faculty are strongly committed to the growth and success of an integrative cancer research program and welcome qualified candidates to apply for this exciting position.

Applicants are requested to submit a curriculum vitae and personal statement describing motivation for application and strengths related to building an integrated cancer research program. Please submit documents online at http://jobs.texastech.edu (job requisition #73143). Questions or inquiries are welcome and should be directed to:

Marjorie R. Jenkins, MD
Search Committee Chair
Co-Director, Women's Health Research Institute
1400 Coulter Drive Amarillo, Texas 79106
(806)354-5480
Marjorie.Jenkins@ttuhsc.edu

TTUHSC is an Equal Employment Opportunity Employer (EOE)

Staff Biochemist

Perform electrophysiological studies to determine effects of novel drugs on spinal cord neuron activity following inflammation or neuropathy. Eva. analgesic activity of novel drugs for inflammatory & neuropathic pain. Design experiments, collect, analyze & summarize data using various math & statistical software/prog languages. Min Req MS in Bio, Chem Eng or Biomed Eng & 2 yrs of lab exp performing electrophysiological & behavioral studies w/ rodents. Job location West Point, PA. CV to J. Kennedy Merck Research Labs, WP1-3, 770 Sumneytown Pike, PO Box 4, West Point PA 19486. Merck is an equal opportunity employer M/F/D/V + proudly embracing diversity in all of its manifestations.

CHAIR
Molecular and Medical Genetics
School of Medicine
Oregon Health & Science University

The School of Medicine at Oregon Health & Science University invites applications and nominations for the position of Professor and Chair, Department of Molecular and Medical Genetics

The Department has a long history of excellence in teaching, research and service. Currently there are 29 primary faculty, 21 joint faculty and 6 adjunct faculty. The areas of research and teaching in the department include molecular genetics, molecular biology, somatic cell genetics, cytogenetics, molecular cytogenetics, population genetics, biochemical genetics, and stem cell function. Examples of ongoing projects include genome stability in cancer and inherited diseases, genetics of rare disorders, gene therapy, human genomics, and epigenetics in cancer. The Department has close clinical and research interactions with the Doernbecher Children's Hospital, the Child Development and Rehabilitation Center, and with the Oregon Cancer Institute. The OHSU School of Medicine ranks in the top 30 of all research-orientated medical schools with more than $300 million in extramural support. OHSU was funded in the first round of the Clinical and Translational Science Awards, the department has a key role in University translational and interdisciplinary research efforts. In addition, there are numerous opportunities for interactions with the other schools and centers at OHSU, including the Oregon National Primate Research Center, the Vollum Institute for Advanced Biomedical Research, the Schools of Nursing and Dentistry and the Oregon Graduate Institute of Science and Engineering.

We seek candidates with an M.D. and/or Ph.D. degree that are internationally recognized for their research, have a strong commitment to teaching and demonstrate the leadership skills needed to expand and enhance the department's clinical and service activities. The successful applicant must be a skilled communicator with a clear vision for departmental growth and development. In addition to a generous start-up package for the chairperson, there is also strong institutional support for hiring new faculty. Overall, this recruitment is part of a major investment at OHSU to expand genetics and genomics research.

OHSU places a high priority on cultural diversity; thus, we seek candidates with a demonstrated sensitivity to and understanding of the diverse academic, socioeconomic, cultural, disabled and ethnic backgrounds of OHSU's students and employees. Interested individuals should submit a Curriculum Vitae and the names of three references to: **Search Committee – Molecular and Medical Genetics, c/o Nicole Lockart, Dean's Office – School of Medicine, Oregon Health & Science University, 3181 SW Sam Jackson Park Road, Portland, OR 97239-3098; or e-mail, lockartn@ohsu.edu**. Review of applications will commence immediately and continue until the position is filled.

OHSU is an Affirmative Action, Equal Opportunity Employer. Women, minorities, disabled persons, Vietnam era and disabled veterans are encouraged to apply. OHSU is a smoke-free workplace.

MAYO CLINIC

Faculty Position in Cancer Pharmacology

The Division of Oncology Research and the Department of Molecular Pharmacology and Experimental Therapeutics of the Mayo Clinic College of Medicine seek an outstanding research investigator in the area of cancer pharmacology. Research within the Division is highlighted at **http://cancercenter.mayo.edu/mayo/research/developmental_therapeutics/**

Applications for either an Assistant Professor or more senior level appointment are welcomed. Investigators with expertise in the areas of proliferative signaling, cell cycle checkpoints, DNA repair, cancer pharmacogenomics and/or rational drug design are particularly encouraged to apply.

A curriculum vitae, selected publications and a statement of research interests, should be submitted by **March 31, 2007** to:

Deb Strauss (strauss.debra@mayo.edu)
or to
Scott Kaufmann, M.D., Ph.D.
Search Committee Chair
Guggenheim 1301
Mayo Clinic
Rochester, MN 55905

James Graham Brown Cancer Center
Tumor Immunology Faculty Position

A tenure-track faculty position at the rank of Assistant Professor has opened in a collaborative research group focused on cellular and molecular tumor immunology. The successful candidate will be provided with generous start-up funds, a competitive salary, a primary tenure-track academic appointment in the Department of Microbiology and Immunology within the School of Medicine, and ample research laboratory space in proximity to the extensive core facilities of the Brown Cancer Center. Successful candidates will have, or be expected to establish, a productive extramurally funded research program and will bring teaching and mentoring capability to the immunology Ph.D. graduate program. Preference will be given to candidates with current NCI funding and/or who are capable of establishing collaborative research interactions with several of the existing members of the Tumor Immunobiology Program. The rank of Associate Professor will be considered for individuals who have an established research program and significant extramural research funding.

Additional information on the research programs may be found at **http://www.louisville.edu/medschool/immunology** and **http://browncancercenter.org/bcc2005/research/program.aspx**. Applicants must have 2 or more years of postdoctoral research experience with clear evidence of productivity and fundability. The search will remain open until the position is filled. Applicants must apply on line at **www.louisville.edu/jobs** and attach a c.v. containing an abstract of research interest. Arrange for 4 letters of reference to be sent to:

Robert D. Stout, Ph.D., Professor and Chairman
Department of Microbiology and Immunology
School of Medicine
University of Louisville, Health Sciences Center
Louisville, KY 40292

University of Louisville is an Equal Opportunity Employer

Karolinska Institutet

PROFESSOR IN MEDICAL BIOCHEMISTRY

Karolinska Institutet seeks applicants for a position as full professor in Medical Biochemistry. The position is profiled towards research in biochemistry and includes teaching at the under-graduate and post-graduate level. The holder is expected to carry out outstanding research and teaching at a high international level.

The research of the applicant should be based on experimental approaches and can represent a variety of areas in the fields of biochemistry and molecular biology, preferentially with emphasis on medically important questions. The applicants should have a broad and well-documented experience in modern biochemistry. Further information concerning this position may be obtained from **Professor Karl Tryggvason**, Department of Medical Biochemistry and Biophysics, Karolinska Institutet, **phone +46 8-524 8770, fax: +46 8-31 61 65, E-mail: karl.tryggvason@ki.se**

Deadline for applications is **March 26, 2007**

Letter of application, curriculum vitae, qualifications, written synopsis of future research, 10 scientific publications of your choice, should be sent in 4 copies by **March 26, 2007** to **Registrator, Karolinska Institutet, S-171 77 Stockholm, Sweden**. For more detailed information, please look at **http://info.ki.se** for the entire advertisement and the Qualifications Portfolio.

UNIVERSITY OF DELAWARE

One of the oldest institutions of higher education in this country, the University of Delaware today combines tradition and innovation, offering students a rich heritage along with the latest in instructional and research technology. The University of Delaware is a Land-Grant, Sea Grant, Urban-Grant, and Space Grant institution with its main campus in Newark, DE, located halfway between Washington, DC and New York City. Please visit our website at **www.udel.edu.**

Phytoplankton Oceanographer
Assistant Professor

The College of Marine and Earth Studies invites applications for a 9-month tenure-track position in Biological Oceanography. The position is available after September 2007 and is located at the Lewes campus, which has modern laboratory facilities and easy access to diverse marine habitats. Responsibilities will include development of a vigorous research program, teaching, and advisement of graduate students. We are looking for candidates with expertise in phytoplankton ecology who will establish an integrated field and laboratory program using modern techniques such as those from molecular biology. The successful candidate will be expected to interact with scientists from diverse disciplines and will receive a competitive salary and attractive startup package. For more information on the College, please visit our website at **www.ocean.udel.edu.**

Candidates should submit a letter of interest, hard copy and email as a single pdf document) describing research and teaching interests, curriculum vitae and the names and contact information of three references to David L. Kirchman (phytosearch@cms.udel.edu), College of Marine and Earth Studies, University of Delaware, Lewes, DE 19958. Review of applications will begin on March 5, 2007 and will continue until the position is filled.

Curriculum vitae and all application materials will be shared with departmental faculty.

The UNIVERSITY OF DELAWARE is an Equal Opportunity Employer which encourages applications from Minority Group Members and Women

MGH 1811

MASSACHUSETTS GENERAL HOSPITAL
HARVARD STEM CELL INSTITUTE

The Center for Regenerative Medicine (CRM) at Massachusetts General Hospital invites applications for a tenure-track assistant professor position. Outstanding scientists in the field of stem cell biology who have the demonstrated ability to develop a strong independent research program will be considered. Successful candidate(s) will be members of the **Harvard Stem Cell Institute** and faculty of Harvard University. Candidates must hold a PhD and or MD and have a history of innovative interactive research. Women and minority candidates are urged to apply.

Applicants should send an electronic copy of (1) letter of interest (2) research plan and (3) current curriculum vitae to **Dr David Scadden c/o Chris Shambaugh** cpasker@partners.org. Three letters of recommendation should also be sent directly to:

Center for Regenerative Medicine Search Committee
Attention: Chris Shambaugh
Massachusetts General Hospital
185 Cambridge St.
CPZN-3265A
Boston, MA 02114

MGH is an Equal Opportunity, Affirmative Action Employer

NC STATE UNIVERSITY

ASSOCIATE DEAN FOR RESEARCH AND GRADUATE PROGRAMS

The College of Veterinary Medicine (CVM) at North Carolina State University (**http://www.cvm.ncsu.edu/**) invites applications for Associate Dean for Research and Graduate Programs. The College seeks exceptional candidates who will capitalize on the many existing strengths of the CVM and the University. This individual will play a pivotal role in the future development of one of the nation's premier veterinary schools in the areas of research and graduate education.

The College excels in basic, translational and clinical research, the training of veterinary and graduate students, and the provision of outstanding patient care. In 2005, the CVM faculty successfully competed for $9.9 million in extramural research funding, placing the College among the top five U.S. veterinary schools. The College is located near the Research Triangle Park of North Carolina and in close proximity to other highly distinguished universities and industrial partners, including the biotechnology and agribusiness sectors. It is expected that the incumbent of this position will take advantage of opportunities for developing effective collaborations with these local resources. The Associate Dean should be an effective communicator who will serve as a catalyst in support of new and innovative research programs, including the areas of genomics and proteomics, food safety, antimicrobial resistance, cancer biology, nanotoxicology as well as allergic, immunologic, infectious diseases. The Associate Dean will facilitate the continued development of programs that are underway, including the newly funded Center for Comparative Medicine and Translational Research (**http://www.cvm.ncsu.edu/research/ccmtr/**) and the Center for Chemical Toxicology Research and Pharmacokinetics (**http://ctrp.ncsu.edu/**). The College seeks an Associate Dean who will play a pivotal role in moving the College forward in its aspirations of becoming the nation's premier site for basic, translational and clinical animal research and recognized center for the training of clinician scientists. The individual will help the College promote the concept of "One Medicine" for the benefit of society.

The College is home to a number of graduate programs spanning a variety of biomedical disciplines leading to MS, MSV/PM, PhD and DVM/PhD degrees. The Associate Dean will provide leadership to direct and expand these training programs as well as a vision for the future that facilitates and encourages interdisciplinary collaborations within the University and with academic and non-academic partners. The successful candidate will also administer and coordinate the College's research facilities, including laboratory animal resources.

Candidates must hold a Ph.D., MD and/or DVM degree and have demonstrated excellence in research as judged by their publication and extramural funding record, with experience and accomplishments equivalent to those required for the rank of Full Professor. There is an expectation that the Associate Dean will maintain an active research program.

Applications must be submitted online and should include a current Curriculum Vitae and the names and addresses of three references. For additional information and to apply online, please visit **http://jobs.ncsu.edu** and reference position #B 6440701. The Search Committee will begin reviewing applications on March 15, 2007 and the search will remain open until a suitable candidate is found. For further information please contact:

Dr. Chris McGahan, Chair
Search Committee for the
Associate Dean for Research and Graduate Programs
Department Head
Molecular Biomedical Sciences
College of Veterinary Medicine
North Carolina State University
4700 Hillsborough St.
Raleigh, NC 27606

North Carolina State University is an equal opportunity and affirmative action employer. In addition, North Carolina State University welcomes all persons without regard to sexual orientation. For ADA accommodations please contact (919) 513-3148.

NC STATE achieve!
Innovation in Action

2 Great Career Events

Science/UCSF Biotech Industry Career Fair

(in partnership with AAAS Annual Meeting)

Make your next career move easier. *Science* Careers and UCSF are co-hosting a career fair in conjunction with the upcoming AAAS Annual Meeting. Come meet recruiters face to face and explore career opportunities for all levels of scientists.

Thursday, 15 February 2007
1:00 pm – 4:30 pm
UCSF Mission Bay Campus
Robertson Auditorium
San Francisco, CA

For information on exhibiting, contact Darrell Bryant at (202) 326-6533. Exhibitors receive free access to *Science*'s Resume/CV Database for 3 months.

Making the Most of Your Career Fair

If you'll be attending the career fair, maximize your experience by first attending our free seminar, *Making the Most of Your Career Fair*. Learn how to promote yourself quickly and professionally.

Tuesday, 13 February 2007
6:00 pm — reception to follow
UCSF Mission Bay Campus
Genentech Auditorium
San Francisco, CA

Making the Most of Your Career Fair is sponsored by Genentech

Genentech
IN BUSINESS FOR LIFE

For more information on these events, visit
www.sciencecareers.org/ucsf

ScienceCareers.org
We know science AAAS

Big Improvements

to *Science* Technology and *Science* Careers Features

The *Science* Technology and *Science* Careers Features now offer you more. Readers will notice a redesigned and revitalized Feature section with:

- Fresh perspectives by leading science writers
- Strengthened science content
- Relevant, timely, and topical subject matter
- Balance of global commercial and academic voices
- Brand new look
- Read in print or online

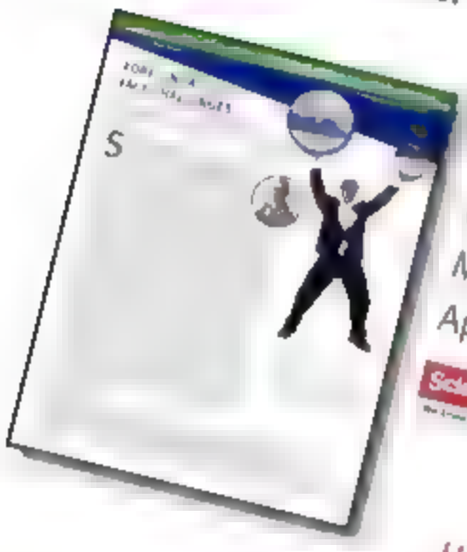

Upcoming *Science* Careers Features include:

February 2 — Faculty Positions
March 2 — International Career Report – Science in Europe
April 6 — Careers in Cancer Research

Upcoming *Science* Technology Features include:

February 23 — Clinical Proteomics
March 16 — Genomics
April 6 — Cell Signaling

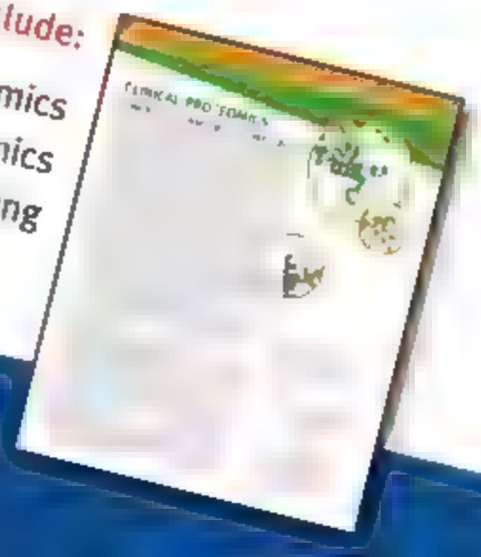

Featured Employers

Search **ScienceCareers.org** for job postings from these employers. Listings updated three times a week.

Abbott Laboratories www.abbott.com

Elan Pharmaceuticals www.elan.com/careers

Genentech www.gene.com

Kelly Scientific Resources
www.kellyscientific.com

Novartis Institutes for BioMedical Research
www.nibr.novartis.com

Pfizer Inc.
www.pfizer.com

Philip Morris
www.canIbeattheexperience.com

Pioneer Hi-Bred
www.pioneer.com

If you would like to be a featured employer, call 202-326-6543

Issue Date
2 March 2007

Booking Deadline:
13 February 2007

Contacts:
Tracy Holmes, Christina Harrison, or Svitlana Barnes
ads@science-int.co.uk
+44 (0) 1223 326500

THE STATE UNIVERSITY OF NEW JERSEY
RUTGERS

Dean
Ernest Mario School of Pharmacy

Rutgers, The State University of New Jersey, seeks an outstanding leader and eminent scholar for the position of Dean of the Ernest Mario School of Pharmacy. Scientists with an exceptional record of scholarly accomplishment and a passionate commitment to excellence in pharmaceutical education both in academe and in clinical practice are encouraged to apply. The Dean is the chief academic and administrative officer of the School and reports directly to the Rutgers Executive Vice President for Academic Affairs.

Rutgers is one of the nation's oldest and largest institutions of higher education, and is a member of the prestigious Association of American Universities. The Ernest Mario School of Pharmacy (EMSP) has a strong academic reputation as one of the top-ranked schools of pharmacy in the country. It is the only school of pharmacy in New Jersey, a leading state in the pharmaceutical and medical technology industry. EMSP is part of a vibrant biomedical and health sciences research and teaching community at Rutgers University, including major academic programs in the life sciences, biotechnology, neuroscience, and bio-engineering, and collaborative relationships with the Center for Advanced Biotechnology and Medicine, the Environmental and Occupational Health Sciences Institute, the Cancer Institute of New Jersey, The School of Public Health, The Robert Wood Johnson Medical School, the New Jersey Center for Biomaterials, the Stem Cell Institute of New Jersey, the Human Genetics Institute, and other related centers and programs. Admission to the EMSP is highly selective and enrolls approximately 250 full-time students. With seventy-six full-time faculty members representing strength in both the basic sciences and clinical practice, the EMSP offers a fully accredited six-year professional degree program leading to the Doctor of Pharmacy. EMSP faculty members are also deeply involved in M.S. and Ph.D. programs in Pharmaceutics, Medicinal Chemistry, Toxicology and related areas. The School is located in central New Jersey, close to New York City, Philadelphia, beaches and countryside.

The Dean will provide the vision and energy to continue the advancement of the EMSP by assuring that the school is at the forefront of pharmacy education, clinical practice and pharmaceutical research. The Dean will foster collaborations with faculty in other Rutgers units, and play a lead role in strengthening the University's involvement with the state's extensive pharmaceutical industry and medical university. The Dean is responsible for both the School's academic strategy and its fiscal management. Additionally, the Dean serves as a strong advocate for the School in communicating its mission and goals to internal and external constituencies and in raising funds from external sources. Candidates for the position should have an earned doctorate in an appropriate field, a minimum of five years of administrative experience, and a significant record of teaching and scholarly or professional achievement.

The salary range is competitive, commensurate with experience and qualifications. The appointment start date is July 1, 2007. Review of nominations and applications has begun and will continue until the position is filled. Applicants should submit a letter of interest, a current vitae, and the names and contact information for at least three references who will be contacted only with the explicit permission of the candidate. All correspondence will be held in confidence and should be mailed or emailed to:

Professor Kathryn Ulrich, Chair,
EMSP Dean Search Committee
Office of the Executive Vice President for Academic Affairs
Rutgers, The State University of New Jersey
83 Somerset Street, Room 302
New Brunswick, NJ 08901-1281
e-mail: emspdsc@rci.rutgers.edu, phone: (732) 932-8792

An Affirmative Action/Equal Opportunity Employer

http://pharmacy.rutgers.edu

Does your next career step need direction?

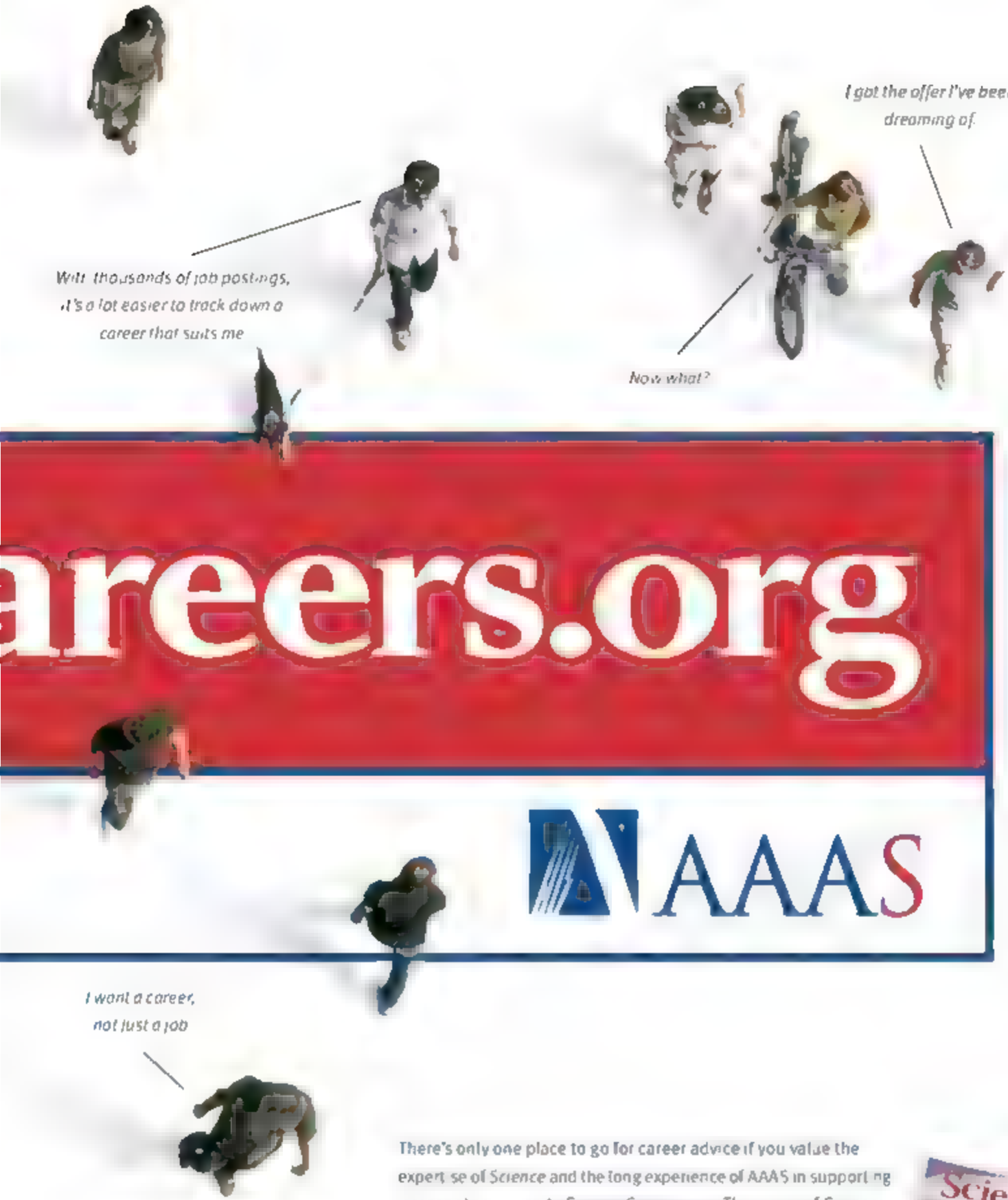

There's only one place to go for career advice if you value the expertise of *Science* and the long experience of AAAS in supporting career advancement. ScienceCareers.org. The pages of *Science* and our website ScienceCareers.org offer

- Thousands of job postings
- Funding information
- Career advice articles and tools
- Networking opportunities

www.sciencecareers.org

POSITIONS OPEN

BIOLOGY EDUCATOR ASSISTANT PROFESSOR

The Biological Sciences Department at California State Polytechnic University, Pomona, invites applications for a tenure-track position in biological education at the rank of Assistant Professor to begin September 2007. The new faculty member will teach classes in science/content methods leading to the teaching credential, develop specialty courses and workshops for science teachers, and will be expected to establish and maintain an externally funded research program in science education involving undergraduate and Master's level students. The successful candidate will also be expected to assist in curriculum development, advise students, serve on Department, College, and University committees, and engage in professional activities. Ph.D. required from an accredited institution in biology by August 2007, a combination of graduate degree and/or work experience in both biology and science education, and possess or be qualified to obtain a California teaching credential in a single subject area. Application review will begin March 1, 2007 and will continue until position is filled.

Address all nominations, inquiries, and requests to:

Dr. Gil Brum and Tina Hartney
Co-Chairs, Biology Educator Search Committee
Biological Sciences Department
California State Polytechnic University, Pomona
3801 West Temple Avenue
Pomona, CA 91768
Telephone: 909-869-4036, fax: 909-869-4078
E-mail: gdbrum@csupomona.edu

FACULTY POSITION IN COMPARATIVE IMMUNOBIOLOGY OR HOST PARASITE/SYMBIONT INTERACTIONS
University of Louisiana at Lafayette

The Department of Biology at the University of Louisiana at Lafayette invites applications for a tenure-track position at the **ASSISTANT PROFESSOR** level in comparative immunobiology or the biology of host parasite or host symbiont interactions. We seek a promising scientist using an experimental approach to investigate the cellular/molecular basis of pathogenic, parasitic, or symbiotic interactions. Applicants must have a Ph.D. in a biological science, with postdoctoral experience preferred. This individual will be expected to establish a vigorous, externally funded research program involving graduate students to complement our doctoral program in environmental and evolutionary biology, and teach courses in immunobiology and other areas of specialty. Information about the Department is available at **website: http://biology.louisiana.edu/.** Applicants should send their curriculum vitae and statements of research and teaching, and have three letters of recommendation sent to: **Immunobiology Search Committee, Department of Biology, University of Louisiana at Lafayette, P.O. Box 42451, Lafayette, LA 70504.** Review of applications will begin on February 22, 2007. Inquiries may be addressed to Joe Neigel, Chair, Immunobiology Search Committee, e-mail: immunosearch@louisiana.edu.

University of Louisiana at Lafayette is an Equal Employment Opportunity/Affirmative Action employer.

The Department of Animal Sciences, Purdue University, West Lafayette, Indiana, invites applications for a **TENURE-TRACK FACULTY** position. The successful candidate will be expected to develop a research program on aspects of adipose biology and/or lipid metabolism that are relevant to growth, obesity or the metabolic syndrome. Candidate will participate in teaching and advising of both undergraduate and graduate students. Suitable candidate must possess a Ph.D. in life sciences or a related area, postdoctoral experience is preferred. Detailed position announcement and application details can be found at **website: http://www.ansc.purdue.edu/positions/Bio%20Obesity%2006.pdf.** Review of applications will begin February 1, 2007 and continue until the position is filled. *Purdue University is an Equal Opportunity/Equal Access/Affirmative Action employer.*

POSITIONS OPEN

PLANT CELL WALL BIOCHEMISTRY

The Department of Biochemistry, Biophysics, and Molecular Biology (**website: http://www.bbmb.iastate.edu**) at Iowa State University (ISU) seeks to hire a tenure-track **ASSISTANT PROFESSOR.** The Department is particularly interested in candidates with expertise and research interests in the biochemistry, molecular biology, and biotechnology of plant cell walls. The Department offers an interactive research environment with excellent research facilities, including a full range of core facilities to support research in genomics, proteomics, metabolomics, nuclear magnetic resonance, and microscopy. Applicants should have a Ph.D. in a relevant field, postdoctoral experience, and are expected to establish a vigorous, externally funded research program. All successful applicants are expected to actively participate in graduate and undergraduate teaching. The expected appointment is at the level of Assistant Professor (tenure track). Excellent laboratory space and a generous start-up package will be provided.

Please provide curriculum vitae, three names of recommenders, a brief description of your research plans, and a statement of your teaching philosophy and interests by March 1, 2007 to: **Search Committee, Department of Biochemistry, Biophysics, and Molecular Biology, 1210 Molecular Biology Building, Iowa State University, Ames, IA 50011.**

ISU is an Equal Opportunity/Affirmative Action Employer.

DIRECTOR, NEW YORK SEA GRANT

Stony Brook University (SUNY) and Cornell University invite nominations and applications for Director of the New York Sea Grant Institute (NYSGI). The Director will be based at Stony Brook University where she/he will also hold an adjunct faculty position. NYSGI's mission is to develop and deliver science that addresses issues of New York's marine and Great Lakes coasts. The Director provides leadership to ensure that the research, education, and outreach programs of NYSGI continue to be among the nation's best. Candidates should send a letter of application with curriculum vitae and contact information for at least five references to: **Dean David Conover, Search Committee Chair, 121 Discovery Hall, Stony Brook University, Stony Brook, NY 11794-5001.** List of qualifications and full job description are available at **website: http://www.seagrant.sunysb.edu/nysgdirector.** To apply online (strongly preferred) visit **website: http://www.stonybrook.edu/cjo.** Review of applications will begin on February 19, 2007. The search will remain open until a suitable candidate is selected.

Equal Opportunity/Affirmative Action Employer.

ASSISTANT/ASSOCIATE PROFESSOR
Medical Genetics
Mercer University School of Medicine
Macon, Georgia

Mercer University School of Medicine invites applications for a 12-month salaried, tenure-track position in genetics at the rank of **ASSISTANT** or **ASSOCIATE PROFESSOR.** The successful candidate will [illegible] education excellence in a multidisciplinary, case-based curriculum and will be expected to develop an independent, externally funded research program. Applicants should have a doctoral degree with an expertise in human genetics and three years of postdoctoral training. Review of applications will continue until the position is filled. For online submission of applications, visit **website: https://www.mercerjobs.com.** *Affirmative Action/Equal Opportunity Employer [illegible]*

The University of Manitoba (Winnipeg, Canada) invites applications for **HEAD** of the **DEPARTMENT OF BIOLOGICAL SCIENCES.** The successful candidate will lead the development of a newly formed Department comprised of 34 full-time academic members with diverse research interests in plant and animal biology. Complete job description and application instructions can be found at **website: http://umanitoba.ca/faculties/science.**

MEETINGS

11th International TNF Conference

MAY 13 - 16 2007 Asilomar, CA, USA

The 11th International TNF Conference program will cover new discoveries and advances in basic science and clinical research.

The scientific program will cover topics ranging from basic science to translational research. Invited speakers, authors of selected abstracts, and poster presenters will report on new developments in our understanding of the structure, signaling mechanisms, and roles in biology and disease of TNF superfamily ligands and receptors.

Please join us for what promises to be an exciting meeting and a magnificent setting at the beautiful historic site of the Asilomar Conference Grounds on the Pacific Ocean coast near Monterey, California (approximately a 2 hour drive south of San Francisco).

FOR MORE INFORMATION AND TO REGISTER, PLEASE GO TO: www.TNF2007.org

ORGANIZING COMMITTEE
Co-Chairs
Avi Ashkenazi (Genentech, USA)
Jeff Browning (Biogen Idec, USA)

SCIENTIFIC ORGANIZING COMMITTEE
Sarah Hymowitz (Genentech, USA)
Michael Karin (UC San Diego, USA)
George Kollias (Biomedical Sciences Research Center, Greece)
Fabienne MacKay (Garvin Institute, Australia)
Jurg Tschopp (University of Lausanne, Switzerland)
David Wallach (Weizmann Institute, Israel)
Carl Ware (La Jolla Institute, USA)

KEYNOTE LECTURE
Vishva Dixit (Genentech, USA)

CONFIRMED SPEAKERS
Jonathan Ashwell (NCI, USA)
Gail Bishop (University of Iowa, USA)
Yongwon Choi (University of Pennsylvania, USA)
Mick Croft (La Jolla Institute, USA)
Yang Xin Fu (University of Chicago, USA)
Sarah Hymowitz (Genentech, USA)
Yong Jun Liu (MD Anderson Cancer Center, USA)
Flavius Martin (Genentech, USA)
Shu Mi (Biogen Idec, USA)
Jurg Tschopp (University of Lausanne, Switzerland)
David Wallach (Weizmann Institute, Israel)
Milton Werner (Rockefeller University, USA)

POSITIONS OPEN

ASSISTANT PROFESSOR
Ponce School of Medicine

The Department of Physiology and Pharmacology at the Ponce School of Medicine invites applications for a full-time faculty position at the level of **ASSISTANT PROFESSOR.** We are seeking individuals with a Ph.D., M.D., or equivalent, and postdoctoral experience. Fluency in spoken and written Spanish and English is preferred. The successful candidate will be expected to participate in the medical and graduate student programs in the physiology and/or pharmacology course(s) and to develop an independent research program. Review of candidates will begin immediately and will continue until position is filled. Send curriculum vitae, a statement of goals, and names and addresses of three references to:

Dr. León Ferder
Chairman, Physiology and Pharmacology Department
Ponce School of Medicine
P.O. Box 7004
Ponce, Puerto Rico 00732
E-mail: leferder@psm.edu

The Ponce School of Medicine is an Equal Opportunity/Affirmative Action Employer. Women and minorities are encouraged to apply.

WATERSHED HYDROLOGIST

The Tropical Agriculture Program of the Earth Institute at Columbia University, New York, seeks applications for a Watershed Hydrologist at the **RESEARCH SCIENTIST** or **ASSOCIATE RESEARCH SCIENTIST** level. The position, focusing on rural African livelihoods and environment, involves basic and applied research. The Watershed Hydrologist will develop scientific framework, models, and applications of sustainable small-scale water capture and management by rural African communities for consumption, agriculture, and ecosystem services. A Ph.D. in hydrology or related sciences is preferred. The position requires research experience in rural Africa and ability to perform in a multidisciplinary and multicultural environment; extensive travel involved. Women and minorities are encouraged to apply. Send letter of application with curriculum vitae and names of three references to: **Dr. Carlos Perez, Associate Director, Tropical Agriculture, Columbia University, Lamont Hall, P.O. Box 1000, Palisades, NY 10964; e-mail: cperez@ei.columbia.edu.**

Columbia University is an Affirmative Action/Equal Opportunity Employer.

CHAIR, DEPARTMENT OF PHARMACEUTICAL SCIENCES. Applications are invited at the **ASSOCIATE PROFESSOR** or **PROFESSOR** level with teaching, research, and service responsibilities. Successful applicants must possess a Ph.D. in medicinal chemistry, pharmaceutics, pharmacology, or a closely related biomedical science. Postdoctoral research experience with a minimum of five to ten years of academic experience is required. A record of continued academic and professional accomplishments in research, teaching, and service must be demonstrated. The Chair is expected to provide leadership and vision in building the Department's research activities and funding to a nationally recognized level, while fulfilling departmental responsibilities within the School of Pharmacy. E-mail a letter of interest and curriculum vitae to the: **Committee Chair, John Krstenansky, e-mail: jkrstenansky@llu.edu.**

POSTDOCTORAL ASSOCIATE position available to study the role of extracellular proteins in pathogenesis of heart failure. The work will focus on osteopontin and integrin signaling. Highly motivated individuals (M.D. and/or Ph.D.) with experience in molecular signaling, cardiac physiology, or cell biology will be preferred. Send curriculum vitae to: **Dr. Krishna Singh, Department of Physiology, East Tennessee State University, P.O. Box 70576, Johnson City, TN 37614-1708; e-mail: singhm@etsu.edu.** *Affirmative Action/Equal Opportunity Employer.*

POSITIONS OPEN

NIH POSTDOCTORAL TRAINING
in Molecular Therapy
The Children's Hospital of Philadelphia/University of Pennsylvania

National Heart Lung and Blood Institute Training Grant, Training in Molecular Therapeutics for Pediatric Cardiology, supporting studies of cardiovascular disease mechanisms and molecular therapies. Project fields include: cardiac and pulmonary development, heart valve disease, regenerative medicine, stem cell biology, and pharmacology. Competitive salary and full benefits. Only applicants with Ph.D. and/or M.D. *(who must be a resident alien or U.S. citizen status)* should send their curriculum vitae and the names of three references to:

Robert J. Levy, M.D.
William J. Rashkind Endowed Chair
University of Pennsylvania School of Medicine
Training Program Director
The Children's Hospital of Philadelphia, 702 ARC
3615 Civic Center Boulevard
Philadelphia, PA 19104
Fax: 215-590-5454
E-mail: levyr@email.chop.edu

Equal Opportunity Employer. Minorities/Females/Persons with Disabilities/Veterans.

POSTDOCTORAL POSITION

New Mexico Highlands University is accepting applications for a Postdoctoral Position that is available as part of a multiyear NIH program carrying out the synthesis, spectroscopy, and bio-testing of compounds for photodynamic therapy. Successful candidates are likely to have experience with computer simulations or modeling. Applicants should have a Ph.D. in chemistry, biochemistry, or related field. Starting date is February 1, 2007. Interested applicants should submit curriculum vitae, a list of courses taken, a letter of interest, and three letters of reference to: **New Mexico Highlands University, Postdoctoral Fellows Search, Academic Affairs, P.O. Box 9000, Las Vegas, NM 87701.** *For disabled access or services, call telephone: 505-454-3311 or TDD 505-454-3003. Equal Opportunity Employer.*

TENURE-TRACK FACULTY POSITION FOR AN ESTABLISHED T CELL IMMUNOLOGIST
Loyola University Chicago
Department of Microbiology and Immunology

Successful applicant will have an active externally funded research program, and will develop synergistic research relationships with existing immunologists in the Department as well as with immunologists in the Oncology Institute, Burn Shock Trauma Institute, and/or the newly developed Institute for Infectious Diseases and Immunology.

Submit letters of application, curriculum vitae, research interests, and names and addresses of three references to: **Katherine L. Knight, Ph.D., Search Committee Chair, Department of Microbiology and Immunology, Loyola University Medical Center, 2160 S. First Avenue, Maywood, IL 60153.**

POSTDOCTORAL POSITIONS are available at the University of Washington in Seattle to characterize cellular proteins and genes involved in cholesterol transport. Experience in molecular and cellular biology is required. Send curriculum vitae and letters of recommendation to: **Dr. John F. Oram, Department of Medicine, Box 356426, University of Washington, Seattle, WA 98115-6426. E-mail: joram@u.washington.edu.**

POSTDOCTORAL POSITION to study vascular routes to the cartilaginous growth plate during postnatal bone development, using multiphoton microscopy. Prior background in live animal imaging and cell biology helpful but not essential. Send curriculum vitae and names of three references to: **Dr. Cornelia Farnum, Department of Biomedical Sciences, Cornell University, Ithaca, NY 14853. E-mail: cef2@cornell.edu.**

POSITIONS OPEN

BIOMEDICAL ENGINEERING FACULTY POSITION

Stony Brook University's Department of Biomedical Engineering invites applications for a **TENURE-TRACK ASSISTANT** or **TENURED ASSOCIATE** or **FULL PROFESSOR** position to begin in the fall of 2007. Recruitment will be within the broad areas of biomedical engineering, with particular emphasis on the quantitative imaging at the molecular and cellular levels. The successful candidate is expected to establish and maintain a competitive, federally funded, interdisciplinary research program in bioimaging, and to excel in teaching at both the graduate and undergraduate levels. Collaboration with Brookhaven National Laboratory's Medical Department, Center for Functional Nanomaterials, and/or the National Synchrotron Light Source is encouraged. For further information, visit **website: http://www.bme.stonybrook.edu.** Those interested should submit a complete application, including curriculum vitae, statement of research and teaching interests, and the names of four references to: **Ki Chon, Ph.D, Bioimaging Search Committee, Department of Biomedical Engineering, Health Science Center L18, R030, Stony Brook University, Stony Brook, NY 11794-8181,** *Equal Opportunity/Affirmative Action Employer.*

ASSISTANT PROFESSOR, BIOLOGICAL OCEANOGRAPHER
The Florida State University

The Department of Oceanography is seeking applications for a Ph.D.-level Biological Oceanographer for a nine-month, tenure-earning appointment at the Assistant Professor level to begin as soon as August 2007. We are particularly interested in a person who studies the role of zooplankton in ecological processes. The position involves research, teaching (primarily at the graduate level), and service. Please send the PDF files of your letter of application, curriculum vitae, and contact information for three references to **e-mail: position@ocean.fsu.edu.**

Starting salary is negotiable, dependant upon qualifications, with a minimum salary of $59,000.

Closing date is 1 May 2007. Application review will begin on 1 June 2007; however, the advertising and search process will remain active until the position is filled.

The Florida State University subscribes to equal opportunity and complies with the Americans with Disabilities Act. All eligible candidates are invited to apply for position vacancies as appropriate. The Florida State University is a public records agency pursuant to Chapter 119, Florida Statutes. An Equal Opportunity/Access/Affirmative Action Employer.

A POSTDOCTORAL POSITION is open to study the role of the cell cycle and stress kinases in models of kidney insufficiency. Collaborations with the transgenic core laboratory at the Arkansas Cancer Research Center will be involved. Candidates with a background in recombinant technologies including in vivo mouse work are encouraged to send their curriculum vitae and three references to: **Peter M. Price, Ph.D., University of Arkansas for Medical Sciences, VA Medical Center, 4300 West 7th Street, Mail Route 151VA, Little Rock, AR 72205. E-mail: pricepeterm@uams.edu.**

MARKETPLACE

Believe it!

DNA Sequencing for $2.50 per reaction.

- Read length up to 900 bases.
- High quality electropherograms.
- Fast turnaround.
- Plasmid and PCR purification available.

$2.50 per reaction!

POLYMORPHIC
Polymorphic DNA Technologies, Inc.

www.polymorphicdna.com
info@polymorphicdna.com

1125 Atlantic Ave., Ste. 102
Alameda, CA 94501

Polymorphic exclusively uses ABI 3730XL sequencers.
Data delivered via secure FTP, email or CD.
No charge for standard sequencing primers.
384 sample minimum order.
96 well plates only—no tubes.

888.362.0888

For more information please visit
www.polymorphicdna.com

THE KEYS TO HIGH PERFORMANCE

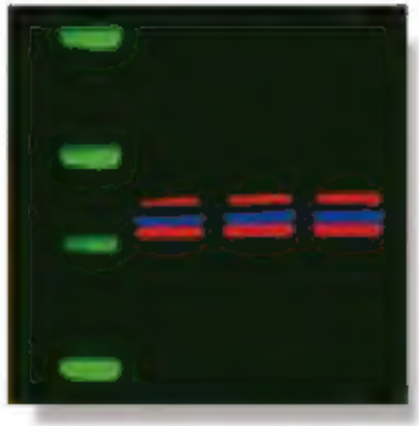

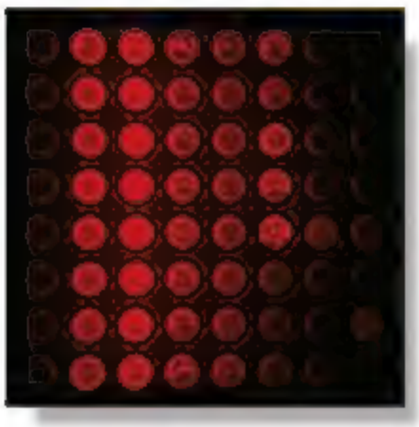

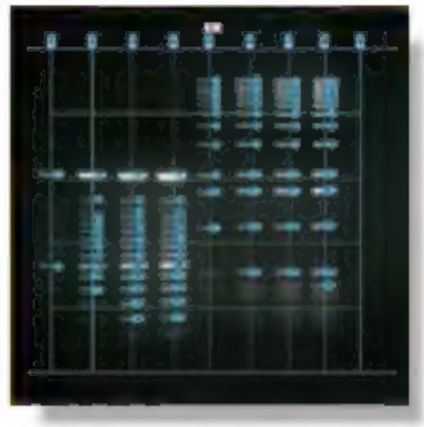

Introducing the Kodak Image Station 4000MM PRO: the newest addition to the industry standard Image Station line brings precision automation and ease of use to an entirely new level. The IS4000MM PRO features a new automated high-performance 10X zoom lens and computer-controlled 10 excitation and 4 emission filter systems, providing reproducible and quantitative imaging of chemiluminescent, fluorescent, and chromogenic labels in gels, blots, plates and more. With 4-million pixel resolution, >4 OD dynamic range and optional x-ray and radioisotopic imaging capabilities, the Kodak Image Station 4000MM PRO provides the optimal combination of precision, performance and versatility.

www.kodak.com/go/imagestation5
Call toll free:
U.S. 1-877-747-4357, exp. code 7
International +1-203-786-5657

Kodak
Molecular Imaging Systems